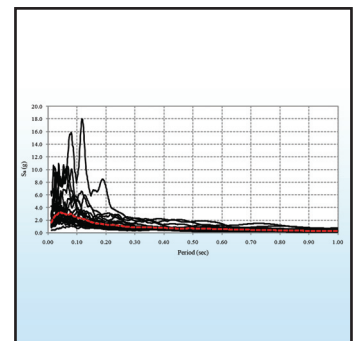
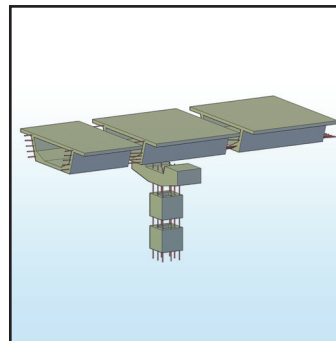
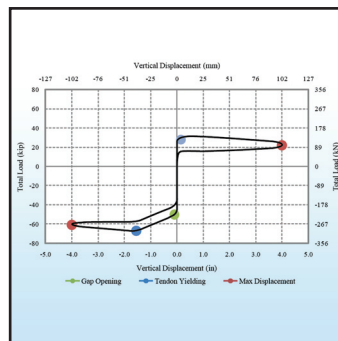
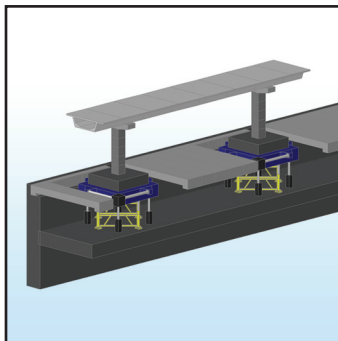


Seismic Design and Analysis of a Precast Segmental Concrete Bridge Model

by
Myrto Anagnostopoulou,
Andre Filiatrault and Amjad Aref



Technical Report MCEER-11-0002

September 15, 2011

NOTICE

This report was prepared by the University at Buffalo, State University of New York, as a result of research sponsored by the Federal Highway Administration. Neither MCEER, associates of MCEER, its sponsors, the University at Buffalo, State University of New York, nor any person acting on their behalf:

- a. makes any warranty, express or implied, with respect to the use of any information, apparatus, method, or process disclosed in this report or that such use may not infringe upon privately owned rights; or
- b. assumes any liabilities of whatsoever kind with respect to the use of, or the damage resulting from the use of, any information, apparatus, method, or process disclosed in this report.

Any opinions, findings, and conclusions or recommendations expressed in this publication are those of the author(s) and do not necessarily reflect the views of MCEER or its sponsors.

Seismic Design and Analysis of a Precast Segmental Concrete Bridge Model

by

Myrto Anagnostopoulou,¹ Andre Filiatrault² and Amjad Aref²

Publication Date: September 15, 2011

Submittal Date: January 14, 2011

Technical Report MCEER-11-0002

Task Number 020-2.2

FHWA Contract Number DTFH61-07-C-00020

- 1 Structural and Test Engineer, Structural and Earthquake Engineering and Simulation Laboratory, Department of Civil, Structural and Environmental Engineering, University at Buffalo, State University of New York
- 2 Professor, Department of Civil, Structural and Environmental Engineering, University at Buffalo, State University of New York

MCEER

University at Buffalo, State University of New York

Red Jacket Quadrangle, Buffalo, NY 14261

Phone: (716) 645-3391; Fax (716) 645-3399

E-mail: mceer@buffalo.edu; WWW Site: <http://mceer.buffalo.edu>

Preface

MCEER is a national center of excellence dedicated to the discovery and development of new knowledge, tools and technologies that equip communities to become more disaster resilient in the face of earthquakes and other extreme events. MCEER accomplishes this through a system of multidisciplinary, multi-hazard research, in tandem with complimentary education and outreach initiatives.

Headquartered at the University at Buffalo, The State University of New York, MCEER was originally established by the National Science Foundation in 1986, as the first National Center for Earthquake Engineering Research (NCEER). In 1998, it became known as the Multidisciplinary Center for Earthquake Engineering Research (MCEER), from which the current name, MCEER, evolved.

Comprising a consortium of researchers and industry partners from numerous disciplines and institutions throughout the United States, MCEER's mission has expanded from its original focus on earthquake engineering to one which addresses the technical and socio-economic impacts of a variety of hazards, both natural and man-made, on critical infrastructure, facilities, and society.

The Center derives support from several Federal agencies, including the National Science Foundation, Federal Highway Administration (FHWA), and the Department of Homeland Security/Federal Emergency Management Agency, State of New York, other state governments, academic institutions, foreign governments and private industry.

The Center's Highway Project, primarily funded by the FHWA since 1992, focuses on the development of improved seismic design, evaluation, and retrofit methodologies and strategies for new and existing bridges and other highway structures. Over the years, MCEER has produced a new seismic retrofitting manual, consisting of two parts (bridges and other highway structures), as well as research products on the seismic retrofitting of truss bridges, seismic isolation manual and Risks from Earthquake Damage to Roadway System (REDARS).

In 2007, MCEER was awarded a new contract, "Innovative Technologies and Their Applications to Enhance the Seismic Performance of Highway Bridges." The major focus of the research program is on the development of detailed technology to apply accelerated bridge construction (ABC) in seismic regions, and the development of innovative seismic protection technologies that can enhance the seismic performances of precast reinforced concrete bridges with an emphasis on ABC.

The primary objective of this study is to investigate the response of precast segmental concrete bridge structures, designed according to Accelerated Bridge Construction (ABC) techniques, when subjected to earthquake loading. A large-scale model of a single-span segmental bridge was designed to be tested on the dual six-degree of freedom shake tables of the Structural Engineering and Earthquake Simulation Laboratory (SEESL) at the University of Buffalo. The AASHTO

LRFD Bridge Design Specifications and the PCI Bridge Design Manual were used for the design of the bridge model. A key concept incorporating post-tensioned internal unbonded tendons acting as the only continuous reinforcement between adjacent segments of both the superstructure and substructure was introduced in the design. Unbonded tendons can allow the triggering of a gap opening mechanism between adjacent segments and the system's self-centering response when subjected to seismic loads. In a companion effort, a two-dimensional numerical model of the segmental bridge superstructure was developed to verify its behavior under vertical seismic loads. The numerical model was analyzed under a series of vertical seismic excitations using nonlinear time-history dynamic analysis methods and its seismic response was evaluated considering different seismic intensities. The development and design of the segmental bridge model as well as the response of the superstructure's numerical model under vertical seismic loads are presented in this report.

ABSTRACT

Precast segmental concrete bridge construction has witnessed increasing attention both in the United States and around the world due to the advantages it offers over the more traditional cast-in-place techniques. Despite the apparent advantages of the segmental bridge construction methods, concerns have arisen regarding the performance of such structural systems in regions of moderate to high seismicity.

This report studies the response of a precast segmental bridge model, designed according to the Accelerated Bridge Construction (ABC) techniques, when subjected to earthquake induced loads. A prototype bridge system is selected [Megally et al., 2002] and modified to comply with the ABC requirements for precast segmental bridges. The segmental bridge model is then scaled down to a 1/2.39-scale experimental model. The superstructure of the scaled bridge model consists of a single-span single-cell box girder, and its substructure consists of two square hollow piers. By means of modern structural experimental techniques, such as shake table dynamic testing, the large-scale precast segmental bridge specimen will provide valuable information on the behavior of such systems under seismic loading.

The large-scale bridge specimen is initially designed according to current American Bridge Design specifications: the AASHTO LRFD Bridge Design Specifications [2007] and the PCI Bridge Design Manual [2003]. A key concept is introduced in the design: the use of internal unbonded pre-stressing tendons as the only continuous reinforcement along the length of both the superstructure and substructure. Unbonded tendons can allow the triggering of a gap opening mechanism between adjacent segments of the deck and piers when the bridge is subjected to seismic loading.

In order to verify the behavior of the designed superstructure model under vertical seismic loads, a two-dimensional numerical model is developed incorporating material and geometric nonlinearities. The numerical model is analyzed under a series of vertical seismic excitations using non-linear dynamic analysis methods, and its seismic response is evaluated considering different seismic intensities. A complete numerical model of the large-scale bridge specimen will be presented in a future study, together with results on the specimen's response under uniaxial and multiaxial seismic excitations of various intensities.

The precast segmental bridge specimen described in this study was tested on the dual shake tables of the Structural Engineering and Earthquake Simulation Laboratory (SEESL) at the University at Buffalo, on April/May 2010 [Sideris et al., 2010]. The results of the experimental investigation of the precast segmental bridge specimen, as conducted at SEESL, will be discussed in a future study and will be used to calibrate the bridge's numerical model.

ACKNOWLEDGEMENTS

The authors would like to acknowledge the Federal Highway Administration of the U.S. Department of Transportation for providing funding for this research.

Special thanks are due to Mr. Petros Sideris, Ph.D. Candidate in the Department of Civil, Structural & Environmental Engineering at the University at Buffalo, State University of New York, for his valuable contribution to much of the content of this report. The report was reviewed by the FIGG Engineering Group, leading experts in bridge engineering and segmental bridge industry practices. Their comments and suggestions are greatly appreciated.

TABLE OF CONTENTS

Section	Title	Page
1	INTRODUCTION.....	1
1.1	Precast Segmental Bridges.....	4
1.2	Previous Research.....	6
1.3	Research Objectives.....	13
1.4	Report Layout	15
2	BRIDGE MODEL.....	17
2.1	Prototype Structure	17
2.2	Similitude Requirements.....	19
2.3	Scaling Procedure	22
2.4	Superstructure Model.....	29
2.5	Substructure Model.....	31
2.6	Construction Procedure of Bridge Model.....	31
3	SUPERSTRUCTURE DESIGN	35
3.1	Material and Cross-Section Properties.....	36
3.2	Design Loads	38
3.2.1	Dead Loads	38
3.2.2	Live Loads	39
3.2.3	Earthquake Loads.....	40
3.3	Design Load Combinations.....	43
3.4	Stress Limits for Pre-stressing Tendons and Concrete	45
3.5	Preliminary Design	46
3.5.1	Service III Limit State.....	47
3.5.2	Lifting of Superstructure.....	49
3.5.3	Extreme Event I Limit State, Vertical Earthquake	50
3.5.4	Tendon Geometry	50
3.6	Pre-stress Loss Estimation	50
3.6.1	Losses due to Friction	52
3.6.2	Losses due to Elastic Shortening	53
3.6.3	Losses due to Anchorage Set.....	55
3.6.4	Losses due to Concrete Shrinkage	56
3.6.5	Losses due to Concrete Creep.....	57
3.6.6	Tendon Stresses after Losses	58
3.7	Service III Limit State.....	60
3.8	Service I Limit State	62
3.9	Strength I Limit State.....	63
3.10	Extreme Event I Limit State	65
3.10.1	Vertical Earthquake Load	65
3.10.2	Horizontal Transverse Earthquake Load	66
3.11	Reinforcement Limits	66

TABLE OF CONTENTS (CONT'D)

Section	Title	Page
4	SUBSTRUCTURE DESIGN.....	69
4.1	Material Properties.....	70
4.2	Section Properties	71
4.3	Design Loads	71
4.3.1	Dead Loads	71
4.3.2	Live Loads	71
4.3.3	Earthquake Loads.....	72
4.4	Design Load Combinations.....	75
4.5	Preliminary Design	75
4.5.1	Extreme Event I Limit State	76
4.5.2	Tendon Geometry	77
4.5.3	Slenderness Effects	77
4.6	Prestress Loss Estimation	78
4.6.1	Losses due to Friction	78
4.6.2	Losses due to Elastic Shortening	78
4.6.3	Losses due to Anchorage Set	79
4.6.4	Losses due to Concrete Shrinkage	79
4.6.5	Losses due to Concrete Creep.....	79
4.6.6	Tendon Stresses after Losses	79
4.7	Service III Limit State.....	80
4.8	Service I Limit State	81
4.9	Strength I Limit State.....	81
4.10	Extreme Event I Limit State	82
4.10.1	Uniaxial Earthquake Load	82
4.10.2	Biaxial Earthquake Loads.....	82
4.11	Reinforcement Limits	83
4.11.1	Minimum Reinforcement.....	83
4.11.2	Limits for Reinforcement.....	83
4.12	Shear Design	84
4.12.1	Minimum Transverse Reinforcement	85
4.12.2	Nominal Shear Resistance	85
4.12.3	Effective Shear Depth, d_v	86
4.12.4	Shear Resistance	86
4.12.5	Required Area of Shear Reinforcement.....	88
5	SUPERSTRUCTURE NUMERICAL MODEL.....	91
5.1	Two-Segment Model Geometry	91
5.2	Modeling Approach	92
5.3	Two-Segment Model Response	96
5.3.1	Influence of Joint Length.....	99
5.3.2	Influence of Loading Duration.....	104

TABLE OF CONTENTS (CONT'D)

Section	Title	Page
5.3.3	Influence of Critical Damping	105
5.4	Eight-Segment Model Response.....	106
6	SEISMIC RESPONSE OF SUPERSTRUCTURE MODEL	117
6.1	Design Response Spectra	117
6.2	Ground Motion Set	120
6.3	Seismic Response.....	126
7	CONCLUSIONS	135
8	REFERENCES.....	139
	APPENDIX A	141

LIST OF FIGURES

Figure	Title	Page
1-1	Precast segmental ‘span-by-span’ construction [FHWA, 2004].....	2
1-2	Precast segmental ‘balanced cantilever’ construction [FHWA, 2004].....	2
1-3	Typical bridge superstructure cross-section with internal tendons [FHWA, 2004]	3
1-4	Typical precast piers with continuous strand tendons [FHWA, 2004].....	3
1-5	Joint opening of segmental box girder superstructure under vertical loading [Rombach, 2002].....	6
1-6	Phase I test unit elevation and cross-section [Megally et al., 2002].....	7
1-7	Phase I vertical loading sequence [Megally et al., 2002]	8
1-8	Phase II test unit elevation and cross-section [Megally et al., 2002].....	8
1-9	Phase II vertical loading sequence [Megally et al., 2002]	9
1-10	Phase III experimental test set-up [Burnell et al., 2005].....	10
1-11	Phase III test unit superstructure cross-section [Burnell et al., 2005]	10
1-12	Single joint model [Veletzos et al., 2006].....	11
1-13	Multiple joint model [Veletzos et al., 2006].....	11
1-14	Precast column test units [Hewes et al., 2002]	12
1-15	Precast column test set-up [Hewes et al., 2002]	13
2-1	Elevation of prototype structure [Megally et al., 2002].....	17
2-2	Cross-section of prototype superstructure [Megally et al., 2002].....	17
2-3	Elevation of prototype bridge test unit.....	19
2-4	Overall view of the Structural Engineering and Earthquake Simulation Laboratory (SEESL) at the University at Buffalo (see www.nees.buffalo.edu).....	22
2-5	Dual shake tables (with extension platforms) at the SEESL at the University at Buffalo (see www.nees.buffalo.edu)	23
2-6	Cross-section of superstructure test model	30
2-7	Box pier segment dimensions [AASHTO-PCI-ASBI, 2000]	32
2-8	Elevation of 1/2.39-scale bridge test model on the dual shake tables of SEESL (UB).....	33
2-9	Three-dimensional bridge test model on the dual shake tables of SEESL (UB).....	33
3-1	Bridge test unit and design superstructure model.....	35
3-2	Superstructure design cross-section.....	37
3-3	Design Truck according to AASHTO, 2007.....	38
3-4	Seismic response coefficient for the prototype bridge and scaled test model [AASHTO, 2007].....	41
3-5	Tendon configuration at mid-span, support and cantilever end sections.....	51
3-6	Elevation view of tendon geometry along the superstructure.....	52
3-7	Plan and elevation view of tendon geometry along the superstructure	60
4-1	Longitudinal elevation of bridge test model.....	69
4-2	Transverse elevation of bridge test model and pier cross-section	69
4-3	Pier cross-section and tendon configuration.....	76

LIST OF FIGURES (CONT'D)

Figure	Title	Page
5-1	Elevation view of the two-segment model.....	92
5-2	Bi-linear elastic rule for the unbonded tendons [Carr, 2007]	93
5-3	Compression spring geometry along the contact zone	94
5-4	Bi-linear with slackness hysteresis for modeling joint gap opening [Carr, 2007].....	94
5-5	Elevation view of the two-segment numerical model.....	96
5-6	First mode of vibration of the two-segment numerical model.....	97
5-7	Second mode of vibration of the two-segment numerical model	97
5-8	Third mode of vibration of the two-segment numerical model	97
5-9	Fourth mode of vibration of the two-segment numerical model	98
5-10	Fifth mode of vibration of the two-segment numerical model	98
5-11	Vertical cyclic sinusoidal displacement-controlled loading (T=12.0sec) applied at mid-span joint of the two-segment numerical model.....	100
5-12	History of total load versus displacement of the two-segment numerical model and effective joint length equal to $h/4$	100
5-13	History of total load versus displacement of the two-segment numerical model and effective joint length equal to $h/9$, $h/4$, $h/2$	101
5-14	Axial force versus axial elongation of the two-segment bottom compression spring (spring 11) at mid-span contact zone	102
5-15	Deflection profile of the two-segment numerical model due to pre-stress	103
5-16	Deflection profile of the two-segment numerical model due to maximum upward loading of mid-span contact joint	103
5-17	Deflection profile of the two-segment numerical model due to maximum downward loading of mid-span contact joint.....	104
5-18	Vertical cyclic sinusoidal displacement-controlled loads of 6, 12 and 24 seconds period applied at mid-span joint of the two-segment numerical model.....	104
5-19	History of total load versus displacement of the two-segment numerical load and loading periods equal to 6, 12 and 24 seconds.....	105
5-20	History of total load versus displacement of the two-segment numerical load and 3%, 5% and 10% critical damping.....	106
5-21	Elevation view of the eight-segment model.....	106
5-22	Elevation view of the eight-segment numerical model.....	106
5-23	First mode of vibration of the eight-segment numerical model.....	107
5-24	Second mode of vibration of the eight-segment numerical model	107
5-25	Third mode of vibration of the eight-segment numerical model	107
5-26	Fourth mode of vibration of the eight-segment numerical model	108
5-27	Fifth mode of vibration of the eight-segment numerical model	108
5-28	Sixth mode of vibration of the eight-segment numerical model.....	108
5-29	Vertical cyclic sinusoidal displacement-controlled loads (T=50.0sec) applied at contact joints of the eight-segment numerical model	110
5-30	History of total load versus displacement of mid-span Joint 4 for the eight- segment numerical model	111

LIST OF FIGURES (CONT'D)

Figure	Title	Page
5-31	History of total load versus displacement of Joint 3 for the eight-segment numerical model.....	111
5-32	History of total load versus displacement of Joint 2 for the eight-segment numerical model.....	112
5-33	History of total load versus displacement of Joint 1 for the eight-segment numerical model.....	113
5-34	Deflection profile of the eight-segment numerical model due to maximum downward loading.....	114
5-35	Deflection profile of the eight-segment numerical model due to maximum upward loading.....	114
5-36	Deflection profile of the eight-segment numerical model due to maximum downward loading of the mid-span joint	115
5-37	Deflection profile of the eight-segment numerical model due to maximum upward loading of the mid-span joint	115
6-1	Seismic response coefficient for the prototype bridge, elastic and design scaled test model [AASHTO, 2007]	118
6-2	Design and Maximum Considered Earthquake response spectra for a prototype bridge located at Western United States and City of Los Angeles [USGS, ASCE/SEI 7-05].....	119
6-3	Design and Maximum Considered Earthquake response spectra for the prototype bridge and scaled bridge model located at the City of Los Angeles [USGS, ASCE/SEI 7-05].....	120
6-4	Acceleration response spectra of the horizontal components of similitude-scaled ATC-63 ground motions and median acceleration response spectrum, 5% critical damping.....	122
6-5	Acceleration response spectra of the vertical component of the original ATC-63 ground motions and median acceleration response spectrum, 5% critical damping .	123
6-6	Acceleration response spectra of the vertical component of the similitude-scaled ATC-63 ground motions and median acceleration response spectrum, 5% critical damping.....	123
6-7	Acceleration response spectra of the vertical similitude-scaled ATC-63 ground motions for Design Earthquake (DE) intensity level, 5% critical damping	125
6-8	Acceleration response spectra of the vertical similitude-scaled ATC-63 ground motions for Maximum Considered Earthquake (MDE) intensity level, 5% critical damping.....	125
6-9	Cumulative probability distribution function of maximum upward vertical displacement of mid-span cross-section considering the DE and MCE intensity levels	127
6-10	Cumulative probability distribution function of maximum upward vertical displacement of mid-span cross-section considering the DE and MCE intensity levels and different loading directions.....	128

LIST OF FIGURES (CONT'D)

Figure	Title	Page
6-11	Cumulative probability distribution function of maximum downward vertical displacement of mid-span cross-section considering the DE and MCE intensity levels	129
6-12	Cumulative probability distribution function of maximum downward vertical displacement of mid-span cross-section considering the DE and MCE intensity levels and different loading directions.....	129
6-13	Cumulative probability distribution function of maximum top gap opening of mid-span cross-section considering the DE and MCE intensity levels	131
6-14	Cumulative probability distribution function of maximum top gap opening of mid-span cross-section considering the DE and MCE intensity levels and different loading directions.....	131
6-15	Cumulative probability distribution function of maximum bottom gap opening of mid-span cross-section considering the DE and MCE intensity levels	132

LIST OF TABLES

Table	Title	Page
2-1	Cross-section and material properties of prototype superstructure [Megally et al., 2002].....	18
2-2	List of physical quantities involved in Newton’s 2 nd law.....	20
2-3	Scale factors for earthquake response of structures [Harris and Sabnis, 1999].....	21
2-4	Theoretical performance of SEESL shake tables (see www.nees.buffalo.edu).....	23
2-5	‘Artificial mass’ simulation of a 1/4-scale bridge specimen.....	25
2-6	‘Gravity forces neglected and prototype material’ simulation of a 1/4-scale bridge specimen.....	27
2-7	‘Gravity forces neglected and prototype material’ simulation of a 1/2.5-scale bridge specimen.....	28
2-8	Geometrical and material parameters of 1/2.39-scale bridge specimen.....	29
2-9	Cross-section properties of superstructure test model.....	30
3-1	Design material properties [AASHTO, 2007].....	37
3-2	Design superstructure cross-section properties.....	38
3-3	Member forces due to dead loads.....	38
3-4	Member forces due to live loads.....	39
3-5	Uniform Load Method design parameters for vertical earthquake loads.....	43
3-6	Member forces due to vertical earthquake loads.....	43
3-7	Member forces due to considered load cases.....	44
3-8	Load combinations and load factors [AASHTO, 2007].....	44
3-9	Member forces due to considered load combinations.....	45
3-10	Stress limits for post-tensioned low relaxation strands [AASHTO, 2007].....	46
3-11	Member forces during lifting.....	49
3-12	Tendon eccentricities at superstructure’s critical sections.....	51
3-13	Losses due to friction along the tendons’ length.....	54
3-14	Losses due to elastic shortening.....	55
3-15	Effective length due to anchorage set.....	55
3-16	Losses due to anchorage set along the tendons’ length.....	56
3-17	Total pre-stressing losses and forces after losses along the superstructure’s length.....	59
3-18	Tendon effective forces and eccentricities.....	61
3-19	Concrete stresses for Service III Limit State.....	62
3-20	Concrete stresses for Service I Limit State.....	62
3-21	Flexural resistance of superstructure at mid-span for Strength I limit state.....	64
3-22	Flexural resistance of superstructure at supports for Strength I limit state.....	65
4-1	Design material properties [AASHTO, 2007].....	70
4-2	Pier cross-section properties.....	71
4-3	Member forces due to dead loads.....	72
4-4	Member forces due to live loads.....	72
4-5	Uniform Load Method design parameters for horizontal earthquake loads.....	74
4-6	Member forces due to horizontal earthquake loads.....	74

LIST OF TABLES (CONT'D)

Table	Title	Page
4-7	Member forces due to considered load cases.....	74
4-8	Member forces due to considered load combinations.....	75
4-9	Pier flexural resistance for Extreme Event I limit state	77
4-10	Losses due to friction along the tendons' length	78
4-11	Total pre-stressing losses and forces after losses along the pier's length.....	80
4-12	Tendon geometry and eccentricities	81
4-13	Concrete stresses for Service III limit state	81
4-14	Concrete stresses for Service I limit state	81
4-15	Pier flexural resistance for Extreme Event I limit state	82
4-16	Member forces at support due to biaxial earthquake loading.....	83
5-1	Compression spring location along the contact zone.....	93
5-2	Compression spring stiffness along the contact zone for a joint effective length equal to $h/4$	95
5-3	Periods of vibration of the two-segment numerical model.....	96
5-4	Compression spring stiffness for different values of joint length.....	99
5-5	Periods of vibration of the eight-segment numerical model.....	109
5-6	Fundamental periods of vibration of superstructure model	110
6-1	Seismic ground motion design parameters [USGS, ASCE/SEI 7-05].....	119
6-2	ATC-63 far-field ground motion records [ATC-63, 2008].....	121
6-3	Peak ground acceleration and duration of vertical ATC-63 ground motions	124
6-4	Maximum upward vertical displacement of mid-span cross-section.....	127
6-5	Maximum downward vertical displacement of mid-span cross-section.....	128
6-6	Maximum top gap opening of mid-span cross-section.....	130
6-7	Maximum bottom gap opening of mid-span cross-section.....	132

LIST OF SYMBOLS

A	= Acceleration coefficient
A_c	= Cross section area
A_{cs}	= Spring effective cross section area
A_{sp}	= Pre-stressing strand area
a	= Acceleration
b	= Cross section width
C_c	= Concrete creep coefficient
C_{sm}	= Elastic seismic coefficient
C_u	= Ultimate creep strain
c	= Neutral axis depth
D_p	= Pre-stressing strand diameter
d_p	= Distance from extreme compression fiber to the centroid of the pre-stressing tendons
E_c	= Concrete modulus of elasticity
E_p	= Pre-stressing strand modulus of elasticity
E_s	= Mild reinforcement modulus of elasticity
e_b	= Tendon eccentricity from the bottom cross section fiber
e_m	= Tendon eccentricity at mid-span
e_s	= Tendon eccentricity at pier centerline
e_t	= Tendon eccentricity from the top cross section fiber
F	= Force
F_y	= Yielding force
F_{pu}	= Pre-stressing stress ultimate force
F_{py}	= Pre-stressing stress yield force
f_b	= Concrete stress at bottom face of member
$f_{b,l}$	= Bottom tensile stress due to applied loads
f'_c	= Concrete compression strength
f_{ps}	= Average stress in unbonded tendon
f_{pu}	= Pre-stressing steel ultimate stress
f_{py}	= Pre-stressing steel yield stress
f_t	= Concrete stress at top face of member
$f_{t,l}$	= Top tensile stress due to applied loads
f_y	= Mild reinforcement yield stress
g	= Acceleration of gravity
h	= Cross section depth
I	= Moment of inertia
K	= Lateral stiffness

K_s = Contact spring stiffness
 K_w = Wobble friction coefficient for pre-stressed tendons
 k_c = Product of applicable correction factors for concrete creep
 k_{sh} = Product of applicable correction factors for concrete shrinkage
 L = Length
 l = Linear dimension
 l_e = Effective tendon length
 l_i = Tendon length between anchorages
 l_j = Joint contact length
 M_n = Cross-section nominal flexural resistance
 M_t = Total moment due to considered load combination
 m = Mass
 \bar{m} = Mass per unit length
 N_s = Number of support hinges crossed by the tendon between anchorages.
 P = Pressure
 P_e = Tendon effective pre-stress force
 P_i = Tendon initial pre-stress force
 P_j = Tendon jacking force
 p_e = Equivalent uniform static earthquake load
 p_o = Applied uniform load
 r = Bi-linear factor
 S = Site coefficient
 S_{DS} = Design, 5% damped, spectral response acceleration parameter at short periods
 S_{DI} = Design, 5% damped, spectral response acceleration parameter at a period of 1.0 second
 S_{MS} = Maximum considered earthquake, 5% damped, spectral response acceleration at short periods adjusted for site class effects
 S_{MI} = Maximum considered earthquake, 5% damped, spectral response acceleration at a period of 1.0 second adjusted for site class effects
 S_a = Spectral response acceleration
 S_b = Cross section modulus for extreme bottom fiber
 S_c = Concrete shrinkage coefficient
 S_i = Scaling factor
 S_t = Cross section modulus for extreme top fiber
 S_u = Ultimate shrinkage strain
 T_I = Fundamental period of vibration
 t = Time
 v = Velocity
 v_s = Static displacement
 W = Weight

- w = Anchor set for pre-stressed tendons
- w_c = Concrete unit weight
- z_b = Section centroid from bottom cross section surface
- z_t = Section centroid from top cross section surface
- ΔF_{pA} = Pre-stressing loss due to anchorage set
- ΔF_{pES} = Pre-stressing loss due to elastic shortening
- ΔF_{pF} = Pre-stressing loss due to friction
- ΔF_{pLT} = Pre-stressing losses due to shrinkage and creep of concrete, and relaxation of the steel
- ΔF_{pT} = Total loss of pre-stressing force
- β_1 = Concrete coefficient
- δ = Displacement
- ε = Strain
- θ = Angular change of pre-stressing steel path from jacking end to the point under investigation
- μ = Coefficient of friction for pre-stressed tendons
- ν = Poisson's ratio
- ζ = Percentage of critical damping
- ρ = Material mass density
- σ = Stress
- ω = Frequency

SECTION 1

INTRODUCTION

Recent years have witnessed growing interest in Accelerated Bridge Construction (ABC) both in the United States and Europe, as an answer to the need to reconstruct major highways while minimizing delay and community disruption. In addition to simply reducing on-site construction time, current ABC concepts imply traffic impacts minimization, work zone safety improvement, environmental disruption decrease, construction quality increase and reduced life-cycle costs.

A representative example of ABC is related to the adoption of precast segments forming the bridge's superstructure and substructure. In contrast to 'classical' monolithic bridge constructions, a segmental bridge consists of discrete precast elements stressed together by prestressed tendons. Precast segmental construction began in Europe in the 1950s; the first segmental concrete bridge, built in 1950, was cast-in-place across the Lahn River in Balduinstein, in Germany. Moreover, the first precast segmental concrete bridge, built in 1962, crossed the Seine River in France. In the United States, the first precast segmental concrete bridge was built in 1973 near Corpus Christi, Texas and the first cast-in-place segmental bridge was built in 1974 near San Diego, California.

The precast construction process involves the segmental manufacturing of bridge components in precast yards or plants which are then transported to the construction site in order to be assembled. Two common assembly procedures exist for precast segmental bridge superstructures - the 'span-by-span method' (see Figure 1-1) and the 'balanced cantilever method' (see Figure 1-2). In the span-by-span method, entire spans are constructed and then lifted into place or constructed in place on a temporary steel truss. In the balanced cantilever method, segments are installed one at a time on either side of the piers. Comparing with conventional cast-in-place construction, precast segmental construction has the advantage of accelerated construction while maintaining construction quality due to the better working environment of a precast factory.

Box girders are widely used in forming the superstructure cross-section of precast segmental bridges. The precast elements are connected by external or combination of external and internal post-tensioning acting as the continuity reinforcement between the adjacent segments. For the case of internal post-tensioning, the tendons are located within the box girder cell (see Figure 1-3) and are grouted; whereas external post-tensioning ducts are located outside the structural member, generally inside the box girder cell, and are grouted to protect the strands from corrosion.

Hollow section precast concrete segmental piers are widely used in precast segmental bridges. Vertical post-tensioning of the precast pier segments consists of either post-tensioned bars for short to moderate pier heights or strand tendons for tall piers. Bars or tendons are typically anchored in the footings and extend to the pier caps. Strand tendons are usually continuous and

extend from an anchor in the cap on one side of the pier, down the pier, loop through the footing and up the opposite side to another anchor in the cap (see Figure 1-5).

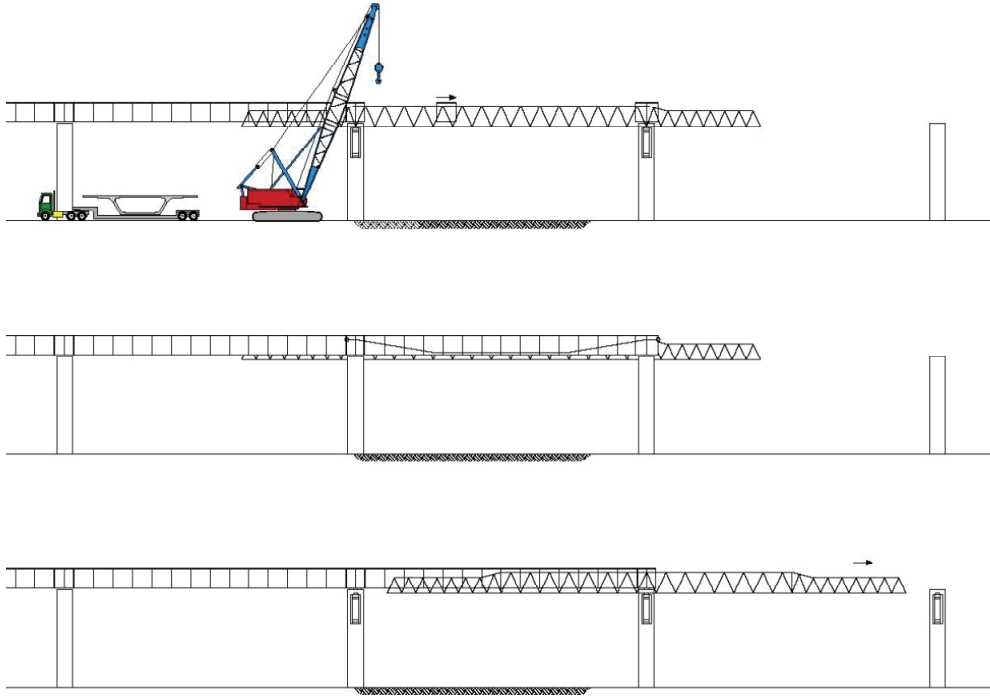


Figure 1-1: Precast segmental 'span-by-span' construction [FHWA, 2004]

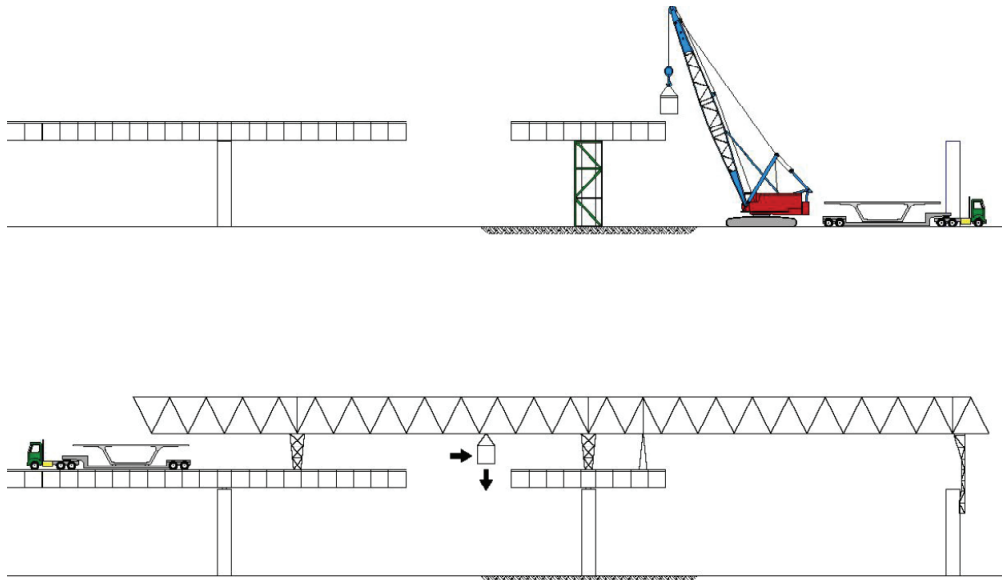


Figure 1-2: Precast segmental 'balanced cantilever' construction [FHWA, 2004]

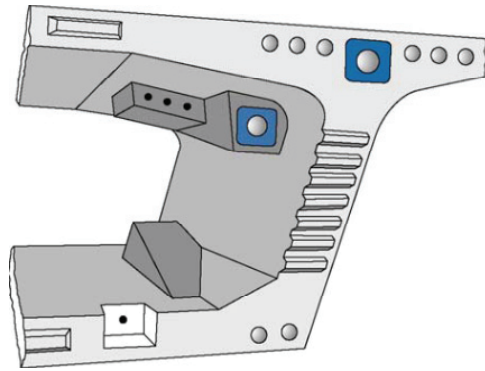


Figure 1-3: Typical bridge superstructure cross-section with internal tendons [FHWA, 2004]

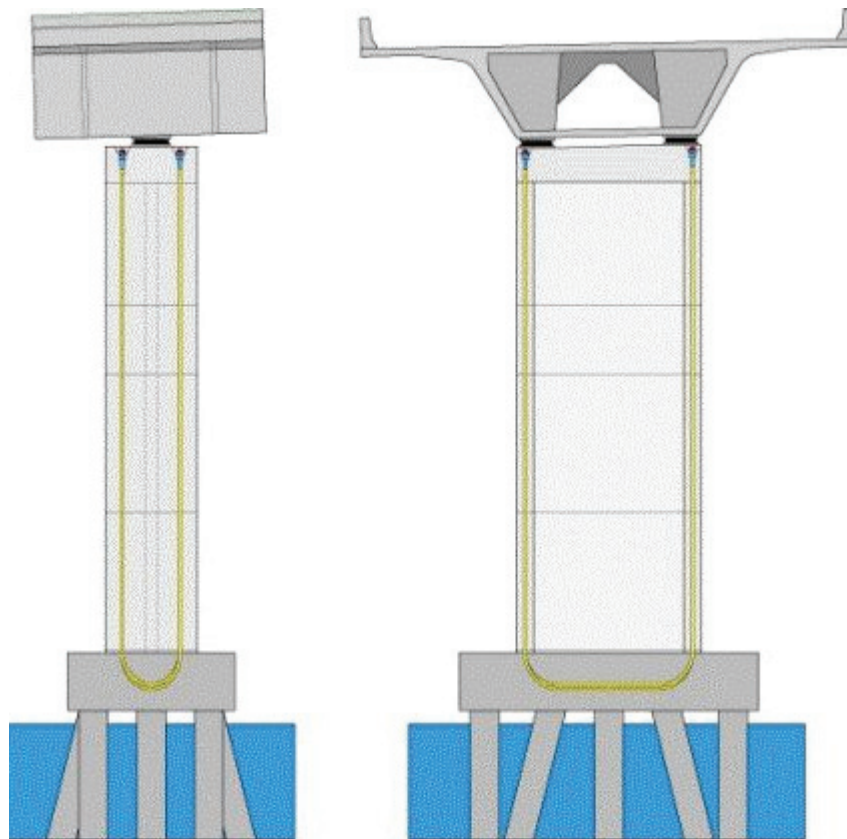


Figure 1-4: Typical precast piers with continuous strand tendons [FHWA, 2004]

The number of applications of precast segmental bridges designed according to the ABC techniques has increased during the last years however; most of them have been in regions of low seismicity. One of the factors that have attributed to that is the relatively unknown behavior of such systems under moderate or high levels of seismic excitation. In particular, a concern arises regarding the effect of the vertical component of ground motions on the generation of significant joint opening between adjacent superstructure segments. Moreover, the behavior of segmental

bridges under combined horizontal and vertical seismic excitation requires extensive investigation.

1.1 Precast Segmental Bridges

Precast segmental bridge construction was introduced in the 1960s and it is characteristic for this type of construction that segments are match cast, which means that each segment is cast against the previous one so that the end face of one segment will be an imprint of the neighbor segment, ensuring a perfect fit at the erection.

Comparing cast-in-place segmental construction with precast segmental construction the following features are to be noted:

- Cast-in-place segmental bridges may be erected on falsework by the free cantilever technique, by span-by-span lifting of spans cast at the bridge site, or by incremental launching. As a result, cast-in-place construction is a relatively slower construction method compared to precast segmental construction given that the work is performed *in situ* and therefore is exposed to weather conditions.
- Precast segmental construction is a fast construction method determined by the time required for the erection. The major part of the work is performed in the pre-casting yard, protected against inclement weather. The time-dependent deformations of the concrete become less important, as the concrete may have reached a higher age by the time the segments are placed in their final position.

Based on the aforementioned arguments, precast segmental construction can be considered as an Accelerated Bridge Construction (ABC) technique.

Precast segmental bridges can be erected using ‘span-by-span’ or ‘balanced cantilevering’ assembly procedures. In span-by-span construction method, construction starts at one end and proceeds continuously to the other end (see Figure 1-1). On the other hand, in balanced cantilevering construction method, construction commences from the piers and proceeds in a ‘balanced’ manner to mid-span (see Figure 1-2).

Span-by-span construction method is performed primarily at the deck level and typically implemented for long viaducts having numerous spans. The formwork is supported either on the bridge piers, on the edge of the previously erected span and the next pier or, at the ground level. The precast segments, which are constructed off site, are placed and adjusted on a steel erection girder spanning from pier to pier, then post-tensioned together in one operation.

Extending segmental construction to balanced cantilevering, the need for erection trusses is eliminated by achieving a self-supporting behavior of the bridge’s superstructure at all stages. The success of this method relies heavily on accurate geometry control during match casting, whereas the size and weight of precast segments are limited by the capacity of transportation and placing equipment.

In terms of typical precast segmental superstructure cross-sections, single-cell box girders provide the most efficient section for casting. The thickness of the top and bottom slabs as well as the thickness of the webs should be carefully selected in order to allow the placing of the conventional and pre-stressing reinforcement and comply with the design requirements of the bridge structure. The depth of the superstructure cross-section can vary along the span length resulting in lower gravitational forces.

The adjacent segments of precast segmental bridges are stressed together by internal or combination of internal and external post-tensioning tendons. Internal tendons are located inside the box girder cell and are grouted following post-tensioning (bonded tendons). On the other hand, external tendons run inside the box girder cell, along the bridge's length through deviators that provide the desired profile. Common bridge engineering practice requires that external tendons be grouted after post-tensioning to protect the strands from corrosion in the long term.

Precast concrete segmental piers can be thin-walled hollow segments, match-cast or mass-produced with a thin mortar between segments. Post-tensioned bars or strands are generally inserted in ducts cast in the segments and stressed. Later, the ducts are grouted.

According to AASHTO LRFD Bridge Design Specifications [2007], precast segmental bridges shall utilize shear keys between adjacent segments to prevent relative sliding between them. The segments are usually match-cast with epoxied joints.

The design of a segmental superstructure under the design dead and live loads requires that the superstructure behaves as a monolithic structure and maintains an allowable concrete compression or tension state for the serviceability limit state while it allows the joints between the segments to open under ultimate loads. In the mid-span joint, the greatest bending moment is expected whereas high negative bending moments and shear forces are developed in the joints adjacent to the supports. The opening of the joints under ultimate loads results in a significant cross-section stiffness reduction due to crushing of the concrete in the outer fibers of the joint. A typical joint opening due to applied positive and negative bending moments is illustrated in Figure 1-5. The behavior of precast segmental superstructures under dynamic loading is more complex but follows the general concept of allowing some portion of the structure to yield and dissipate energy.

In the case of precast post-tensioned bridge columns under lateral loads, the stresses under the precast segments result from a combination of the normal force induced by pre-stressing and the moments induced by the lateral load. Once the average stress reaches a zero value at a point under a segment, any increase in the lateral load leads to an opening between that segment and the one beneath it. Under seismic loads, pre-stressed columns exhibit a self-centering ability combined with negligible residual drifts and spalling of the concrete in the region near the compression toe of the column.

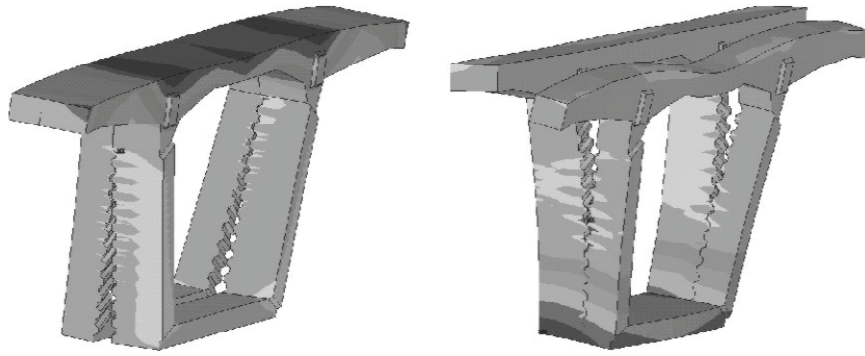


Figure 1-5: Joint opening of segmental box girder superstructure under vertical loading [Rombach, 2002]

Although it is possible to dissipate energy by allowing the cyclic opening and closure of the joints between adjacent segments, concerns have arisen related to the behavior of segmental bridge structures in regions of moderate to high seismicity. The main concerns during strong earthquake shaking are related to the effects of significant joint opening on the global stability of the structural system and, to the response of such systems under combined horizontal and vertical ground excitations.

Seismic design specifications for segmental structures are provided in AASHTO LRFD Bridge Design Specifications [2007] as well as the PCI Bridge Design Manual [2003]. AASHTO LRFD [2007] specifications allow precast-segmental construction without reinforcement across the joint, when the following requirements are met: for Seismic Zones 3 and 4 either cast-in-place or epoxied joints are required; at least 50% of the pre-stress force should be provided by internal tendons; and the internal tendons alone should be able to carry 130% of the dead load.

The following section will briefly review previous research and experimental studies related to the behavior of precast segmental post-tensioned bridge components and their results.

1.2 Previous Research

Several research programs examining issues involving the use of precast segmental bridge structures in seismic areas have been conducted at the University of California at San Diego (UCSD). One of the research projects focused on the seismic performance of precast segmental bridge superstructures and was completed in three phases. The first two phases of the program examined specific segment-to-segment connections in bridge superstructures, whereas the third one examined the seismic behavior of a precast, post-tensioned, segmental bridge superstructure with a cast-in-place hollow rectangular column. Another research project focusing on the seismic design and performance of precast concrete segmental bridge columns was also completed at UCSD.

The first two phases of the program conducted by Megally et al. [2002] investigated the performance of segment-to-segment joints in bridge superstructures under simulated seismic fully reversed cyclic loading for varying ratios of internal and external post-tensioning. The study focused on superstructure joints close to mid-span where high moments and low shears are

induced (Phase I), as well as on superstructure joints close to the supports where high negative moments and high shears are induced (Phase II). The test units for Phase I and II are shown in Figure 1-6 and Figure 1-8. Four 2/3-scale test specimens of a prototype precast segmental bridge were designed and constructed. The test units investigated different post-tensioning layouts. Two test specimens used 100% internal tendons; one of these units had cast-in-place closure joints with mild reinforcement crossing the joints between segments. The third specimen used 100% external tendons whereas the fourth one used 50% internal and 50% external tendons. The major objectives of the research were to investigate the seismic behavior with respect to the opening and closing of the joints under cyclic seismic loading (see Figure 1-7 and Figure 1-9), the crack development and propagation and the failure modes.

In the case of Phase I, all test units achieved large rotations prior to failure whereas the failure modes varied from rupture of the post-tensioning, to crushing of the extreme concrete fibers. Additionally to the experimental testing two numerical models, one two dimensional model and one three-dimensional finite element model, were developed for each test unit.

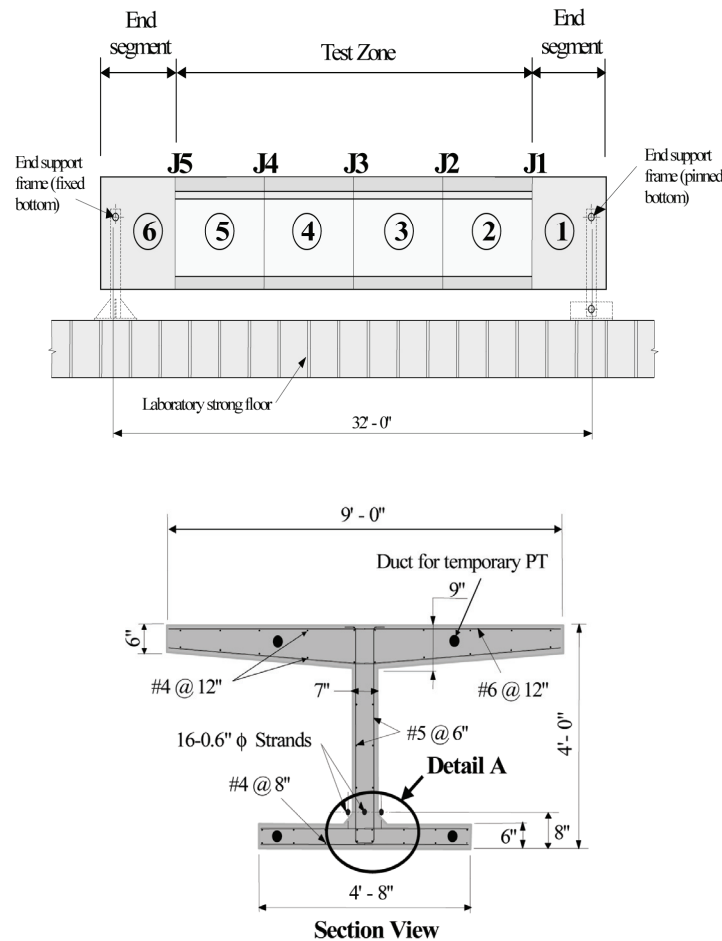


Figure 1-6: Phase I test unit elevation and cross-section [Megally et al., 2002]

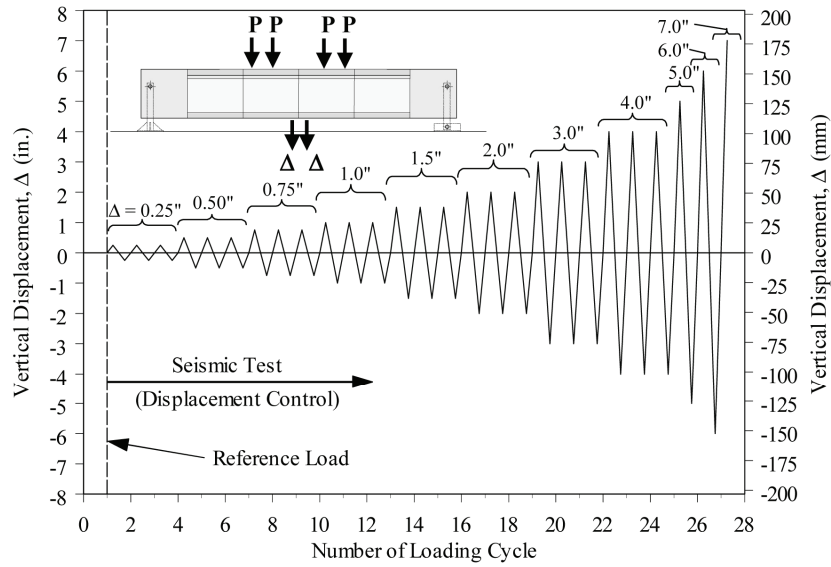


Figure 1-7: Phase I vertical loading sequence [Megally et al., 2002]

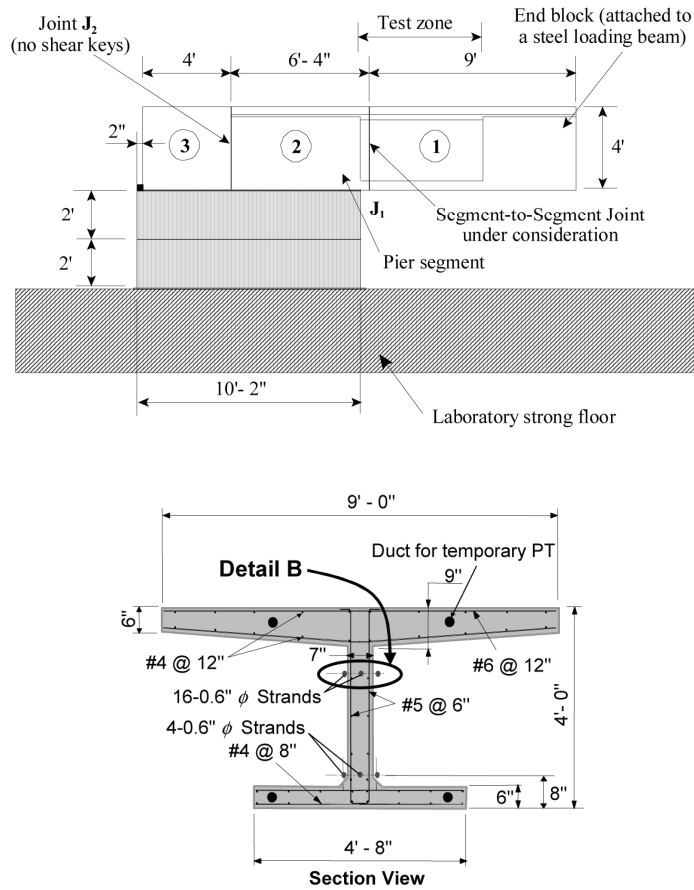


Figure 1-8: Phase II test unit elevation and cross-section [Megally et al., 2002]

The main conclusion of Phase I underlines that the superstructure segment-to-segment joints can undergo significant joint openings without failure. Test units with internally bonded tendons experience explosive failure whereas test units with 100% external tendons undergo ductile failure. Moreover, the combination of internal and external post-tensioning of precast segmental bridge superstructures is not recommended in high seismic zones.

The results of Phase II were similar to the ones of Phase I in that all test units achieved large rotations prior to failure, whereas no relative shear slip between segments was observed prior to flexural failure. In addition to the test units, detailed three-dimensional models were developed for each of the units.

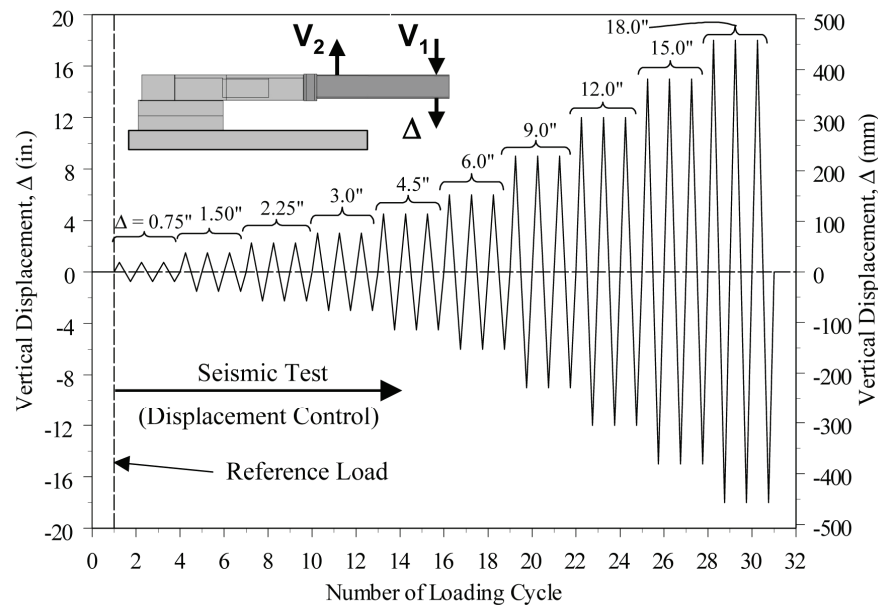


Figure 1-9: Phase II vertical loading sequence [Megally et al., 2002]

The third phase of the program conducted by Burnell et al. [2005] investigated the performance of a half-scale specimen of a prototype bridge from mid-span to mid-span and down to mid-height of the column. The test set-up and superstructure cross-section are shown in Figure 1-10 and Figure 1-11, respectively. The testing program was split into two stages. The first stage pre-stressing level was designed to achieve no joint openings while achieving a column displacement ductility of 4.0 and utilizing 100% of the superstructure dead load. The second stage involved removing some of the tendons to enable inelastic deformations of the joints in the superstructure and impose higher loads on the joints near the columns. The testing continued from the achieved displacement ductility of 4.0 up to ductility 8.0 and utilized 175% of the superstructure dead load to account for vertical accelerations and approximately 75% of the post-tensioning of the first stage. The results from this stage indicated that segment-to-segment joints open during testing but they closed when the earthquake loading was removed.

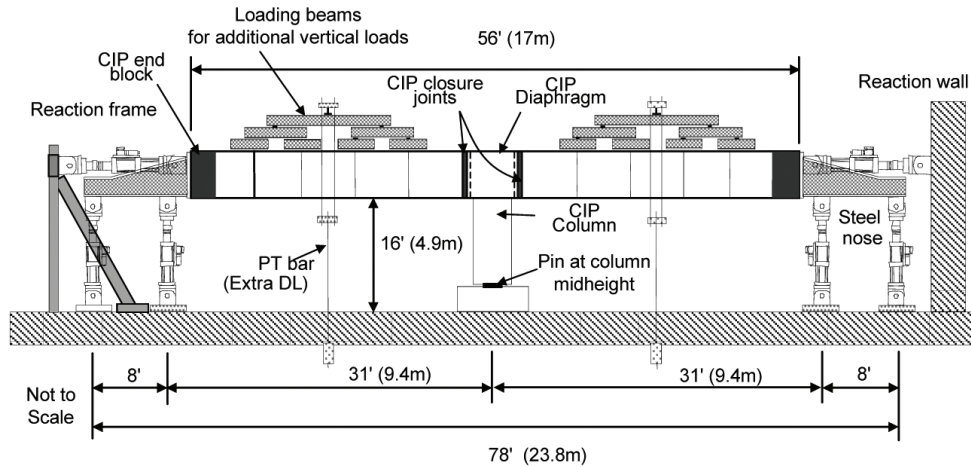


Figure 1-10: Phase III experimental test set-up [Burnell et al., 2005]

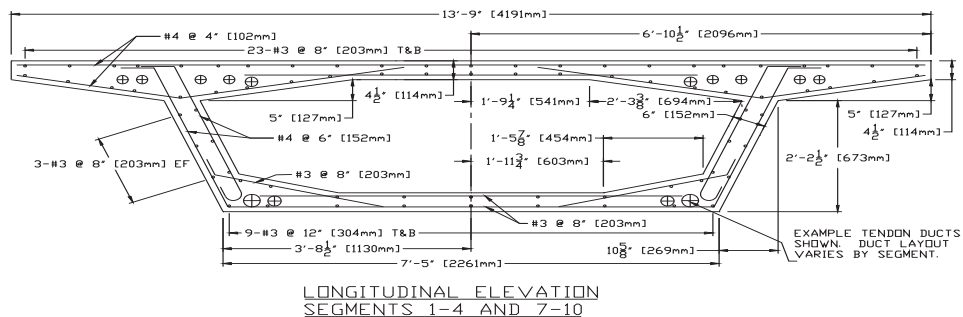


Figure 1-11: Phase III test unit superstructure cross-section [Burnell et al., 2005]

Further numerical research was conducted by Veletzos et al. [2006] that aimed at capturing the behavior of the superstructure segment-to-segment joints (Phases I and II) as well as of the superstructure-pier system (Phase III) and validating the experimental results. The single joint model (see Figure 1-12) was constructed in order to capture the moment rotation response of a single segment-to-segment joint; whereas the multiple joint model (see Figure 1-13) aimed at capturing the response at the system level, including deformations of the precast segments and joint opening.

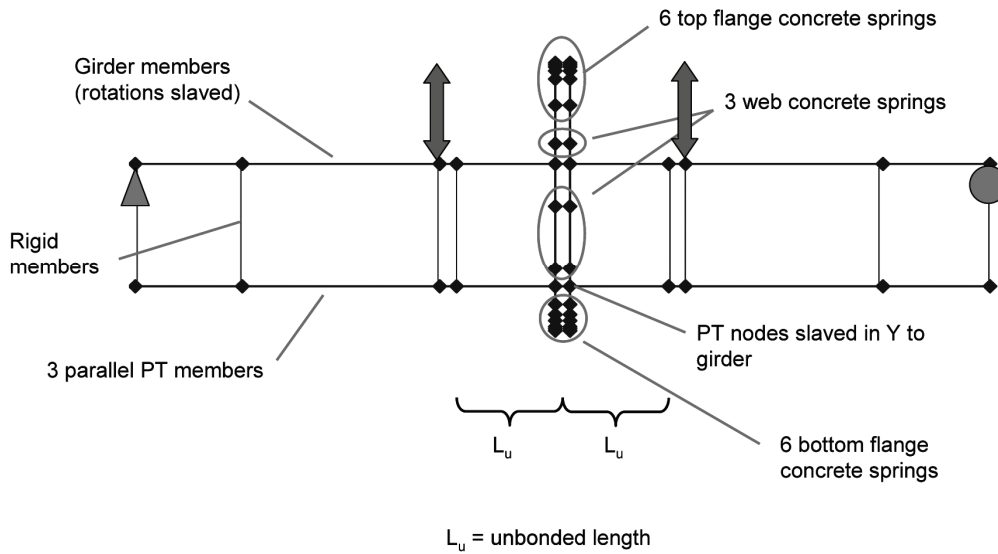


Figure 1-12: Single joint model [Veletzos et al., 2006]

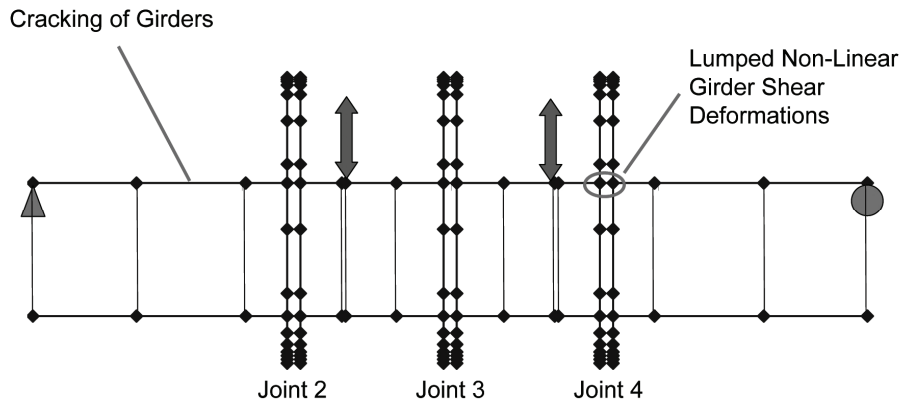
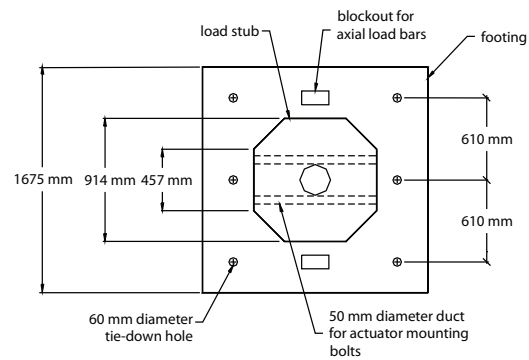
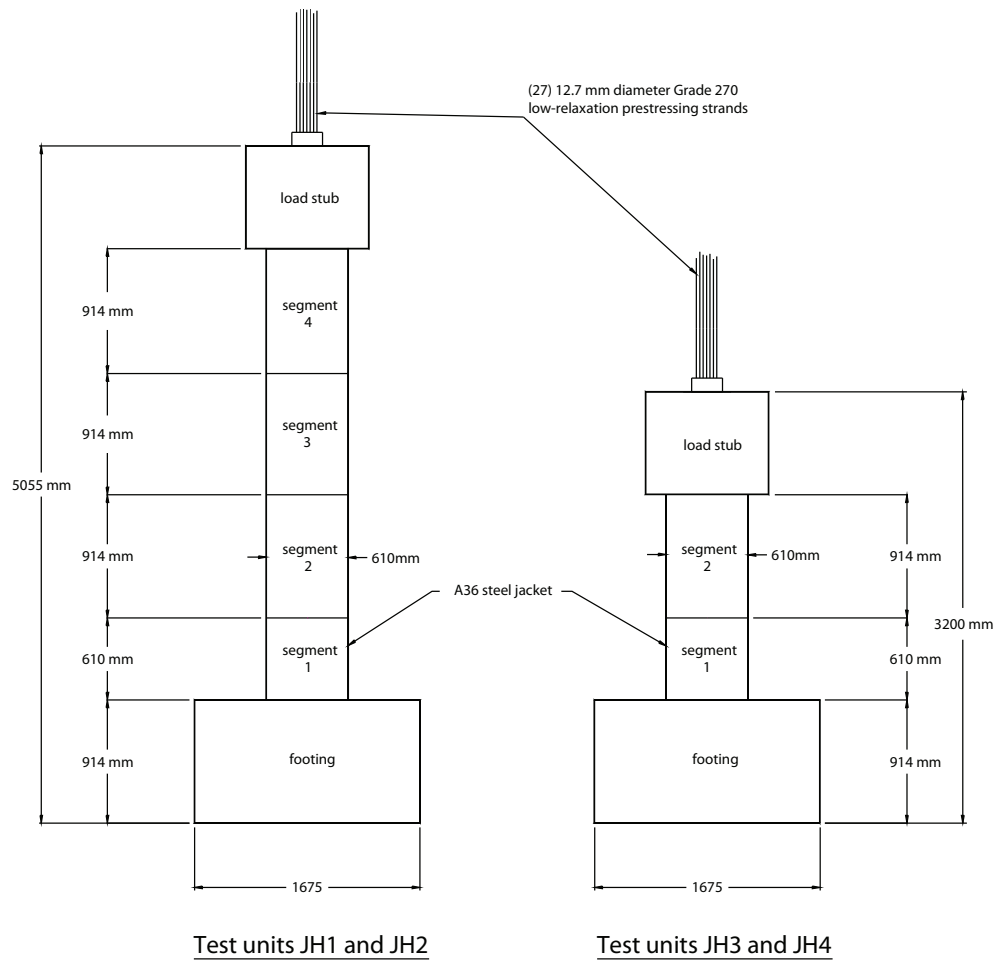


Figure 1-13: Multiple joint model [Veletzos et al., 2006]

In addition, two full scale bridge models were developed based on the Otay River Bridge and San Francisco-Oakland Bay Bridge in California of typical span lengths of 300 feet (91m) and 525 feet (160m), respectively. The models were subjected to a suite of near field earthquake records. The results indicated the significant contribution of vertical earthquake motions to the joint response, whereas the influence of vertical motion on the joint response increased as span length increased.

The research conducted by Hewes et al. [2002] involved the investigation of the performance of unbonded post-tensioned precast concrete segmental bridge columns under lateral earthquake loading. Column specimens with high and low aspect ratios were tested under simulated lateral seismic loading as shown in Figure 1-14 and Figure 1-15.



Top view of test units

Figure 1-14: Precast column test units [Hewes et al., 2002]

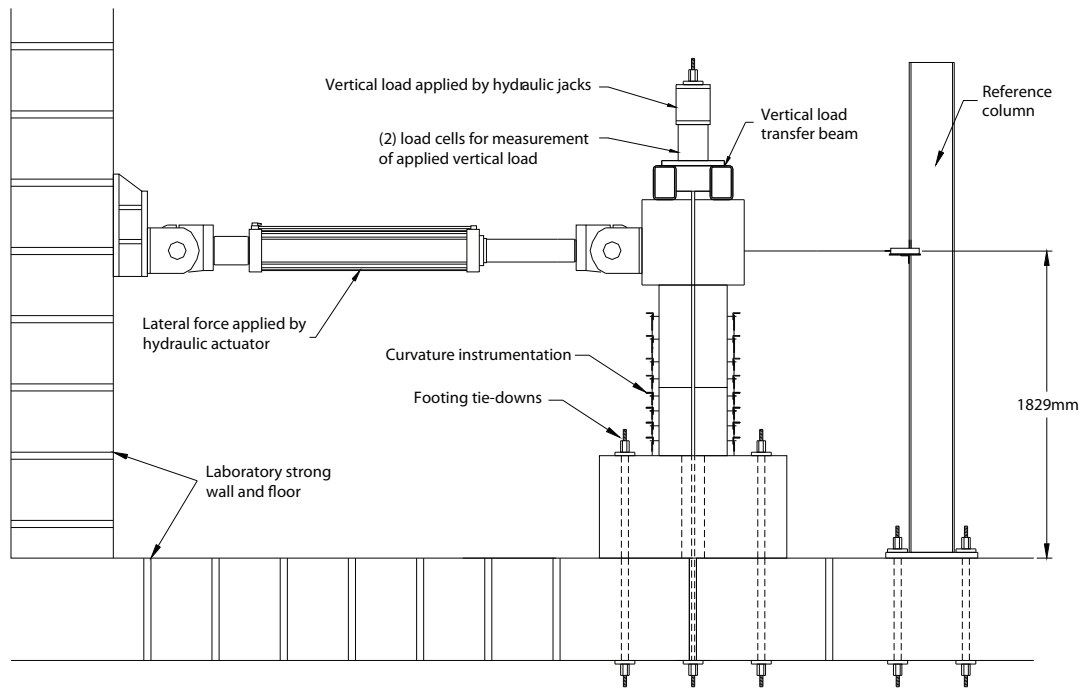


Figure 1-15: Precast column test set-up [Hewes et al., 2002]

The study of Hewes et al. [2002] concludes on the fact that concrete bridge columns built using segmental construction, and reinforced longitudinally with unbonded pre-stressing steel can safely and effectively resist lateral earthquake forces. The columns are capable of undergoing large nonlinear displacements without experiencing significant or sudden loss of strength. Residual displacements after the seismic event are minimal and the damage incurred low. Only minor repair work would be required after the earthquake, thus reducing costs and limiting the amount of disruption of normal use of the bridge structure. Preliminary recommendations for the seismic design of precast concrete segmental columns are also discussed.

In addition, several research studies have demonstrated the enhanced self-centering behavior of post-tensioned precast segmental piers with unbonded tendons [Ou et al. 2010, Yamashita et al. 2009 and Wang et al. 2008].

1.3 Research Objectives

The primary objective of this study is to investigate the response of precast segmental concrete bridge structures, designed according to the Accelerated Bridge Construction (ABC) techniques, when subjected to earthquake loading. A key concept incorporating post-tensioned internal unbonded tendons acting as the continuous reinforcement between adjacent segments of both the superstructure and substructure is introduced in the design. The use of post-tensioned internal unbonded tendons in precast segmental bridge superstructures has never been reported in the

literature, whereas several research studies have demonstrated the enhanced self-centering behavior of post-tensioned precast segmental piers with unbonded tendons.

The concept of internal unbonded tendons has been considered in several research studies focusing on the seismic performance and design of segmental bridge piers [Ou et al. 2010, Yamashita et al. 2009, Wang et al. 2008, Hewes 2007]. Bonded tendons tend to provide emulative response; that is, behavior similar to conventional cast-in-place piers. On the other hand, unbonded tendons allow the segmental structural element to display rocking behavior through opening and closing of the joints between adjacent segments [Christopoulos and Filiatrault, 2006]. As a result, rocking systems with unbonded tendons display a self-centering response under seismic loads while controlling the seismic forces applied to the system. Despite the advantages of using internal unbonded tendons in precast segmental bridges, there are issues that require careful investigation such as: the design of high stress zones adjacent to the joints and the protection of the tendons against environmental effects.

In this study, a large-scale test bridge specimen is designed as part of ongoing research on precast segmental bridges undertaken by the Department of Civil, Structural and Environmental Engineering (CSEE) at the University at Buffalo and the Multidisciplinary Center for Earthquake Engineering Research (MCEER). The objective of this experimental investigation is to study the behavior of such systems when subjected to earthquake induced loads. The prototype bridge system considered by Megally et al. [2002] is modified in order to comply with the ABC techniques as applied for precast segmental systems. Internal unbonded tendons are considered as the only continuous reinforcement along the length of both the superstructure and substructure. The unbonded tendons can allow the triggering of gap opening mechanism between adjacent segments and the system's self-centering response when subjected to seismic loads.

Initially, the segmental bridge model is scaled in order to meet the performance specifications of the dual shake tables of the Structural Engineering and Earthquake Simulation Laboratory (SEESL), at the University at Buffalo. The superstructure and substructure of the bridge test unit are then designed according to AASHTO LRFD Bridge Design Specifications [2007] and PCI Bridge Design Manual [2003].

Moreover, a two-dimensional numerical model of the segmental bridge superstructure is developed and analyzed under a series of vertical seismic excitations and intensities using non-linear time-history dynamic analysis methods. A complete numerical model of the large-scale bridge specimen will be presented in future studies together with results on its response when subjected to uniaxial and multiaxial earthquake induced loads of various intensities.

The large-scale bridge specimen was constructed and tested on the dual shake tables of SEESL during the months of April and May 2010. The description of the test set-up can be found at Sideris et al. [2010]. The results on the experimental investigation of the precast segmental bridge specimen, as conducted at SEESL, will be discussed in future reports along with, further design considerations and numerical investigations for precast segmental bridge systems subjected to earthquake loadings.

1.4 Report Layout

This report contains seven chapters, a list of references, and one appendix.

Chapter 1 provides an introduction to precast segmental bridge structures and the objectives of the current research study. Chapter 2 describes the prototype bridge system, the precast segmental bridge test unit as well as the scaling procedure of the prototype system to meet the performance specifications of SEESL's dual shake tables. Chapter 3 presents the design of the scaled superstructure model according to AASHTO LRFD Bridge Design Specifications [2007] and PCI Bridge Design Manual [2003]. Chapter 4 discusses the design of the scaled substructure model according to the same specifications. Chapter 5 describes the two-dimensional numerical model that was developed in order to investigate the behavior of the segmental superstructure model under vertical earthquake excitation. Chapter 6 evaluates the response of the developed numerical model under a series of historical vertical earthquake ground motions, as defined in ASCE/SEI 7-05 [2005], considering different intensities. Chapter 7 provides the conclusions of the current research study and discusses future research topics on precast segmental bridge systems.

Appendix A contains the shop drawings used for the fabrication of the test specimen. The drawings present the geometry of the bridge test unit - superstructure and substructure, the tendon configuration and the mild reinforcement details for a typical superstructure and pier segment.

SECTION 2

BRIDGE MODEL

2.1 Prototype Structure

The prototype bridge structure used for the design of the test specimen is the one considered in Megally et al. [2002]. It is a single-cell box girder bridge that consists of five spans with three interior spans of 100 feet (30.48 m) and exterior spans of 75 feet (22.86 m) for a total length of 450 feet (137.16 m), as shown in Figure 2-1. Each span of the prototype structure is post-tensioned with a harped shape tendon. Due to the short span length it is assumed that the prototype structure is constructed by the ‘span-by-span’ method.

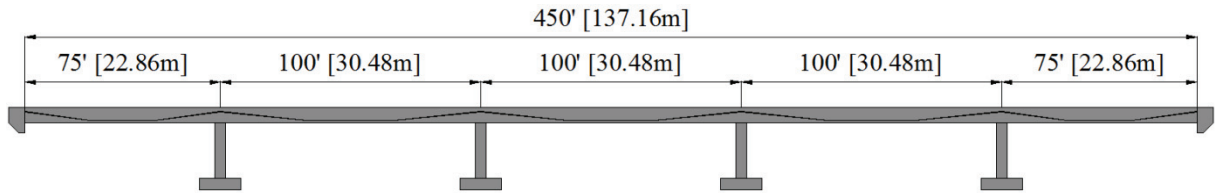


Figure 2-1: Elevation of prototype structure [Megally et al., 2002]

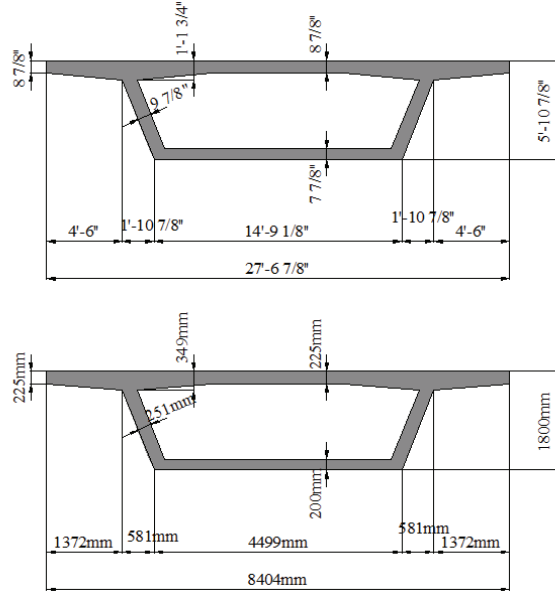


Figure 2-2: Cross-section of prototype superstructure [Megally et al., 2002]

The typical cross-section of the prototype bridge complies with the AASHTO-PCI-ASBI Segmental Box Girder Standards for Span-by-Span and Balanced Cantilever Construction [2000], as shown in Figure 2-2. The height of the piers is approximately 25.0 feet (7.62 m) measured from the centroid of the superstructure’s cross-section to the top surface of the foundation. No information on the geometry of the piers cross-section is provided by Megally et al. [2002].

The section and material properties used for this study match the ones considered by Megally et al. [2002] and are summarized in Table 2-1.

Table 2-1: Cross-section and material properties of prototype superstructure [Megally et al., 2002]

Properties	Symbol	Value	
Cross-section area	A_c	6034 in ²	3.89 m ²
Moment of inertia	I	4.29E6 in ⁴	1.79 m ⁴
Section centroid from bottom surface	z_b	45.2 in	1.15 m
Section centroid from top surface	z_t	25.7 in	0.65 m
Tendon eccentricity at mid-span	e_m	33.2 in	0.84 m
Tendon eccentricity at pier centerline	e_s	6.7 in	0.17 m
Concrete strength	f'_c	5.0 ksi	34.5 MPa
Concrete modulus of elasticity	E_c	4287 ksi	29.6 GPa
Pre-stressing steel ultimate strength	f_{pu}	270 ksi	1860 MPa
Pre-stressing steel modulus of elasticity	E_p	28500 ksi	196.5 GPa

The interest in the performance of segment-to-segment joints in bridge superstructures under vertical seismic loading is focused on joints close to mid-span where high moments and low shears are induced and on joints close to the supports where high negative moments and high shears are induced. Moreover, the interest in the performance of segment-to-segment joints in bridge substructures under horizontal seismic loading is focused on joints close to the supports where high moments and shears develop.

Given the geometric symmetry of the prototype structure only one span of the prototype bridge will be considered for the development of this experimental set-up. In order to match the tendon geometry of the prototype bridge, a cantilever on each side of the supports is considered. The length of each cantilever is set equal to 25% of the interior span length. The total length of the superstructure model – one span and two overhangs – is 150 feet (45.7 m), as shown in Figure 2-3.

In order to comply with the Accelerated Bridge Construction (ABC) techniques for precast segmental bridges, both the superstructure and substructure of the modeled bridge system are divided into segments. The uniform behavior of the system is achieved through the post-tensioning of the segments whereas; the segments are in direct contact to their adjacent ones. The

superstructure model is designed to consist of six interior segments 20 feet (0.51 m) long and two exterior ones 15 feet (0.38 m) long (see Figure 2-3). A segment-to-segment joint is provided at the mid-span section where maximum relative displacement of the segments is expected. Moreover, one segment is placed at the centerline of each support to provide the necessary support conditions between the superstructure and the columns. Each of the piers consists of five 5.0 feet long (1.52 m) segments, as shown in Figure 2-3.

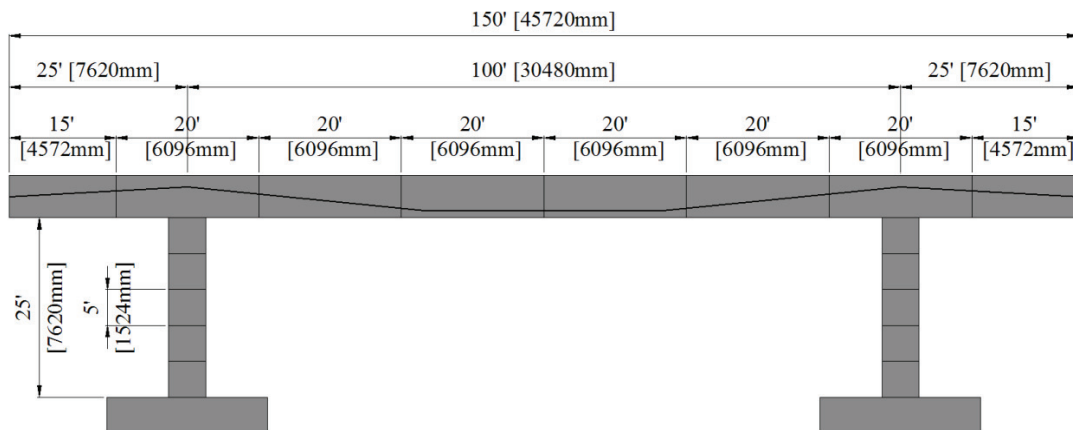


Figure 2-3: Elevation of prototype bridge test unit

2.2 Similitude Requirements

A structural model is defined as any structural element or assembly of structural elements built to a reduced scale in comparison with full size structures, which is to be tested and for which laws of similitude must be employed to interpret test results. This definition encompasses a broad class of modeling studies on prototype (full-size) structures such as buildings and bridges taking into account various loading cases such as static and seismic effects. The majority of reduced-size structural elements or structures play an important experimental role in problems dealing with education, research and design.

A representative structural model is a Strength Model or Replica Model, which is a geometrically similar model to the prototype made of materials that are similar to the prototype materials such that the model will predict the prototype behavior up to failure.

Any structural model must be designed, loaded and interpreted according to a set of similitude requirements that relate the model to the prototype structure. The similitude requirements are based upon the theory of modeling which can be derived from a dimensional analysis of the physical phenomena involved in the behavior of the structure. The fundamental measures related to the mechanical – static and dynamic – physical problems are: the length, the force or mass and the time. Through dimensional analysis all the variables involved in a mechanical problem can be grouped and expressed as functions of the fundamental measures resulting to a subsequent reduction of the unknown quantities of the problem.

The main physical parameters (variables) involved in the similitude procedure of a structure when subjected to seismic loading are related by the Newton's second law of motion:

$$F = \frac{d(mv)}{dt} \quad (2-1)$$

The physical quantities involved in the above expressions and the corresponding units are presented in Table 2-2.

Table 2-2: List of physical quantities involved in Newton's 2nd law

Quantity	Units
Seismic force, F	F
Mass, m	FL ⁻¹ T ²
Acceleration, α	LT ⁻²

The fundamental equation of Newton's second law can be expressed in dimensionless products taking into account the physical quantities involved:

$$F = ma \Leftrightarrow F = m \frac{l}{t^2} \Leftrightarrow Ft^2 = ml \rightarrow \frac{Ft^2}{ml} = \frac{FT^2}{FL^{-1}T^2L} \quad (2-2)$$

If this single product were to be made the same for the model and the prototype structure, complete dynamic similarity would be obtained, where m stands for the model and p for the prototype structure:

$$\frac{F_m t_m^2}{m_m l_m} = \frac{F_p t_p^2}{m_p l_p} \quad (2-3)$$

For each physical parameter involved in the scaling procedure of the prototype structure, a scaling factor can be defined as the ratio of the prototype physical parameter to the same model physical parameter:

$$S_X = \frac{X_p}{X_m} \quad (2-4)$$

The model-prototype relation then becomes:

$$S_F S_T^2 = S_m S_l \quad (2-5)$$

or

$$(S_\sigma S_A) S_T^2 = (S_\rho S_V) S_l \Leftrightarrow (S_E S_\varepsilon) S_l^2 S_T^2 = S_\rho S_l^3 S_l \Leftrightarrow S_\rho = \frac{S_E}{S_A S_l} \quad (2-6)$$

In order to apply the above equation directly to any dynamic problem four main physical parameters need to be specified: the acceleration (α), any linear dimension (l), the modulus of elasticity (E) and the mass density of the material (ρ). Any other parameters such as mass, time,

displacements, frequency that can be of interest are linearly related to the four main ones through the laws of physics and mechanics.

However, trying to satisfy all similitude requirements can be sometimes impossible because of the practical restrictions imposed on the model material properties, geometry and testing equipment. A summary of the scale factors obtained from three different similitude considerations for earthquake loading is given in Table 2-3 [Harris and Sabnis, 1999]. Even though a ‘True Replica model’ (Case I) is the most accurate model in terms of capturing the effect of inertial, gravitational and restoring forces of the structural model, it is practically impossible to build. Alternative scaling laws such as the ‘Artificial Mass Simulation’ (Case II) and ‘Gravity Forces Neglected – Prototype Material’ (Case III) have been shown to simulate the behavior of the structure adequately.

Table 2-3: Scale factors for earthquake response of structures [Harris and Sabnis, 1999]

Physical Quantities			Dimension	Scale Factors		
				Case I ¹	Case II ²	Case III ³
Earthquake loading	Force,	F	F	$S_E S_l^2$	$S_E S_l^2$	S_l^2
	Pressure,	q	FL^{-2}	S_E	S_E	1
	Acceleration,	α	LT^{-2}	1	1	S_l^{-1}
	Gravitational acceleration,	g	LT^{-2}	1	1	Neglected
	Velocity,	v	LT^{-1}	$S_l^{1/2}$	$S_l^{1/2}$	1
	Time,	t	T	$S_l^{1/2}$	$S_l^{1/2}$	S_l
Geometry	Linear dimension,	l	L	S_l	S_l	S_l
	Displacement,	δ	L	S_l	S_l	S_l
	Frequency,	ω	T^{-1}	$S_l^{-1/2}$	$S_l^{-1/2}$	S_l^{-1}
Material properties	Modulus of elasticity,	E	FL^{-2}	S_E	S_E	1
	Stress,	σ	FL^{-2}	S_E	S_E	1
	Strain,	ε	-	1	1	1
	Poisson’s ratio,	ν	-	1	1	1
	Mass density,	ρ	$FL^{-4}T^2$	S_E/S_l	$(g\rho l/E)_m=(g\rho l/E)_p$	1
	Energy,	EN	FL	$S_E S_l^3$	$S_E S_l^3$	S_l^3
¹ ‘True Replica Model’ scaling law						
² ‘Artificial Mass Simulation’ scaling law						
³ ‘Gravity Forces Neglected, Prototype Material’ scaling law						

The simulated laws as defined for Case II consider additional material of a non-structural nature (lumped or distributed additional mass) in order to simulate the required scaled density of the model. On the other hand, the simulation law as expressed in Case III applies to the case where gravity stresses can be neglected in the structural behavior and where the same materials are used in both model and prototype to enable the testing to reach failure.

2.3 Scaling Procedure

Based on the geometry of the bridge model, as described in Section 2.1, similitude laws must be satisfied so that the model meets the performance specifications of the dual shaking tables of SEESL, at the University at Buffalo. The two high-performance six-degree of freedom shake tables can be repositioned from directly adjacent to one other to positions up to 100 feet (30.5 m) apart (centre-to-centre), as shown in Figure 2-4 and Figure 2-5. Moreover, together the shake tables can host specimens of up to 100 metric tons (220 kips) and as long as 120 feet (36 m). The specimens can be subjected to fully in-phase or totally uncorrelated dynamic excitations. The two shake tables are designed for the theoretical performance listed in Table 2-4. The use of modern testing techniques - such as pseudo-dynamic and real-time dynamic hybrid testing - are possible, along with conventional dynamic, quasi-static and static force techniques.

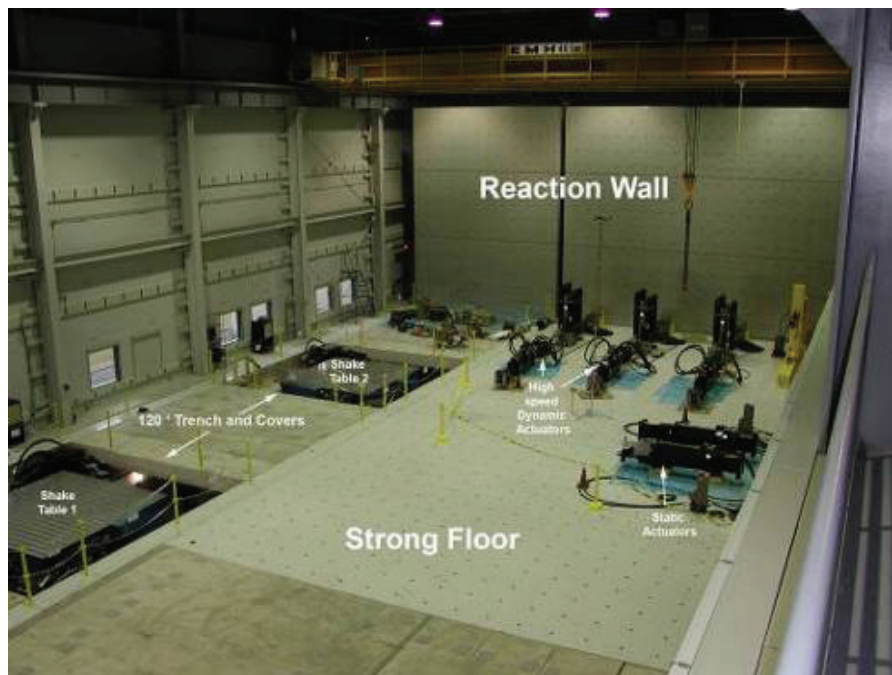


Figure 2-4: Overall view of the Structural Engineering and Earthquake Simulation Laboratory (SEESL) at the University at Buffalo (see www.nees.buffalo.edu)



Figure 2-5: Dual shake tables (with extension platforms) at the SEESL at the University at Buffalo (see www.nees.buffalo.edu)

Table 2-4: Theoretical performance of SEESL shake tables (see www.nees.buffalo.edu)

Table platform size without table extension:	11.8 ft × 11.8 ft (3.6 m × 3.6 m)
Table platform size with extension platform in place:	23.0 ft × 23.0 ft (7.0 m × 7.0 m)
Maximum specimen mass:	110.2 kips (50 ton) max; 44.1 kips (20 ton) nominal
Maximum specimen mass with table extension platform in place:	88.2 kips (40 ton) max
Maximum overturning moment:	332 kips-ft (46 ton-m)
Maximum off centre loading moment:	108 kips-ft (15 ton-m)
Frequency of operation:	0.1~50 Hz nominal; 100 Hz max
Stroke (X axis, Y axis, Z axis):	±6.0 in; ±6.0 in, ±3.0 in (±1.50 m, ±1.50 m, ±0.75 m)
Velocity (X axis, Y axis, Z axis):	50 in/sec, 50 in/sec, 20 in/sec (1250 mm/sec, 1250 mm/sec, 500 mm/sec)
Acceleration (X axis, Y axis, Z axis):	±1.15 g ±1.15 g ±1.15 g

For comparison purposes two different simulation laws will be considered: the ‘Artificial Mass’ simulation and the ‘Gravity Forces Neglected, Prototype Material’ simulation.

In the case of ‘Artificial Mass’ simulation the following iterative procedure is followed and summarized in Table 2-5:

- assume a linear dimension scaling factor, S_l . In addition, consider unit scaling factors for the acceleration and material modulus of elasticity, S_a and S_E , respectively. The later assumption implies application of un-scaled inertia forces on the model structure as well as use of the same material for both model and prototype structures;
- compute the scale factors, S_i , for all involved physical quantities using the relationships given in Table 2-5;
- assuming that the material mass density of the model and prototype structures is the same - S_p is set equal one, re-compute the mass and frequency scaling factors and account for the additional mass required of a non-structural nature material (lumped or distributed);
- compare the total mass of the bridge model to the maximum allowable specimen mass on the shake tables (see Table 2-4);
- check if the acceleration and frequency values of the model structure meet the performance specifications of the shaking tables and repeat the procedure until all requirements are satisfied.

Based on the results presented in Table 2-5 for a 1/4-scale model, the total superstructure mass equals 58.93 kips (26.8 ton). Taking into account the additional mass of the bent caps, piers and footings of the bridge test specimen, the total weight of the bridge model would not exceed the maximum allowable specimen mass according to the performance specifications of the dual shake tables (see Table 2-4). However, a high amount of additional non-structural mass (44.2 kips or 20.1 ton) is required in order to satisfy the similitude requirements. The additional non-structural mass can be concentrated or distributed along the specimen length. In both cases, difficulties should be expected in lumping the structural and non-structural mass together and achieving a uniform behavior of the model under any dynamic excitation.

Table 2-5: ‘Artificial mass’ simulation of a 1/4-scale bridge specimen

Physical Quantities		Prototype Structure	Scale Factors, S_i			Model Structure
Length of superstructure,	l	150 ft (45720 mm)	S_l	4		37.5 ft (11430 mm)
Acceleration,	α	-	S_α	1		-
Modulus of elasticity,	E	4287 ksi (29.6 GPa)	S_E	1		4287 ksi (29.6 GPa)
Mass density,	ρ	0.15 kips/ft ³ (23.56 kN/m ³)	$S_E/S_\alpha S_l$	0.25	1	0.15 kips/ft ³ (23.56 kN/m ³)
Seismic force,	F	-	$S_E S_l^2$	16		-
Mass of superstructure,	m	943 kips (430 ton)	$S_\rho S_l^3$	16	64	14.73 kips (6.7 ton)
Gravitational acceleration,	g	32.17 ft/sec ² (9.81 m/sec ²)	1	1		32.17 ft/sec ² (9.81 m/sec ²)
Velocity,	v	-	$(S_l S_\alpha)^{1/2}$	2		-
Time,	t	-	$(S_l/S_\alpha)^{1/2}$	2		-
Cross-section area of superstructure,	A_c	6034 in ² (3.89 m ²)	S_l^2	16		377 in ² (0.24 m ²)
Moment of inertia of superstructure,	I	4289863 in ⁴ (1.79 m ⁴)	S_l^4	256		16757 in ⁴ (0.007 m ⁴)
Volume of superstructure,	V	6286 ft ³ (178 m ³)	S_l^3	64		98 ft ³ (2.8 m ³)
Displacement,	δ	-	S_l	4		-
Frequency,	ω	-	$S_l^{-1}(S_E/S_\rho)^{1/2}$	0.50	0.25	-
Stress,	σ	-	S_E	1		-
Strain,	ϵ	-	1	1		-
Poisson’s ratio,	ν	-	1	1		-

Note: Structural mass equals 14.73 kips (6.7 ton) whereas additional non-structural mass 44.2 kips (20.1 ton) for a total mass of 58.93 kips (26.8 ton).

In the case of ‘Gravity Forces Neglected and Prototype Material’ simulation, the following iterative procedure is followed and summarized in Table 2-6:

- assume a linear dimension scaling factor, S_l . In addition, consider unit scaling factors for the modulus of elasticity and the material mass density, S_E and S_ρ , respectively. It should be noted that by assuming unit scaling factor for the mass density (mass over volume) and given that the volume of the model structure is decreased compared to the prototype one, the mass of the model is lower as well. Consequently, the gravity forces of the structure are considered to be neglected given that the gravitational acceleration is the same in both cases. This assumption is reasonable considering the low gravity forces typically applied to bridge piers;
- compute the scale factors, S_i , for all involved physical quantities using the relationships given in Table 2-5;
- compare the total mass of the bridge model to the maximum allowable specimen mass on the shake tables (see Table 2-4);
- check if the acceleration and frequency values of the model structure meet the performance specifications of the shaking tables and repeat the procedure until all requirements are satisfied.

According to the second similitude procedure shown in Table 2-6, the superstructure of a 1/4-scale model weights 14.73 kips (6.7 ton), which is a very low value compared to the maximum allowable specimen mass according to the performance specifications of the dual shake tables (see Table 2-4). As mentioned above, in that case the gravity forces of the structure are neglected given that the volume of the model structure is lower than that of the prototype one; whereas the material mass density is the same in both cases. This assumption is reasonable considering the negligible effect of gravitational forces on the bridge superstructure and substructure. Consequently, a lower scaling factor can be chosen resulting in a larger model specimen; however, attention should be paid to the scaling requirements of the acceleration, time and frequency.

The ‘Gravity Forces Neglected and Prototype Material’ similitude procedure (Case III) is chosen as the basis for the design procedure of the bridge model, as it leads to a larger scaled model with no additional non-structural weights. Following the same iteration procedure as described above, a linear dimension scaling factor that equals to 2.50 is introduced, as shown in Table 2-7. The 1/2.5-scale bridge test specimen is expected to meet the performance specifications of the SEESL dual shake tables.

Table 2-6: ‘Gravity forces neglected and prototype material’ simulation of a 1/4-scale bridge specimen

Physical Quantities		Prototype Structure	Scale Factors, S_i		Model Structure
Length of superstructure,	l	150 ft (45720 mm)	S_l	4	37.5 ft (11430 mm)
Modulus of elasticity,	E	4287 ksi (29.6 GPa)	S_E	1	4287 ksi (29.6 GPa)
Mass density,	ρ	0.15 kips/ft ³ (23.56 kN/m ³)	$S_E/S_\alpha S_l$	1	0.15 kips/ft ³ (23.56 kN/m ³)
Acceleration,	α	-	S_α	0.25	-
Seismic force,	F	-	$S_E S_l^2$	16	-
Mass of superstructure,	m	943 kips (430 ton)	$S_\rho S_l^3$	64	14.73 kips (6.7 ton)
Gravitational acceleration,	g	32.17 ft/sec ² (9.81 m/sec ²)	1	1	32.17 ft/sec ² (9.81 m/sec ²)
Velocity,	v	-	$(S_l S_\alpha)^{1/2}$	1	-
Time,	t	-	$(S_l/S_\alpha)^{1/2}$	4	-
Cross-section area of superstructure,	A_c	6034 in ² (3.89 m ²)	S_l^2	16	377 in ² (0.24 m ²)
Moment of inertia of superstructure,	I	4289863 in ⁴ (1.79 m ⁴)	S_l^4	256	16757 in ⁴ (0.007 m ⁴)
Volume of superstructure,	V	6286 ft ³ (178 m ³)	S_l^3	64	98 ft ³ (2.8 m ³)
Displacement,	δ	-	S_l	4	-
Frequency,	ω	-	$S_l^{-1} (S_E/S_\rho)^{1/2}$	0.25	-
Stress,	σ	-	S_E	1	-
Strain,	ε	-	1	1	-
Poisson’s ratio,	ν	-	1	1	-

Table 2-7: ‘Gravity forces neglected and prototype material’ simulation of a 1/2.5-scale bridge specimen

Physical Quantities		Prototype Structure	Scale Factors, S_i		Model Structure
Length of superstructure,	l	150 ft (45720 mm)	S_l	2.5	60 ft (18288 mm)
Modulus of elasticity,	E	4287 ksi (29.6 GPa)	S_E	1	4287 ksi (29.6 GPa)
Mass density,	ρ	0.15 kips/ft ³ (23.56 kN/m ³)	$S_E/S_\alpha S_l$	1	0.15 kips/ft ³ (23.56 kN/m ³)
Acceleration,	α	- -	S_α	0.4	- -
Seismic force,	F	- -	$S_E S_l^2$	6.25	- -
Mass of superstructure,	m	943 kips (430 ton)	$S_\rho S_l^3$	15.6	60.3 kips (27.4 ton)
Gravitational acceleration,	g	32.17 ft/sec ² (9.81 m/sec ²)	1	1	32.17 ft/sec ² (9.81 m/sec ²)
Velocity,	v	- -	$(S_l S_\alpha)^{1/2}$	1	- -
Time,	t	- -	$(S_l/S_\alpha)^{1/2}$	2.5	- -
Cross-section area of superstructure,	A_c	6034 in ² (3.89 m ²)	S_l^2	6.25	965 in ² (0.62 m ²)
Moment of inertia of superstructure,	I	4289863 in ⁴ (1.79 m ⁴)	S_l^4	39.1	109820 in ⁴ (0.046 m ⁴)
Volume of superstructure,	V	6286 ft ³ (178 m ³)	S_l^3	15.6	402 ft ³ (11.4 m ³)
Displacement,	δ	- -	S_l	2.5	- -
Frequency,	ω	- -	$S_l^{-1} (S_E/S_\rho)^{1/2}$	0.4	- -
Stress,	σ	- -	S_E	1	- -
Strain,	ε	- -	1	1	- -
Poisson’s ratio,	ν	- -	1	1	- -

The scaled superstructure is initially designed to be 60 feet long, corresponding to a linear dimension scaling factor equal to 2.50 (see Table 2-7). However, in order for the model to comply with the geometry specifications of the dual shake tables, the superstructure's length between its two supports is redefined to be 41.875 feet (12.76 m) corresponding to a length scaling factor equal to 2.39. As a result, the total length of the superstructure will be 61.875 feet (18.86 m) and the length of each cantilever will be 10 feet (3.05 m). Each of the six interior segments of the scaled superstructure model is 8.375 feet (2.55 m) long and each of the exterior ones 5.813 feet (1.77 m) long, as shown in Figure 2-8. Moreover, the total length of each pier is 10.0 feet (3.05 m) and each of the five segments is 2.0 feet (0.61 m) long. Table 2-8 summarizes all geometrical and material parameters considered for the similitude procedure and the final values of the corresponding scaling factors.

Table 2-8: Geometrical and material parameters of 1/2.39-scale bridge specimen

Physical Quantities	Prototype Structure	Scale Factors, S_i
Length of superstructure,	150 ft (45.72 m)	2.39
Length of piers,	25 ft (7.62 m)	2.39
Concrete modulus of elasticity,	4287 ksi (29.6 GPa)	1.0
Concrete mass density,	0.15 kips/ft ³ (23.56 kN/m ³)	1.0
Mass of superstructure,	943 kips (430 ton)	13.62
Gravitational acceleration,	32.17 ft/sec ² (9.81 m/sec ²)	1.0
Cross-section area of superstructure,	6034 in ² (3.89 m ²)	5.70
Moment of inertia of superstructure,	4289863 in ⁴ (1.79 m ⁴)	32.52
Volume of superstructure,	6286 ft ³ (178 m ³)	13.62

2.4 Superstructure Model

Due to the slenderness of the prototype superstructure's cross-section (see Figure 2-2) and given the 1/2.39-scale requirement, a change in the thickness of the top plate, bottom plate and webs of the cross-section is considered necessary. Moreover, attention should be paid so that the thickness

of the plates and webs allows the placement of the pre-stressing and mild reinforcement in the cross-section.

As shown in Figure 2-6, a thickness of 3 1/2" (89 mm) is chosen for the top and bottom plate. The thickness of the webs is set equal to 5" (127 mm). The width and height of the model cross-section are the exact scaled values of the prototype cross-section. The modified properties of the model superstructure cross-section are presented in Table 2-9. The design of the superstructure according to current design codes is presented in Chapter 3.

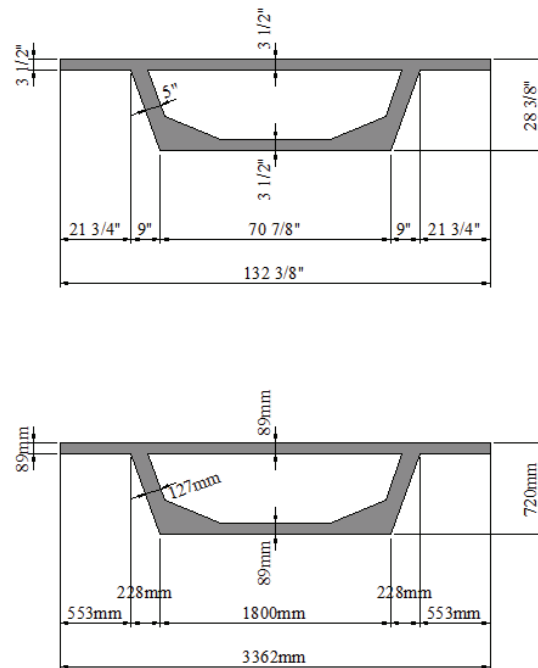


Figure 2-6: Cross-section of superstructure test model

Table 2-9: Cross-section properties of superstructure test model

Properties	Value	
Length, L	61.875 ft	18.86 m
Cross-section area, A_c	1047 in ²	0.67 m ²
Moment of inertia about y-y, I_y	124266 in ⁴	0.052 m ⁴
Moment of inertia about z-z, I_z	1193266 in ⁴	0.499 m ⁴
Section centroid from bottom surface, z_b	15.85 in	0.40 m
Section centroid from top surface, z_t	12.50 in	0.32 m

Given that the total length of the superstructure is 61.875 feet (18.86 m), its total weight equals 69.23 kips (31.5 ton). The maximum specimen mass on each shake table considering the extension platform in place equals 40 ton (88 kips), as shown in Table 2-4. The difference between the maximum allowable mass on each shake table (40 ton or 88 kips) and the mass of the superstructure acting on each support (34.6 kips or 15.75 ton) should accommodate the total weight resulting from the piers, cap beams and footings.

2.5 Substructure Model

As discussed in Section 2.3, the total length of each pier of the bridge model equals 10.0 feet (3.05 m) and each pier is divided in five 2.0 feet (0.61 m) long segments. The distance between the superstructure's supports equals 41.875 feet (12.76 m) so that the piers are centrally placed in respect to the shake tables.

The AASHTO-PCI-ASBI Segmental Standards Manual [2000] provides typical box pier segments cross-section details for span-by-span and balanced cantilever bridge construction (see Figure 2-7). In this study, a square hollow cross-section is considered for the piers. The width of the pier is set equal to 25" (635 mm) and the web thickness equal to 5" (127 mm) which results to a total weight of 4.2 kips (1.9 ton) for each pier and 77.6 kips (35.3 ton) for the superstructure and both piers. The design of the piers according to current design codes is presented in Chapter 4.

The geometry of the scaled bridge test unit is presented in Figure 2-8.

2.6 Construction Procedure of Bridge Model

The bridge test unit, tested on the dual shaking tables of the Structural Engineering and Earthquake Simulation Laboratory (SEESL) at the University at Buffalo, is described in detail by Sideris et al. [2010]. It consisted of the precast segmental superstructure - as described in Section 2.4, two precast cap beams, two precast segmental piers - as described in Section 2.5 and two footings. All members – superstructure, cap beams, piers and footings - were manufactured in a precast plant and delivered to the Laboratory. Based on the 'span-by-span' construction procedure, assembly and pre-stressing of the superstructure segments were carried out on the Laboratory Floor whereas; assembly and pre-stressing of the piers and cap beams were carried out on the two shake tables (one pier per table). Finally, the superstructure was lifted using a 40-ton crane and placed onto the cap beams and piers.

A three-dimensional view of the bridge model on the dual shake tables at SEESL is presented in Figure 2-9.

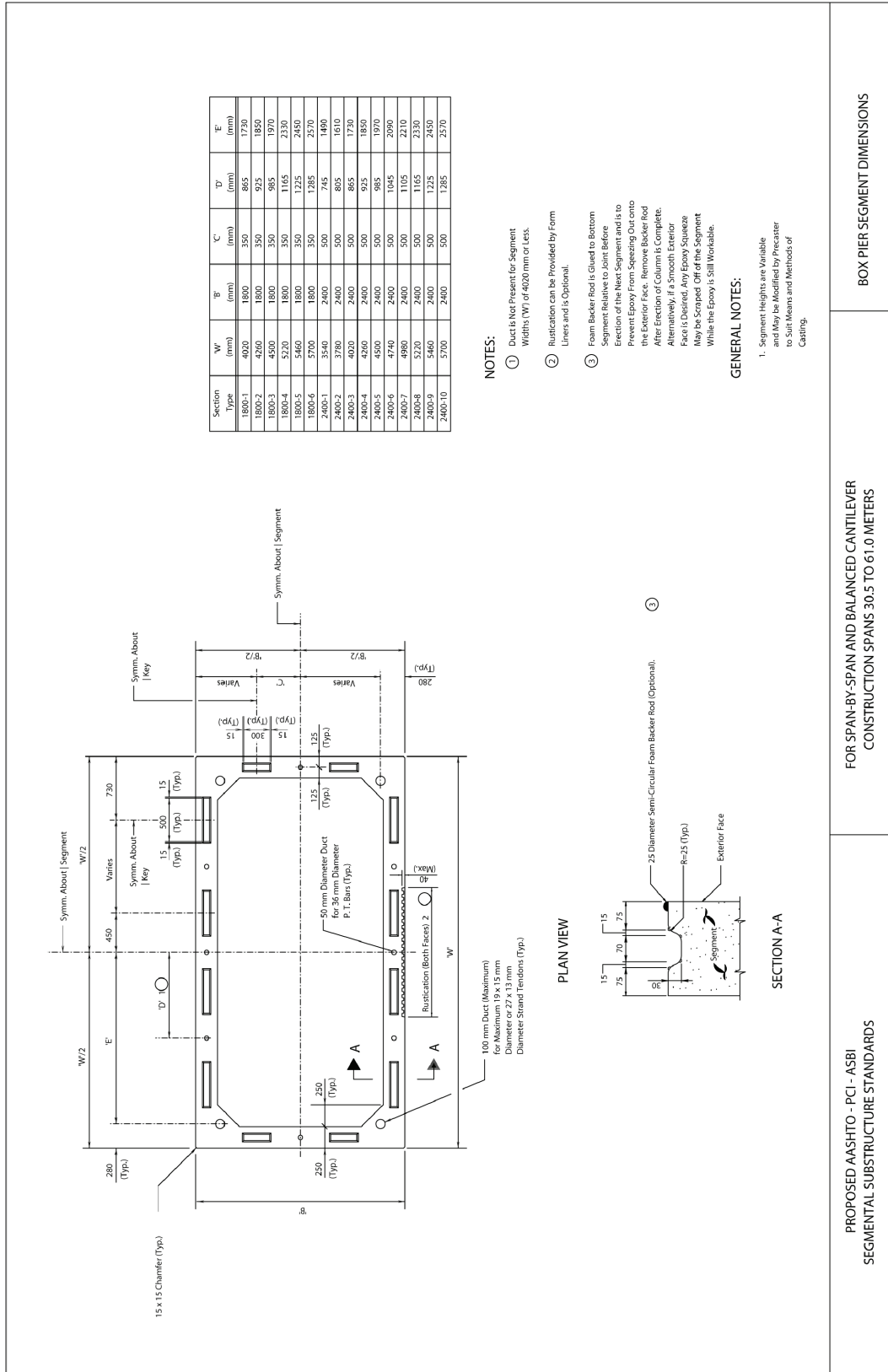


Figure 2-7: Box pier segment dimensions [AASHTO-PCI-ASBI, 2000]

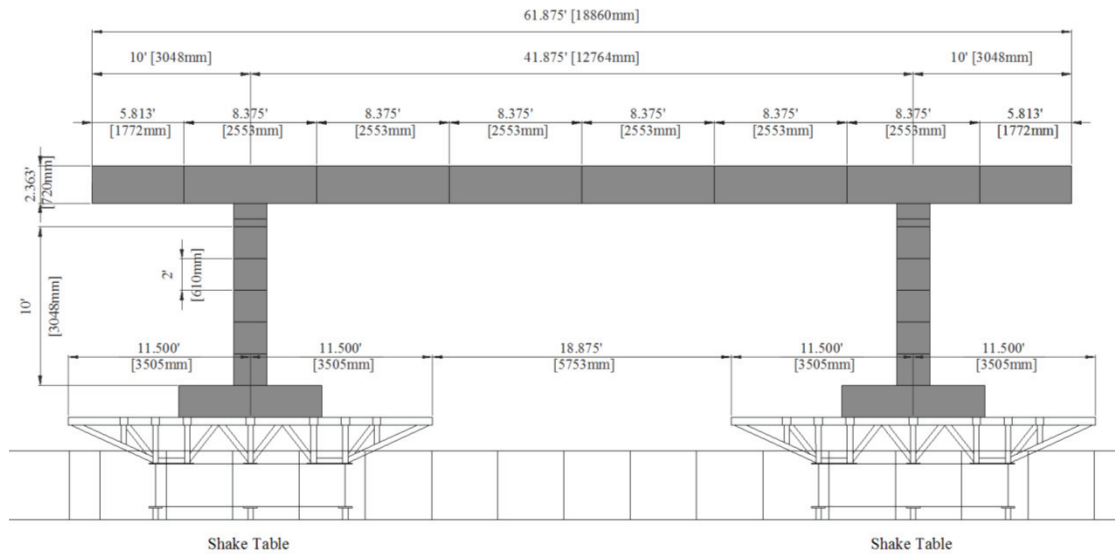


Figure 2-8: Elevation of 1/2.39-scale bridge test model on the dual shake tables of SEESL (UB)

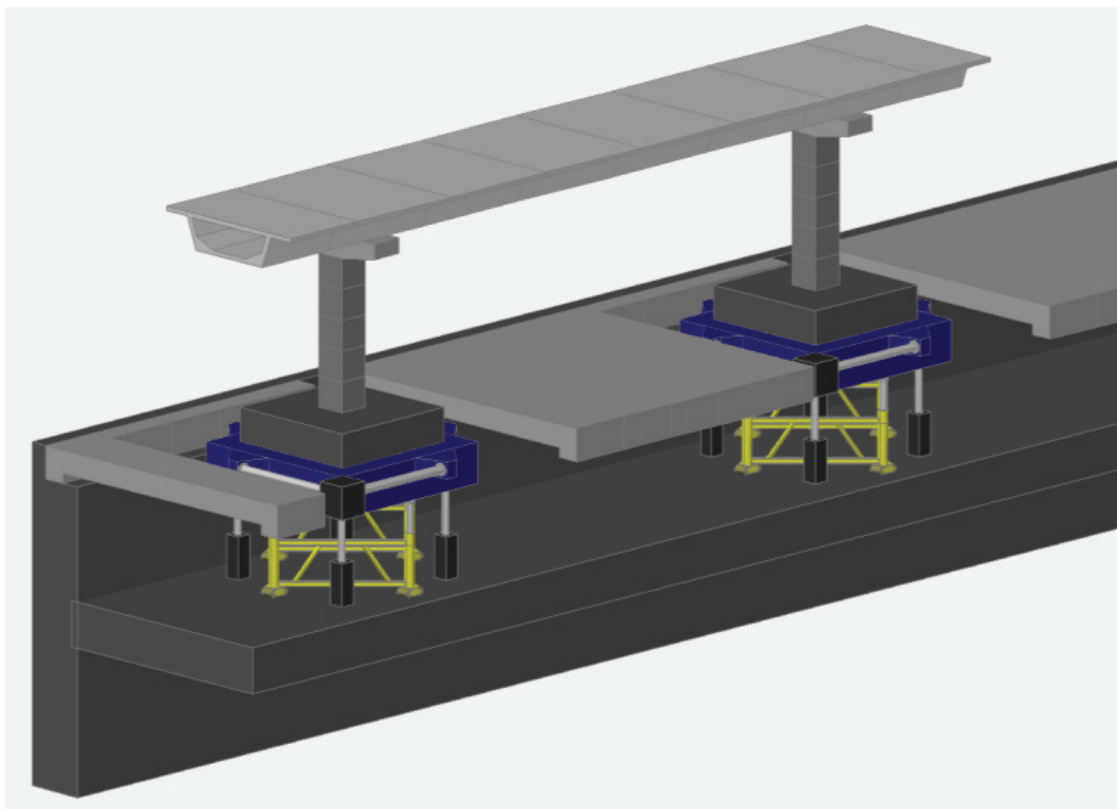


Figure 2-9: Three-dimensional bridge test model on the dual shake tables of SEESL (UB)

SECTION 3

SUPERSTRUCTURE DESIGN

The superstructure of the bridge test specimen, as described in Section 2.4, is designed hereafter according to AASHTO LRFD Bridge Design Specifications [2007] and PCI Bridge Design Manual [2003].

The AASHTO LRFD [2007] design specifications refer to the design and analysis procedures of segmentally constructed bridges and their components. Joints in precast segmental bridges shall be either cast-in-place closures or match-cast epoxied joints and shear keys should be provided to prevent relative sliding between segments. Moreover, the use of internal or combination of internal and external pre-stressing reinforcement is allowed in zones of moderate or high seismicity considering that at least 50% of the pre-stress force should be provided by internal tendons. The design of precast segmental bridges with pre-stressing continuity reinforcement requires that structural members behave as monolithic under serviceability limit states whereas; joints between segments may open under ultimate limit states.

In this study, the superstructure of the bridge specimen is considered to be simply supported on the cap beams and piers. Following the AASHTO LRFD [2007] specifications, the superstructure model is assumed to be continuous and the code provisions for segmentally constructed bridges are employed for its design. The geometry of the bridge test unit and the design superstructure model is illustrated in Figure 3-1.

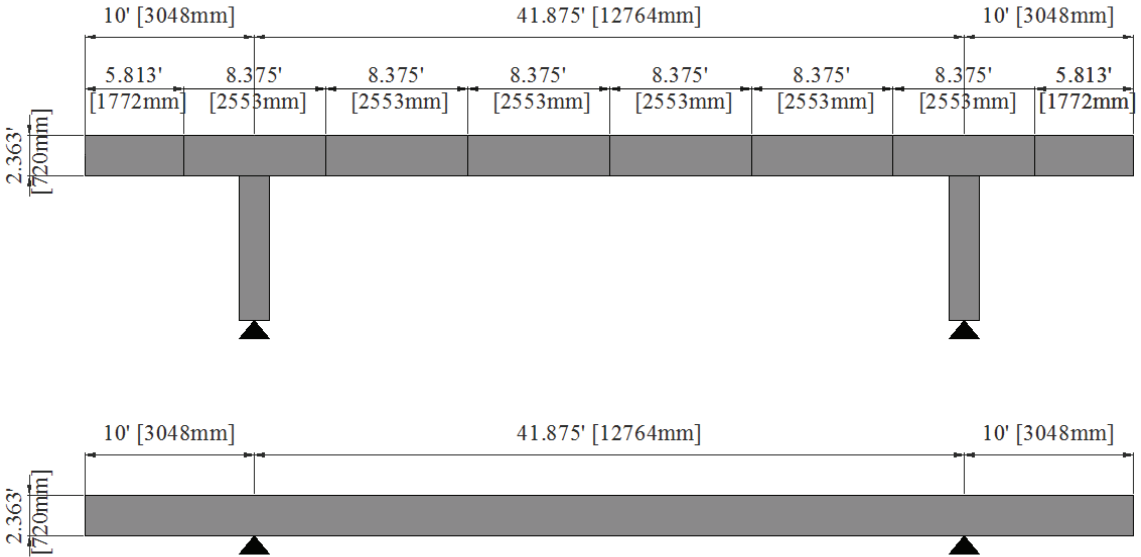


Figure 3-1: Bridge test unit and design superstructure model

3.1 Material and Cross-Section Properties

According to the AASHTO LRFD Bridge Design Specifications [2007], the specified 28-day concrete compressive strength is 5000 psi (34.5 MPa) and the modulus of elasticity is 4287 ksi (29.6 GPa). Grade 60 reinforcement steel is specified for mild steel with yield strength that equals 60 ksi (414 MPa) and modulus of elasticity equal to 29000 ksi (200 GPa).

In terms of the pre-stressing reinforcement, AASHTO LRFD [2007] allows the use of internal and external tendons in zones of moderate or high seismicity (Zones 3 and 4) given that at least 50% of the pre-stress force should be provided by internal tendons. According to the provisions, both internal and external tendons are grouted after post-tensioning.

Several research studies have demonstrated the enhanced self-centering behavior of post-tensioned precast segmental columns when internal unbonded tendons are used as the only continuous reinforcement along the member's length [Ou et al. 2010, Yamashita et al. 2009, Wang et al. 2008, Hewes 2007]. Bonded tendons in precast segmental structures lead to conventional cast-in-place behavior of the system whereas; unbonded tendons allow opening and closing of the joints between adjacent segments and therefore rocking behavior of the system.

Based on the above, a key concept incorporating post-tensioned internal unbonded tendons acting as the only continuous reinforcement between both the superstructure and substructure segments is introduced in the design. Contrary to AASHTO's design provisions, neither shear keys nor epoxied joints are considered in this study. It should be noted that use of post-tensioned internal unbonded tendons in precast segmental bridge superstructures has never been reported in the literature.

Due to the small dimensions of the superstructure cross-section (see Figure 2-6), a mono-strand post-tensioning system has been selected [DYWIDAG DSI, 2009]. The mono-strand tendons are typically made from cold-drawn, low relaxation 7-wire strand Grade 270 (1860 MPa). The strand diameter is 0.5" (12.7 mm) and is sheathed inside a high density polyethylene duct having a diameter of approximately 1" (25.4 mm). The mono-strands are unbonded and therefore free to slide inside the duct.

The material properties used in the design of the superstructure model are summarized in Table 3-1. Moreover, the geometry of the superstructure's cross-section is illustrated in Figure 3-2 and the cross-sectional properties used for the design are summarized in Table 3-2.

Table 3-1: Design material properties [AASHTO, 2007]

Material	Property	Symbol	Value
Concrete	Compression strength (28 days)	f'_c	5000 psi (34.5 MPa)
	Unit weight	w_c	150 lbs/ft ³ (2403 kg/m ³)
	Modulus of elasticity	E_c	4287 ksi (29.6 GPa)
Pre-stressing Strands	Strand diameter	D_p	0.5 in (12.77 mm)
	Strand area	A_{sp}	0.153 in ² (98.71 mm ²)
	Ultimate strength	F_{pu}	41.3 kips (183.7 kN)
	Yield strength	F_{py}	37.2 kips (165.3 kN)
	Modulus of elasticity	E_p	28500 ksi (196.5 GPa)
Reinforcing Bars	Yield stress	f_y	60 ksi (414 MPa)
	Modulus of elasticity	E_s	29000 ksi (200 GPa)

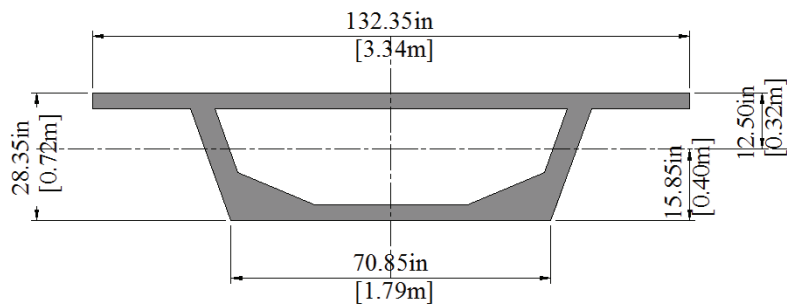


Figure 3-2: Superstructure design cross-section

Table 3-2: Design superstructure cross-section properties

Property	Symbol	Value
Area	A_c	1047 in ² (0.67 m ²)
Depth	h	28.35 in (0.72 m)
Width	b	132.35 in (3.34 m)
Moment of inertia (y-y)	I_y	124266 in ⁴ (0.052 m ⁴)
Moment of inertia (z-z)	I_z	1193266 in ⁴ (0.499 m ⁴)
Distance of center of gravity from top fiber	z_t	12.50 in 0.32 m
Distance of center of gravity from bottom fiber	z_b	15.85 in 0.40 m
Section modulus for extreme top fiber	$S_{y,t}$	9944 in ³ (0.159 m ³)
Section modulus for extreme bottom fiber	$S_{y,b}$	7839 in ³ (0.126 m ³)

3.2 Design Loads

3.2.1 Dead Loads

The dead loads on the model structure include the superstructure self-weight (DC) and the permanent loads from barriers and future surfacing (DW) which are conservatively assumed to be equal to 30 percent of the superstructure's self-weight. The dead loads and the corresponding member forces are presented in Table 3-3.

Table 3-3: Member forces due to dead loads

Load Case	Load Value	Moment	
		Mid-span	Support
Self-weight, DC	1.09 kips/ft (15.92 kN/m)	185 kips-ft (251 kN-m)	-55 kips-ft (-75 kN-m)
Barriers and Surfacing, DW	0.33 kips/ft (4.77 kN/m)	55 kips-ft (75 kN-m)	-17 kips-ft (-23 kN-m)

3.2.2 Live Loads

According to AASHTO LRFD Bridge Design Specifications [2007] and PCI Bridge Design Manual [2003], the vehicular live loads on bridges, designed as HL-93, consist of a combination of the Design Truck and the Design Lane loads. The Design Truck load is represented by three concentrated loads 8, 32 and 32 kips (35, 145 and 145 kN) in a distance of 14 and 14 to 30 feet (4.30 and 4.30 to 9.00 m) respectively, as shown in Figure 3-3. The Design Lane load consists of a uniform load of 0.64 kips/ft (9.35 kN/m).

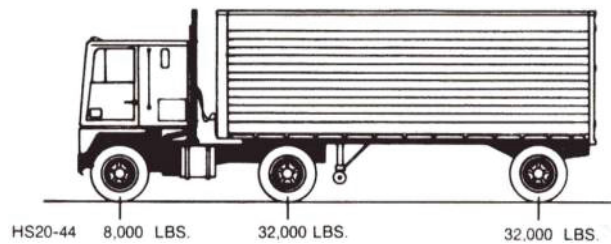


Figure 3-3: Design Truck according to AASHTO, 2007

The static effects of the Design Truck shall be increased by a percentage defined as Dynamic Load Allowance (IM) in order to account for wheel load impact from moving vehicles. The factor to be applied to the static load shall be taken as $(1+IM/100)$ where IM equals 33% for all limit states except from fatigue and fracture limit states.

In order to compute the most critical bending moments developed in the mid-span section, the Design Truck is placed at the centre line of the interior span and the distance between the two 32 kips (145 kN) point loads is considered equal to 14 feet (4.30 m). The distributed load is placed only in the interior span.

Taking into account that the live loads will be applied to the scaled superstructure design model, their values and location shall be scaled down to match the model requirements. The scale factor for the static forces, S_{Fst} , equals $S_E \times S_l^3$ whereas; according to Table 2-7, the scale factor for the seismic forces, S_{Fse} , equals $S_E \times S_l^2$. The member forces resulting from the applied live loads are presented in Table 3-4.

Table 3-4: Member forces due to live loads

Load Case	Load Value	Moment	
		Mid-span	Support
Design Truck, <i>LL</i>	0.59/ 2.35 kips (2.62/ 10.45 kN)	47 kips-ft (64 kN-m)	-
Design Lane, <i>LL</i>	0.11 kips/ft (1.61 kN/m)	25 kips-ft (34 kN-m)	-

3.2.3 Earthquake Loads

Earthquake loads, as defined in AASHTO LRFD Bridge Design Specifications [2007], are given by the product of the elastic seismic coefficient C_{sm} and the equivalent weight of the structural system.

The superstructure of the bridge test specimen is considered to be simply supported on the piers and therefore solely vertical earthquake loads are considered for its design. The method of analysis to be used is the Uniform Load Method which is based on the superstructure's fundamental mode of vibration in the vertical direction. The period of this mode is taken as that of an equivalent single mass-spring oscillator whereas, the stiffness of this equivalent spring is calculated using the maximum displacement that occurs when an arbitrary uniform vertical load is applied to the bridge's superstructure. The elastic seismic coefficient, C_{sm} , is used to calculate the equivalent uniform seismic load from which seismic force effects are found.

The Uniform Load Method is described below:

- calculate the static vertical displacements, $v_s(x)$, due to a corresponding unit uniform load, p_o , which is applied over the length of the bridge's superstructure;
- calculate the stiffness of the superstructure, K , as the ratio of the uniform load times its total length over the maximum static displacement of the superstructure, v_{max} ;
- calculate the total weight, W , of the bridge superstructure;
- calculate the fundamental period of the bridge, T_1 , using the following expression:

$$T_1 = 2\pi \sqrt{\frac{W}{gK}} \quad (3-1)$$

- calculate the elastic seismic coefficient, C_{sm} , as indicated hereafter and then calculate the equivalent static earthquake loading, p_e , along the superstructure's length, L , from the expression:

$$p_e = \frac{C_{sm}W}{L} \quad (3-2)$$

- calculate the displacements and member forces to be used for the design by applying the equivalent static earthquake loading, p_e , to the structure and performing a second static analysis.

The elastic seismic response coefficient, C_{sm} , for the system's first mode of vibration is defined as:

$$C_{sm} = \frac{1.2AS}{T_1^{2/3}} \leq 2.5A \quad (3-3)$$

where T_1 the fundamental period of vibration, A the acceleration coefficient and S the site coefficient.

The acceleration coefficient, A , is obtained from the seismic hazard maps presented in AASHTO [2007] which correspond to a 10 percent probability of exceedance in 50 years (475-year return period). Four different soil profiles, S , are specified in AASHTO [2007] which correspond to different site effect coefficients. In locations where the soil properties are not sufficiently known, the site coefficient for soil profile type II shall be used.

Considering a prototype bridge located at a site in the Western United States, the acceleration coefficient, A , and the site coefficient, S , are set equal to 0.25 (Seismic Zone 3) and 1.20 (Soil profile type II), respectively.

In order to relate the seismic behavior of the prototype structure to the model one, the period and acceleration scale factors should be taken into account. According to the similitude requirements and Table 2-7, the scale factors for the acceleration S_A , site coefficient S_S and fundamental period S_T , are:

$$S_A = 1/S_L = 1/2.39$$

$$S_S = 1.0$$

$$S_T = S_L = 2.39$$

The elastic seismic response coefficient, C_{sm} , as defined in Equation (3-3) is illustrated in Figure 3-4 for both the prototype and scaled bridge model and a range of periods from zero to two seconds.

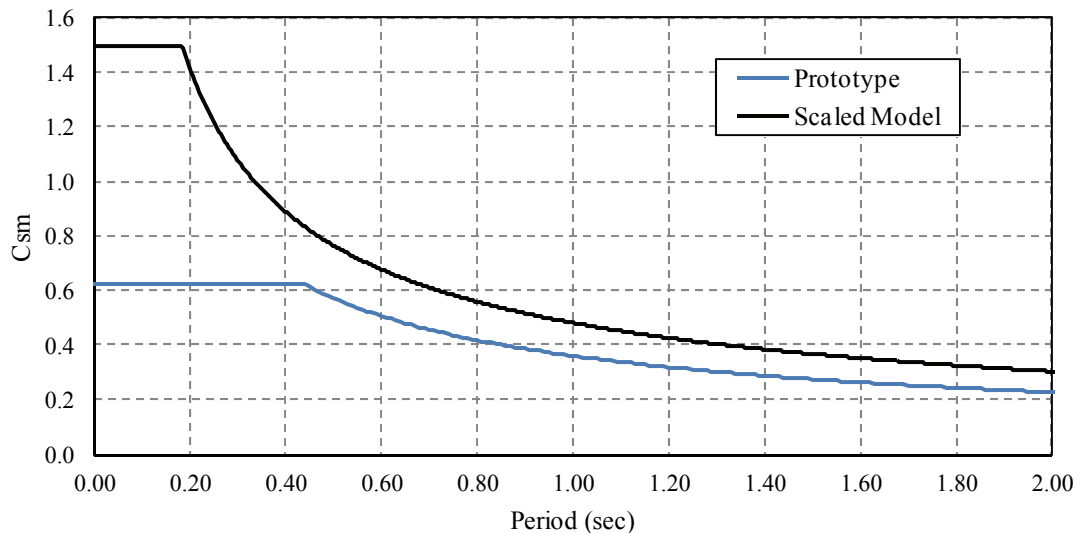


Figure 3-4: Seismic response coefficient for the prototype bridge and scaled test model [AASHTO, 2007]

The superstructure's seismic mass results from: the self-weight of the superstructure (DC Load Case in Table 3-3), the permanent loading from the barriers and future surfacing (DW Load Case in Table 3-3) as well as, 30 percent of the design lane live load (Design Lane LL Load Case in Section 3.2.2). The total considered weight, W , of the scaled superstructure equals 89.8 kips (40.75 tons).

The AASHTO LRFD Bridge Design Specifications [2007] considers only horizontal seismic loads for the design of bridge systems whereas; the effect of vertical seismic loads is neglected. Given the significant impact of vertical seismic loading on the behavior of the segmental superstructure system, the vertical equivalent static earthquake load is assumed to be equal to 2/3 of the corresponding horizontal one.

Applying the Uniform Load Method, as described above, the vertical static displacement at the superstructure's mid-span cross-section due to a corresponding unit uniform load (1 kip/ft = 14.59 kN/m) is equal to 0.09 inches (2.40 mm). Consequently, the stiffness of the bridge superstructure under vertical loading, K_{ver} , equals 7872 kips/ft (114883 kN/m). Given that the total considered weight, W , is 89.8 kips (40.75 tons) and g equals 32.17 ft/sec² (9.81 m/sec²), the model's fundamental period of vibration under vertical loading, $T_{l,v}$, is computed to be 0.118 seconds.

Using Equation (3-3), the model's elastic seismic response coefficient due to vertical earthquake loading, $C_{sm,v}$, is:

$$C_{sm,v} = \frac{1.2 \cdot (0.25 \cdot 2.39) \cdot 1.2}{0.118^{2/3}} = 3.58 > 2.5 \cdot (0.25 \cdot 2.39) = 1.49 \Rightarrow C_{sm,v} = 1.49$$

The equivalent vertical static earthquake load, $p_{e,v}$, acting along the superstructure's length will therefore be equal to:

$$p_{e,v} = \frac{2}{3} \frac{C_{sm} W}{L} = 1.44 \text{ kips/ft} \quad (3-4)$$

According to AASHTO LRFD [2007], the design seismic loads result from the elastic seismic loads divided by the response modification factor, R . The superstructure of a bridge system is considered to remain elastic when subjected to earthquake induced loads and therefore the response modification factors, R , equals to unity. However, the proposed segmental superstructure system with internal unbonded tendons is expected to have higher ductility and energy dissipation capabilities comparing to the conventional monolithic systems. Consequently, a greater R -factor equal to 2.50 is selected for the design of the bridge's superstructure and substructure [Sideris et al., 2010]. The design vertical earthquake load, $p_{d,v}$, along the superstructure's length will therefore be:

$$p_{d,v} = \frac{p_{e,v}}{R} = \frac{1.44}{2.50} = 0.58 \text{ kips/ft} \quad (3-5)$$

The design vertical earthquake load equals 0.58 kips/ft (8.46 kN/m).

It should be noted that, the period of vibration in the vertical direction corresponds to a very stiff structure resulting to a maximum elastic seismic response coefficient value. Table 3-5 summarizes the considered design parameters for the bridge's superstructure under vertical earthquake loading.

Table 3-5: Uniform Load Method design parameters for vertical earthquake loads

Parameter	Symbol	Vertical EQ
Maximum static displacement,	v_{max}	0.09 in (2.40 mm)
Stiffness,	K	7872 kips/ft (114883 kN/m)
Model fundamental period,	T_1	0.118 sec
Elastic seismic response coefficient,	C_{sm}	1.49
Equivalent static earthquake loading,	p_e	1.44 kips/ft (21.02 kN/m)
Design earthquake load,	p_d	0.58 kips/ft (8.46 kN/m)

The section forces resulting from the application of the design vertical earthquake loads on the bridge's superstructure are presented in Table 3-6 whereas; section forces resulted from all considered load cases are summarized in Table 3-7.

Table 3-6: Member forces due to vertical earthquake loads

Load Case	Load Value	Moment	
		Mid-span	Support
Vertical EQ, EQ_v	0.58 kips/ft (8.46 kN/m)	98 kips-ft (133 kN-m)	-29 kips-ft (-39 kN-m)

3.3 Design Load Combinations

According to the AASHTO LRFD Bridge Design Specifications [2007], bridge components and connections should be designed in order to satisfy the each of the following limit states:

- Service I: compression in pre-stressed concrete components is investigated using this load combination;
- Service III: is the load combination for longitudinal analysis related to tension in pre-stressed concrete superstructures with the objective of crack control;
- Strength I: is the basic load combination related to the normal vehicular use of a bridge. The ultimate strength of all bridge components is computed;

- Extreme Event I: is the load combination including earthquake.

The load factors for the various load combinations are presented in Table 3-8 and, the member forces for all considered load combinations are presented in Table 3-9.

Table 3-7: Member forces due to considered load cases

Load Case	Moment	
	Mid-span	Support
Self-weight, <i>DC</i>	185 kips-ft (251 kN-m)	-55 kips-ft (-75 kN-m)
Barriers and Surfacing, <i>DW</i>	55 kips-ft (75 kN-m)	-17 kips-ft (-23 kN-m)
Design Truck, <i>LL</i>	47 kips-ft (64 kN-m)	-
Design Lane, <i>LL</i>	25 kips-ft (34 kN-m)	-
Vertical EQ, <i>EQ_v</i>	98 kips-ft (133 kN-m)	-29 kips-ft (-39 kN-m)

Table 3-8: Load combinations and load factors [AASHTO, 2007]

		Load Factors				
		<i>DC</i>	<i>DW</i>	<i>LL</i>	<i>EQ</i>	
Load Combinations	<i>Service I</i>	1.00	1.00	1.00	-	
	<i>Service III</i>	1.00	1.00	0.80	-	
	<i>Strength I</i>	max	1.25	1.50	1.75	-
		min	0.90	0.65	1.75	-
	<i>Extreme Event I</i>	max	1.25	1.50	0.50	1.00
		min	0.90	0.65	0.50	1.00

A preliminary design is conducted in order to compute the number of tendons and their geometry along the superstructure's length. The critical load combinations considered in the preliminary design are: Service III limit state; Extreme Event I limit state for vertical earthquake loading and; the lifting of the superstructure as described in Section 3.5.2. Following the preliminary design, all time dependant and non-dependant losses due to pre-stressing are computed. The superstructure's stresses and section forces for all considered load combinations are computed and compared to the design limit states ones.

Table 3-9: Member forces due to considered load combinations

Load Combination		Moment	
		Mid-span	Support
Service I		328 kips-ft (445 kN-m)	-72 kips-ft (-98 kN-m)
Service III		311 kips-ft (422 kN-m)	-72 kips-ft (-98 kN-m)
Strength I	max	467 kips-ft (633 kN-m)	-95 kips-ft (-129 kN-m)
	min	356 kips-ft (483 kN-m)	-61 kips-ft (-83 kN-m)
Extreme Event I, Vertical EQ Load	downward	max	456 kips-ft (618 kN-m)
		min	345 kips-ft (468 kN-m)
	upward	max	260 kips-ft (353 kN-m)
		min	149 kips-ft (202 kN-m)

3.4 Stress Limits for Pre-stressing Tendons and Concrete

The magnitude of pre-stressing force in a concrete member is not constant, but assumes different values during the life of the member. The greatest force that acts on the member is during the jacking operation and is referred as Jacking force, P_j . Upon transfer of force to the concrete member, there is an immediate reduction of the jacking force to a lower value defined as the Initial Pre-stress force, P_i , as a consequence of all instantaneous losses such as anchorage slip, elastic shortening and friction. With the passage of time, the pre-stress force is further reduced. The result of time-dependent effects, including concrete shrinkage and creep and steel relaxation, is that the initial pre-stress force is gradually reduced to what will be termed the Effective Pre-stress force, P_e . For the case of unbonded pre-stressed tendons, slip can occur between the steel and the surrounding concrete when flexural loading is applied. The result is that the elongation of the steel is distributed over the entire length of the tendon.

Most specifications for pre-stressed concrete members impose certain limitations on stresses in the concrete and steel at particular loading stages. According to AASHTO LRFD Bridge Design Specifications [2007] and PCI Bridge Design Manual [2003], the tendon stress shall not exceed the tensile strength limit values specified in Table 3-10 for the different design Limit States.

Table 3-10: Stress limits for post-tensioned low relaxation strands [AASHTO, 2007]

Limit States	Condition	Stress Limit
Service	Prior to seating,	$0.90 f_{py}$
	At anchorages and couplers immediately after anchor set,	$0.70 f_{pu}$
	Elsewhere along length of member away from anchorages and couplers immediately after anchor set,	$0.74 f_{pu}$
	At service limit state after all losses (f_{pe}),	$0.80 f_{py}$
Strength and Extreme Event	Tensile strength,	f_{pu}
	Yield strength,	f_{pu}

The stress limits for concrete account for temporary stresses before losses and stresses at Service Limit states after losses. The concrete compressive and tensile stress limits according to AASHTO LRFD [2007] and PCI Bridge Design Manual [2003] are summarized below.

The stress limits for concrete at release before losses are:

- Compression for pre-tensioned or post-tensioned members, $0.60f'_c$;
- Tension:
 - i. in areas without bonded reinforcement, $0.0948\sqrt{f'_c} \leq 0.2$ ksi;
 - ii. in areas with bonded reinforcement sufficient to resist the tensile force in the concrete assuming an uncracked section, $0.24\sqrt{f'_c}$ ksi.

At Service Limit state for fully pre-stressed components, the concrete stress limits are:

- Compression using the load combination for Service I Limit state:
 - i. due to effective prestress and permanent (dead) load, $0.45f'_c$;
 - ii. due to effective prestress and permanent and dead and live loads, $0.60f'_c$;
- Tension using the load combination for Service III Limit state:
 - i. for components with bonded pre-stressing tendons or reinforcement subjected to not worse than moderate corrosive conditions, $0.19\sqrt{f'_c}$ ksi;
 - ii. for components with unbonded pre-stressing, no tension is allowed.

3.5 Preliminary Design

The preliminary design of the number of tendons and their geometry along the length of the superstructure will be governed by the developed concrete tensile stresses. The jacking force, P_j , as well as the effective pre-stressing force, P_e , should be estimated and the concrete stresses computed so that, no tensile concrete stresses are developed.

The concrete stress at the top face of any post-tensioned member, f_t , and at the bottom face, f_b , can be found by superimposing axial and bending effects due to the applied pre-stress force and the dead and live loads [Nilson, 1978]:

$$f_t = -\frac{\sum P_e}{A_c} \pm \frac{\sum P_e e_i}{S_t} \mp \frac{M_t}{S_t} \quad (3-6)$$

$$f_b = -\frac{\sum P_e}{A_c} \pm \frac{\sum P_e e_i}{S_b} \mp \frac{M_t}{S_b} \quad (3-7)$$

where P_e is the effective pre-stress force acting on the cross-section, A_c is the superstructure cross-section area, e_i the strand eccentricity from the center of gravity of the cross-section, S_t the superstructure's top fiber modulus, S_b the superstructure's bottom fiber modulus and M_t the total moment at the specific location due to the considered load combination (see Table 3-9).

As listed in Table 3-10 and according to AASHTO LRFD Bridge Design Specifications [2007], the effective tendon limit stress at Service limit states, after all losses, is $0.80f_{py}$. A more conservative value is recommended by the mono-strand manufacturers [DYWIDAG DSI, 2009], equal to $0.65F_{pu}$ assuming that the percentage of total losses is 35. Based on that, the effective pre-stressing force is initially assumed to be equal to $0.65F_{pu}$ or 26.9 kips/strand (119.4 kN/strand) whereas; the jacking force equals $0.80F_{pu}$ or 33 kips/strand (146.8 kN/strand) [DYWIDAG DSI, 2009].

In the following sections, the stresses at mid-span and support sections are computed and the number of tendons required as well as, their geometry along the superstructure's length.

3.5.1 Service III Limit State

As mentioned in Section 3.4, Service III Limit State will govern the design of the bridge superstructure in terms of the developed cross-sectional tensile concrete stresses. In particular, for unbonded pre-stressed tendons no tensile stresses are allowed to develop.

The bottom tensile stress at mid-span cross-section equals:

$$f_{b,m} = \frac{M_{b,m}}{S_b} \quad (3-8)$$

By substituting into Equation (3-8) $M_{b,m}$, the total moment due to Service III loads at mid-span equal to 311 kips-ft (422 kN-m) and S_b equal to 7839 in³ (0.126 m³), the bottom tensile stress $f_{b,m}$ at mid-span is 0.476 ksi (3.28 MPa).

Assuming that the distance between the centre of gravity of strands and the bottom fiber of the superstructure cross-section is 1.75 inches (45 mm), the total effective pre-stressing force can be computed using Equation (3-7). Given that the concrete tension stress limit for unbonded tendons is zero and that $f_{b,m}$ at mid-span is 0.476 ksi (3.28 MPa), A_c is 1047 in² (0.67 m²) and e_i is 14.10 inches (358 mm), the total effective pre-stressing force after all losses is 173 kips (770 kN).

The number of strands required is approximately seven ($173/26.9 \approx 7$). A total number of ten 1/2-inch tendons (T.1 to T.10) is selected with a total area of 1.53 in^2 (987.1 mm^2) and a total effective pre-stress force of 269 kips (1197 kN).

The top tensile stress at the centerline of the support cross-section equals:

$$f_{t,s} = \frac{M_{t,s}}{S_t} \quad (3-9)$$

By substituting into Equation (3-9) $M_{t,s}$, the total moment due to Service III loads at the support equal to 72 kips-ft (98 kN-m) and S_t equal to 9944 in^3 (0.159 m^3), the top tensile stress $f_{t,s}$ at support is 0.087 ksi (0.60 MPa).

Assuming that the distance between the strands' centre of gravity and the top fiber of the superstructure cross-section equals 1.75 inches (45 mm), the effective pre-stress can be computed using Equation (3-6). Given that the concrete tension stress limit for unbonded tendons is zero and that $f_{t,s}$ at support is 0.087 ksi (0.60 MPa), A_c is 1047 in^2 (0.67 m^2) and e_t is 10.75 inches (273 mm), the total effective pre-stress force after all losses is 43 kips (191 kN).

The number of the strands required is approximately two ($43/26.9 \approx 2$). It can be therefore noted that, the number of tendons required at the support is significantly different than the one at required at mid-span. Because of that, the design will consider that two of the mid-span strands (T.1 and T.10) will reach the support with a parabolic geometry and an eccentricity from the top fiber equal to 1.75 inches (45 mm) whereas; the eight remaining tendons (T.2 to T.9) will reach the support with an unknown average eccentricity, e_i .

Following the reverse procedure than the one described above, the unknown average eccentricity, e_i , can be computed:

$$f_{t,s} = 0.087 = \frac{10 \cdot 26.9}{A} + \frac{2 \cdot 26.9 \cdot 10.75}{S_t} + \frac{(10 - 2) \cdot 26.9 \cdot e_i}{S_t}$$

Given that A_c equals 1047 in^2 (0.67 m^2) and S_t equals 9944 in^3 (0.159 m^3), e_i equals 10.53 inches (267 mm) below the neutral axis of the superstructure's cross-section.

At the cantilever end sections, where zero moments are developed, the total number of strands will reach in order to be tensioned from one side and fixed from the other. So, the geometry of tendons from the support to the end of cantilever should be such as the centre of gravity of tendons at the cantilever end coincides with the centre of gravity of the cross-section.

Summarizing the results we obtained for Service III Limit State, the design of the superstructure will incorporate ten tendons (T.1 to T.10) with a 1/2-inch diameter (12.7 mm). The geometry of the tendons will be parabolic along the superstructure's length. The eccentricity of the ten tendons at the mid-span section is 1.75 inches (45 mm) from the extreme bottom fiber of the cross-section whereas; two of the tendons (T.1 and T.10) reach the support with an eccentricity of 1.75 inches (45 mm) and eight of them (T.1 to T.9) with an average eccentricity of 23.03 inches (585 mm)

from the top fiber of the superstructure's cross-section. It should be noted that in order to account for the small size of the scaled superstructure model and to facilitate the construction of the specimen, the internal unbonded tendons are considered continuous along the superstructure's length and draped in the webs of the cross-section.

3.5.2 Lifting of Superstructure

The bridge superstructure designed hereafter is considered to be a simply supported beam with two overhangs of equal length (Figure 3-1). Following the assembly and pre-stressing of the superstructure's precast segments as described in Section 2.6, a crane will lift it up to its supports. The only load acting on the superstructure during lifting is its own self-weight.

Based on the lifting equipment of the SSEL Laboratory and the superstructure's total weight, two lifting points have been selected. The span between the lifting points is 15.625 feet long (4.76 m) whereas; the two overhangs are 23.125 feet (7.05 m) long. Considering that the self-weight of the superstructure equals 1.09 kips/ft (15.91 kN/m), the resulting design forces are calculated and presented in Table 3-11.

Table 3-11: Member forces during lifting

Load Case	Load Value	Moment	
		Mid-span	Lifting Points
Lifting	1.09 kips/ft (15.91 kN/m)	-258 kips-ft (-350 kN-m)	-292 kips-ft (-396 kN-m)

As shown in Table 3-11, the top fiber of the superstructure's cross-section is in tension along its total length during lifting. Consequently, a number of tendons should be provided at the top plate of the cross-section and along the total length of the superstructure in order to prevent the development of any tensile stresses during lifting. The design will incorporate four additional tendons (T.11 to T.14) lying at a fixed distance of 1.75 inches (45 mm) from the top fiber of the superstructure's cross section with an effective pre-stress force of 26.9 kips/strand (119.4 kN/strand).

By substituting into Equation (3-6), $M_{t,m}$ the total moment due to lifting at mid-span equal to 258 kips-ft (350 kN-m), S_t equal to 9944 in³ (0.159 m³), A_c equal to 1047 in² (0.67 m²) and e_i equal to 10.75 inches (273.05 mm) for tendons T.11 to T.14 and 14.40 inches (366 mm) for tendons T.1 to T.10 from the center of gravity of the superstructure's cross section:

$$f_{t,m} = -\frac{14 \cdot 26.9}{1047} - \frac{4 \cdot 26.9 \cdot 10.75}{9944} + \frac{10 \cdot 26.9 \cdot 14.10}{9944} + \frac{258 \cdot 12}{9944} = -0.068 \text{ ksi}$$

Consequently, the concrete stresses at the top fiber of the superstructure's cross-section during lifting are compressive.

Summarizing the results we obtained above, the design of the superstructure will incorporate fourteen tendons (T.1 to T.14) with a 1/2-inch diameter (12.7 mm). The geometry of tendons T.1 to T.10 will be parabolic, as mentioned in Section 3.5.1 whereas; tendons T.11 to T.14 will be lying at a distance of 1.75 inches (45 mm) from the top fiber of the superstructure's cross-section and along its length during the lifting of the superstructure.

3.5.3 *Extreme Event I Limit State, Vertical Earthquake*

As tabulated in Table 3-9, no negative moments are developed at the mid-span of the superstructure when subjected to either downward or upward vertical seismic loading [AASHTO, 2007]. Even though no tension stresses are expected to develop at the top fiber of the mid-span cross-section according to the design seismic loads, this might differ during the actual testing of the bridge model on the two shake tables.

As mentioned in Section 3.5.2, four additional tendons (T.11 to T.14) are incorporated in the design in order to account for the developed tensile stresses during lifting of the superstructure. Initially, all fourteen tendons (T.1 to T.14) are placed and tensioned in order to lift the superstructure to its final position. Afterwards, two tendons (T.12 and T.13) will be released and the twelve remaining tendons (T.1 to T.10, T.11 and T.14) will provide the required pre-stressing forces to the superstructure.

3.5.4 *Tendon Geometry*

Based on the above calculations and the requirements of the AASHTO LRFD Bridge Design Specifications [2007] concerning the minimum vertical and horizontal clear spacing between the ducts, the tendons are distributed in the cross-section as shown in Table 3-12 and Figure 3-5 for the mid-span, support and cantilever end sections. The geometry of the tendons along the span's length is illustrated in Figure 3-6. As noted before, the tendons are draped in the webs of the superstructure's cross-section.

It should be mentioned that e_t and e_b as listed in Table 3-12, refer to the tendon eccentricity above and below the center of gravity of the superstructure's cross-section, respectively.

3.6 **Pre-stress Loss Estimation**

The total pre-stress losses in post-tensioned members as defined in AASHTO LRFD Bridge Design Specifications [2007] may be taken as:

$$\Delta F_{pT} = \Delta F_{pF} + \Delta F_{pA} + \Delta F_{pES} + \Delta F_{pLT} \quad (3-10)$$

where ΔF_{pT} is the total loss of pre-stressing force, ΔF_{pF} is the loss due to friction, ΔF_{pA} is the loss due to anchorage set, ΔF_{pES} is the sum of all losses due to elastic shortening or extension at the time of application of pre-stress and external loads and ΔF_{pLT} is the losses due to long-term shrinkage and creep of concrete, and relaxation of the steel.

Table 3-12: Tendon eccentricities at superstructure's critical sections

Tendons	#	Mid-span		Support		Cantilever End		Units
		e_t	e_b	e_t	e_b	e_t	e_b	
T.1, T.10	2	-	14.10 (358)	10.75 (273)	-	10.75 (273)	-	in (mm)
T.2, T.9	2	-	14.10 (358)	-	5.10 (129)	5.60 (142)	-	in (mm)
T.3, T.8	2	-	14.10 (358)	-	8.10 (206)	0.10 (2.5)	-	in (mm)
T.4, T.7	2	-	14.10 (358)	-	11.10 (282)	-	5.40 (137)	in (mm)
T.5, T.6	2	-	14.10 (358)	-	14.10 (358)	-	10.90 (277)	in (mm)
T.11 to T.14	4	10.75 (273)	-	10.75 (273)	-	10.75 (273)	-	in (mm)

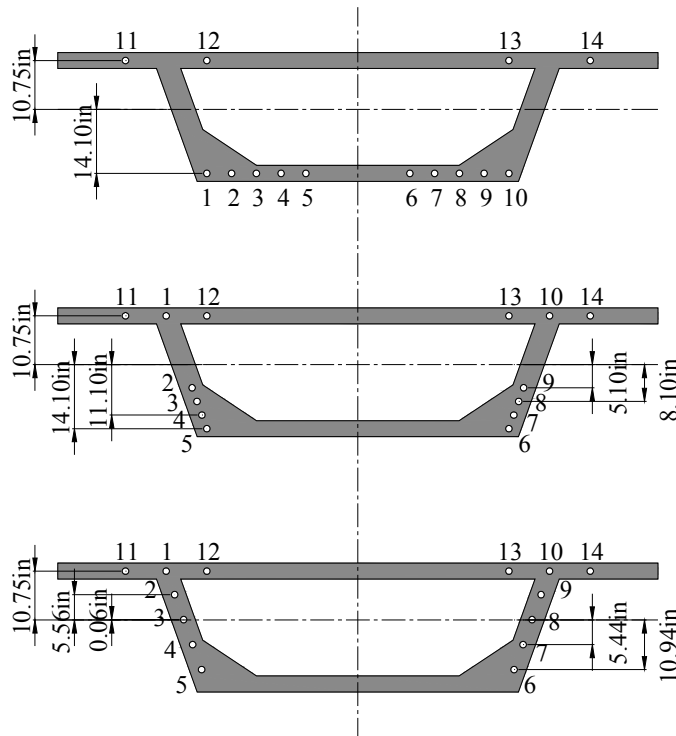


Figure 3-5: Tendon configuration at mid-span, support and cantilever end sections

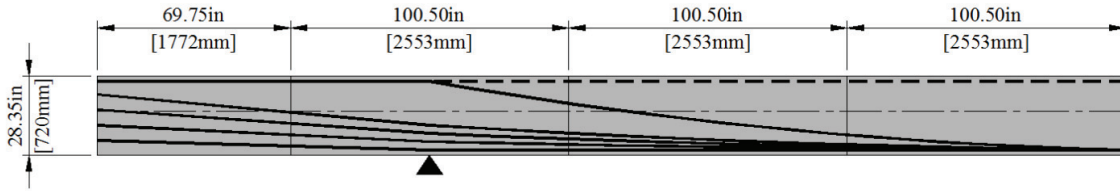


Figure 3-6: Elevation view of tendon geometry along the superstructure

3.6.1 Losses due to Friction

For post-tensioned members, usually the tendons are anchored at one end and stretched with the jacks at the other end. The total friction loss is the sum of the ‘wobble friction’ due to unintentional misalignment, and the ‘curvature friction’ due to the intentional curvature of the tendon.

According to AASHTO LRFD Bridge Design Specifications [2007], losses due to friction between the internal pre-stressing tendons and the duct wall may be taken as:

$$\Delta F_{pF} = P_j (1 - e^{-(K_w x + \mu \theta)}) \quad (3-11)$$

where ΔF_{pF} the loss due to friction, P_j the force in the pre-stressing steel at jacking, x the length of pre-stressing tendon from the jacking end to any point under consideration, K_w the wobble friction coefficient, μ the coefficient of friction and θ the sum of the absolute values of angular change of pre-stressing steel path from jacking end to the point under investigation.

The jacking force, P_j , is set equal to 30 kips (133.4 kN) and not 33 kips (146.8 kN) which is the maximum value of jacking force specified by the strand manufacturer [DYWIDAG DSI, 2009]. The wobble coefficient K_w is set equal to 0.0002 /ft whereas the coefficient of friction μ equals 0.23 /rad for polyethylene ducts [AASHTO, 2007].

Given that the tendons are curved in both horizontal and vertical plane, the total angular change θ_i shall be obtained by adding the total vertical angular change, $\theta_{v,i}$, and the total horizontal angular change, $\theta_{h,i}$. Since the developed elevation and plan of the tendons is of parabolic geometry, the angular change θ_i can be computed as:

$$\theta = \sqrt{\theta_{v,i}^2 + \theta_{h,i}^2} \quad (3-12)$$

Each of the vertical and horizontal angular change can be computed as:

$$\theta_i = \frac{4y_i}{x_i} \quad (3-13)$$

where θ_i the total vertical or horizontal angular change, y_i the vertical distance between top and bottom points of the parabola and x_i the horizontal distance between top and bottom points of the parabola.

Moreover, the expected elongation of the tendons is also computed according to:

$$elongation = \sum \frac{P_{i,av} x}{E_p A_{ps}} \quad (3-14)$$

where $P_{i,av}$ the average pre-stressing force after friction losses between adjacent location points, x the length of pre-stressing tendon from the jacking end to any point under consideration, E_p the modulus of elasticity of the pre-stressing strands and A_{ps} the total area of pre-stressing strands.

The losses are computed for each tendon at five points - jacking end, left support, mid-span, right support and dead end. The results are presented in Table 3-13.

3.6.2 Losses due to Elastic Shortening

Elastic shortening is the immediate shortening of the member under the application of pre-stressing forces. For a post-tensioned member with several tendons stressed simultaneously, there is no elastic shortening loss, since jacking will proceed until the desired pre-stress force is reached. However, in the case of tendons tensioned sequentially, after the first tendon the tensioning of any subsequent tendon will reduce the force in those already anchored, with the exception of the last tendon which will suffer no loss.

The loss due to elastic shortening in post-tensioned members, according to AASHTO LRFD Bridge Design Specifications [2007], may be computed as:

$$\Delta f_{pES} = \frac{N-1}{2N} \frac{A_{ps} f_{pbt} (I_g + e_m^2 A_c) - e_m M_g A_c}{A_{ps} (I_g + e_m^2 A_c) + \frac{A_c I_g E_c}{E_p}} \quad (3-15)$$

where A_{ps} the area of pre-stressing steel, A_c the area of the gross concrete section, E_c the modulus of elasticity of concrete at transfer, E_p the modulus of elasticity of pre-stressing tendons, e_m the tendon average eccentricity, f_{pbt} the stress in pre-stressing steel immediately prior to transfer, I_g the moment of inertia of the gross concrete section, M_g the moment due to self-weight at location under consideration and N the number of identical pre-stressing tendons.

The ratio $(N-1/2N)$ is assumed to be equal to 0.50 whereas A_{ps} equals 2.14 in² accounting for fourteen tendons, A_g equals 1047 in², E_c equals 4287 ksi, E_p equals 28500 ksi, f_{pbt} equals 218.7 ksi and I_g equals 124266 in⁴.

The losses due to elastic shortening are computed for the cantilever end, support and mid-span sections and presented in Table 3-14.

Table 3-13: Losses due to friction along the tendons' length

Tendon	P_j (kips)	θ (rad)	x (in)	ΔF_{pF} (kips)	P_{i,pF} (kips)	P_{i,av} (kips)	Elongation (in)
T.1, T.10	30.0	0.000	0.00	0.00	30.00		
		0.000	120.00	0.06	29.94	29.97	0.82
		0.210	371.25	1.59	28.41	29.17	1.68
		0.421	622.50	3.05	26.95	27.68	1.59
		0.421	742.50	3.10	26.90	26.93	0.74
4.84							
T.2, T.9	30.0	0.000	0.00	0.00	30.00		
		0.098	120.00	0.72	29.28	29.64	0.82
		0.197	371.25	1.51	28.49	28.88	1.66
		0.297	622.50	2.27	27.73	28.11	1.62
		0.395	742.50	2.94	27.06	27.39	0.75
4.85							
T.3, T.8	30.0	0.000	0.00	0.00	30.00		
		0.076	120.00	0.58	29.42	29.71	0.82
		0.190	371.25	1.46	28.54	28.98	1.67
		0.305	622.50	2.32	27.68	28.11	1.62
		0.380	742.50	2.85	27.15	27.41	0.75
4.86							
T.4, T.7	30.0	0.000	0.00	0.00	30.00		
		0.054	120.00	0.43	29.57	29.79	0.82
		0.195	371.25	1.49	28.51	29.04	1.67
		0.336	622.50	2.52	27.48	28.00	1.61
		0.389	742.50	2.91	27.09	27.29	0.75
4.86							
T.5, T.6	30.0	0.000	0.00	0.00	30.00		
		0.031	120.00	0.28	29.72	29.86	0.82
		0.205	371.25	1.56	28.44	29.08	1.68
		0.379	622.50	2.79	27.21	27.83	1.60
		0.411	742.50	3.04	26.96	27.09	0.75
4.85							
T.11 to T.14	30.0	0.000	0.00	0.00	30.00		
		0.000	120.00	0.06	29.94	29.97	0.82
		0.000	371.25	0.19	29.81	29.88	1.72
		0.000	622.50	0.31	29.69	29.75	1.71
		0.000	742.50	0.37	29.63	29.66	0.82
5.08							

Table 3-14: Losses due to elastic shortening

		Cantilever end	Support	Mid-span
e_m ,	(in)	-3.29	0.88	7.00
M_g ,	(kips-ft)	0.00	55	185
Δf_{pES} ,	(ksi)	1.60	1.49	1.65
ΔF_{pES} ,	(kips)	0.24	0.23	0.25

3.6.3 Losses due to Anchorage Set

In post-tensioned members, when the jacking force is released, the steel tension is transferred to the concrete through the anchorages. Inevitably there is a small amount of slip at the anchorages upon transfer, as the wedges seat themselves into the tendons or as the anchorage hardware deforms. The magnitude of anchorage set depends on the particular pre-stressing system.

Losses due to anchorage set will be computed based on the recommendations of PCI Bridge Design Manual [2003]. An average value of anchor set, w , equal to 0.375 inches (9.525 mm) is chosen.

After the post-tensioning tendon is anchored the drop in tendon stress due to anchorage set is affecting a length, x_a , which can be approximated as:

$$x_a = \sqrt{\frac{A_{sp} E_p w L}{\Delta P}} \quad (3-16)$$

where A_{sp} the area of the pre-stressing strand, E_p the modulus of elasticity of the pre-stressing tendons, w the anchor set, L the total length of the tendon and ΔP the difference in the pre-stressing force between the jacking end and the dead end due to friction losses as computed above.

Table 3-15: Effective length due to anchorage set

Tendon	x_a (in)
T.1, T.10	599.95
T.2, T.9	616.76
T.3, T.8	626.63
T.4, T.7	620.50
T.5, T.6	606.31
T.11 to T.14	1800.74

The loss of the pre-stressing force due to anchorage set can be then calculated along any point, x_i , of the tendon length:

$$\Delta F_{pA} = \frac{2\Delta P(x_a - x_i)}{L} \quad (3-17)$$

The calculations for all tendons are summarized in Table 3-16.

Table 3-16: Losses due to anchorage set along the tendons' length

Location (in)	Anchorage Set Losses (kips)					
	T.1, T.10	T.2, T.9	T.3, T.8	T.4, T.7	T.5, T.6	T.11 to T.14
0.00	5.45	5.30	5.22	5.27	5.39	1.82
120.00	4.36	4.27	4.22	4.25	4.33	1.70
371.25	2.08	2.11	2.13	2.12	2.09	1.44
622.50	0.00	0.00	0.03	0.00	0.00	1.19
742.50	0.00	0.00	0.00	0.00	0.00	1.07

3.6.4 Losses due to Concrete Shrinkage

Drying shrinkage of concrete permits a reduction of strain in the pre-stressing steel equal to the shrinkage of the concrete. The resulting steel stress reduction is an important component of the total pre-stress loss.

According to the PCI Bridge Design Manual [2003], the concrete shrinkage coefficient, S_c , is given by the equation:

$$S_c(t, t_o) = \frac{(t - t_o)}{35 + (t - t_o)} S_u \quad (3-18)$$

where t the age of concrete, t_o the age of concrete at the end of the initial curing period and S_u the ultimate shrinkage strain.

An average value for the ultimate shrinkage strain is suggested:

$$S_u = 545k_{sh}10^{-6} \quad (3-19)$$

$$k_{sh} = k_{cp}k_hk_s \quad (3-20)$$

where k_{cp} the correction factor for initial curing period equal to 0.86 for 28 days moist curing period, k_h the correction factor for relative humidity equal to 1.00 for 70% average ambient relative humidity and k_s the size correction factor:

$$k_s = 1.2e^{-0.12V/S} \quad (3-21)$$

where V the volume of concrete and S the surface area of concrete exposed to drying.

For a ratio of the section volume over the concrete area exposed to drying equal to 3.42, k_s is computed to be equal to 0.80, k_{sh} equals 0.68 and S_u equals 0.37%. Using Equation (3-18):

$$S_c(180,28) = \frac{(180 - 28)}{35 + (180 - 28)} 0.37 \cdot 10^{-3} = 0.30 \cdot 10^{-3}$$

$$\Delta f_{p,Sc} = S_c E_p = 8.65 \text{ ksi} \quad (3-22)$$

The losses due to concrete shrinkage, $\Delta F_{p,Sc}$, are estimated to be 1.32 kips.

3.6.5 Losses due to Concrete Creep

For unbonded post-tensioned members, the reduction in steel stress due to concrete creep is more or less uniform along the entire length of the tendon.

According to the PCI Bridge Design Manual [2003], the concrete creep coefficient, C_c , is given by the equation:

$$C_c(t, t_o) = \frac{(t - t_o)^{0.6}}{10 + (t - t_o)^{0.6}} C_u \quad (3-23)$$

where t the age of concrete, t_o the age of concrete at the end of the initial curing period and C_u the ultimate creep strain.

An average value for the ultimate creep strain is suggested:

$$C_u = 1.88k_c \quad (3-24)$$

$$k_c = k_{la} k_h k_s \quad (3-25)$$

where k_{la} the correction factor for loading age equal to 0.84 for 28 days moist cured loading age, k_h the correction factor for relative humidity equal to 1.00 for 70% average ambient relative humidity and k_s the size correction factor:

$$k_s = \frac{2}{3} \left(1 + 1.13e^{-0.54V/S} \right) \quad (3-26)$$

where V the volume of concrete and S the surface area of concrete exposed to drying.

For a ratio of the section volume over the concrete area exposed to drying equal to 3.42, k_s is computed to be equal to 0.79, k_c equals 0.66 and C_u equals 1.24. Using Equation (3-23):

$$C_c(180,28) = \frac{(180 - 28)^{0.6}}{10 + (180 - 28)^{0.6}} 1.24 = 0.832$$

The loss in tension due to concrete creep will be calculated at the maximum moment section at mid-span, for the condition of self-weight plus pre-stress. The losses due to concrete creep, $\Delta F_{p,Cc}$, are estimated to be 0.26 kips.

3.6.6 Tendon Stresses after Losses

After having computed both instantaneous and time-dependant losses, the pre-stress level should be estimated at two stages of the considered pre-stressed concrete superstructure. First, an estimate of the pre-stressing forces is needed immediately following transfer of pre-stress which may result from subtracting all instantaneous losses – friction, anchorage set and elastic shortening – from the jacking force:

$$P_{p,tr} = P_j - (\Delta F_{pF} + \Delta F_{pES} + \Delta F_{pA}) \quad (3-27)$$

The second stage requires an estimate of the effective pre-stress after all instantaneous and time-dependant losses have occurred:

$$P_{ef} = P_j - (\Delta F_{pF} + \Delta F_{pES} + \Delta F_{pA}) - (\Delta F_{p,Sc} + \Delta F_{p,Cc}) \quad (3-28)$$

Both the pre-stressing forces at transfer, $P_{p,tr}$ and the effective force, P_{ef} , along the tendon length are tabulated in Table 3-17.

Table 3-17: Total pre-stressing losses and forces after losses along the superstructure's length

Tendon	Distance (in)	P _j (kips)	Losses					P _{p,tr} (kips)	P _{ef} (kips)
			ΔF _{pF} (kips)	ΔF _{pES} (kips)	ΔF _{pA} (kips)	ΔF _{p,Sc} (kips)	ΔF _{p,Cc} (kips)		
T.1, T.10	0.00	30.00	0.00	0.24	5.23	1.32	0.26	24.53	22.95
	120.00		0.06	0.23	4.22			25.49	23.91
	371.25		1.59	0.25	2.13			26.03	24.45
	622.50		3.05	0.23	0.03			26.70	25.12
	742.50		3.10	0.24	0.00			26.65	25.07
T.2, T.9	0.00	30.00	0.00	0.24	5.09	1.32	0.26	24.67	23.09
	120.00		0.72	0.23	4.14			24.91	23.33
	371.25		1.51	0.25	2.15			26.09	24.51
	622.50		2.27	0.23	0.16			27.34	25.76
	742.50		2.94	0.24	0.00			26.82	25.24
T.3, T.8	0.00	30.00	0.00	0.24	5.01	1.32	0.26	24.74	23.16
	120.00		0.58	0.23	4.09			25.11	23.53
	371.25		1.46	0.25	2.16			26.13	24.55
	622.50		2.32	0.23	0.23			27.22	25.64
	742.50		2.85	0.24	0.00			26.90	25.32
T.4, T.7	0.00	30.00	0.00	0.24	5.06	1.32	0.26	24.70	23.12
	120.00		0.43	0.23	4.12			25.22	23.65
	371.25		1.49	0.25	2.15			26.10	24.52
	622.50		2.52	0.23	0.19			27.07	25.49
	742.50		2.91	0.24	0.00			26.85	25.27
T.5, T.6	0.00	30.00	0.00	0.24	5.17	1.32	0.26	24.58	23.00
	120.00		0.28	0.23	4.19			25.30	23.72
	371.25		1.56	0.25	2.14			26.05	24.47
	622.50		2.79	0.23	0.08			26.90	25.33
	742.50		3.04	0.24	0.00			26.72	25.14
T.11-T.14	0.00	30.00	0.00	0.24	1.80	1.32	0.26	27.95	26.37
	120.00		0.06	0.23	1.68			28.03	26.45
	371.25		0.19	0.25	1.43			28.13	26.55
	622.50		0.31	0.23	1.18			28.28	26.70
	742.50		0.37	0.24	1.06			28.32	26.74

According to AASHTO LRFD Bridge Design Specifications [2007] and Table 3-10, the pre-stressing force limit for tendons immediately after anchor set, $P_{p, tr}$, is 28.9 kips (128.6 kN) at anchorages and 30.6 kips (136.1 kN) elsewhere along the member length and away from anchorages whereas; according to Table 3-17 the maximum developed pre-stressing force equals 28.32 kips (126.0 kN). Moreover, the pre-stressing force limit for tendons at Service Limit state after all losses, P_{ef} , is 29.7 kips (132.1 kN) whereas; the maximum developed effective pre-stressing force equals 26.74 kips (118.9 kN).

The tendon geometry along the span is illustrated in Figure 3-7 (plan view and elevation). Due to geometric symmetry of the superstructure, only half of the superstructure's geometry is presented.

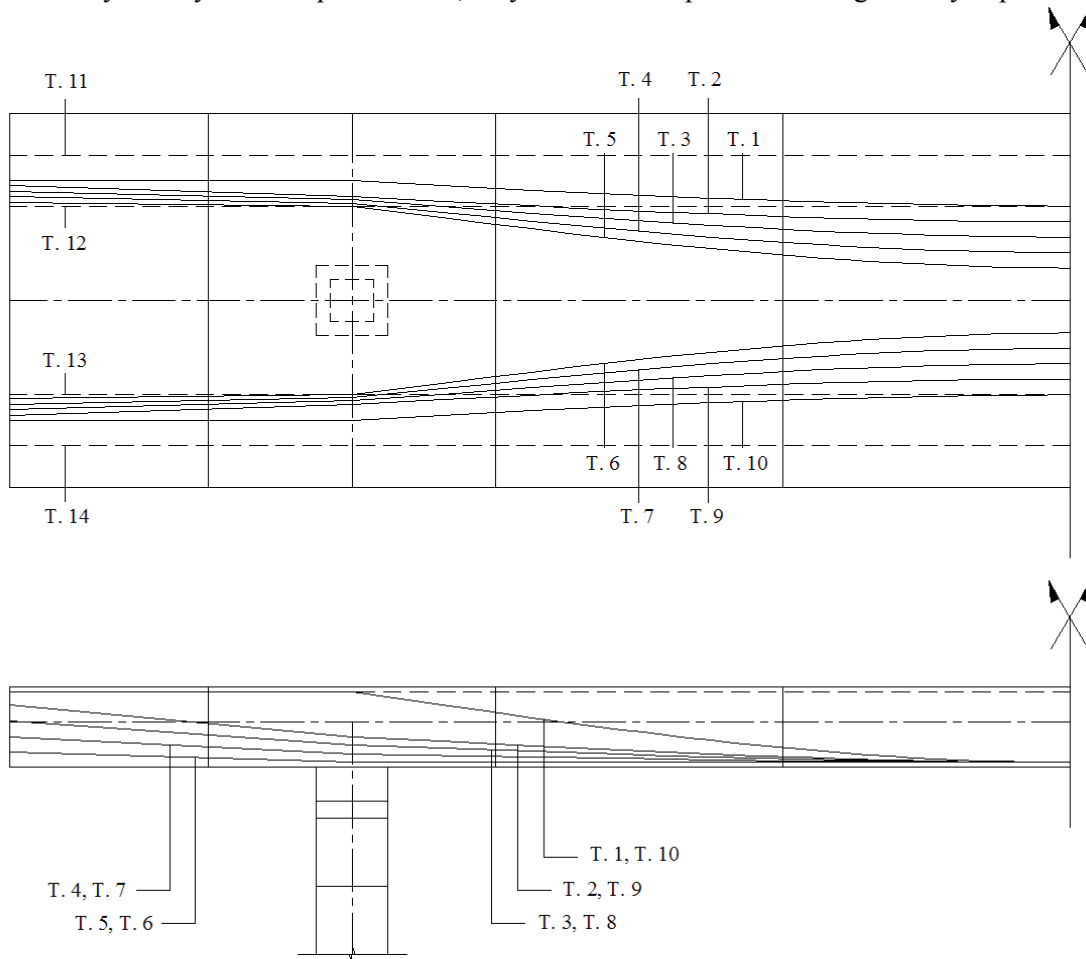


Figure 3-7: Plan and elevation view of tendon geometry along the superstructure

3.7 Service III Limit State

According to AASHTO LRFD Bridge Design Specifications [2007] and Section 3.4, no tensile concrete stress are allowed for fully pre-stressed unbonded components at Service III Limit State.

The maximum developed moments due to Service III load combination are 311 kips-ft (422 kN-m) for the mid-span section and -72 kips-ft (-98 kN-m) for the support, as presented in Table 3-9.

By substituting into Equations (3-6) and (3-7) the values of effective pre-stressing forces P_{ef} and eccentricities e_t or e_b as presented in Table 3-18, S_t equal to 9944 in³ (0.159 m³), A_c equal to 1047 in² (0.67 m²) and S_b equal to 7839 in³ (0.126 m³) the top and bottom concrete stresses along the superstructure's length can be computed. It should be mentioned that e_t and e_b refer to the tendon eccentricity above and below the center of gravity of the superstructure's cross-section, respectively. The concrete stresses due to Service III Limit State are listed in Table 3-19 and it becomes evident that no tensile stresses are developed.

Table 3-18: Tendon effective forces and eccentricities

Location	T.1, T.10			T.2, T.9		
	P_{ef} (kips)	e_t (in)	e_b (in)	P_{ef} (kips)	e_t (in)	e_b (in)
jack end	22.95	10.75	-	23.09	5.95	-
left support	23.91	10.75	-	23.33	-	5.10
mid-span	24.45	-	14.10	24.51	-	14.10
right support	25.12	10.75	-	25.76	-	5.10
dead end	25.07	10.75	-	25.24	5.95	-

Location	T.3, T.8			T.4, T.7		
	P_{ef} (kips)	e_t (in)	e_b (in)	P_{ef} (kips)	e_t (in)	e_b (in)
jack end	23.16	0.45	-	23.12	-	5.05
left support	23.53	-	8.10	23.65	-	11.10
mid-span	24.55	-	14.10	24.52	-	14.10
right support	25.64	-	8.10	25.49	-	11.10
dead end	25.32	0.45	-	25.27	-	5.05

Location	T.5, T.6			T.11, T.14		
	P_{ef} (kips)	e_t (in)	e_b (in)	P_{ef} (kips)	e_t (in)	e_b (in)
jack end	23.00	-	10.55	26.37	10.75	-
left support	23.72	-	14.10	26.45	10.75	-
mid-span	24.47	-	14.10	26.55	10.75	-
right support	25.33	-	14.10	26.70	10.75	-
dead end	25.14	-	10.55	26.74	10.75	-

Table 3-19: Concrete stresses for Service III Limit State

Location	f_t (ksi)	f_b (ksi)
jack end	-0.335	-0.189
left support	-0.116	-0.480
mid-span	-0.370	-0.177
right support	-0.122	-0.512
dead end	-0.357	-0.209

3.8 Service I Limit State

According to the AASHTO LRFD Bridge Design Specifications [2007] and Section 3.4, the compression limit stresses for the service limit state Load Combination I are $0.45f_c'$ due to effective pre-stress and permanent (dead) load and $0.60f_c'$ due to effective pre-stress and permanent and transient loads (all dead loads and live loads). In particular, the compression limit stress is equal to 2.25 ksi (15.5 MPa) due to effective pre-stress and dead load and 3.00 ksi (20.7 MPa) due to effective pre-stress and dead and live loads.

The maximum developed moments due to Service I load combination are 240 kips-ft (325 kips-ft) for the mid-span section and -72 kips-ft (-98 kN-m) for the support accounting for permanent loads whereas; 328 kips-ft (445 kN-m) for the mid-span section and -72 kips-ft (-98 kN-m) for the support, for permanent and transient loads, as presented in Table 3-9.

The concrete stresses due to Service I Limit State are listed in Table 3-20 and it becomes evident that compressive concrete stresses are significantly lower than the corresponding limits.

Table 3-20: Concrete stresses for Service I Limit State

Location	Permanent Loads		Permanent and Transient Loads	
	f_t (ksi)	f_b (ksi)	f_t (ksi)	f_b (ksi)
jack end	-0.335	-0.189	-0.335	-0.189
left support	-0.116	-0.480	-0.116	-0.480
mid-span	-0.284	-0.285	-0.390	-0.151
right support	-0.122	-0.512	-0.122	-0.512
dead end	-0.357	-0.209	-0.357	-0.209

3.9 Strength I Limit State

The flexural resistance of the superstructure's mid-span cross-section is computed based on the approach developed in AASHTO LRFD Bridge Design Specifications [2007] for flexural members with unbonded tendons.

The average stress in the unbonded steel may be taken as:

$$f_{ps} = f_{ef} + 914 \left(\frac{d_p - c}{l_e} \right) \leq f_{py} \quad (3-29)$$

$$l_e = \frac{2l_i}{2 + N_s} \quad (3-30)$$

where f_{ef} the effective stress in pre-stressing steel at section under consideration after all losses, d_p the distance from extreme compression fiber to the centroid of the pre-stressing tendons, c the distance from extreme compression fiber to the neutral axis assuming that the tendon pre-stressing steel has yield, l_e the effective tendon length, f_{py} the yield strength of pre-stressing steel, l_i the length of tendon between anchorages and N_s the number of support hinges crossed by the tendon between anchorages.

In addition, the standard assumption of concrete stresses at ultimate flexure being represented by a rectangular stress block is adopted, with the intensity equal to $0.85f_c'$ and the depth equal to β_1c where β_1 is a coefficient equal to 0.80 for the specified concrete strength.

Given the complexity of the superstructure cross-section geometry, its nominal flexural resistance, M_n , is computed using the Strain Compatibility approach, the basis of which lays on maintaining equilibrium between the sum of steel tension forces and concrete compression forces developed in the cross-section. The process is iterative because both steel stresses and depth of the neutral axis are unknown, as shown in Equation (3-29).

The maximum developed moments due to Strength I load combination are 467 kips-ft (633 kN-m) for the mid-span section and -95 kips-ft (-129 kN-m) for the support, as presented in Table 3-9. Moreover, f_{py} equals 243 ksi (1675 MPa), l_i equals 742.5 in (18.86 m) and N_s equals 2 and; using Equation (3-30) l_e equals 371.3 in (9.43 m).

Given that only the pre-stressing reinforcement connects the superstructure segments, it is the only reinforcement to be considered for the calculation of the flexural resistance of the superstructure whereas; non-prestressing reinforcement is neglected.

Regarding the superstructure's mid-span section, the neutral axis c is assumed to be lying in the top plate of the cross-section. An iterative procedure is followed and a value of c equal to 0.87 inches (22.3 mm) is obtained.

Based on Equation (3-29), the stresses in the unbonded pre-stressing steel are listed in Table 3-21 and result to a sum of tensile pre-stressing steel forces equal to 395.61 kips (1760 kN) for Strength I Limit State.

Table 3-21: Flexural resistance of superstructure at mid-span for Strength I limit state

Tendon	P_{ef} (kips)	f_{ef} (ksi)	d_{pi} (in)	#	f_{ps} (ksi)	P_{ps} (kips)
T.1	24.45	159.8	26.60	1	223.1	34.13
T.2	24.51	160.2	26.60	1	223.5	34.20
T.3	24.55	160.4	26.60	1	223.7	34.23
T.4	24.52	160.3	26.60	1	223.6	34.21
T.5	24.47	160.0	26.60	1	223.3	34.16
T.6	24.47	160.0	26.60	1	223.3	34.16
T.7	24.52	160.3	26.60	1	223.6	34.21
T.8	24.55	160.4	26.60	1	223.7	34.23
T.9	24.51	160.2	26.60	1	223.5	34.20
T.10	24.45	159.8	26.60	1	223.1	34.13
T.11, T.14	26.55	173.5	1.75	2	175.7	26.88
Sum	-	-	-	12	-	395.61

The total compressive concrete force, P_c , equals 395.99 kips (1761 kN) given that f'_c equals 5.0 ksi (34.5 MPa), c equals 0.87 in (22.3 mm) and b_t equals 132.35 in (3.34 m) and:

$$P_c = (0.85 \cdot f'_c)(0.80 \cdot c)b_t \quad (3-31)$$

Based on the above, the nominal flexural capacity, M_n , of the superstructure's cross-section at mid-span equals 754 kips-ft (1022 kN-m). Assuming a resistance factor, ϕ , equal to 0.90 for flexural components with unbonded tendons, the factored flexural resistance, M_r , equals 679 kips-ft (921 kN-m) which is greater than the maximum developed moment at mid-span due to Strength I load combination that equals 467 kips-ft (633 kN-m).

The same procedure is followed for the superstructure's support sections. The neutral axis c is assumed to be lying in the bottom plate of the cross-section and a value of c equal to 1.54 inches (39.4 mm) is obtained following an iterative process.

Based on Equation (3-29), the stresses in the unbonded pre-stressing steel are listed in Table 3-22 and result to a sum of tensile pre-stressing steel forces equal to 370.15 kips (1646 kN) for Strength I Limit State.

Table 3-22: Flexural resistance of superstructure at supports for Strength I limit state

Tendon	P_{ef} (kips)	f_{ef} (ksi)	d_{pi} (in)	#	f_{ps} (ksi)	P_{ps} (kips)
T.1	23.91	156.3	1.75	1	156.8	23.99
T.2	23.33	152.5	17.60	1	192.0	29.38
T.3	23.53	153.8	20.60	1	200.7	30.70
T.4	23.65	154.5	23.60	1	208.9	31.95
T.5	23.72	155.1	26.60	1	216.8	33.16
T.6	23.72	155.1	26.60	1	216.8	33.16
T.7	23.65	154.5	23.60	1	208.9	31.95
T.8	23.53	153.8	20.60	1	200.7	30.70
T.9	23.33	152.5	17.60	1	192.0	29.38
T.10	23.91	156.3	1.75	1	156.8	23.99
T.11, T.14	26.45	172.9	26.60	2	234.6	35.89
Sum	-	-	-	12	-	370.15

The total compressive concrete force, P_c , equals 370.01 kips (1646 kN) by substituting into Equation (3-31) f_c' equal to 5.0 ksi (34.5 MPa), c equal to 1.54 in (39.4 mm) and b_b equal to 70.85 in (1.80 m).

Based on the above, the nominal flexural capacity, M_n , of the superstructure's cross-section at the supports equals 611 kips-ft (828 kN-m). Assuming a resistance factor, ϕ , equal to 0.90 for flexural components with unbonded tendons, the factored flexural resistance, M_r , equals 550 kips-ft (746 kN-m) which is significantly greater than the maximum developed moment at mid-span due to Strength I load combination that equals 95 kips-ft (129 kN-m).

3.10 Extreme Event I Limit State

3.10.1 Vertical Earthquake Load

The maximum developed moments due to Extreme Event I Limit State and vertical earthquake loading are 456 kips-ft (618 kN-m) for the mid-span section and -124 kips-ft (-168 kN-m) for the support, as presented in Table 3-9.

According to Section 3.9, the factored flexural resistance, M_r , of the superstructure's cross-section equals 679 kips-ft (921 kN-m) for the mid-span and 550 kips-ft (746 kN-m) for the support sections, which are greater than the maximum developed moments due to the considered loads.

3.10.2 Horizontal Transverse Earthquake Load

The flexural resistance of the superstructure's cross-section is computed under a horizontal transverse earthquake loading. Following the same procedure as the one described in Section 3.9 and considering as critical section the mid-span one, the factored flexural resistance, $M_{r,y}$, of the superstructure's cross-section is computed to be equal to 1780 kips-ft (2413 kN-m).

3.11 Reinforcement Limits

According to AASHTO LRFD Bridge Design Specifications [2007], at any section of a flexural component the amount of pre-stressed and non-prestressed tensile reinforcement shall be adequate to develop a factored flexural resistance, M_r , at least equal to the lesser of 1.20 times the cracking strength, M_{cr} , determined on the basis of elastic stress distribution and the modulus of rupture, f_r , and 1.33 times the factored moment required by the applicable strength load combination.

The cracking moment, M_{cr} , is defined as:

$$M_{cr} = S_c (f_r + f_{cpe}) - M_{dnc} \left(\frac{S_c}{S_{nc}} - 1 \right) \geq S_c f_r \quad (3-32)$$

where f_{cpe} the compressive stress in concrete due to effective pre-stress forces only (after allowance for all pre-stress losses) at extreme fiber of section where tensile stress is caused by externally applied loads, M_{dnc} the total unfactored dead load moment acting on the monolithic or non-composite section, S_c the section modulus for the extreme fiber of the composite section where tensile stress is caused by externally applied loads, S_{nc} the section modulus for the extreme fiber of the monolithic or non-composite section where tensile stress is caused by externally applied loads and f_r the modulus of rupture.

For the case of monolithic sections Equation (3-32) reduces to:

$$M_{cr} = S_c (f_r + f_{cpe}) \geq S_c f_r \quad (3-33)$$

$$f_r = 0.24 \sqrt{f'_c} \quad (3-34)$$

The calculations regarding the critical mid-span section of the superstructure are performed hereafter. Given that S_b equals 7839 in³ (0.126 m³), f_r equals 0.537 ksi (3.70 MPa) and f_{cpe} equals 0.653 ksi (4.50 MPa) according to Section 3.7, M_{cr} is computed to be equal to 777 kips-ft (1053 kN-m).

In order to compute the flexural resistance, M_r , of the superstructure's cross-section at mid-span, the number and distance of pre-stressing and non-prestressing reinforcement from the cross-section's extreme fiber in tension needs to be specified. The Strain Compatibility approach is used and the strain at each layer of non-prestressing reinforcement is computed assuming that the maximum concrete compressive strain is 0.003. On the other hand, the stresses developed in the pre-stressing reinforcement are computed as described in Section 3.9.

The diameter of non-prestressing reinforcement is selected to be 3/8" (9.53 mm) for #3 bars whereas; their yielding stress is 60 ksi (414 MPa).

Assuming that the neutral axis, c , is lying in the top plate of the superstructure's cross-section at mid-span, a value of 1.82 inches (46.2 mm) is obtained. Moreover, the nominal flexural capacity, M_n , of the superstructure's cross-section at mid-span equals 1032 kips-ft (1399 kN-m) and assuming a resistance factor, ϕ , equal to 0.90 for flexural components with unbonded tendons, the factored flexural resistance, M_r , equals 928 kips-ft (1258 kN-m).

Based on the above and given that the factored moment at mid-span due to Strength I load case is 467 kips-ft:

$$M_r = 928 > \min\{1.2 \cdot 777, 1.33 \cdot 467\} = \min\{932, 621\} = 621 \text{ kips-ft}$$

Consequently, the amount of pre-stressed and non-prestressed tensile reinforcement is considered to be adequate according to AASHTO LRFD Bridge Design Specifications [2007].

The reinforcement details of the superstructure test unit – pre-stressing strands and mild reinforcement - are presented in Appendix A.

The superstructure test specimen, designed according to AASHTO LRFD Bridge Design Specifications [2007] and PCI Bridge Design Manual [2003], will be used to develop a two-dimensional analytical model. In Chapters 5 and 6, the numerical model will be analyzed under a series of vertical seismic excitations of different intensities using non-linear dynamic analysis methods.

SECTION 4

SUBSTRUCTURE DESIGN

The substructure of the bridge model, as described in Section 2.5, is designed hereafter according to AASHTO LRFD Bridge Design Specifications [2007] and PCI Bridge Design Manual [2003].

The piers are considered to act as cantilevers with a fixed support between the pier's end segment and the foundation block. The cap beams, piers and foundation blocks are post-tensioned together whereas; the superstructure is simply supported on the cap beams. Following the AASHTO LRFD [2007] specifications, the piers are considered to behave as continuous members and the code provisions for segmentally constructed bridges are employed for their design. The geometry of the design model is illustrated in Figure 4-1 and Figure 4-2.

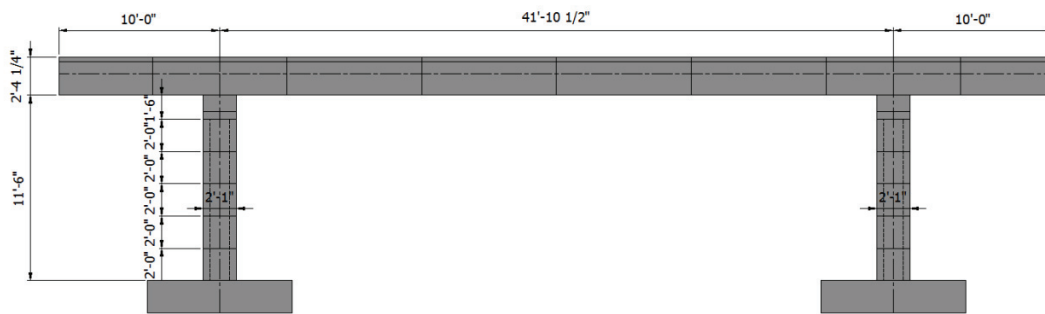


Figure 4-1: Longitudinal elevation of bridge test model

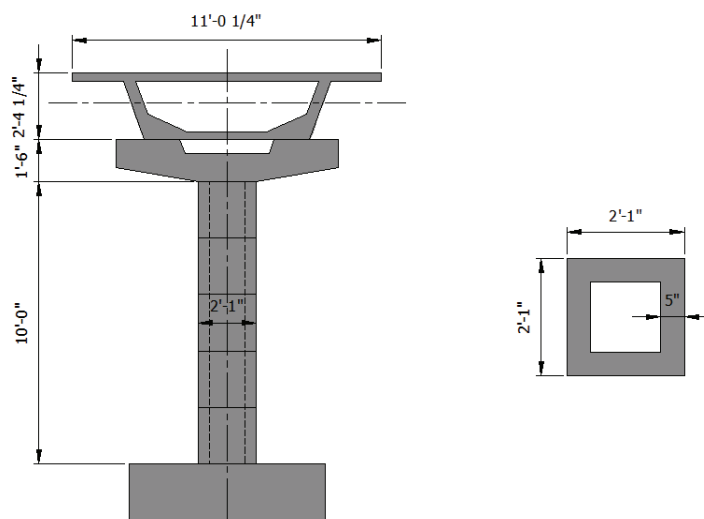


Figure 4-2: Transverse elevation of bridge test model and pier cross-section

4.1 Material Properties

The material properties used for the design of the bridge's substructure match the ones used for the design of its superstructure, as described in Section 3.1. For the post-tensioning of the piers, the same mono-strand system as the one used for the pre-stressing of the superstructure has been selected [DYWIDAG DSI, 2009]. The diameter of the strand is 0.6" (15.2 mm) and the strand is sheathed inside a high density polyethylene duct having a diameter of approximately 1" (25.4 mm).

The key concept of incorporating post-tensioned internal unbonded tendons acting as the continuous reinforcement between the pier segments is incorporated in the design as for the case of the bridge's superstructure (see Section 3.1). Neither shear keys nor epoxied joints are considered between the pier's segments.

The material properties used in the design of the piers are summarized in Table 3-1.

Table 4-1: Design material properties [AASHTO, 2007]

Material	Property	Symbol	Value
Concrete	Compression strength (28 days)	f_c'	5000 psi (34.5 MPa)
	Unit weight	w_c	150 lbs/ft ³ (2403 kg/m ³)
	Modulus of elasticity	E_c	4287 ksi (29.6 GPa)
Pre-stressing Strands	Strand diameter	D_p	0.6 in (15.24 mm)
	Strand area	A_{sp}	0.217 in ² (134.00 mm ²)
	Ultimate strength	F_{pu}	58.6 kips (260.7 kN)
	Yield strength	F_{py}	52.7 kips (234.4 kN)
	Modulus of elasticity	E_p	28500 ksi (196.5 GPa)
Reinforcing Bars	Yield stress	f_y	60 ksi (414 MPa)
	Modulus of elasticity	E_s	29000 ksi (200 GPa)

4.2 Section Properties

The geometry of the pier cross-section is illustrated in Figure 4-2 and the cross-sectional properties used for the design are summarized in Table 4-2.

Table 4-2: Pier cross-section properties

Property	Symbol	Value
Area	A_c	400 in ² (0.26 m ²)
Depth	h	25.0 in (635 mm)
Width	b	25.0 in (635 mm)
Thickness	t_i	5.0 in (127 mm)
Height	H	120.0 in (3.05 m)
Moment of inertia	I	28333 in ⁴ (0.012 m ⁴)

4.3 Design Loads

4.3.1 Dead Loads

The dead loads acting on the piers include the superstructure self-weight (DC), the permanent loads from barriers and future surfacing (DW) acting on the superstructure and the self-weight of the cap beams (DC). According to Section 3.2.1 and Table 3-3, the uniform load resulting from the superstructure self-weight and the permanent loads from barriers and future surfacing equal 1.09 kips/ft (15.92 kN/m) and 0.33 kips/ft (4.82 kN/m), respectively. The geometry of the cap beams is illustrated in Sideris et al. [2010] and its weight is approximately 3.8 kips (1.7 ton).

The loads and the corresponding member forces are presented in Table 4-3.

4.3.2 Live Loads

The live loads acting on the superstructure of the bridge model are described in detail in Section 3.2.2 and Table 3-4.

The member forces resulting from the applied live loads on the piers are presented in Table 4-4.

Table 4-3: Member forces due to dead loads

Load Case	Load Value	Axial Force
Superstructure self-weight, <i>DC</i>	1.09 kips/ft (15.92 kN/m)	33.8 kips (150.3 kN)
Barriers and surfacing, <i>DW</i>	0.33 kips/ft (4.82 kN/m)	10.1 kips (44.9 kN)
Cap beam self-weight, <i>DC</i>	3.8 kips (16.9 kN)	3.8 kips (16.9 kN)

Table 4-4: Member forces due to live loads

Load Case	Load Value	Axial Force
Design Truck, <i>LL</i>	0.59/ 2.35 kips (2.62/ 10.45 kN)	2.9 kips (12.9 kN)
Design Lane, <i>LL</i>	0.11 kips/ft (1.61 kN/m)	2.4 kips (10.7 kN)

4.3.3 Earthquake Loads

Earthquake loads as defined in AASHTO LRFD Bridge Design Specifications [2007] are given by the product of the elastic seismic coefficient C_{sm} and the equivalent weight of the structural system.

Each pier is designed as a cantilever with a concentrated earthquake load at its top. The method of analysis to be used is the Uniform Load Method which is based on the corresponding fundamental mode of vibration of the bridge. The period of this mode is taken as that of an equivalent single mass-spring oscillator whereas; the stiffness of this equivalent spring is calculated using the maximum displacement that occurs when an arbitrary uniform lateral load is applied to the bridge structure. The elastic seismic coefficient, C_{sm} , is used to calculate the equivalent uniform seismic load from which seismic force effects are found.

The Uniform Load Method is described in detail in Section 3.2.3. The elastic seismic response coefficient C_{sm} , as defined in Equation (3-3), is illustrated in Figure 3-4 for both the prototype and scaled bridge model.

The following loads are considered for computing the seismic mass acting on each pier: the self-weight of the superstructure (see Table 3-3); the permanent loading from the barriers and future surfacing acting on the superstructure (see Table 3-3); 30 percent of the design lane live load acting on the superstructure (see Table 3-4); the self-weight of the cap beams (see Table 4-3) and 50 percent of the self-weight of each pier equal to 2.1 kips (0.95 ton). The total considered weight, W , acting on each pier equals 50.5 kips (22.4 tons).

The static displacement at the top of each pier due to a horizontal unit point load (1 kip = 4.448 kN) is equal to 0.01 inches (0.25 mm). Consequently, the stiffness of the piers, K , equals 1201 kips/ft (17527 kN/m). Given that the total considered weight, W , is 50.5 kips (22.4 tons) and g equals 32.17 ft/sec² (9.81 m/sec²), the pier's fundamental period of vibration under horizontal earthquake loading, T_1 , is computed to be 0.227 seconds.

Based on Equation (3-3), the elastic seismic response coefficient, C_{sm} , due to horizontal earthquake loading is:

$$C_{sm} = \frac{1.2 \cdot (0.25 \cdot 2.39) \cdot 1.2}{0.227^{2/3}} = 2.31 > 2.5 \cdot (0.25 \cdot 2.39) = 1.49 \Rightarrow C_{sm} = 1.49$$

The equivalent static horizontal earthquake load, P_e , acting on the pier equals 75.30 kips (335.0 kN).

According to AASHTO LRFD Bridge Design Specifications [2007], the design seismic loads result from the elastic seismic loads divided by the response modification factor, R . For single bridge columns the response modification factor, R , equals to 1.5, 2.0 and 3.0 for 'critical', 'essential' and 'other' importance bridge categories, respectively. According to Section 3.2.3, an overall R -factor equal to 2.50 is selected for the segmental bridge system described in this study. Considering the case of a 'critical' importance bridge category, the response modification factor for the case of segmental bridge columns with internal unbonded tendons will be:

$$R = 1.5 \cdot 2.5 = 3.75 \quad (4-1)$$

The design horizontal earthquake load, P_d , acting on the pier will therefore be:

$$P_d = \frac{P_e}{R} = \frac{75.30}{3.75} = 20.08 \text{ kips (89.3 kN)} \quad (4-2)$$

Table 4-5 summarizes the considered design parameters for the bridge's substructure under horizontal earthquake loading.

The section forces resulting from the application of the design horizontal earthquake loading on the piers are presented in Table 4-6. In order to calculate the design moment at the base of the piers, the height between the superstructure's center of gravity and the base of the pier including the height of the cap beam is considered. The total considered height equals 153.85 inches (3.9 m).

The section forces resulted from all considered load cases are summarized in Table 4-7.

Table 4-5: Uniform Load Method design parameters for horizontal earthquake loads

Parameter	Symbol	Vertical EQ
Maximum static displacement,	v_{max}	0.01 in (0.25 mm)
Stiffness,	K	1201 kips/ft (17527 kN/m)
Model fundamental period,	T_1	0.227 sec
Elastic seismic response coefficient,	C_{sm}	1.49
Equivalent static earthquake loading,	P_e	75.30 kips (335.0 kN)
Design earthquake load,	P_d	20.08 kips (89.3 kN)

Table 4-6: Member forces due to horizontal earthquake loads

Load Case	Load Value	Moment	Shear Force
Horizontal EQ, EQ_h	20.08 kips (89.3 kN)	257 kips-ft (348 kN-m)	20.1 kips (89.3 kN)

Table 4-7: Member forces due to considered load cases

Load Case	Axial Force	Moment	Shear Force
Superstructure self-weight, DC	33.8 kips (150.3 kN)	- -	- -
Barriers and surfacing, DW	10.1 kips (44.9 kN)	- -	- -
Cap beam self-weight, DC	3.8 kips (16.9 kN)	- -	- -
Design Truck, LL	2.9 kips (12.9 kN)	- -	- -
Design Lane, LL	2.4 kips (10.7 kN)	- -	- -
Horizontal EQ, EQ_h	- -	257 kips-ft (348 kN-m)	20.1 kips (89.3 kN)

4.4 Design Load Combinations

According to the AASHTO LRFD Bridge Design Specifications [2007], bridge components and connections should be designed in order to satisfy the Service I, Service III, Strength I and Extreme Event I limit states, as described in Section 3.3.

The load factors for the various load combinations are presented in Table 3-8 whereas; the member forces for all considered load combinations are summarized in Table 4-8.

A preliminary design is conducted in order to compute the number of tendons and their geometry along the pier length. Afterwards, all time dependant and non-dependant losses due to pre-stressing are computed as well as, the stresses and section forces developed along the pier length for all considered load combinations and compared to the design limit states ones.

The stress limits for the pre-stressing tendons and concrete are presented in Section 3.4, according to AASHTO LRFD Bridge Design Specifications [2007] and PCI Bridge Design Manual [2003].

Table 4-8: Member forces due to considered load combinations

Load Combination	Axial Force	Moment	Shear Force
Service I	53.9 kips (239.8 kN)	- -	- -
Service III	52.6 kips (234.0 kN)	- -	- -
Strength I (max)	71.3 kips (317.2 kN)	- -	- -
Extreme Event I, Horizontal EQ Load (max)	64.7 kips (287.8 kN)	257 kips-ft (348 kN-m)	20.1 kips (89.3 kN)

4.5 Preliminary Design

For pre-stressing the precast pier segments, continuous straight unbonded tendons are used. The strands are anchored in the footings and extend to the pier caps. Eight mono-strand tendons [DYWIDAG DSI, 2009] with a 0.6” diameter are used along the pier’s length, as illustrated in Figure 4-3.

The design of the piers will be governed by the jacking force, P_j , and the effective pre-stressing force, P_e of the tendons. According to AASHTO LRFD Bridge Design Specifications [2007] and Table 3-10, the effective tendon limit stress at Service limit states, after all losses, is $0.80f_{py}$. A more conservative value is recommended by the mono-strand manufacturers [DYWIDAG DSI, 2009], equal to $0.65F_{pu}$ assuming that 35 percent of total losses. Based on the second approach, the effective pre-stressing force is initially assumed to be equal to $0.65F_{pu}$ or 38.1 kips/strand (169.4 kN/strand) and the maximum jacking force equals $0.80F_{pu}$ or 46.9 kips/strand (208.6 kN/strand) [DYWIDAG DSI, 2009].

The pier's preliminary design will be governed by the flexural resistance of the cross-section under the Extreme Event I load combination. The calculations are presented hereafter.

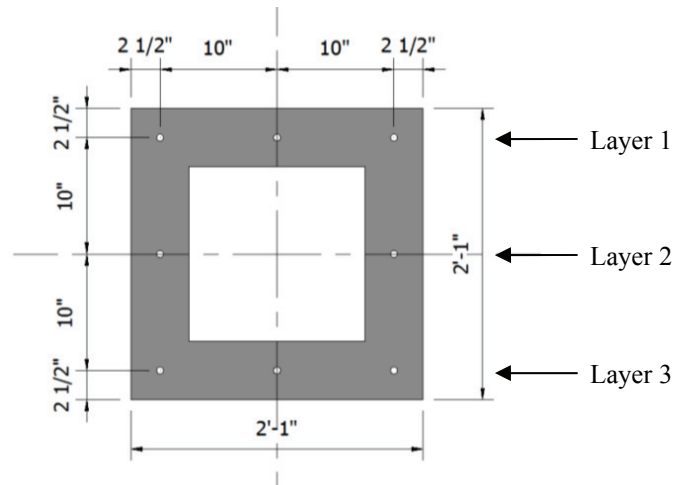


Figure 4-3: Pier cross-section and tendon configuration

4.5.1 Extreme Event I Limit State

The flexural resistance of the pier cross-section is computed based on the approach developed in AASHTO LRFD Bridge Design Specifications [2007] for flexural members with unbonded tendons. The average stress in the unbonded steel, the concrete stresses and the nominal flexural resistance, M_n , of the pier cross-section are computed according to Section 3.9.

The maximum developed moment due to Extreme Event I load combination is 257 kips-ft (348 kN-m) for the fixed cantilever end, as tabulated in Table 4-8. Moreover, f_{py} equals 243 ksi (1675 MPa), l_t equals 120.0 inches (3.05 m) and N_s equals zero and; using Equation (3-30) l_e equals 120.0 inches (3.05 m).

The pre-stressing reinforcement is the only reinforcement to be considered for the calculation of the flexural resistance of the piers; non-prestressing reinforcement is neglected.

Initially, an assumption on the neutral axis c is made and an iterative procedure is followed until equilibrium of forces is satisfied. A value of c equal to 5.01 inches (127.3 mm) is obtained.

Based on Equation (3-29), the stresses in the unbonded pre-stressing steel are presented in Table 4-9 and result to a sum of tensile pre-stressing steel forces equal to 360.9 kips (1605.5 kN) for Extreme Event I Limit State.

The total compressive concrete force, P_c , equals 425.7 kips (1893.6 kN) by substituting into Equation (3-31) f_c' equal to 5.0 ksi (34.5 MPa), c equal to 5.01 inches (127.3 mm) and b equal to 25 inches (0.63 m).

Table 4-9: Pier flexural resistance for Extreme Event I limit state

Tendon	P_e (kips)	f_{ef} (ksi)	d_{pi} (in)	#	f_{ps} (ksi)	P_{ps} (kips)
Layer 1	38.1	175.5	2.50	3	156.4	101.8
Layer 2	38.1	175.5	12.50	2	232.5	100.9
Layer 3	38.1	175.5	22.50	3	243.0	158.2
Sum	-	-	-	8	-	360.9

Finally, the maximum developed axial force due to Extreme Event I load combination is 64.7 kips (287.8 kN), as presented in Table 4-8. Based on the above, the nominal flexural capacity, M_n , of the pier cross-section equals 419 kips-ft (568 kN-m). Assuming a resistance factor, ϕ , equal to 0.90 for flexural components with unbonded tendons, the factored flexural resistance, M_r , equals 377 kips-ft (511 kN-m) which is greater than the maximum developed moment due to Extreme Event I load combination that equals 257 kips-ft (348 kN-m).

4.5.2 Tendon Geometry

Based on the above calculations and the requirements of the AASHTO LRFD Bridge Design Specifications [2007] concerning the minimum vertical and horizontal clear spacing between the ducts, the tendons are distributed in the cross-section as shown in Figure 4-3. The tendons follow a straight path along the pier length.

4.5.3 Slenderness Effects

For concrete columns that undergo appreciable lateral deflections resulting from combinations of vertical or vertical and lateral loads force effects should be determined. A slenderness ratio is defined as Kl_u/r where K the effective length factor, l_u the unbraced length of the member and r the radius of gyration of the member.

According to AASHTO LRFD Bridge Design Specifications [2007] and for members not braced against sideways, the effects of slenderness may be neglected where the slenderness ratio is less than 22. Otherwise, the member's factored moments should be increased to reflect effects of large deformations. It should be noted that these procedures were developed for reinforced concrete columns but are currently used for pre-stressed concrete columns as well.

Considering the pier as a cantilever fixed at its interface with the foundation block, the effective length factor, K , is set equal to 2.10. The unbraced length, l_u , equals 120.0 inches (3.05 m) and the radius of gyration, r , equals 8.42 inches (214 mm) given that I equals 28333 in⁴ (0.012 m⁴) and A_c equals 400 in² (0.26 m²). As a result, the slenderness ration is computed as:

$$\frac{Kl_u}{r} = \frac{2.10 \cdot 120}{8.42} = 30 > 22$$

For a slenderness ratio equal to 30, the piers may be considered slightly slender and according to AASHTO LRFD Bridge Design Specifications [2007] the large deformation effects should be taken under consideration. However given that the piers are constructed by precast post-tensioned segments and the slenderness ratio of the corresponding monolithic member is relatively low, large deflection analysis is not considered in this study.

Moreover, the wall slenderness ratio of a hollow rectangular cross-section, λ_w , shall be taken as:

$$\lambda_w = \frac{X_u}{t} \quad (4-3)$$

where X_u is the clear length of the constant thickness portion of a wall between other walls or fillets between walls and t the thickness of the wall.

Given that X_u equals 15.0 inches (381 mm) and t equals 5.0 inches (127 mm), the wall slenderness ratio is equal to 3.0 and consequently the equivalent rectangular stress block method may be used for the design of the section based on a compression strain of 0.003 [AASHTO, 2007].

4.6 Prestress Loss Estimation

The total prestress losses in post-tensioned members, as defined in AASHTO LRFD Bridge Design Specifications [2007], are calculated according to Section 3.6 and Equation (3-10). The detailed calculations are presented hereafter.

4.6.1 Losses due to Friction

The tendon losses due to friction are computed according to Section 3.6.1 at three points: jacking end, mid-span and dead end. The results are presented in Table 4-10.

Table 4-10: Losses due to friction along the tendons' length

Tendon	P_j (kips)	θ_i (rad)	x (in)	ΔF_{pF} (kips)	$P_{i,pF}$ (kips)	$P_{i,av}$ (kips)	Elongation (in)
Layers 1, 2, 3	46.0	0.000	0.00	0.00	46.00		
		0.000	60.00	0.05	45.95	45.98	0.45
		0.000	120.00	0.09	45.91	45.93	1.45
							0.89

4.6.2 Losses due to Elastic Shortening

The tendon losses due to elastic shortening of the member are calculated using Equation (3-15) and Section 3.6.2. The ratio $(N-1/2N)$ is assumed to be equal to 0.50 whereas A_{ps} equals 1.74 in² accounting for eight tendons, A_c equals 400 in², E_c equals 4287 ksi, E_p equals 28500 ksi, f_{pb} equals 218.7 ksi, I equals 28333 in⁴ and M_g equals to zero.

Using Equation (3-15), the losses due to elastic shortening, Δf_{pES} , are estimated to be 3.07 ksi or 0.67 kips.

4.6.3 Losses due to Anchorage Set

Losses due to anchorage set will be computed based on the recommendations of PCI Bridge Design Manual [2003]. According to Section 3.6.3, an average value of anchor set, w , equal to 0.375 inches (9.525 mm) is chosen.

The loss of the pre-stressing force due to anchorage set can be calculated as:

$$\Delta F_{pA} = \frac{wE_p}{L} \quad (4-4)$$

For E_p equal to 28500 ksi and L equal to 120 in, the losses due to tendon anchorage set, Δf_{pAs} , are estimated to be 89.06 ksi or 19.33 kips.

4.6.4 Losses due to Concrete Shrinkage

The losses due to concrete shrinkage are computed according to Section 3.6.4. For a ratio of the section volume over the concrete area exposed to drying, V/S , equal to 4.00, k_s is computed to be equal to 0.74, k_{sh} equals 0.64 and S_u equals 0.35%. Using Equation (3-18) and (3-22):

$$S_c(180,28) = \frac{(180 - 28)}{35 + (180 - 28)} \cdot 0.35 \cdot 10^{-3} = 0.28 \cdot 10^{-3}$$

$$\Delta f_{p,Sc} = S_c E_p = 8.06 \text{ ksi}$$

The losses due to concrete shrinkage, $\Delta F_{p,Sc}$, are estimated to be 1.75 kips.

4.6.5 Losses due to Concrete Creep

The losses due to concrete shrinkage are computed according to Section 3.6.5. For a ratio of the section volume over the concrete area exposed to drying, V/S , equal to 4.00, k_s is computed to be equal to 0.75, k_c equals 0.63 and C_u equals 1.19. Using Equation (3-23):

$$C_c(180,28) = \frac{(180 - 28)^{0.6}}{10 + (180 - 28)^{0.6}} \cdot 1.19 = 0.798$$

The losses due to concrete creep, $\Delta f_{p,Cc}$, are estimated to be 3.64 ksi or 0.79 kips.

4.6.6 Tendon Stresses after Losses

After having computed both instantaneous and time-dependant losses, the pre-stress level of the piers should be estimated at two stages. First, an estimate of the pre-stressing forces immediately following transfer of pre-stress is needed according to Equation (3-27) and; the second stage requires an estimate of the effective prestress after all instantaneous and time-dependant losses have occurred according to Equation (3-28). Both the pre-stressing forces at transfer, $P_{p,tr}$ and the

effective force, P_{ef} , along the tendon length are presented in Table 4-11. The tendon geometry is shown in Figure 4-3.

Table 4-11: Total pre-stressing losses and forces after losses along the pier's length

Tendon	Distance (in)	P_j (kips)	Losses					$P_{p,tr}$ (kips)	P_e (kips)
			ΔF_{pF} (kips)	ΔF_{pES} (kips)	ΔF_{pA} (kips)	$\Delta F_{p,Sc}$ (kips)	$\Delta F_{p,Cc}$ (kips)		
Layers 1, 2, 3	0.00	46.0	0.00	0.67	19.33	2.26	0.79	26.01	23.47
	60.00		0.05					25.96	23.42
	120.00		0.09					25.92	23.38

According to AASHTO LRFD Bridge Design Specifications [2007] and Table 3-10, the pre-stressing force limit for tendons immediately after anchor set, $P_{p,tr}$, is 41.0 kips (182.4 kN) at anchorages and 43.4 kips (193.1 kN) elsewhere along the member length and away from anchorages whereas; according to Table 4-11 the maximum developed pre-stressing force equals 26.01 kips (115.7 kN). Moreover, the pre-stressing force limit for tendons at Service Limit state after all losses, P_e , is 42.2 kips (187.7 kN) whereas; the maximum developed effective pre-stressing force equals 23.47 kips (104.4 kN).

4.7 Service III Limit State

The concrete stress at any post-tensioned member, f_c , can be computed by superimposing axial and bending effects due to the applied pre-stress force and the dead and live loads [Nilson, 1978]:

$$f_c = -\frac{N_u + \sum P_e}{A_c} \pm \frac{\sum P_e e_i}{S_c} \mp \frac{M_u}{S_c} \quad (4-5)$$

where N_u is the axial load at the specific location due to the considered load combination, P_e is the effective prestress force acting on the cross-section, A_c is the pier cross-section area, e_i the strand eccentricity from the center of gravity of the cross-section, S_c the pier's modulus, and M_u the total moment at the specific location due to the considered load combination.

According to AASHTO LRFD Bridge Design Specifications [2007] and Section 3.4, no tensile concrete stress are allowed for fully pre-stressed unbonded components at Service III Limit State.

As summarized in Table 4-8, no flexural moments are developed along the pier length due to Service III load combination.

By substituting into Equation (4-5) the eccentricities, e_i , as presented in Table 4-12; the effective pre-stressing forces, P_e , as presented in Table 4-11; S_c equal to 2267 in³ (0.037 m³) and A_c equal to 400 in² (0.26 m²), the concrete stresses along the pier's length can be computed. The concrete stresses due to Service III Limit State are tabulated in Table 4-13 and it becomes evident that no tensile stresses are developed.

Table 4-12: Tendon geometry and eccentricities

Tendon	e_i (in)	#
Layer 1	10.0	3
Layer 2	0.0	2
Layer 3	10.0	3

Table 4-13: Concrete stresses for Service III limit state

Location	Distance (in)	P_e (kips)	N_u (kips)	M_u (kips-in)	f_c (ksi)
Jack end	0.00	23.47	48.45	0.0	-0.591
Mid-section	60.00	23.42	50.53	0.0	-0.595
Dead end	120.00	23.38	52.62	0.0	-0.599

4.8 Service I Limit State

According to the AASHTO LRFD Bridge Design Specifications [2007] and Section 3.4, the compression limit stresses for Service I load combination are $0.45f_c'$ due to effective prestress and permanent (dead) load and $0.60f_c'$ due to effective prestress and permanent and transient loads (all dead loads and live loads). In particular, the compression limit stress is equal to 2.25 ksi (15.5 MPa) due to effective prestress and dead load and 3.00 ksi (20.7 MPa) due to effective prestress and dead and live loads.

As summarized in Table 4-8, no flexural moments are developed along the pier length due to Service I load combination.

The concrete stresses due to Service I Limit State are computed according to Section 4.7 and are presented in Table 4-14. It is evident that compressive concrete stresses are significantly lower than the corresponding limits.

Table 4-14: Concrete stresses for Service I limit state

Location	Distance (in)	P_e (kips)	N_u (kips)	M_u (kips-in)	f_c (ksi)
Jack end	0.00	23.47	49.69	0.0	-0.594
Mid-section	60.00	23.42	51.77	0.0	-0.598
Dead end	120.00	23.38	53.85	0.0	-0.602

4.9 Strength I Limit State

As summarized in Table 4-8, no flexural moments are developed along the pier length due to Strength I load combination and no further calculations are required.

4.10 Extreme Event I Limit State

4.10.1 Uniaxial Earthquake Load

The maximum developed moment due to Extreme Event I Limit State is 257 kips-ft (348 kN-m) for the fixed cantilever end, as summarized in Table 4-8.

Following the procedure described in Section 4.5.1., an assumption on the neutral axis c of the pier cross-section is made and an iterative procedure is followed until equilibrium of forces is satisfied. A value of c equal to 4.22 inches (107.2 mm) is obtained.

In Table 4-15, the stresses in the unbonded pre-stressing steel are tabulated based on Equation (3-29) resulting to a sum of tensile pre-stressing steel forces for Extreme Event I Limit State equal to 293.9 kips (1307.3 kN).

Using Equation (3-31) and given that f_c' equals 5.0 ksi (34.5 MPa), c equals 4.22 inches (107.2 mm) and b equals 25 inches (0.63 m), the total compressive concrete force, P_c , equals 358.6 kips (1595.1 kN).

Table 4-15: Pier flexural resistance for Extreme Event I limit state

Tendon	P_c (kips)	f_{ef} (ksi)	d_{pi} (in)	#	f_{ps} (ksi)	P_{ps} (kips)
Layer 1	23.38	107.7	2.50	3	94.6	61.61
Layer 2	23.38	107.7	12.50	2	170.8	74.12
Layer 3	23.38	107.7	22.50	3	243.0	158.19
Sum	-	-	-	8	-	293.9

The maximum developed axial force due to Extreme Event I load combination is 64.7 kips (287.8 kN), as summarized in Table 4-8. Based on the above, the nominal flexural capacity, M_n , of the pier cross-section equals 403.6 kips-ft (547 kN-m). Assuming a resistance factor, ϕ , equal to 0.90 for flexural components with unbonded tendons, the factored flexural resistance, M_r , equals 363.3 kips-ft (493 kN-m) which is greater than the maximum developed moment due to Extreme Event I load combination that equals 257 kips-ft (348 kN-m).

4.10.2 Biaxial Earthquake Loads

According to AASHTO LRFD Bridge Design Specifications [2007], the elastic seismic force effects on each of the pier's principle axes resulting from analysis in the two perpendicular directions shall be combined. Given the symmetry of the pier's cross-section, 100 percent of the absolute value of the force effects in one of the perpendicular directions is combined with 30 percent of the absolute value of the force effects in the other perpendicular direction. The corresponding moments for the critical fixed cantilever end cross-section are presented in Table 4-16.

Table 4-16: Member forces at support due to biaxial earthquake loading

Extreme Event I	%	N_u (kips)	M_y (kips-ft)	M_z (kips-ft)
EQ Load in y-y	100	64.7	257	-
EQ Load in z-z	30	-	-	77

Given that the factored axial load equals 64.7 kips (287.8 kN) and is less than $0.10\phi f'_c A_g$, the following relationship should be satisfied considering the earthquake loads acting on each pier:

$$\frac{|M_y|}{M_{r,y}} + \frac{|M_z|}{M_{r,z}} \leq 1.0 \Rightarrow \frac{257}{363.3} + \frac{77}{363.3} = 0.92 < 1.0 \quad (4-6)$$

4.11 Reinforcement Limits

4.11.1 Minimum Reinforcement

According to AASHTO LRFD Bridge Design Specifications [2007] and Section 3.11, the calculation of the pier cracking strength, M_{cr} , is required. Given that S_c is equal to 2267 in³ (0.037 m³), f_r equals 0.537 ksi (3.70 MPa) and f_{cpe} equals 2.155 ksi (14.86 MPa) the cracking moment, M_{cr} , is computed to be equal to 508 kips-ft (689 kN-m).

The diameter of non-prestressing reinforcement is selected to be 3/8" (9.53 mm) for #3 bars and, their yielding stress is 60 ksi (414 MPa).

Initially, an assumption on the neutral axis c is made and an iterative procedure is followed until equilibrium of forces is satisfied. A value of c equal to 1.71 inches (43.4 mm) is obtained. Moreover, the nominal flexural capacity, M_n , of the pier's cross-section equals 860 kips-ft (1166 kN-m) and assuming a resistance factor, ϕ , equal to 0.90 for flexural components with unbonded tendons, the factored flexural resistance, M_r , equals 774 kips-ft (1049 kN-m).

Based on the above and given that the factored moment at mid-span due to Extreme Event I load case is 257 kips-ft:

$$M_r = 774 > \min\{1.2 \cdot 508, 1.33 \cdot 257\} = \min\{610, 342\} = 342 \text{ kips-ft}$$

Consequently, the amount of pre-stressed and non-prestressed tensile reinforcement is considered to be adequate according to AASHTO LRFD Bridge Design Specifications [2007].

4.11.2 Limits for Reinforcement

According to AASHTO LRFD Bridge Design Specifications [2007], the maximum area of pre-stressed and non-prestressed longitudinal reinforcement for compression members shall be such that:

$$\frac{A_s}{A_c} + \frac{A_{ps} f_{pu}}{A_c f_y} \leq 0.08 \quad (4-7)$$

$$\frac{A_{ps} f_{ef}}{A_c f_c'} \leq 0.30 \quad (4-8)$$

where A_s the area of non-prestressed steel, A_c the gross area of the section, A_{ps} the area of pre-stressing steel, f_{py} the specified tensile strength of pre-stressing steel, f_y the specified yield strength of reinforcing bars, f_c' the specified compressive stress of concrete and f_{ef} the effective prestress.

Accounting for sixty four non-prestressed steel bars with a diameter equal to 3/8" (9.53 mm) for #3 bars, the area of non-prestressed steel, A_s , is 7.07 in² (4561 mm²). Given that A_c equals 400 in² (0.26 m²), A_{ps} equals 1.74 in² (1123 mm²), f_{pu} equals 270 ksi (1860 MPa), f_y equals 60 ksi (414 MPa), f_c' equals 5 ksi (34.5 MPa) and f_{ef} equals 107.7 ksi (743 MPa), Equations (4-7) and (4-8) yield to:

$$\frac{7.07}{400} + \frac{1.74 \cdot 270}{400 \cdot 60} = 0.037 < 0.08$$

$$\frac{1.74 \cdot 107.7}{400 \cdot 5} = 0.094 < 0.30$$

The minimum area of pre-stressed and non-prestressed longitudinal reinforcement shall be such that:

$$\frac{A_s f_y}{A_c f_c'} + \frac{A_{ps} f_{pu}}{A_c f_c'} \geq 0.135 \quad (4-9)$$

$$\frac{7.07 \cdot 60}{400 \cdot 5} + \frac{1.74 \cdot 270}{400 \cdot 5} = 0.446 > 0.135$$

According to AASHTO LRFD Bridge Design Specifications [2007], for piers in Seismic Zone 3 the area of longitudinal reinforcement shall not be less than 0.01 or more than 0.06 times the gross cross-section area, A_c . The total area of non-prestressed and pre-stressed longitudinal reinforcement is 8.80 in² (5677 mm²) and accordingly:

$$0.1 A_c = 4.0 < A_s + A_{ps} = 8.80 < 0.6 A_c = 24.0$$

4.12 Shear Design

According to AASHTO LRFD Bridge Design Specifications [2007], transverse shear reinforcement shall be provided in regions where:

$$V_u > 0.5\phi(V_c + V_p) \quad (4-10)$$

where V_u the factored shear force, ϕ the resistance factor, V_c the nominal shear resistance of concrete and V_p the component of pre-stressing force in direction of the shear force. The load combination under consideration is the Extreme Event I as shown in Table 4-8.

4.12.1 Minimum Transverse Reinforcement

For post-tensioned concrete bridges, where transverse reinforcement is required, the area of transverse reinforcement, A_v , shall satisfy [AASHTO, 2007]:

$$A_v \geq 0.0316 \sqrt{f'_c} \frac{b_v s}{f_y} \quad (4-11)$$

where f'_c the compressive stress of concrete, b_v the width of web, s the spacing of transverse reinforcement and f_y the yield strength of transverse reinforcement.

Given that f'_c equals 5 ksi (34.5 MPa), b_v equals 10.0 inches (254 mm) considering both webs and f_y equals 60 ksi (414 MPa), Equation (4-11) yields to:

$$\frac{A_v}{s} \geq 0.0316 \sqrt{5} \frac{10}{60} = 0.012 \text{ in}^2/\text{in} \text{ (0.30 mm}^2/\text{mm)}$$

Additionally, for a rectangular pier in Seismic Zone 3 the total gross sectional area, A_{sh} , of rectangular hoop reinforcement shall satisfy either of the following:

$$A_{sh} \geq 0.30 s h_c \frac{f'_c}{f_y} \left[\frac{A_c}{A_{co}} - 1 \right] \quad (4-12)$$

$$A_{sh} \geq 0.12 s h_c \frac{f'_c}{f_y} \quad (4-13)$$

where s the vertical spacing of hoops, A_{co} the area of column core, A_c the gross area of column, A_{sh} the total cross-sectional area of tie reinforcement, f_y the yield strength of transverse reinforcement, h_c the core dimension of tied column in the direction under consideration, f'_c the compressive stress of concrete.

Given that A_{co} equals 192 in² (0.12 m²), A_c equals 400 in² (0.26 m²), f_y equals 60 ksi (414 MPa), h_c equals 8.0 inches (203 mm) considering both webs and f'_c equals 5 ksi (34.5 MPa), Equations (4-12) and (4-13) yield to:

$$\frac{A_{sh}}{s} \geq 0.30 \cdot 8.0 \frac{5}{60} \left[\frac{400}{192} - 1 \right] = 0.217 \text{ in}^2/\text{in} \text{ (5.51 mm}^2/\text{mm)}$$

$$\frac{A_{sh}}{s} \geq 0.12 \cdot 8.0 \frac{5}{60} = 0.08 \text{ in}^2/\text{in} \text{ (2.03 mm}^2/\text{mm)}$$

Consequently, the ratio A_{sh}/s should be greater than 0.217 in²/in (5.51 mm²/mm) in order to comply with the code provisions.

4.12.2 Nominal Shear Resistance

According to AASHTO LRFD Bridge Design Specifications [2007], the nominal shear resistance, V_n , of a concrete member shall be determined as the lesser of:

$$V_n = V_c + V_s + V_p \quad (4-14)$$

$$V_n = 0.25f'_c b_v d_v + V_p \quad (4-15)$$

in which:

$$V_c = 0.0316\beta\sqrt{f'_c}b_v d_v \quad (4-16)$$

$$V_s = \frac{A_v f_y d_v (\cot \vartheta + \cot \alpha) \sin \alpha}{s} \quad (4-17)$$

where b_v the effective web width taken as the minimum web width within the depth d_v , d_v the effective shear depth, s the spacing of stirrups, β the factor indicating ability of diagonally cracked concrete to transmit tension, θ the angle of inclination of diagonal compressive stresses, α the angle of inclination of transverse reinforcement to longitudinal axis, A_v the area of shear reinforcement within a distance c and V_p the component in the direction of the applied shear of the effective pre-stressing force.

4.12.3 Effective Shear Depth, d_v

In order to design the pier for shear, the critical section should be identified as the larger of the effective shear depth, d_v and $0.5d_v \cot \theta$ from the face of the support. The effective shear depth, d_v , taken as the distanced measured perpendicular to the neutral axis between the resultants of the tensile and compressive forces due to flexure, it need not be taken to be less than the greater of:

$$d_v \geq \max \{0.9d_e, 0.72h\} \quad (4-18)$$

where d_e the effective depth from extreme compression fiber to the centroid of the tensile force in the tensile reinforcement and h the section depth.

Given that h equals 25.0 inches (0.64 m) and d_e equals 12.5 inches (0.32 m), the effective d_v depth is computed to be equal to 18.0 inches (457 mm), Equation (4-18) yields to:

$$d_v \geq \max \{0.9 \cdot 12.5, 0.72 \cdot 25.0\} = 18.0 \text{ in (457 mm)}$$

4.12.4 Shear Resistance

For sections containing at least the minimum amount of transverse reinforcement as specified in Section 4.12.1, the values of β and θ are related to the shear stress on the concrete, v_u , and the longitudinal strain, ϵ_x , at the mid-depth of the member when the section is subjected to M_u , N_u and V_u [AASHTO, 2007].

The shear stress on the concrete is determined as [AASHTO, 2007]:

$$v_u = \frac{|V_u - \phi V_p|}{\phi b_v d_v} \quad (4-19)$$

where V_u the factored shear force, ϕ the resistance factor for shear, V_p the component in the direction of the applied shear of the effective pre-stressing force, b_v the effective web width and d_v the effective shear depth.

Given that V_u equals 20.1 kips (89.3 kN), ϕ is 0.85 for shear of unbonded tendons, V_p is zero, b_v is 10.0 inches (254 mm) considering both webs of the pier cross-section and d_v is 18.0 inches (457 mm), the shear stress v_u is computed to be 0.13 ksi (0.9 MPa).

The strain, ϵ_x , at the mid-depth of the pier section when subjected to M_u , N_u and V_u is computed as follows [AASHTO, 2007]:

$$\epsilon_x = \frac{(|M_u|/d_v) + 0.5N_u + 0.5|V_u - V_p| \cot \theta - A_{ps}f_{po}}{2(E_s A_s + E_p A_{ps})} \leq 0.001 \quad (4-20)$$

where M_u the factored moment at the specified section which occurs simultaneously with V_u , N_u the factored axial force taken as positive if tensile and negative if compressive, V_u the factored shear force, V_p the component in the direction of the applied shear of the effective pre-stressing force; positive if resisting the applied shear, θ the angle of inclination of diagonal compressive stresses, A_{ps} the area of pre-stressing steel on the flexural tension side of the member, f_{po} a parameter taken as $0.7f_{pu}$ for post-tensioned members, E_s the modulus of elasticity of non-prestressed steel, A_s the area of non-prestressed steel on the flexural tension side of the member at the section under consideration, A_s the area of non-prestressed steel on the flexural tension side of the member at the section under consideration and E_p the modulus of elasticity of pre-stressed steel.

For the fixed cantilever end of the pier, the forces due to Extreme Event I load combination are: M_u equal to 257 kips-ft (348 kN-m), N_u equal to 64.7 kips (287.8 kN) and V_u equal to 20.1 kips (89.3 kN). The component of the applied shear due to the effective pre-stressing forces, V_p , is zero given that the tendons are lying straight along the pier's length.

Assuming that θ is 35° and considering that A_{ps} equals 0.65 in^2 (419 mm^2) accounting for three tendons lying on the flexural tension side of the member, f_{po} equals 189 ksi (1303 MPa) and E_p equals 28500 ksi (196.5 GPa), ϵ_x is computed according to Equation (4-20):

$$\epsilon_x = \frac{(257 \cdot 12/18) + 0.5 \cdot 64.7 + 0.5 \cdot 20.1 \cdot \cot 35 - 0.65 \cdot 189}{2 \cdot 28500 \cdot 0.65} = 0.026 > 0.001 \Rightarrow \epsilon_x = 0.001$$

It should be noted that the non-prestressed steel on the flexural tension side of the pier section is neglected.

Having computed ϵ_x and v_u/f_c' the values of θ and β can be obtained from AASHTO LRFD Bridge Design Specifications [2007]. Specifically, θ is equal to 36.4° – approximately equal to the initial assumption of 35° and β is equal to 2.23.

Using Equation (4-16), the nominal shear resisted by the concrete, V_c , is computed as:

$$V_c = 0.0316 \cdot 2.23\sqrt{5} \cdot 10.0 \cdot 18.0 = 28.4 \text{ kips (126 kN)}$$

Moreover, according to Equation (4-10):

$$V_u = 20.1 \text{ kips} > 0.5 \cdot 0.85 \cdot (28.4 + 0) = 12.1 \text{ kips (54 kN)}$$

Therefore, transverse shear reinforcement should be provided.

4.12.5 Required Area of Shear Reinforcement

According to AASHTO LRFD Bridge Design Specifications [2007] and Equation (4-10), the transverse reinforcement shear resistance, V_{s_s} , is:

$$V_s \leq V_u / \phi - V_c - V_p \quad (4-21)$$

For V_u equal to 20.1 kips (89.3 kN), ϕ equal to 0.85, V_c equal to 28.4 kips (126 kN) and V_p equal to zero, the shear force carried by the transverse reinforcement, V_{s_s} , is 5.8 kips (25.8 kN).

The amount of transverse shear reinforcement is then computed according to Equation (4-17). Given that V_s is 5.8 kips (25.8 kN), f_y equals 60 ksi (414 MPa), d_v equals 18.0 inches (457 mm), θ equals 36.4° and α equals 90° , the ratio A_v/s can be computed to be $0.004 \text{ in}^2/\text{in}$, which is lower than the minimum ratio of transverse reinforcement that is equal to $0.217 \text{ in}^2/\text{in}$ (see Section 4.12.1).

Assuming a spacing distance s equal to 3.0 inches (76 mm) and using two number 3 closed stirrups per web (diameter of 3/8" or 9.53 mm), the required area of transverse reinforcement is $0.295 \text{ in}^2/\text{in}$ and V_s equals:

$$V_s = \frac{0.884 \cdot 60 \cdot 18.0 (\cot 36.4 + \cot 90) \sin 90}{3.0} = 431 \text{ kips (1917 kN)}$$

Using Equation (4-14), the nominal shear resistance, V_n , of the pier equals 460 kips (2046 kN).

Given that f_c' equals 5 ksi (34.5 MPa), b_v equals 10.0 inches (254 mm) considering both webs, d_v equals 18.0 inches (457 mm) and V_p equals zero, the nominal shear resistance, V_n , of the pier is computed based on Equation (4-15):

$$V_n = 0.25 \cdot 5 \cdot 10.0 \cdot 18.0 = 225 \text{ kips (1001 kN)}$$

According to Section 4.12.2:

$$V_n = \min\{460, 225\} = 225 \text{ kips} > V_u = 20.1 \text{ kips}$$

The reinforcement details of the substructure test units – pre-stressing strands and mild reinforcement - are presented in Appendix A.

SECTION 5

SUPERSTRUCTURE NUMERICAL MODEL

The first step in investigating the behavior of the designed bridge test specimen under seismic induced loads is to consider its superstructure and substructure as two separate numerical models. Later on and using the acquired information on the response of the two systems, a numerical model of the complete bridge system can be developed and subjected to a series of earthquake loads of different intensities. This report focuses on the behavior of the segmental superstructure under vertical earthquake excitations whereas; detailed numerical investigations will be presented in future studies.

In this Chapter, a numerical model of the bridge superstructure designed in Chapter 3 is developed in order to predict its behavior under a series of vertical seismic excitations. The two-dimensional numerical model of the bridge's superstructure incorporating material and geometric nonlinearities is analyzed using the inelastic dynamic analysis software Ruaumoko [Carr, 2007].

The program Ruaumoko is designed to produce time-history responses of various non-linear structures subjected to ground accelerations and varying force or displacement excitations. A wide variety of modeling options are available to represent the structural system such as frame type members, spring and contact members which can follow a large number of different hysteresis rules.

Initially, a two-segment superstructure model with a single gap at the mid-span section is developed and subjected to a vertical displacement controlled load pattern aiming to verify the inelastic behavior of the implemented elements. The geometry of the two-segment simplified model is similar to the geometry of the full eight-segment superstructure bridge model. Based on the modeling assumptions used for the simplified model, a full eight-segment model is developed according to the geometric and material properties of the superstructure design model as presented in the previous Chapters. For the latter both pushover and dynamic time histories analysis are conducted.

The numerical model described hereafter provided a series of pre-test predictions for the experimental investigation of the bridge test specimen that took place at the SEESL Laboratory at the University at Buffalo.

5.1 Two-Segment Model Geometry

The geometry of the two-segment numerical model is similar to that of the full superstructure model. The length of each segment is 140.70 inches (3574 mm) whereas; the span's length equals 201.00 inches (5105 mm) and the overhangs' length equals 40.20 inches (1021 mm). Ten internal unbonded tendons with a parabolic profile run along the superstructure length. The geometry of the tendons is given in Table 3-12 and presented in Figure 3-5 and Figure 3-6. In order to

minimize the number of structural elements, a single tendon is modeled instead of ten, having an equivalent cross-sectional area. Its geometry matches the geometric center of gravity of the ten tendons along the span.

The geometry of the two-segment model is illustrated in Figure 5-1. It should be noted that the cross-section and material properties used are the ones presented in Table 3-1 and Table 3-2.

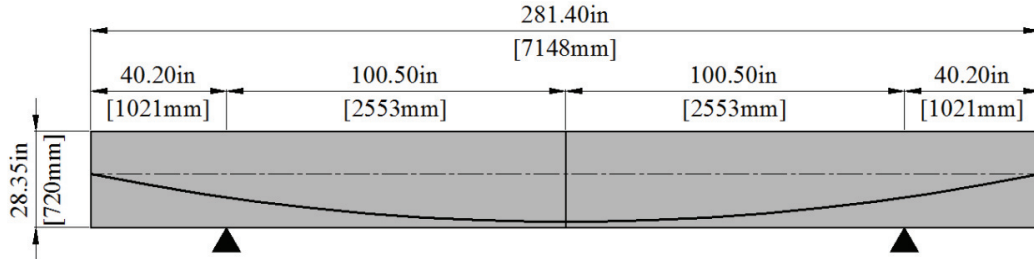


Figure 5-1: Elevation view of the two-segment model

5.2 Modeling Approach

A segmental bridge superstructure, whose segments are joined together by internal unbonded tendons, is characterized by the behavior of its joints and its self-centering ability when subjected to a vertical seismic excitation. The gaps between the joined elements open and the unbonded tendons, which are free to slide inside their ducts, get stretched. In that case, the post-tensioned tendons act as a self-centering mechanism [Christopoulos and Filiatrault, 2006] whereas; the gap opening of the superstructure’s segments result in the dissipation of the seismic energy that is introduced in the system.

Based on the above, the superstructure is modeled with linear elastic frame members with the cross sectional and material properties of the scaled superstructure model. The longitudinal axis of the frame elements coincides with the center of gravity of the superstructure cross-section.

To model the unbonded tendon, several bi-linear elastic spring elements are used in order to match its parabolic geometry. Those springs work in series and their nodes are constrained to the nodes of the superstructure beams in the vertical direction. Moreover, the initial axial stiffness of each spring element represents the total cross-sectional area of the pre-stressing tendons times the modulus of elasticity of pre-stressed steel divided by the length of the spring. The bi-linear factor, r , is set equal to 0.02 whereas the spring elements’ yielding force in tension, F_y , equals the yielding strength of the tendons based on their material properties minus the effective pre-stressing force after all losses. The hysteresis rule used is illustrated in Figure 5-2 [Carr, 2007].

Prior to loading, the joint between two adjacent segments is closed and the whole section is in compression. When a vertical seismic load is applied, the joint opens and a compressive contact zone forms whose depth decreases with increasing gap opening. In order to simulate the contact zone between adjacent segments, a series of bi-linear inelastic springs distributed along the height

of the contact interface is used. These springs, which are connected to the superstructure beam elements with rigid links, provide solely compression resisting forces whereas; they have no tensile strength. Attention should be paid to the fact that all nodes lying along a gap section are constrained to have the same vertical displacement.

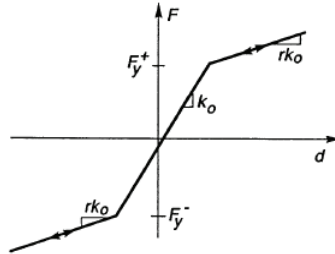


Figure 5-2: Bi-linear elastic rule for the unbonded tendons [Carr, 2007]

The neutral axis of the contact zone between adjacent beam segments is not constant but depends on the loading applied to the model structure. Initially, the compression of the contact zone is uniformly distributed along its height resulting to an infinite theoretical neutral axis. By imposing a vertical load to the section, the compression stresses on one side increase and decrease on the other side. Consequently, as the gap opening increases the neutral axis moves further inside the section. In order to be able to capture the shift of the neutral axis depth along the contact zone height, a representative number of compression springs should be selected [Spieth et al., 2004].

Based on the geometry of the superstructure cross-section, the contact zone between two adjacent segments is modeled with eleven non-linear springs whose position along the section height is given in Table 5-1. The location of each spring is measured from the bottom fiber of the cross-section.

Table 5-1: Compression spring location along the contact zone

Spring	H_i	
	(in)	(mm)
1	28.35	720
2	27.18	690
3	26.02	661
4	24.85	631
5	20.35	517
6	15.85	403
7	9.64	245
8	3.50	89
9	2.33	59
10	1.17	30
11	0.00	0

As shown in Figure 5-3, four compression springs are placed at each of the top and bottom plate of the cross-section where the maximum local deformations due to compression are expected. Moreover, the position of the central spring coincides with the position of the superstructure frame elements.

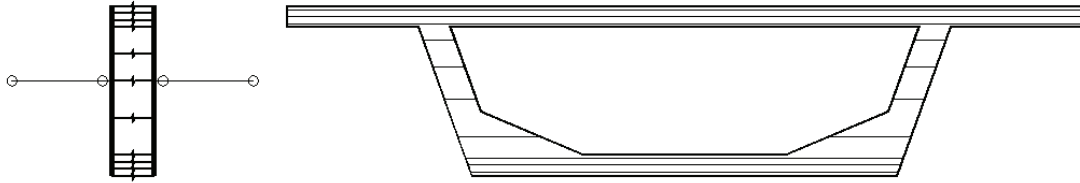


Figure 5-3: Compression spring geometry along the contact zone

The hysteresis rule used to model the springs along the height of the contact zone between two adjacent beam elements is the bi-linear with slackness hysteresis rule as illustrated in Figure 5-4 [Carr, 2007]. In order to ensure that no tensile forces are developed, a high positive gap value is chosen. Additionally, the initial and post-yield stiffness as well as, the negative yielding force of each spring need to be defined.

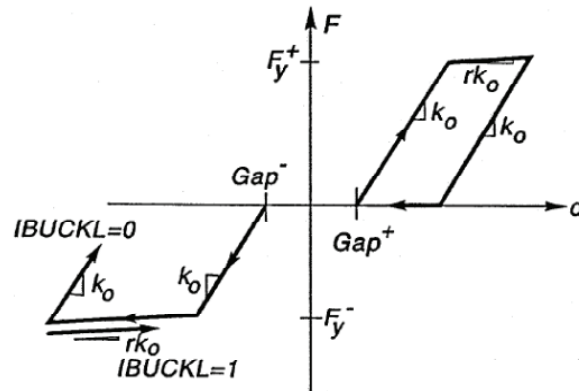


Figure 5-4: Bi-linear with slackness hysteresis for modeling joint gap opening [Carr, 2007]

The initial axial stiffness of the simulated joint represents the effective cross sectional area of each spring, A_{cs} , times the concrete modulus of elasticity, E_c , divided by the length of the joint, l_j . The length of the joint represents an effective length where localized strains in the adjoining beams are expected due to the joint opening and development of compression forces. In order to show and evaluate the influence of the joint length to the contact stiffness, the joint length is taken as $h/2$, $h/4$ and $h/9$ where h is the height of the contact zone. Moreover, the stiffness of the superstructure frame elements adjacent to the gap is increased in order to compensate the additional flexibility due to the joint compression springs and not to change the global stiffness of the model.

In Table 5-2, the axial stiffness of the compression springs along the contact zone are listed assuming a joint effective length equal to $h/4$. The bi-linear factor, r , is set equal to 0.02.

Table 5-2: Compression spring stiffness along the contact zone for a joint effective length equal to $h/4$

Spring	$A_{cs,i}$ (in ²)	E_c (ksi)	L_j (in)	$K_{s,i}$ (kips/in)
1	77	4287	7	47282
2	154			94564
3	154			94564
4	101			61927
5	48			29290
6	57			34880
7	100			61547
8	145			88920
9	85			51826
10	84			51224
11	41			25386

Another decisive influence parameter of the behavior of the contact zone between two adjacent segments is the local compressive strength of the contact zone expressed by the negative yielding force of the compression springs. The limit of elastic behavior of the contact area is represented by the stress level when the concrete in the contact zone starts to deform plastically. Based on that, the yielding force of the compression springs along the contact zone is set equal to the cross sectional area, A_{cs} , times the concrete compression strength, f_c' .

Both supports are constrained with respect to the vertical displacement whereas; one is free to move along the horizontal axis, aiming to capture the axial deformation interaction of the superstructure frame elements, pre-stressed tendon spring elements and compression springs along the gap section.

The model structure is subjected to the vertical loads resulting from its self-weight whereas; pre-stressing is also applied as an external load with a vertical and horizontal component at the end nodes.

The modeling approach described above applies to both considered models, the two-segment and eight-segment ones. Hereafter, the two models are described in detail and their modal response characteristics as well as their inelastic response under vertical displacement-controlled loadings are presented.

5.3 Two-Segment Model Response

The two-segment superstructure numerical model is developed and subjected to a vertical displacement controlled load pattern aiming to verify the inelastic behavior of the implemented elements as well as, investigate the effect of various design parameters on the model's response.

In Figure 5-5, the two-segment model is illustrated as implemented in Ruaumoko [Carr, 2007] and based on the geometry presented in Figure 5-1. The superstructure is divided into a finite number of frame elements which matches the number of pre-stressed tendon spring elements. The end nodes of the superstructure frame elements and tendon spring ones are constrained to have the same vertical displacement.

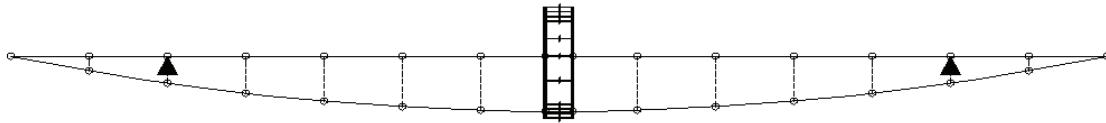


Figure 5-5: Elevation view of the two-segment numerical model

The five first periods of vibration of the two-segment numerical model are presented in Table 5-3. The corresponding mode shapes are presented in Figure 5-6 through Figure 5-10, respectively. Only the self-weight of the superstructure is accounted for the calculation of the periods of vibration and mode shapes of the model.

Table 5-3: Periods of vibration of the two-segment numerical model

Mode	Frequency (Hz)	Period (sec)
1	52.48	0.0191
2	185.00	0.0054
3	277.50	0.0036
4	410.30	0.0024
5	631.70	0.0016

The first, third and fifth mode shapes are symmetrical with respect to the vertical axis passing through the mid-span cross-section of the model, as shown in Figure 5-6, Figure 5-8 and Figure 5-10, respectively. On the other hand, the second and fourth mode shapes are anti-symmetrical with respect to the vertical axis passing through the mid-span cross-section, as shown in Figure 5-7 and Figure 5-9, respectively. Consequently when a symmetric vertical excitation is applied at the mid-span section of the superstructure model, the second and fourth modes (odd numbered modes) are not excited as the mid-span section is a point of inflection for those modes and all the response is due to the first, third and fifth modes (even numbered modes). Moreover, the frequency ratios are roughly in the ratios 1:3:5:8:12.

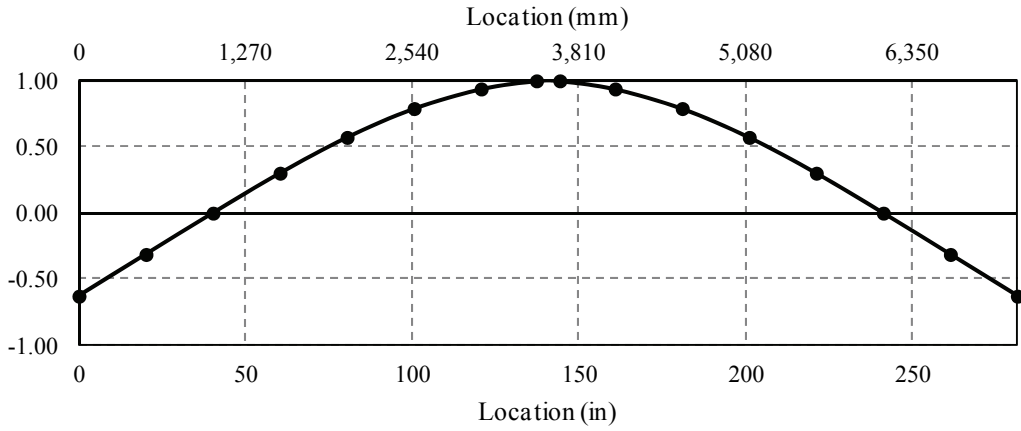


Figure 5-6: First mode of vibration of the two-segment numerical model

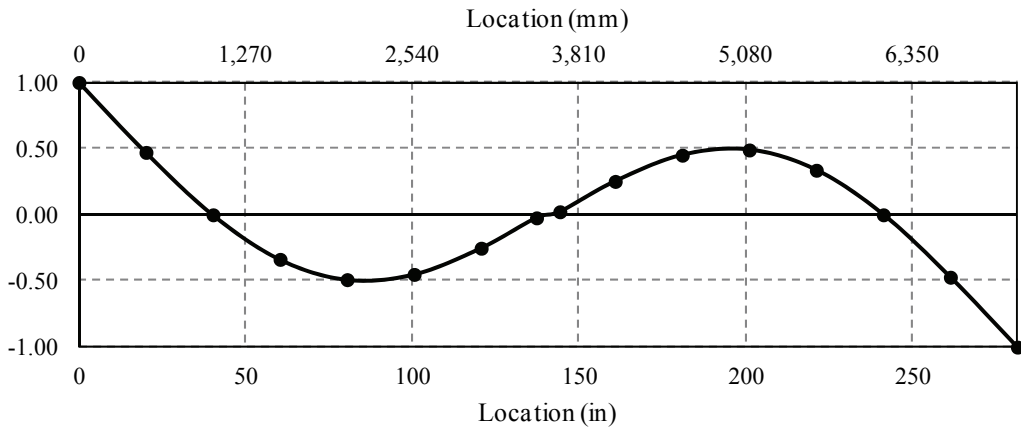


Figure 5-7: Second mode of vibration of the two-segment numerical model

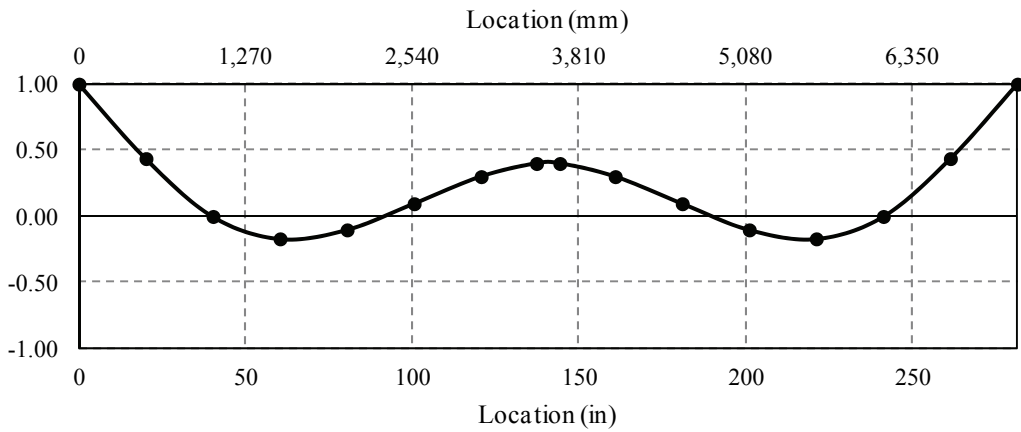


Figure 5-8: Third mode of vibration of the two-segment numerical model

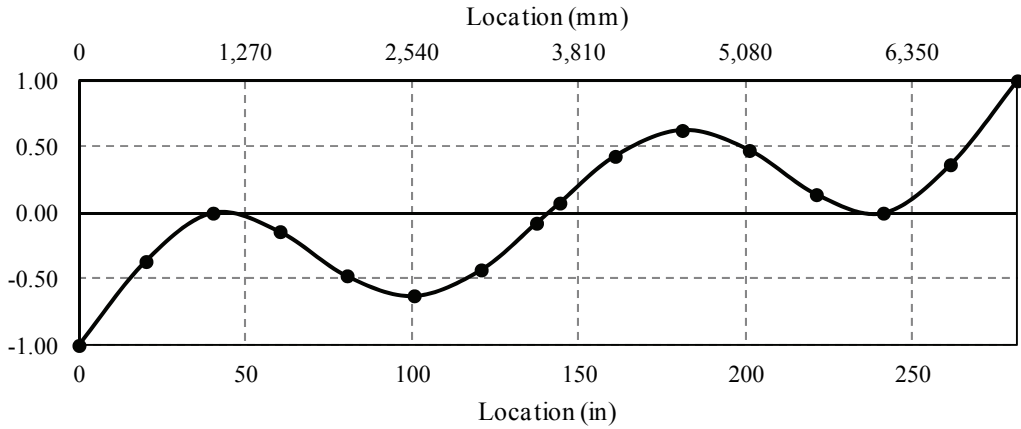


Figure 5-9: Fourth mode of vibration of the two-segment numerical model

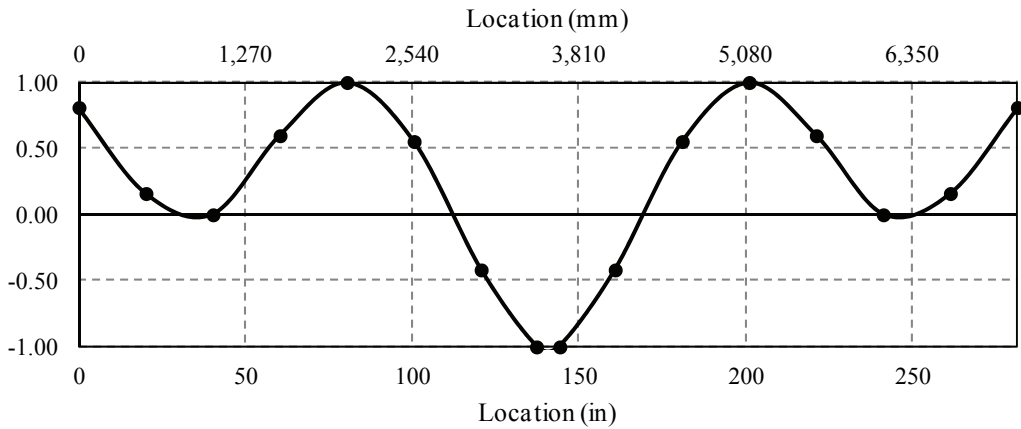


Figure 5-10: Fifth mode of vibration of the two-segment numerical model

In addition, the fundamental period of vibration of a simply supported continuous beam element is computed from the equation [Chopra, 2007]:

$$T_1 = \frac{2L^2}{\pi} \sqrt{\frac{\bar{m}}{E_c I}} \quad (5-1)$$

where L is the superstructure's length, \bar{m} the superstructure's mass per unit length, E_c the concrete modulus of elasticity and I the cross-section moment of inertia. By substituting the cross sectional properties of the two-segment model into Equation (5-1), its fundamental period of vibration is computed to be equal 0.0171 seconds which does not significantly differs from the one tabulated in Table 5-3. This difference may be attributed to the fact that in the first case the model has a gap located at its mid-span resulting to a less stiff structure and consequently to a higher period than the case where a continuous beam element is assumed.

The response of the two-segment superstructure model is investigated by applying a vertical cyclic sinusoidal displacement-controlled loading at the mid-span nodes. The direction of the load is initially downward and then reversed. Different assumptions related to the length of the compression mid-span joint, the value of critical damping assigned to the model and the duration of the displacement-controlled load are considered and presented in the following sections.

5.3.1 Influence of Joint Length

The gap opening between two adjacent superstructure segments results in the development of localized strains along an effective length of the adjoining beams. The effective joint length influences the axial stiffness of the compression springs that are used to model the contact zone between two segments and is expressed as a fraction of the height of the contact zone. In order to show and evaluate the influence of the joint length to the stiffness of the compression springs, the joint length is taken as $h/2$, $h/4$ and $h/9$, respectively where h is the height of the contact zone. The values of the axial stiffness of the eleven springs resulting from those three considered cases are presented in Table 5-4.

The model is then subjected to a cyclic sinusoidal displacement-controlled loading, applied to the mid-span nodes. The maximum amplitude of the applied displacement is 4.0 inches (102 mm) given that the model's span length is 201.0 inches (5106 mm), and its period is set equal to 12.0 seconds, as shown in Figure 5-11.

Table 5-4: Compression spring stiffness for different values of joint length

Spring	$K_{s,i}$ (kips/in)		
	$h/9$	$h/4$	$h/2$
1	110325	47282	23641
2	220649	94564	47282
3	220649	94564	47282
4	144497	61927	30964
5	68344	29290	14645
6	81386	34880	17440
7	143609	61547	30773
8	207481	88920	44460
9	120927	51826	25913
10	119523	51224	25612
11	59235	25386	12693

The damping is modeled using a Rayleigh damping model and assuming a 5% of critical damping applied to the first two modes of the superstructure.

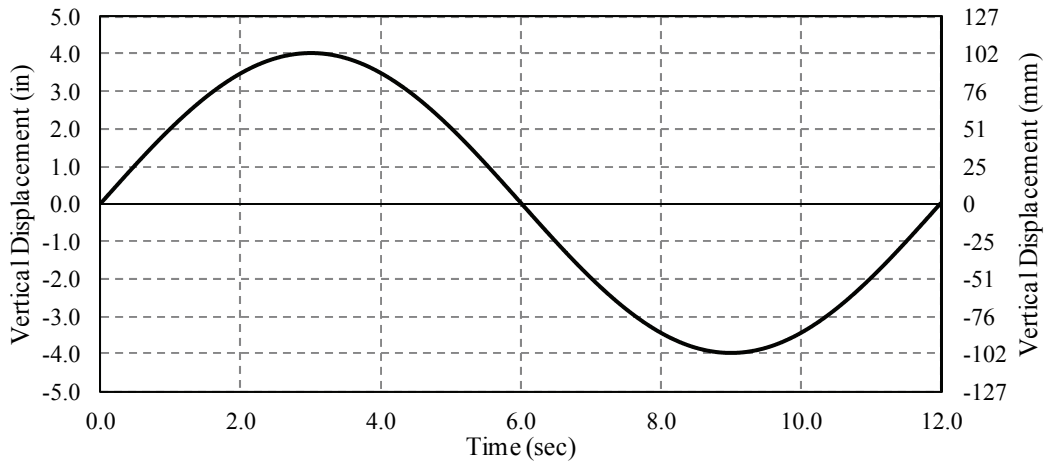


Figure 5-11: Vertical cyclic sinusoidal displacement-controlled loading (T=12.0sec) applied at mid-span joint of the two-segment numerical model

The history of total developed vertical reaction at the support versus the applied vertical displacement for the case of joint length that equals $h/4$ is shown in Figure 5-12.

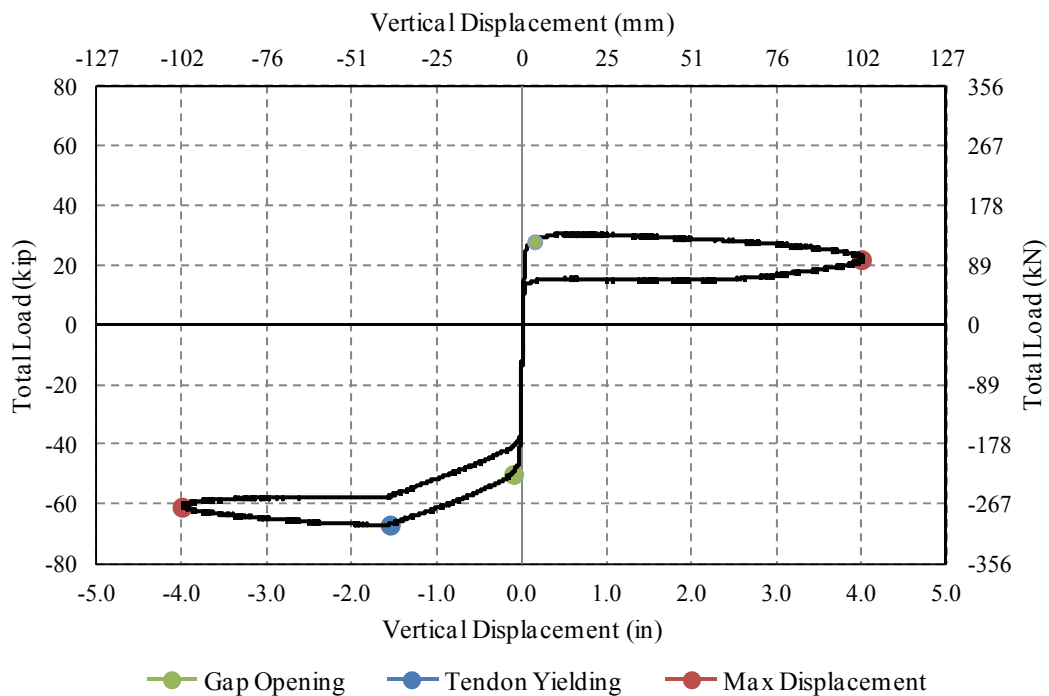


Figure 5-12: History of total load versus displacement of the two-segment numerical model and effective joint length equal to $h/4$

As the model is initially loaded in the downward direction, the initial stiffness is high representing the stiffness of the top compression spring which is activated when the mid-span gap opens. At a load value of approximately -40 kips (-178 kN), a secondary post-yield stiffness slope

is observed resulting from the opening of the mid-span joint and the yielding of the top spring (spring 1). The maximum load of -70 kips (-310 kN) in the downward loading direction is reached at a displacement of -1.5 inches (-38 mm). By further increasing the applied vertical displacement, a third negative stiffness is observed due to the yielding of the pre-stressed tendons. The maximum displacement of -4.0 inches (-102 mm) is reached at a vertical total load of -60 kips (-267 kN). As the loading is reversed, the vertical load versus vertical displacement curve follows the same profile until the point of zero load and displacement. In the upward loading direction, the maximum load of 30 kips (130 kN) is reached followed by yielding of the bottom spring (spring 11) and an approximately stable post-yield stiffness up to the maximum displacement.

After a full cyclic loading the model has returned to its original state behaving as a self-centering system. However, the model exhibits a different behavior when subjected to downward and upward vertical loading due to the location of the unbonded tendon below the centre of gravity of the superstructure's cross-section.

The results of the simulations for different joint lengths, as illustrated in Figure 5-13, show that the model is not very sensitive to the effective joint length as long as it is chosen in a reasonable range. The differences in the response for the cases of $h/4$ and $h/2$ joint length are not significant whereas; they differ from the case of $h/9$ mainly in terms of dissipated energy during one load cycle. Based on that result, an effective joint length of $h/4$ is adopted hereafter.

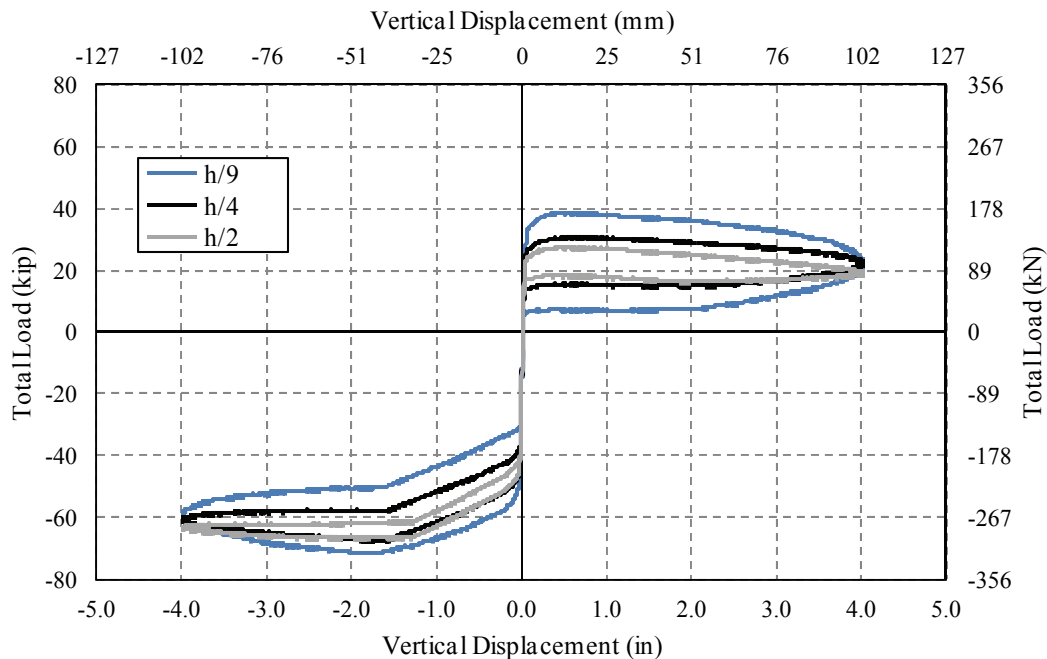


Figure 5-13: History of total load versus displacement of the two-segment numerical model and effective joint length equal to $h/9$, $h/4$, $h/2$

In Figure 5-14, the hysteretic response of the bottom spring (spring 11) of the mid-span joint is presented for the three considered cases of effective joint length. As mentioned before an increased value of joint length results to a decreased stiffness of the springs along the contact area. It should be noted that the spring developed only negative compressive forces and no tension.

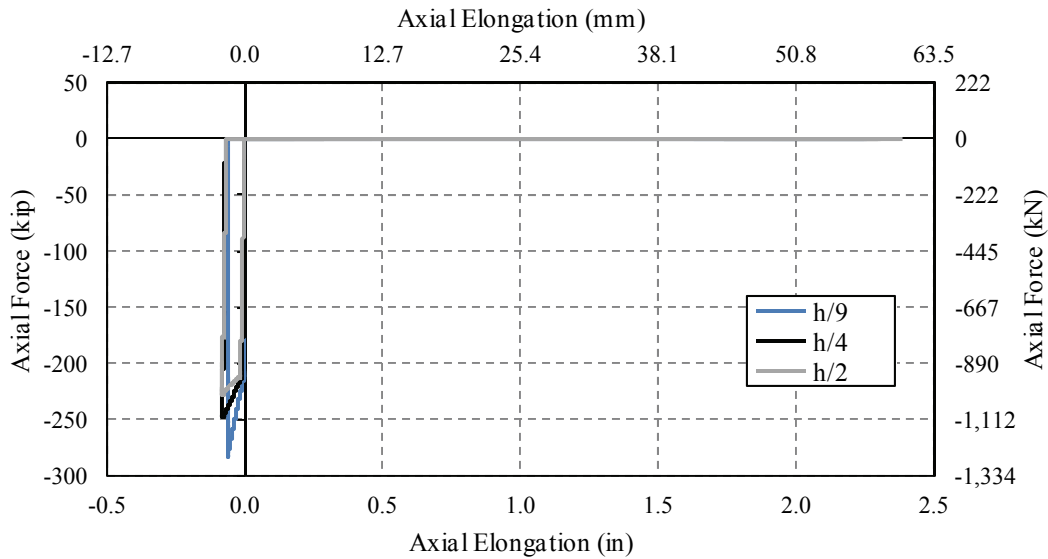


Figure 5-14: Axial force versus axial elongation of the two-segment bottom compression spring (spring 11) at mid-span contact zone

The initial deformed shape of the model due to the applied pre-stressing forces is illustrated in Figure 5-15, where no differences are noted for the three considered cases of joint lengths. Before any vertical loading is applied, the mid-span contact zone is in a state of almost uniform compression.

When a vertical loading is applied, the gap along the mid-span cross section opens and the compression springs along its height are activated. In order to examine the displacement profile of the superstructure model under maximum upward and downward loading, Figure 5-16 and Figure 5-17 are presented hereafter. It is evident that the discontinuity along the model's length resulting from the mid-span gap opening changes the displacement profile of the model from a continuous parabola to a linear shape. Consequently, the two adjacent superstructure segments behave as cantilevers and not as continuous simply-supported beams. The differences in the displacements due to the three cases of varying effective joint length are negligible.

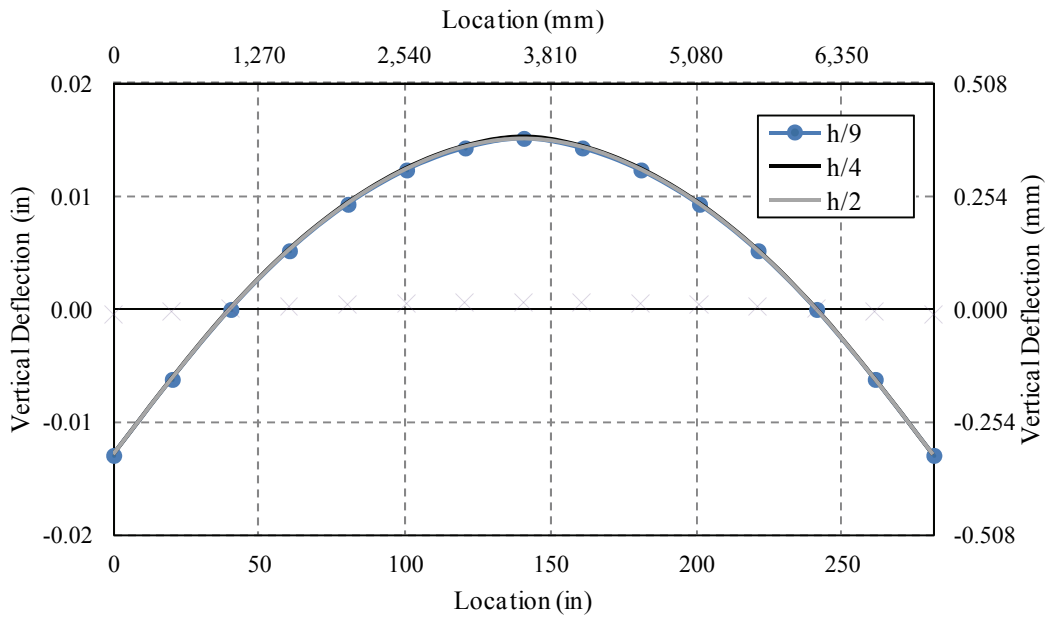


Figure 5-15: Deflection profile of the two-segment numerical model due to pre-stress

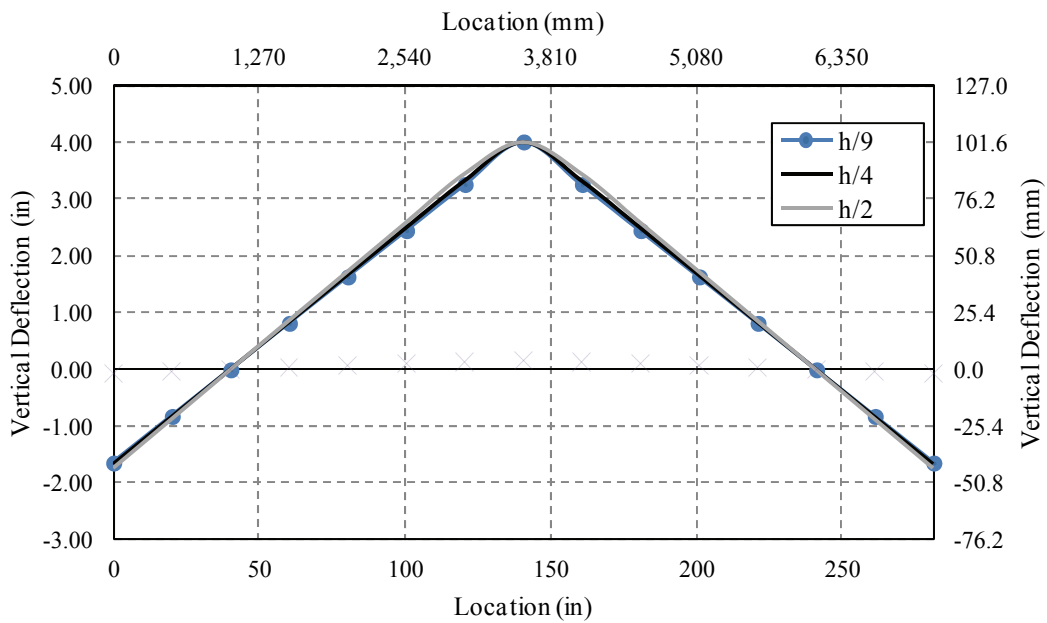


Figure 5-16: Deflection profile of the two-segment numerical model due to maximum upward loading of mid-span contact joint

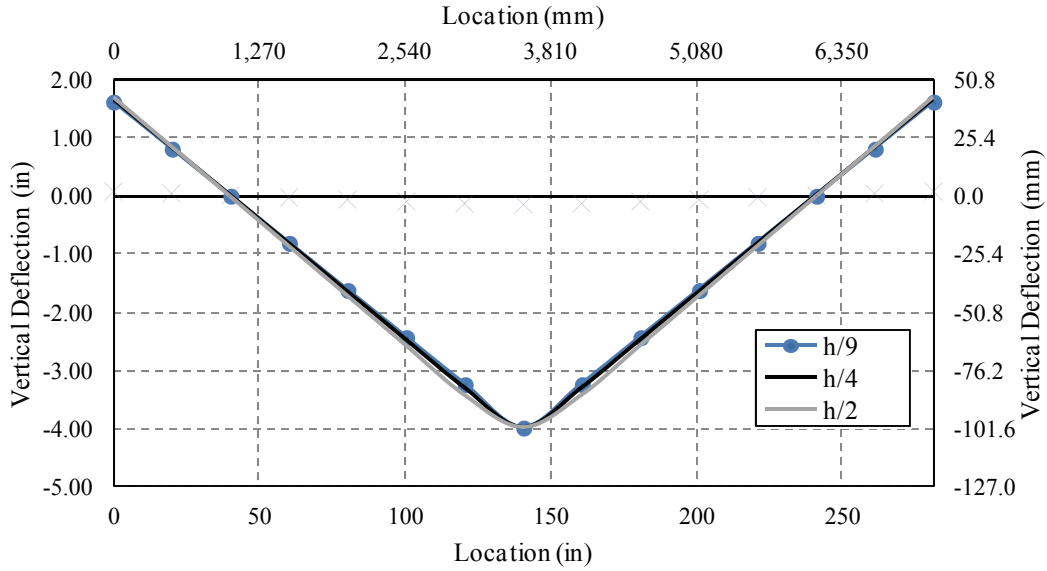


Figure 5-17: Deflection profile of the two-segment numerical model due to maximum downward loading of mid-span contact joint

5.3.2 Influence of Loading Duration

In order to investigate the model’s response under vertical displacement-controlled loading with the same maximum amplitude but different duration, three cases of cyclic sinusoidal loads are considered with periods of 6.0, 12.0 and 24.0 seconds. The three load patterns are illustrated in Figure 5-18, whereas it should be reminded that the fundamental period of vibration of the two-segment model is 0.0191 seconds. For all cases the load is applied at the mid-span joint, while a joint length of $h/4$ is adopted and where h is the height of the contact zone. The viscous damping is assumed to be 5% of critical for all cases.

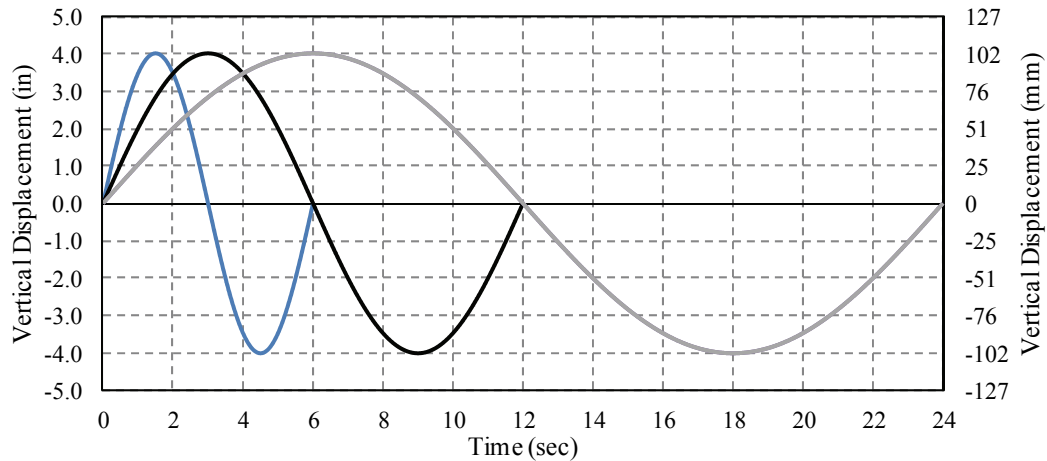


Figure 5-18: Vertical cyclic sinusoidal displacement-controlled loads of 6, 12 and 24 seconds period applied at mid-span joint of the two-segment numerical model

The results of the three considered analysis are evaluated in terms of total developed vertical reaction at the support versus the applied vertical displacement as shown in Figure 5-19. For the case of short period loading equal to 6.0 seconds, high velocities are developed which generate high internal damping forces. Consequently, the forces developed from the model's structural elements are high in order to equilibrate these damping forces, resulting to a wide hysteretic loop. On the other hand, both cases of 12.0 and 24.0 seconds of loading period exhibit narrow hysteretic loops which do not differ significantly.

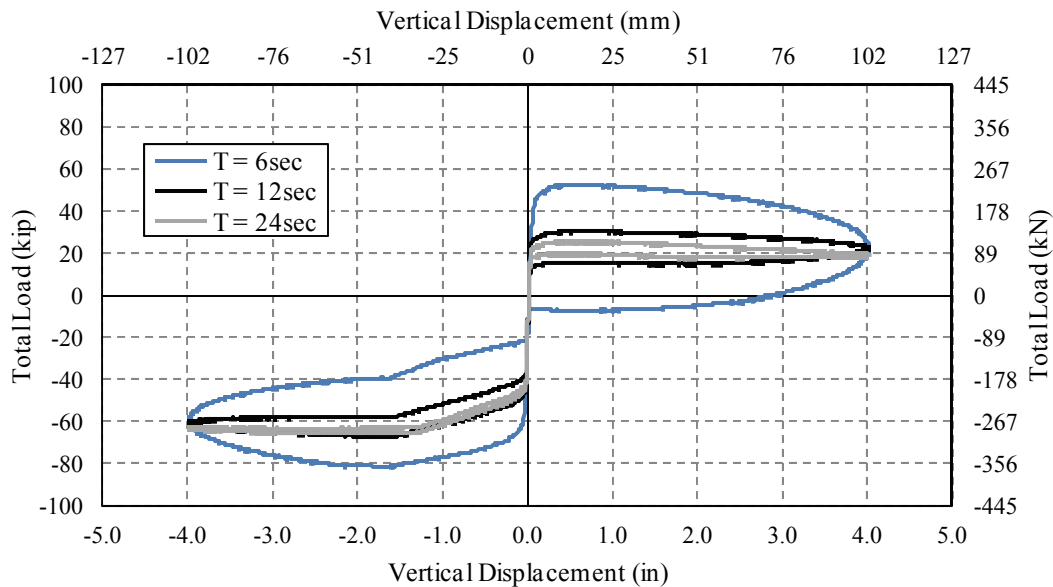


Figure 5-19: History of total load versus displacement of the two-segment numerical load and loading periods equal to 6, 12 and 24 seconds

Consequently if the duration of the load is short, the damping forces are high and the response of the model is significantly affected whereas the model is not very sensitive to the loading duration as far as it is long enough.

5.3.3 Influence of Critical Damping

Hereafter, the effect of critical damping assigned to the structure is investigated. Three cases of 1%, 3% and 10% critical damping are considered applied to the first two modes of vibration whereas; a Rayleigh damping model is defined. The model is loaded with a vertical cyclic sinusoidal displacement-controlled loading of 4.0 inches (102 mm) maximum amplitude and a period of 12.0 seconds as shown in Figure 5-11. For all cases the load is applied at the mid-span joint, while a joint length of $h/4$ is adopted, where h is the height of the contact zone.

As shown in Figure 5-20, the model response is not sensitive to the assigned percentage of critical damping as long as the duration of the loading is long enough. When the loading is slowly applied to the structure, the developed velocities and resulting damping forces are not significant and vice versa. It should be noted that contrary to the case of a displacement-controlled loading whose duration can be carefully chosen in order not to overestimate the developed damping

forces, the duration of a real vertical seismic excitation is explicit. In the latter case, significant attention should be paid in the selected percentage of critical damping.

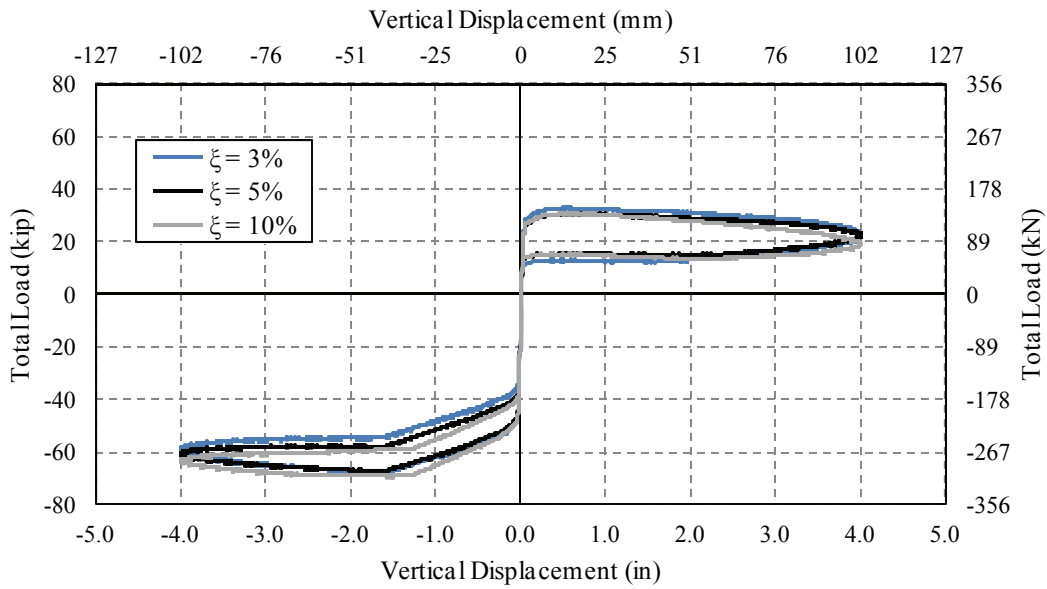


Figure 5-20: History of total load versus displacement of the two-segment numerical load and 3%, 5% and 10% critical damping

5.4 Eight-Segment Model Response

The geometry of the superstructure model as well as the eight-segment model implemented in Ruaumoko [Carr, 2007] is illustrated in Figure 5-21 and Figure 5-22, respectively. It is noted that due to geometric symmetry of the superstructure, only half of the numerical model is presented in Figure 5-22. The end nodes of the superstructure frame elements and tendon spring are constrained to have the same vertical displacement.

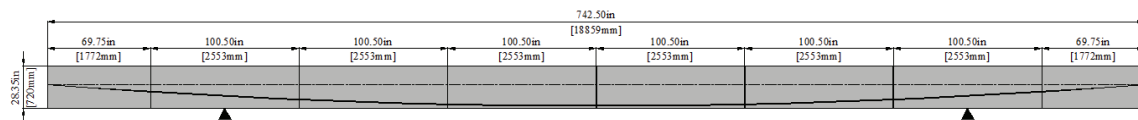


Figure 5-21: Elevation view of the eight-segment model

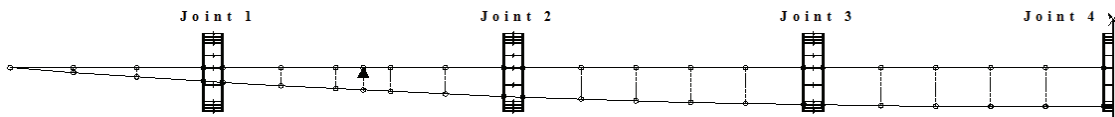


Figure 5-22: Elevation view of the eight-segment numerical model

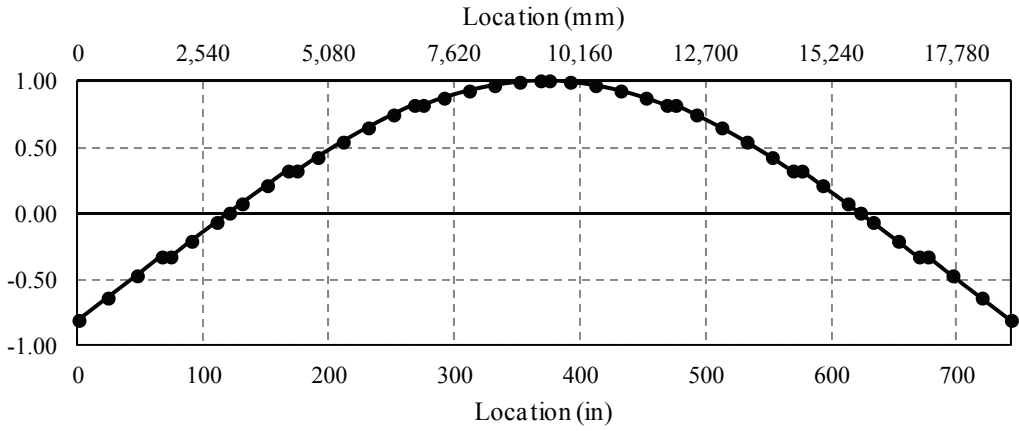


Figure 5-23: First mode of vibration of the eight-segment numerical model

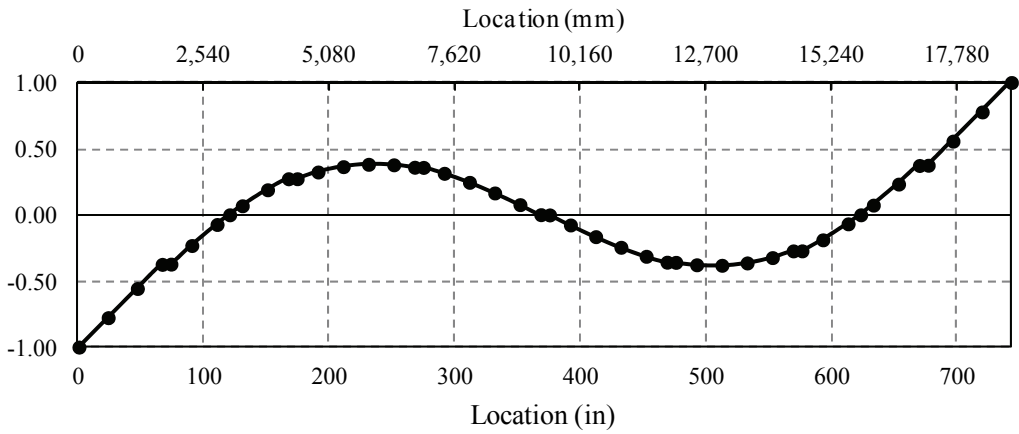


Figure 5-24: Second mode of vibration of the eight-segment numerical model

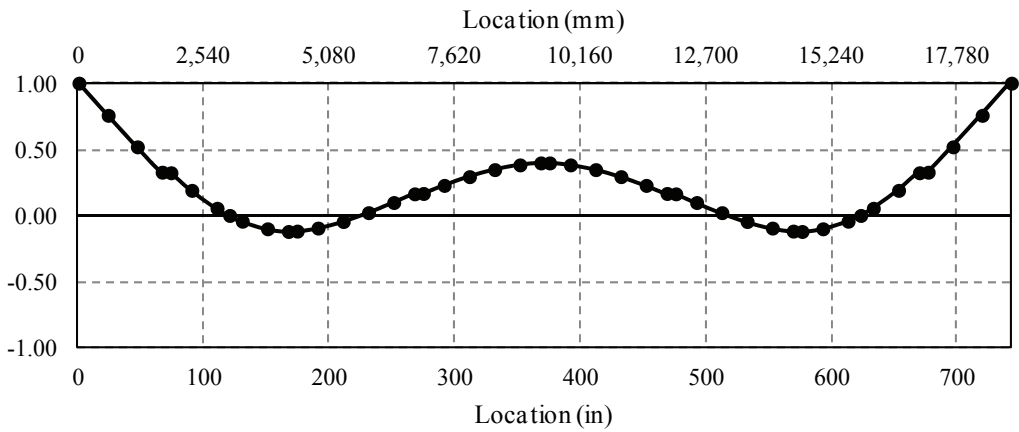


Figure 5-25: Third mode of vibration of the eight-segment numerical model

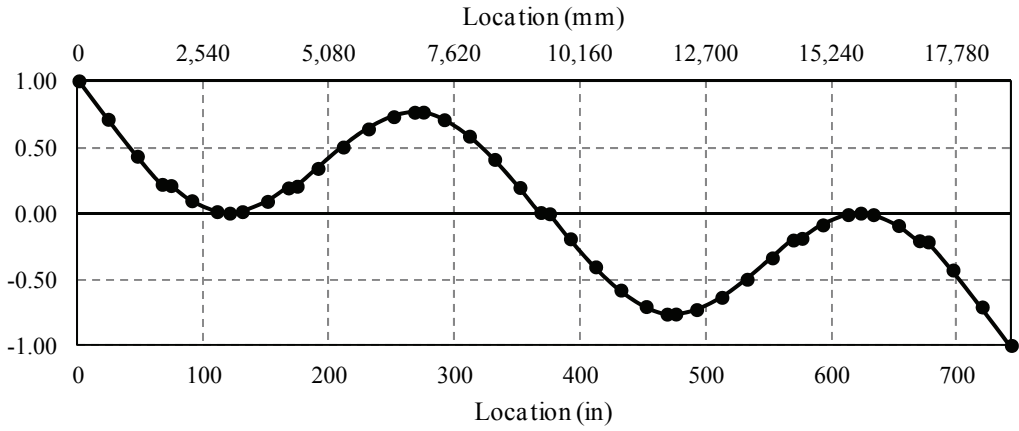


Figure 5-26: Fourth mode of vibration of the eight-segment numerical model

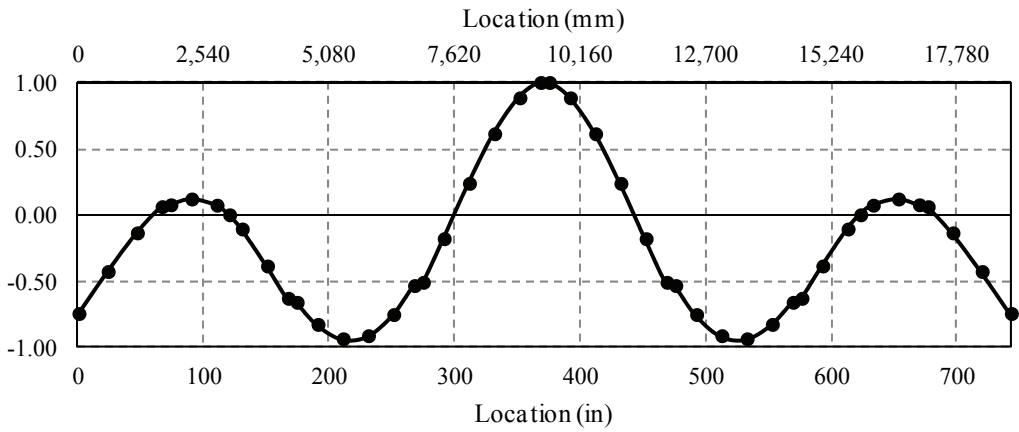


Figure 5-27: Fifth mode of vibration of the eight-segment numerical model

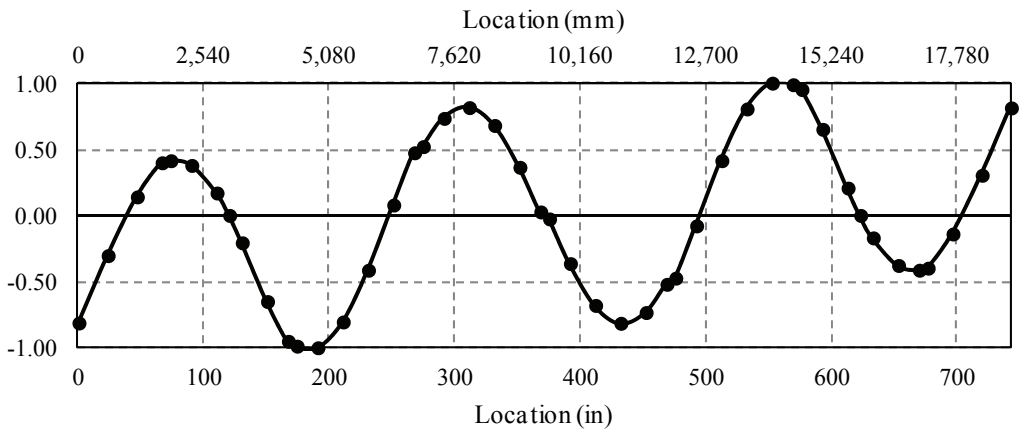


Figure 5-28: Sixth mode of vibration of the eight-segment numerical model

The computed first six mode shapes of the eight-segment numerical model are presented in Figure 5-23 to Figure 5-28, respectively. The associated periods of vibration are listed in Table 5-5. Note that only the self-weight of the superstructure is accounted for the calculation of the periods of vibration and mode shapes of the model.

Table 5-5: Periods of vibration of the eight-segment numerical model

Mode	Frequency (Hz)	Period (sec)
1	8.62	0.116
2	25.51	0.039
3	38.65	0.026
4	59.92	0.017
5	104.40	0.010
6	167.00	0.006

The first, third and fifth mode shapes are symmetrical with respect to the vertical axis passing through the mid-span cross-section of the numerical model as shown in Figure 5-23, Figure 5-25 and Figure 5-27, respectively. On the other hand, the second, fourth and sixth mode shapes are anti-symmetrical as shown in Figure 5-24, Figure 5-26 and Figure 5-28, respectively. Consequently when a symmetric vertical excitation is applied at the mid-span section of the superstructure model, the second, fourth and sixth modes (odd numbered modes) are not excited as the mid-span section is a point of inflection for those modes and all the response is due to the first, third and fifth modes (even numbered modes).

According to the frequency values for the first six modes tabulated in Table 5-5, it is observed that the frequency ratios are roughly in the ratios 1:3:5:7:12:19.

By substituting the cross sectional properties of the eight-segment numerical model into Equation (5-1), its fundamental period of vibration is computed to be equal 0.107 seconds. Moreover, the fundamental period of vibration of the superstructure model computed using the simplified Uniform Load method according to AASHTO LRFD Bridge Design Specification [2007], equals 0.118 seconds as presented in Table 3-5.

In Table 5-6, the values of the first mode of vibration for the superstructure model are summarized, as computed with different procedures mentioned above. All fundamental period values are in the same range however, slight differences are observed. For the periods obtained from the modal analysis of the eight-segment numerical model and Equation (5-1) assuming a continuous simply supported beam, only the self-weight of the superstructure is accounted. On the other hand, for the case of the Uniform Load method according to AASHTO [2007] the superstructure's seismic mass, as presented in Section 3.2.3, accounts for the self-weight of the superstructure as well as, permanent and live loads. Moreover, both the Uniform Load method

and the analytical solution expressed by Equation (5-1) assume a continuous simply supported superstructure beam whereas; the modal analysis incorporates the gaps between the superstructure's segments.

Table 5-6: Fundamental periods of vibration of superstructure model

Method	Period (sec)
Modal analysis	0.116
Analytical solution (Equation 4.1)	0.107
Uniform Load method [AASHTO, 2007]	0.118

In order to capture the response of the eight-segment superstructure model, a vertical cyclic sinusoidal displacement-controlled load pattern is applied to all contact joints along the superstructure's span length. The load pattern follows the shape of the first mode of vibration of the eight-segment numerical model, as shown in Figure 5-23. The maximum amplitudes of the applied displacements are 3.17 inches (81 mm), 8.14 inches (207 mm) and 10.0 inches (254 mm) for Joint 2, Joint 3 and Joint 4 respectively (see Figure 5-22), whereas the period is set equal to 50.0 seconds. The displacement-controlled vertical loads applied to the contact joints are illustrated in Figure 5-29. The direction of the load is initially downward and then reversed.

Based on the response of the two-segment numerical model, the joint length is assumed to be equal to $h/4$, where h is the height of the contact zone whereas the percentage of critical damping is set equal to 5%.

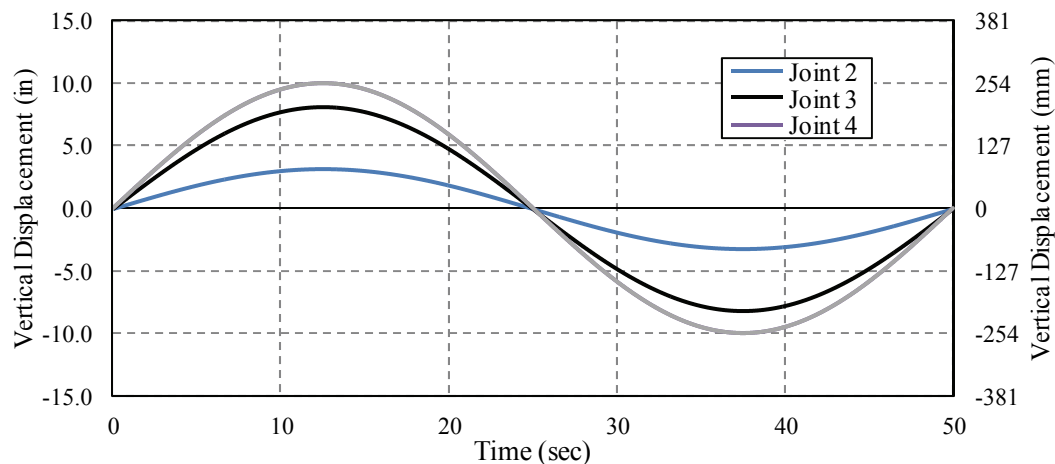


Figure 5-29: Vertical cyclic sinusoidal displacement-controlled loads (T=50.0sec) applied at contact joints of the eight-segment numerical model

The results of the eight-segment numerical model are expressed in terms of total developed vertical reaction at the support versus the applied vertical displacement for all contact joints along the superstructure's span length as shown in Figure 5-30, Figure 5-31 and Figure 5-32, respectively.

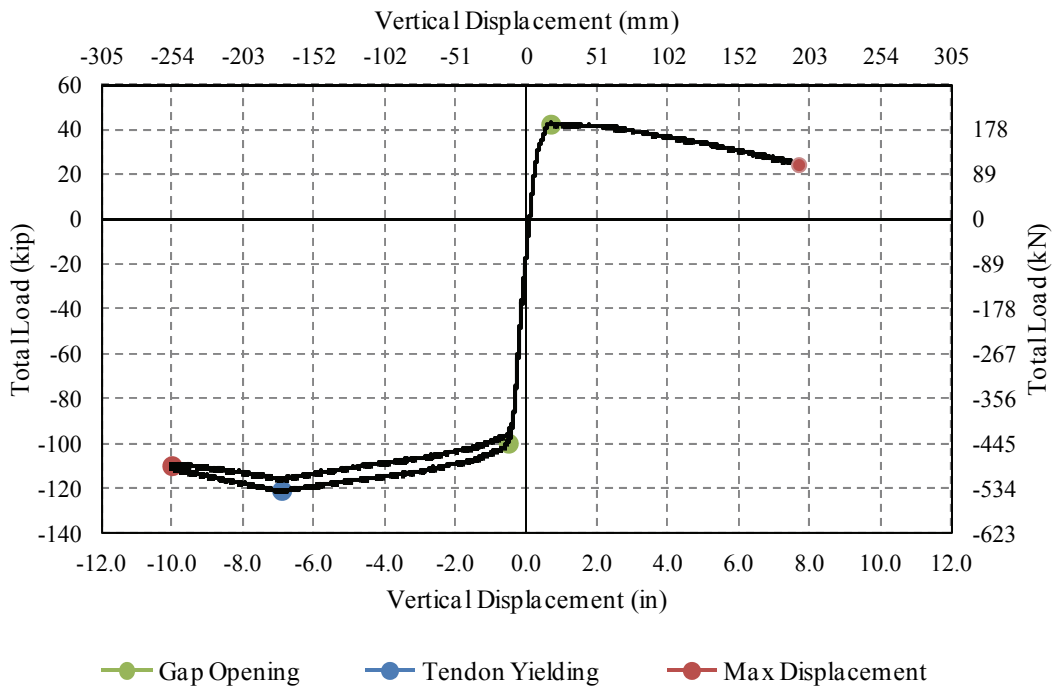


Figure 5-30: History of total load versus displacement of mid-span Joint 4 for the eight-segment numerical model

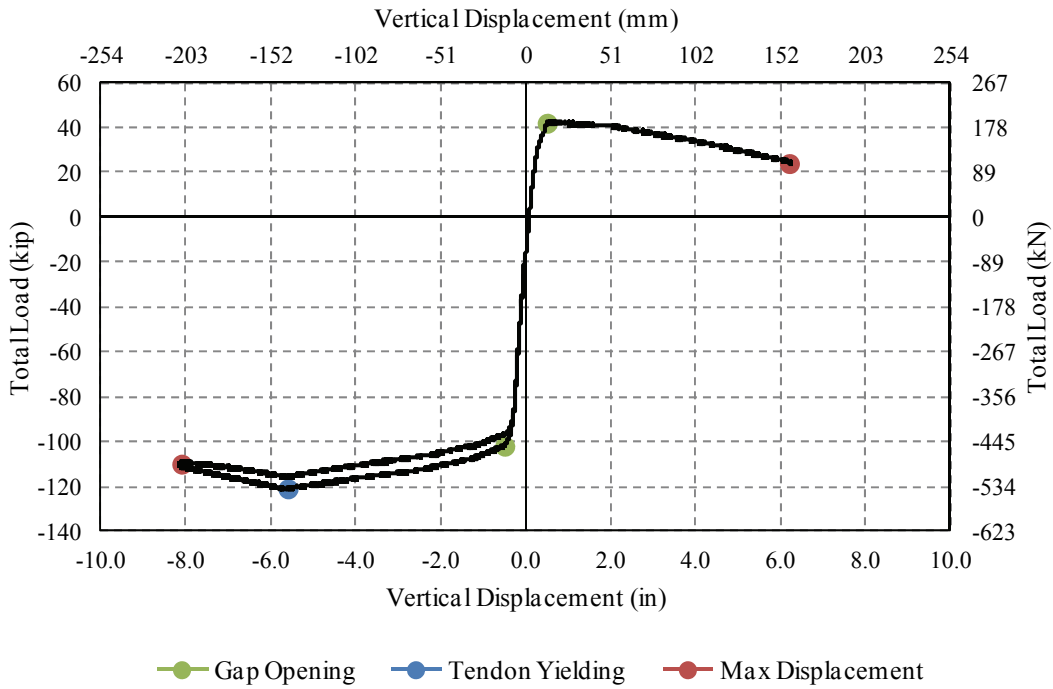


Figure 5-31: History of total load versus displacement of Joint 3 for the eight-segment numerical model

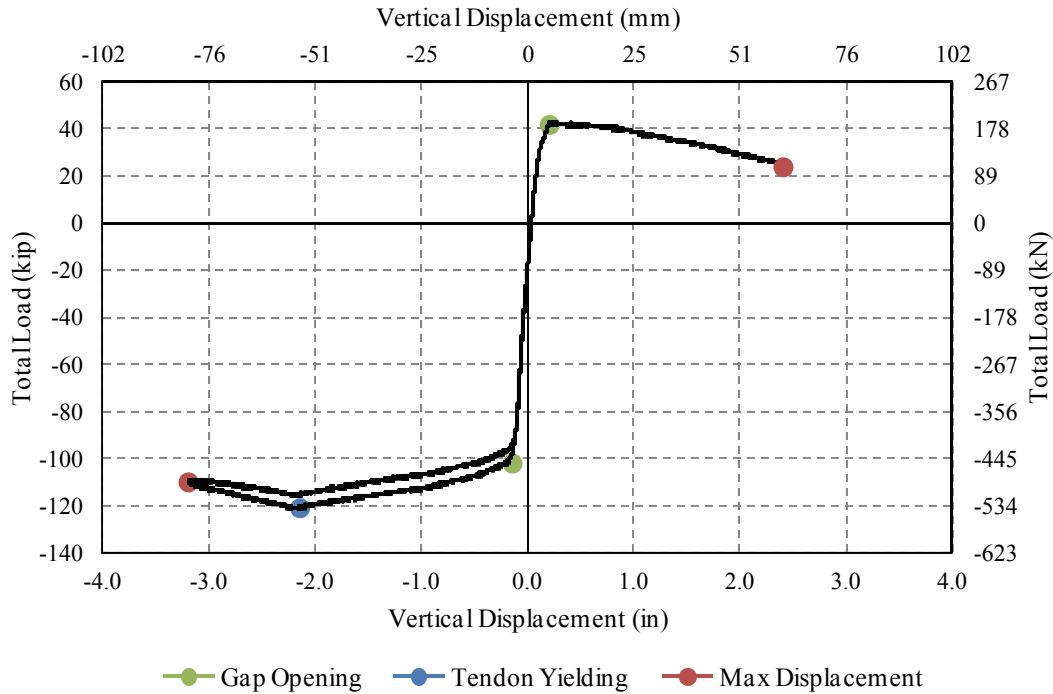


Figure 5-32: History of total load versus displacement of Joint 2 for the eight-segment numerical model

As the model is initially loaded in the downward direction, the initial stiffness is high representing the stiffness of the top compression springs which are activated when the gaps along the span open. At a load value of approximately -100 kips (-445 kN), a secondary post-yield stiffness slope is observed resulting from the opening of the joints and the yielding of the top springs. It should be noted that the compression springs properties are the same for all joints.

The maximum load of -120 kips (-534 kN) in the downward loading direction is reached at a displacement of -2.0 inches (-51 mm), -6.0 inches (-152 mm) and -7.0 inches (-178 mm) for Joint 2, Joint 3 and Joint 4 respectively. By further increasing the applied vertical displacement, a third negative stiffness is observed due to the yielding of the pre-stressed tendons. At a vertical total load of -110 kips (-490 kN), the maximum displacement of -3.0 inches (-76 mm), -8.0 inches (-203 mm) and -10.0 inches (-254 mm) is reached for Joint 2, Joint 3 and Joint 4 respectively. As the loading is reversed, the vertical load versus vertical displacement curve follows the same profile until the point of zero load and displacement.

In the upward loading direction, the maximum load of 40 kips (178 kN) is reached followed by a negative post-yield stiffness up to the maximum displacement which equals 2.5 inches (64 mm), 6.0 inches (152 mm) and 8.0 inches (203 mm) for Joint 2, Joint 3 and Joint 4 respectively.

After a full cyclic loading the eight-segment numerical model has returned to its original state, behaving as a self-centering system. However, the model exhibits a different behavior when subjected to downward and upward vertical loading due to the unbonded tendon lying below the

center of gravity of the model's cross-section. For the case of downward loading a narrow hysteretic loop is observed resulting from the yielding of the top compression springs when the joints open. On the other hand, for the case of upward loading the bottom compression springs have not yield and consequently no hysteretic energy is dissipated.

For the case of Joint 1 placed between the support and the cantilever end section, the history of total developed vertical reaction at the support versus its vertical displacement is illustrated in Figure 5-33.

In order to examine the displacement profile of the superstructure model under maximum downward and upward loading, Figure 5-34 and Figure 5-35 are presented hereafter.

As mentioned earlier, the displacement-controlled load pattern applied to the joints of the eight-segment numerical model was constrained to match the first mode shape. However, if a single displacement-controlled load is applied at the mid-span joint (Joint 4) of the eight-segment numerical model the deflection profile of the model due to downward an upward loading is illustrated in Figure 5-36 and Figure 5-37.

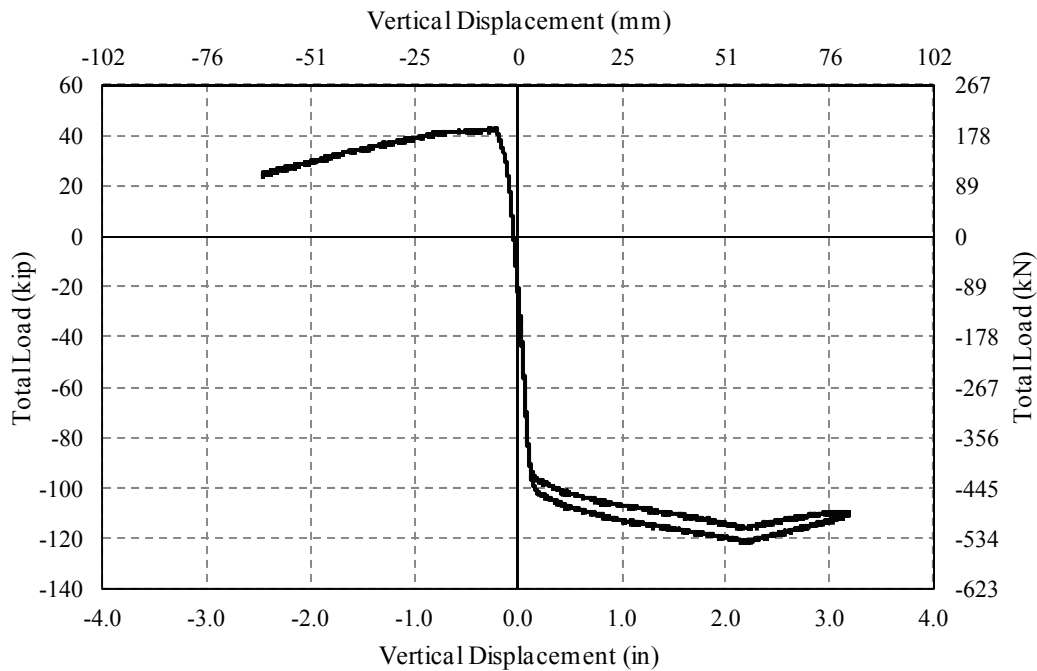


Figure 5-33: History of total load versus displacement of Joint 1 for the eight-segment numerical model

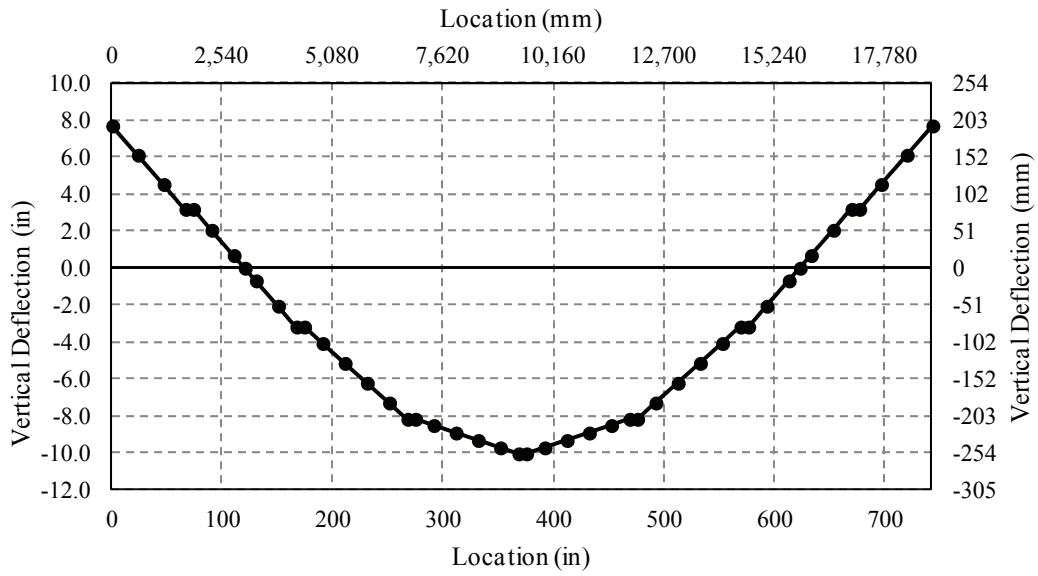


Figure 5-34: Deflection profile of the eight-segment numerical model due to maximum downward loading

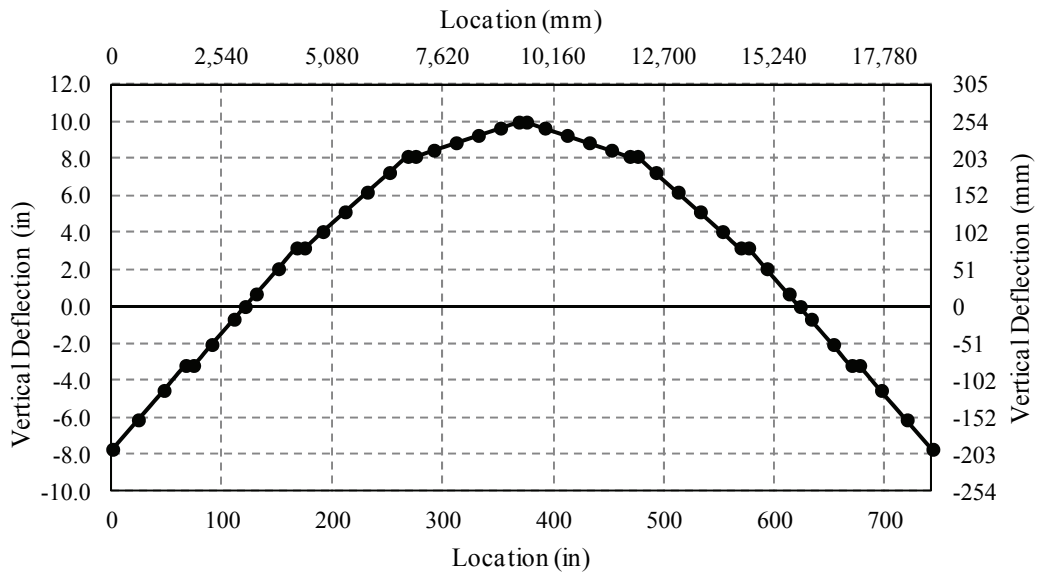


Figure 5-35: Deflection profile of the eight-segment numerical model due to maximum upward loading

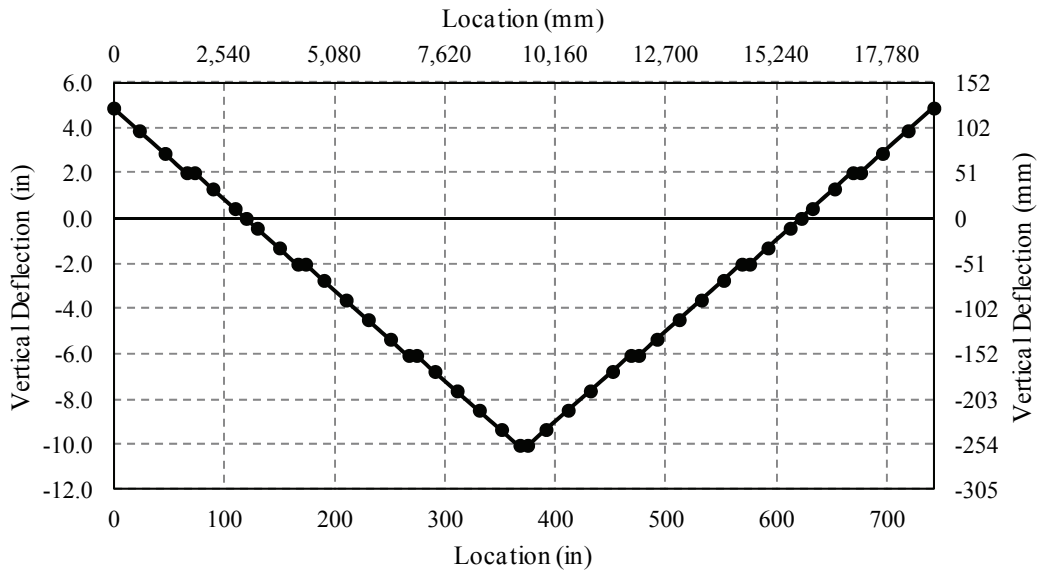


Figure 5-36: Deflection profile of the eight-segment numerical model due to maximum downward loading of the mid-span joint

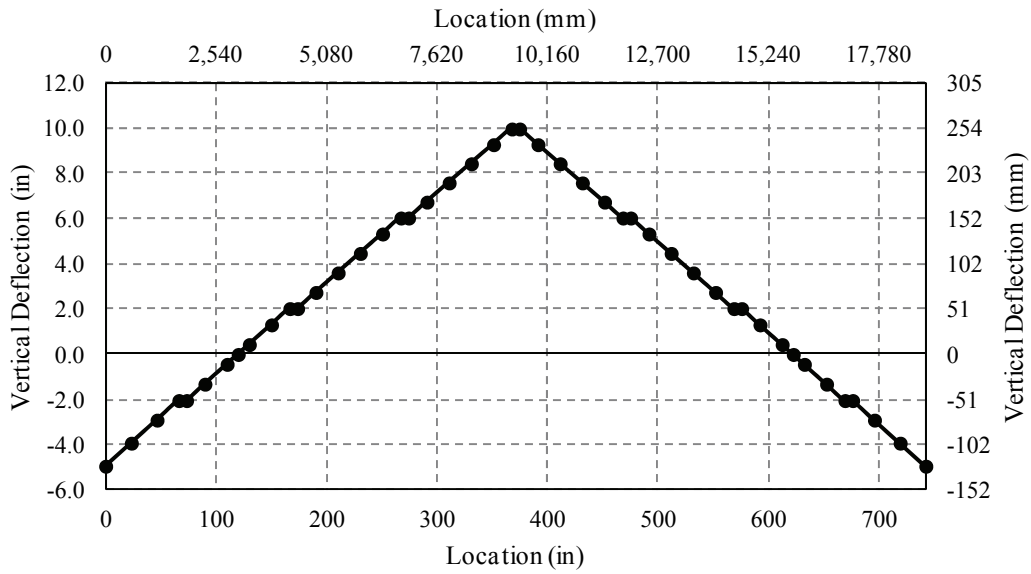


Figure 5-37: Deflection profile of the eight-segment numerical model due to maximum upward loading of the mid-span joint

It is evident that for the case of a single displacement-controlled load applied at the mid-span joint, the deflection profile of the eight-segment numerical model differs from the first period mode shape. However, it matches the results obtained from the two-segment model as presented in Figure 5-16 and Figure 5-17. This response is attributed to the discontinuity along the model's length resulting from the joints gap opening. Consequently, the displacement profile of the model changes from a continuous parabola to a linear shape, matching the deflection profile of a cantilever beam element.

Even though it would be reasonable to evaluate the response of the superstructure's numerical model under a force-controlled load pattern, there are several restrictions concerning this approach mainly because of the difference in the model's response under downward and upward loading. The unbonded pre-stressed tendon which lay below the center of gravity of the superstructure's cross-section imposes an alternation of the model's stiffness when the structure is subjected to a vertical load pattern of opposite directions. For this reason and in order to evaluate the model's response under a vertical force-controlled load pattern, the assigned maximum positive and negative force amplitudes need to be different introducing a considerable amount of uncertainties.

Based on the response obtained from the two-segment and eight-segment numerical models, a series of vertical seismic excitation records are used in order to investigate the model's response under real earthquake vertical motions and identify possible damage limit states. The results of these vertical seismic analyses are discussed in the next Chapter.

SECTION 6

SEISMIC RESPONSE OF SUPERSTRUCTURE MODEL

In this chapter, the response of the superstructure model is evaluated by subjecting the numerical model presented in Chapter 5 to a series of vertical historical earthquake ground motions. Two design performance levels are considered according to the ASCE/SEI 7-05 [2005] specifications: the Design Earthquake (DE) and the Maximum Considered Earthquake (MCE). An ensemble of historical vertical earthquake records is selected based on the FEMA, ATC-63 [2008] guidelines for quantifications of buildings seismic performance.

The seismic response of the superstructure model is evaluated by computing the cumulative probability distribution function of four selected quantities – the maximum upward and downward vertical displacement of the mid-span cross-section as well as, the maximum top and bottom gap opening of the mid-span contact zone, for both design DE and MCE intensity levels.

6.1 Design Response Spectra

According to ASCE/SEI 7-05 [2005] provisions, two intensity levels of design seismic ground motions are defined: the Design Earthquake (DE) and the Maximum Considered Earthquake (MCE). It should be noted that all design specifications presented hereafter apply only to the horizontal components of the seismic ground motions whereas the contribution of the vertical component is neglected.

The acceleration Design Earthquake response spectrum (DE) is developed as described hereafter:

- for periods less than T_0 , the design spectral response acceleration, S_a , equals:

$$S_a = S_{DS} \left(0.4 + 0.6 \frac{T}{T_0} \right) \quad (6-1)$$

- for periods greater than or equal to T_0 and less than or equal to T_s , the design spectral response acceleration, S_a , shall be taken equal to S_{DS} ;
- for periods greater than T_s , the design spectral response acceleration, S_a , equals:

$$S_a = \frac{S_{D1}}{T} \quad (6-2)$$

where S_{DS} is the design spectral response acceleration parameter at short periods, S_{D1} the design spectral response acceleration parameter at 1.0 second period, T the fundamental period of the structure, T_0 equals $0.2S_{D1}/S_{DS}$ and T_s equals S_{D1}/S_{DS} .

The design earthquake spectral response acceleration parameters at short periods, S_{DS} , and at 1.0 second period are determined according to:

$$S_{DS} = \frac{2}{3} S_{MS} \quad (6-3)$$

$$S_{D1} = \frac{2}{3} S_{M1} \quad (6-4)$$

where S_{MS} the maximum considered earthquake (MCE) spectral response acceleration for short periods and S_{M1} the maximum considered earthquake (MCE) spectral response acceleration at 1.0 second period.

The design of the bridge model superstructure under vertical seismic induced loads was based on defining the elastic seismic response coefficient, C_{sm} and the response modification factor, R for the system (see Section 3.2.3). In Figure 6-1, the seismic response coefficient for the prototype bridge, the elastic scaled bridge model and the design scaled model – assuming a R-factor equal to 2.50, is presented for a range of periods from zero to two seconds.

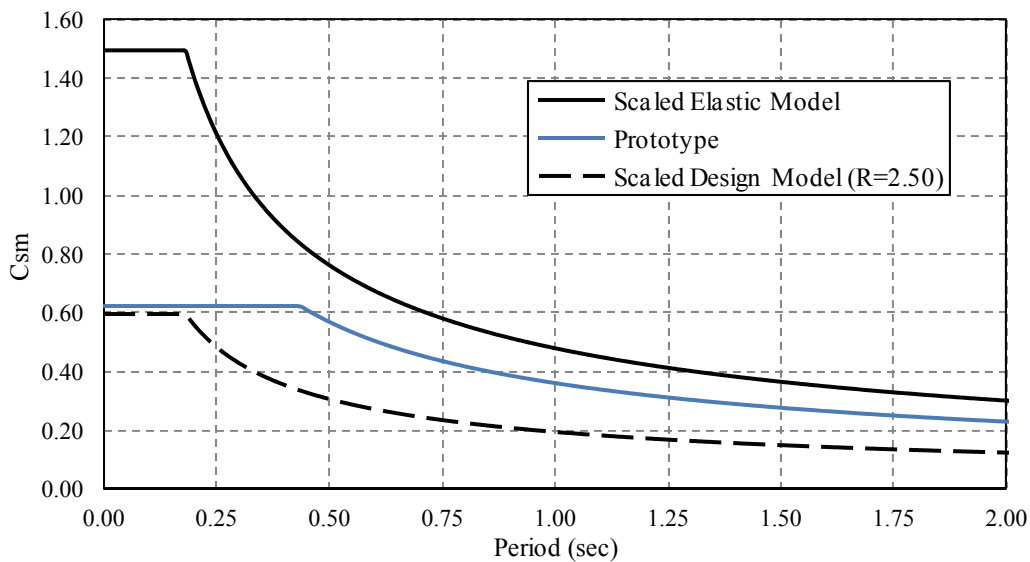


Figure 6-1: Seismic response coefficient for the prototype bridge, elastic and design scaled test model [AASHTO, 2007]

The design earthquake spectral acceleration parameters defined by ASCE/SEI 7-05 [2005] can be computed through correlation with the seismic response coefficient, C_{sm} . As shown in Figure 6-1, the design spectral response acceleration parameter at short periods, S_{DS} equals 0.625 g for the prototype bridge structure.

Using the Seismic Hazard Curves and Uniform Hazard Response Spectra provided by the U.S. Geological Survey website, the design and maximum earthquake spectral response acceleration parameters for a prototype bridge structure located at Western United States (WUS) are: S_{DS} equals 0.625 g, S_{D1} equals 0.273 g, S_{MS} equals 0.938 g and S_{M1} equals 0.410 g. These values are compared to the spectral acceleration parameters of a prototype bridge located at the City of Los Angeles (LAC). The values for both cases are summarized in Table 6-1 and the corresponding DE and MCE acceleration response spectra are illustrated in Figure 6-2, assuming a 5% of critical damping.

Table 6-1: Seismic ground motion design parameters [USGS, ASCE/SEI 7-05]

Quantity	WUS	LAC
S_{MS} (g)	0.938	2.123
S_{MI} (g)	0.410	1.176
S_{DS} (g)	0.625	1.415
S_{DI} (g)	0.273	0.784
T_s (sec)	0.437	0.554

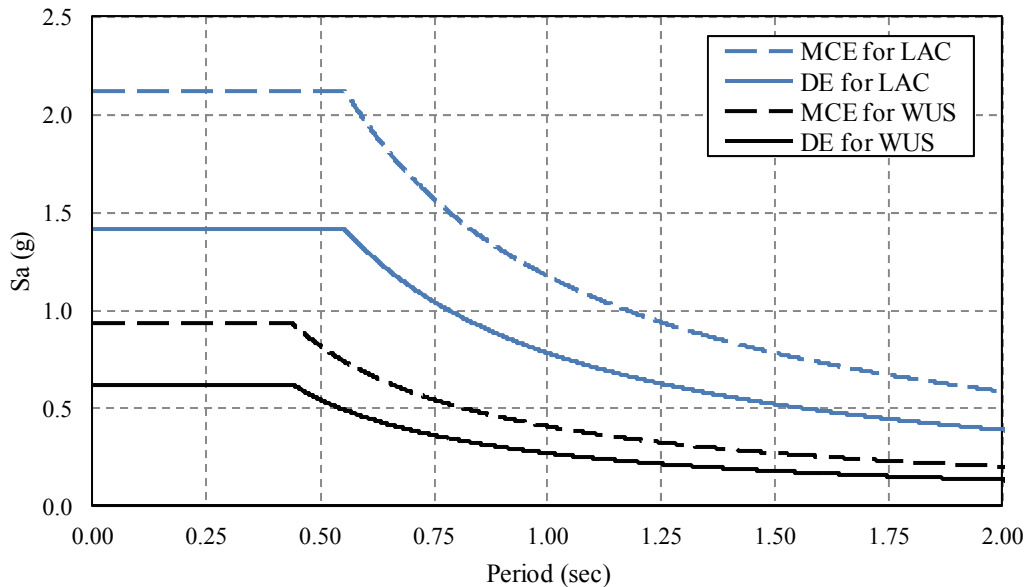


Figure 6-2: Design and Maximum Considered Earthquake response spectra for a prototype bridge located at Western United States and City of Los Angeles [USGS, ASCE/SEI 7-05]

The eight-segment numerical model of the bridge superstructure, as described in Section 5.4, is analyzed for vertical seismic loads that correspond to the earthquake response spectra of both considered locations presented in Table 6-1 and Figure 6-2. According to Section 3.3, the design of the bridge’s superstructure is not governed by the Extreme Event I load combination, including earthquake loads for a prototype bridge structure located at WUS. Consequently, a higher seismic intensity level can be considered such as the case of a prototype bridge located the LAC. The following Sections present the results of the superstructure’s vertical seismic response considering the DE and MCE hazard intensity levels of a bridge located at the LAC.

The DE and MCE acceleration response spectral values, presented in Table 6-1, need to be scaled to match the similitude requirements of the scaled bridge model (see Section 2.3). The time and acceleration scaling factors are:

$$S_t = \frac{t_p}{t_m} = 2.39 \quad (6-5)$$

$$S_a = \frac{a_p}{a_m} = 0.42 \quad (6-6)$$

The scaled DE and MCE acceleration response spectra for LAC are obtained after applying Equations (6-5) and (6-6) to the corresponding prototype response spectra. The plots are presented in Figure 6-3 assuming a 5% of critical damping.

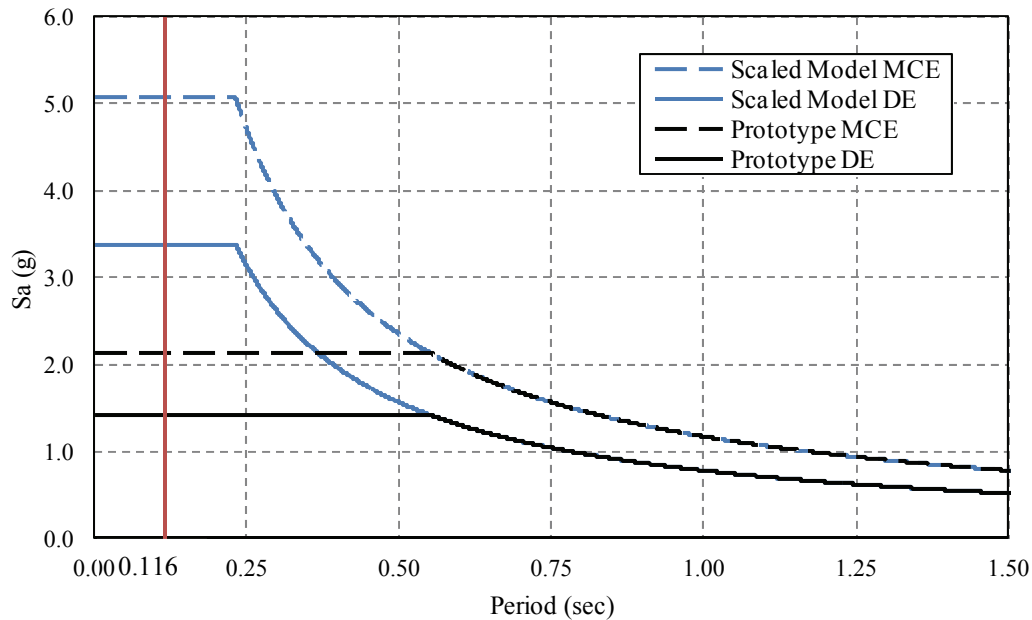


Figure 6-3: Design and Maximum Considered Earthquake response spectra for the prototype bridge and scaled bridge model located at the City of Los Angeles [USGS, ASCE/SEI 7-05]

The fundamental period of vibration of the eight-segment superstructure model equals 0.116 seconds (see Table 5-6), corresponding to the plateau of the scaled DE and MCE acceleration response spectra, as shown in Figure 6-3.

6.2 Ground Motion Set

The seismic response of the superstructure model under historical earthquake motions is investigated based on the ATC-63 far-field earthquake ground motion ensemble [FEMA ATC-63, 2008]. The PEER-NGA database is used to obtain the selected ground motion records. In order to ensure that the selected records represent strong ground motions that may cause structural collapse, minimum limits on event magnitude (> 6.5), peak ground acceleration ($> 0.2g$) and peak ground velocity (15 cm/sec) were imposed. The twenty-two ATC-63 [2008] records are tabulated in Table 6-2.

Table 6-2: ATC-63 far-field ground motion records [ATC-63, 2008]

ID	Magnitude	Year	Earthquake	Station Name
12011	6.7	1994	Northridge	Beverly Hills - 14145 Mulhol
12012	6.7	1994	Northridge	Canyon Country - W Lost Canny
12041	7.1	1999	Duzce, Turkey	Bolu
12052	7.1	1999	Hector Mine	Hector
12061	6.5	1979	Imperial Valley	Delta
12062	6.5	1979	Imperial Valley	El Centro Array #11
12071	6.9	1995	Kobe, Japan	Nishi-Akashi
12072	6.9	1995	Kobe, Japan	Shin-Osaka
12081	7.5	1999	Kocaeli, Turkey	Duzce
12082	7.5	1999	Kocaeli, Turkey	Arcelik
12091	7.3	1992	Landers	Yermo Fire Station
12092	7.3	1992	Landers	Coolwater
12101	6.9	1989	Loma Prieta	Capitola
12102	6.9	1990	Loma Prieta	Gilroy Array #3
12111	7.4	1987	Manjil, Iran	Abbar
12121	6.5	1987	Superstition Hills	El Centro Imp. Co. Cent
12122	6.5	1987	Superstition Hills	Poe Road
12132	7.0	1992	Cape Mendocino	Rio Del Overpass - FF
12141	7.6	1999	Chi-Chi, Taiwan	CHY101
12142	7.6	1999	Chi-Chi, Taiwan	TCU045
12151	6.6	1971	San Fernando	LA - Hollywood Stor FF
12171	6.6	1976	Friuli, Italy	Tolmezzo

According to FEMA ATC-63 [2008], the horizontal components of the considered ground motions were normalized by peak ground velocity in order to remove unwarranted record-to-record variability, and scaled using a method proposed by Kircher [1996] so that the geometric mean of the spectral acceleration at a period of 1.0 second is at a target of 1.0 g.

It should be noted that only the two horizontal components of the twenty two ATC-63 ground motions are considered for the quantification of structural seismic performance according to FEMA ATC-63 [2008] whereas; the vertical component is neglected. It is therefore evident that although information on horizontal acceleration response spectra is widely available, the corresponding vertical spectra are not defined in current seismic codes in the United States.

From the twenty two ATC-63 ground motions, the vertical component of the 12122-record was not provided by the PEER-NGA database and consequently twenty-one ground motions are considered for obtaining the response of the superstructure model.

The time histories of the two horizontal components of the twenty-one historical ground motions are scaled in order to match the similitude requirements of the scaled superstructure model (see Section 2.3). The scaled time histories are obtained by applying Equations (6-5) and (6-6) to the original time histories. The corresponding acceleration response spectra are plotted assuming a 5% of critical damping. The similitude-scaled acceleration response spectra for the two horizontal components of the ATC-63 historical records are presented in Figure 6-4 as well as, the median horizontal acceleration response spectrum.

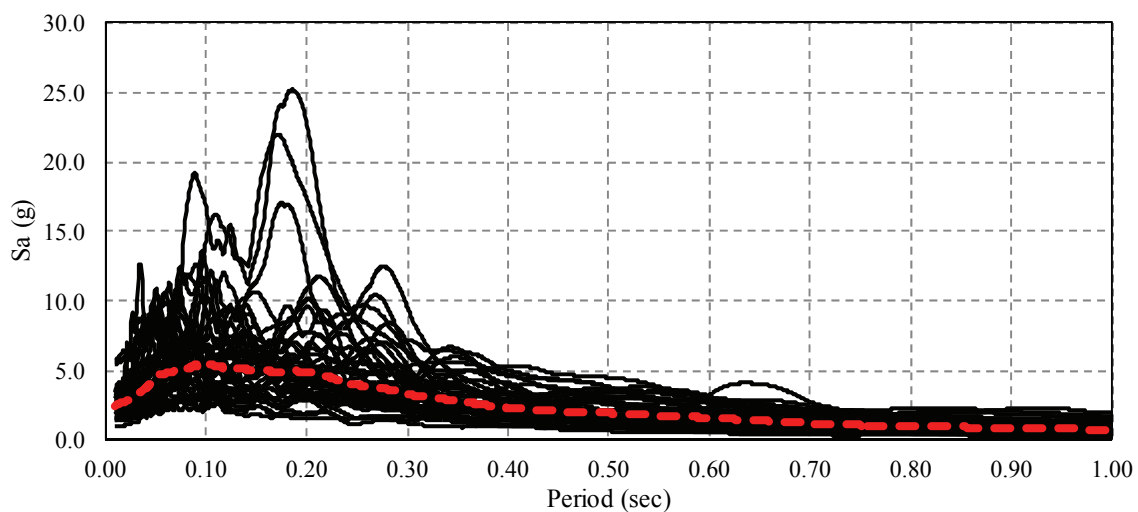


Figure 6-4: Acceleration response spectra of the horizontal components of similitude-scaled ATC-63 ground motions and median acceleration response spectrum, 5% critical damping

A scaling procedure is applied to all ATC-63 similitude-scaled horizontal ground motions in order to match the two considered seismic intensity levels of the Design Earthquake (DE) and the Maximum Considered Earthquake (MCE) for the LAC, as defined in Figure 6-3. For each intensity level and each record, the acceleration response spectrum is multiplied by a factor defined as the ratio of the scaled design spectral acceleration at a target period equal to the fundamental period of vibration of the superstructure model, over the geometric mean of the scaled horizontal spectral accelerations at the same target period. The scaled design spectral acceleration at a period of 0.116 seconds equals 3.380 g and 5.070 g for the case of DE and MCE, respectively (see Figure 6-3). In addition, the geometric mean of the similitude-scaled horizontal spectral accelerations is computed for a period of 0.116 seconds to equal 5.241 g (see Figure 6-4).

Based on the above, the similitude-scaled acceleration response spectra for the horizontal components of the ATC-63 records should be multiplied by a factor of 0.645 and 0.967 for the case of DE and MCE, respectively, so that their median matches the corresponding DE and MCE acceleration design values at a period of 0.116 seconds.

The acceleration response spectra of the original vertical ATC-63 ground motions are presented in Figure 6-5, assuming 5% of critical damping. The corresponding similitude-scaled acceleration response spectra are presented in Figure 6-6, assuming 5% of critical damping.

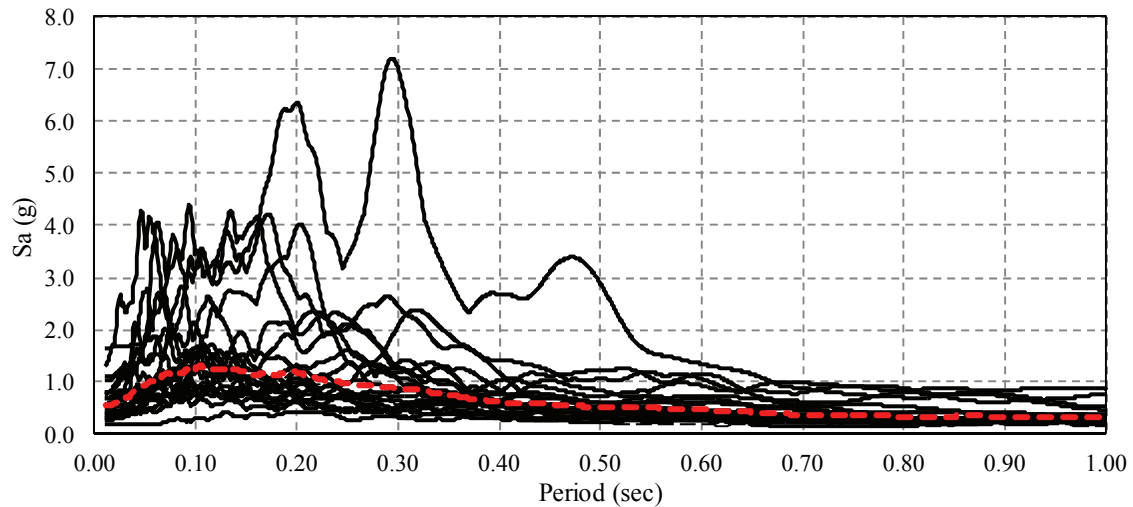


Figure 6-5: Acceleration response spectra of the vertical component of the original ATC-63 ground motions and median acceleration response spectrum, 5% critical damping

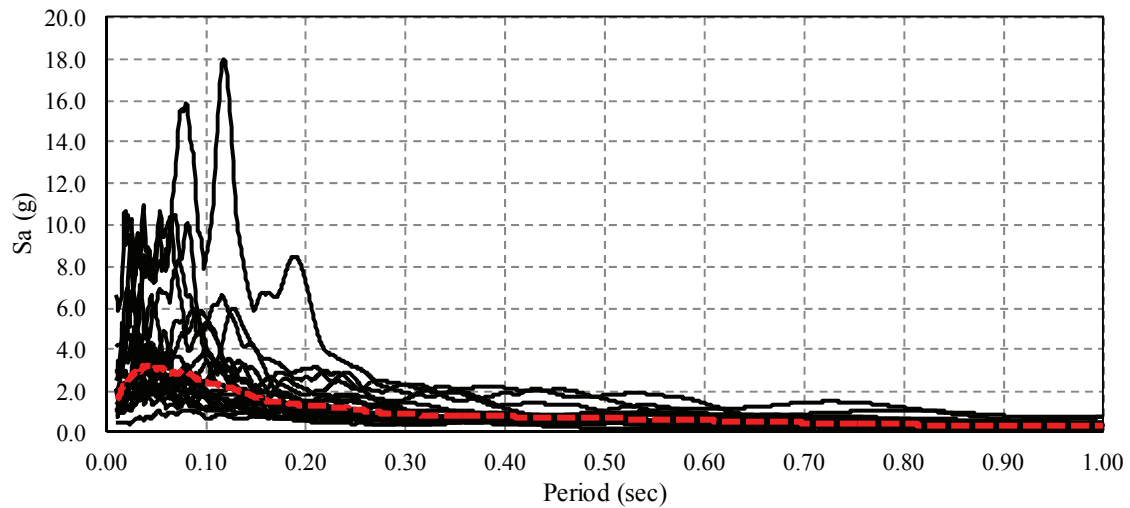


Figure 6-6: Acceleration response spectra of the vertical component of the similitude-scaled ATC-63 ground motions and median acceleration response spectrum, 5% critical damping

Through comparison of Figure 6-5 and Figure 6-6, it becomes evident that the acceleration response spectra of the similitude-scaled vertical ground motions are amplified and shifted towards the high frequency range compare to the response spectra of the original ground motions.

The current bridge design codes provide little guidance on the development of a vertical design spectrum. Thus, the scale factors obtained for the similitude-scaled horizontal ground motions and the two considered seismic intensity levels – DE and MCE, were also used on the similitude-

scaled vertical ground motions. Specifically, the similitude-scaled vertical acceleration response spectra are multiplied by a factor of 0.645 and 0.967 for the case of DE and MCE, respectively.

Table 6-3 presents the peak ground acceleration for each of the vertical ATC-63 ground motion considering the cases of original and similitude-scaled records as well as, the DE and MCE intensity levels. The original and similitude-scaled duration of each record are also presented.

Table 6-3: Peak ground acceleration and duration of vertical ATC-63 ground motions

EQ	PGA (g)				Duration (sec)	
	Original	Scaled	DE	MCE	Original	Scaled
12011	0.67	1.91	1.29	1.93	29.98	11.99
12012	0.70	1.86	1.25	1.88	19.98	7.99
12041	0.34	0.90	0.61	0.91	55.89	22.36
12052	0.43	1.10	0.74	1.11	45.30	18.12
12061	0.57	1.79	1.21	1.81	99.91	39.96
12062	0.37	0.96	0.65	0.97	39.03	15.61
12071	1.66	4.16	2.81	4.21	40.95	16.38
12072	0.17	0.43	0.29	0.43	40.95	16.38
12081	0.42	1.09	0.73	1.10	27.18	10.87
12082	0.31	1.03	0.69	1.04	29.99	12.00
12091	0.37	0.96	0.65	0.97	43.98	17.59
12092	0.49	1.37	0.93	1.39	27.96	11.19
12101	1.31	6.64	4.48	6.72	39.95	15.98
12102	0.79	3.07	2.07	3.11	39.94	15.98
12111	1.11	2.86	1.93	2.89	53.40	21.36
12121	0.29	0.76	0.51	0.77	40.00	16.00
12132	0.80	2.05	1.39	2.08	35.98	14.39
12141	0.28	0.73	0.49	0.74	89.99	36.00
12142	0.54	2.10	1.42	2.13	89.99	36.00
12151	0.77	2.51	1.70	2.55	27.99	11.20
12171	1.02	3.00	2.03	3.04	36.34	14.54

The acceleration response spectra of the vertical component of the similitude-scaled ATC-63 ground motions corresponding to the two considered seismic intensity levels, DE and MCE, are illustrated in Figure 6-7 and Figure 6-8, respectively, assuming a 5% of critical damping.

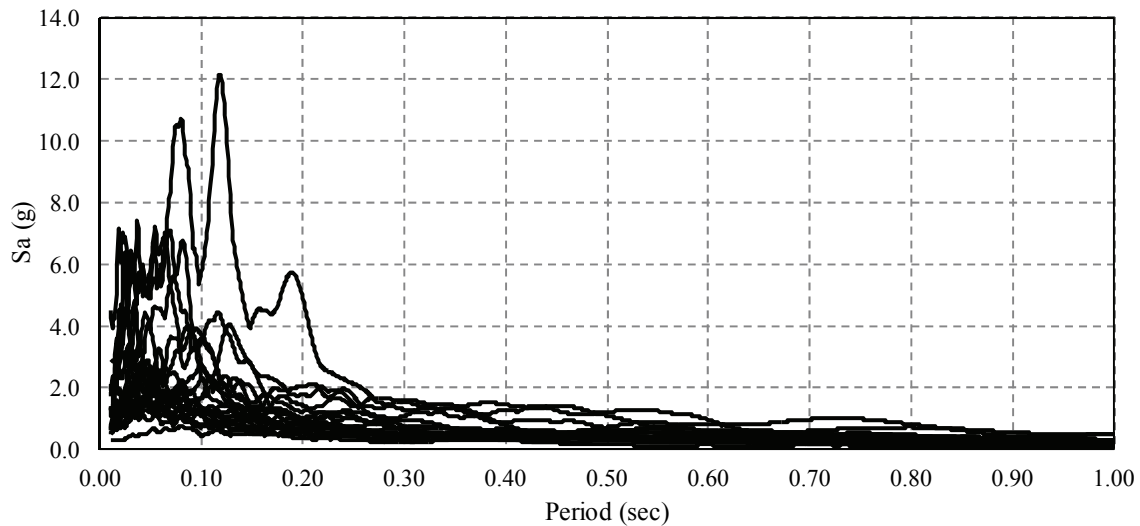


Figure 6-7: Acceleration response spectra of the vertical similitude-scaled ATC-63 ground motions for Design Earthquake (DE) intensity level, 5% critical damping

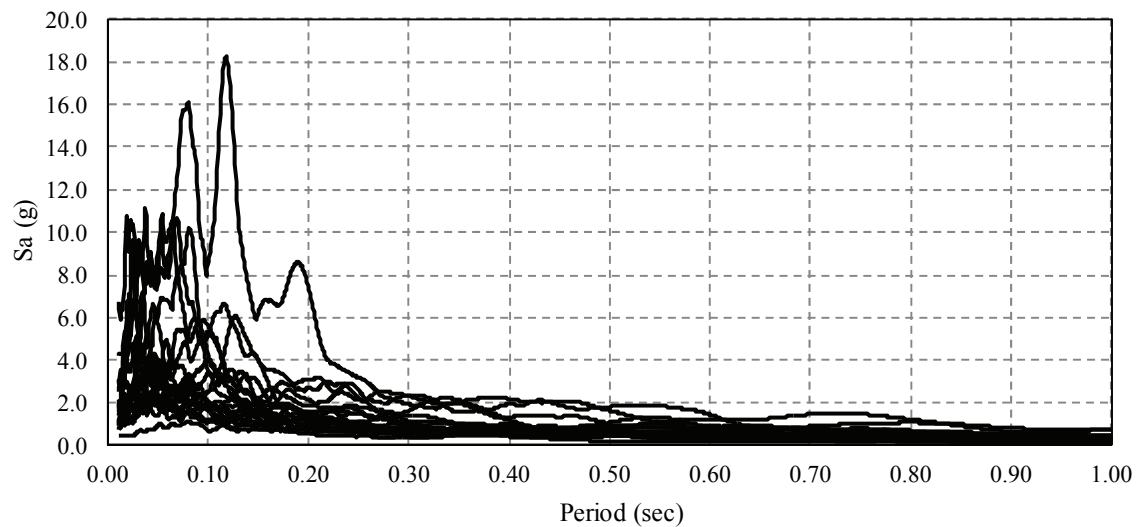


Figure 6-8: Acceleration response spectra of the vertical similitude-scaled ATC-63 ground motions for Maximum Considered Earthquake (MCE) intensity level, 5% critical damping

The same scaling factors are applied to the time histories of the similitude-scaled vertical ground motions. These acceleration time histories are used for conducting non-linear dynamic analyses of the eight-segment numerical model of the superstructure model, as presented in Section 5.4.

Summarizing, from the original twenty one vertical ATC-63 ground motions a series of forty-two acceleration time histories are produced considering the Design Earthquake and Maximum Considered Earthquake intensity levels of a bridge located at the City of Los Angeles [FEMA ATC-63, 2008]. Given that the response of the bridge superstructure differs significantly when subjected to upward and downward vertical loading, the forty-two ground motions will be applied to the numerical model considering both loading directions.

6.3 Seismic Response

The seismic response of the bridge's superstructure model is obtained by subjecting the eight-segment numerical model developed in Section 5.4 to a series of forty-two vertical ground motions. Both upward and downward loading are considered for the analyses.

The non-linear dynamic analyses are conducted using a Rayleigh damping model which is by definition proportional to the mass and stiffness matrix of the numerical model. Additionally, viscous damping, which is proportional to the nodal velocities, is expressed as a percentage of the model's critical damping. Based on the above, high values of inherent damping combined with a high frequency loading can result to unrealistically high values of developed damping forces. Given that a commonly adopted value of viscous damping assigned to regular concrete structures is in the range of 3% to 5% of the critical, a 3% of critical damping is assigned to the superstructure bridge model. The selected value is considered to be conservative enough so to minimize the uncertainties related to the effect of high damping forces to the structural response.

After conducting a series of non-linear dynamic analyses, the seismic response of the superstructure bridge model is evaluated by examining the variation of four response quantities in respect to the Design and Maximum Considered Earthquake intensity levels as well as, the direction of the loading. The selected response quantities are: the maximum upward (top) and downward (bottom) vertical displacement of the mid-span cross-section as well as, the maximum top and bottom gap opening of the mid-span contact zone (maximum elongation of top and bottom compression springs at mid-span section). The results obtained from the conducted dynamic analyses are expressed in terms of probability of non-exceedance of the selected response quantity versus the response quantity.

The maximum vertical displacement of the superstructure's mid-span cross-section is an indicative response quantity of the model's behavior when subjected to vertical seismic loading. Both cases of upward and downward maximum displacement are considered.

In Table 6-4, an indication of the most severe response in terms of maximum upward vertical displacement of the mid-span cross-section is given for both considered intensity levels and loading directions.

Additionally, the cumulative probability distribution function of the same response quantity is presented for both considered intensities, DE and MCE. In Figure 6-9, the probability of non-exceedance for the maximum upward vertical displacement is illustrated independently of the

loading direction whereas; in Figure 6-10 the upward and downward loading curves are presented separately.

Table 6-4: Maximum upward vertical displacement of mid-span cross-section

Max Upward Vertical Displacement		
Intensity	Downward Loading	Upward Loading
DE	0.352 in (8.93 mm)	0.502 in (12.75 mm)
MCE	0.705 in (17.91 mm)	0.524 in (13.32 mm)

The overall maximum response in terms of upward vertical displacement occurs for the case of the MCE and downward loading direction. The maximum response equals 0.705 inches (17.91 mm) whereas the maximum upward vertical displacement of the mid-span section of the eight-segment numerical model for the case of displacement-controlled loading is approximately equal to 8.0 inches (203 mm), as shown in Figure 5-30. Consequently, the superstructure model can be subjected to higher earthquake intensity levels that the ones specified by FEMA ATC-63 [2008] without collapsing.

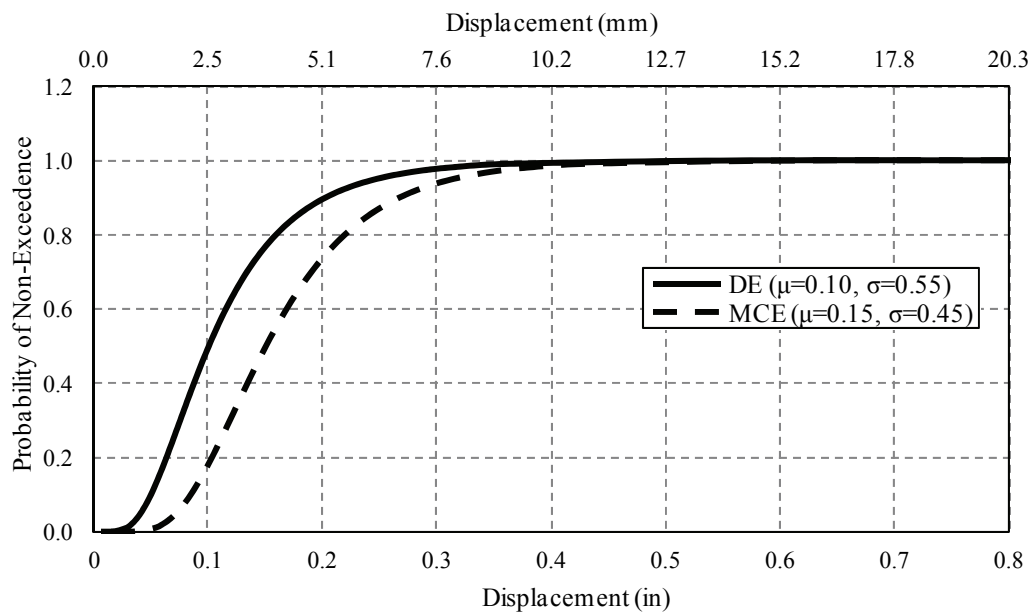


Figure 6-9: Cumulative probability distribution function of maximum upward vertical displacement of mid-span cross-section considering the DE and MCE intensity levels

Given that the superstructure's behavior is affected by the presence of the unbonded tendons lying below the center of gravity of the model's cross-section, it is reasonable that the upward

vertical displacement response is greater for the case of downward loading for both considered intensity levels. However, the difference is not considered significant.

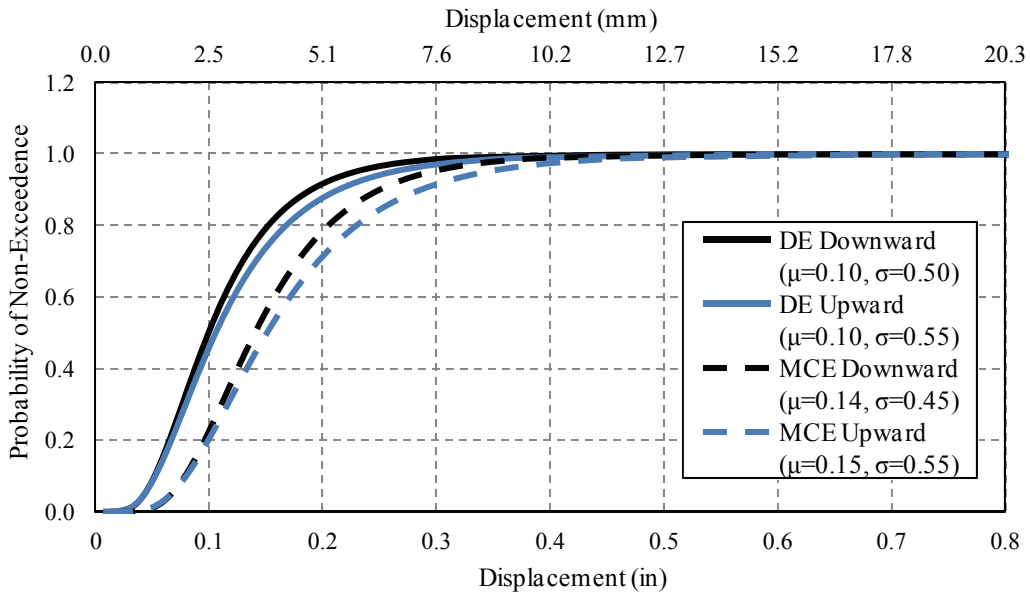


Figure 6-10: Cumulative probability distribution function of maximum upward vertical displacement of mid-span cross-section considering the DE and MCE intensity levels and different loading directions

In Table 6-5, an indication of the most severe response in terms of maximum downward vertical displacement of the mid-span cross-section is given for both considered intensity levels and loading directions.

Table 6-5: Maximum downward vertical displacement of mid-span cross-section

Max Downward Vertical Displacement		
Intensity	Downward Loading	Upward Loading
DE	0.925 in (23.49 mm)	0.703 in (17.85 mm)
MCE	1.149 in (29.18 mm)	0.980 in (24.90 mm)

Additionally, the cumulative probability distribution function of the same response quantity is presented for both considered intensities, DE and MCE. In Figure 6-11, the cumulative probability distribution function of the maximum downward vertical displacement is illustrated independently of the loading direction whereas; in Figure 6-12 the upward and downward loading curves are presented separately.

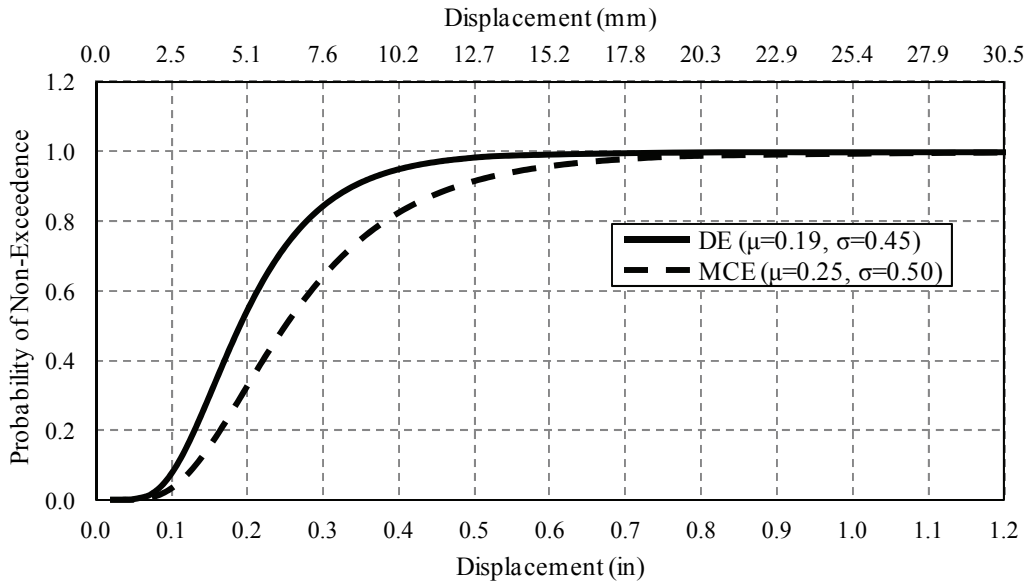


Figure 6-11: Cumulative probability distribution function of maximum downward vertical displacement of mid-span cross-section considering the DE and MCE intensity levels

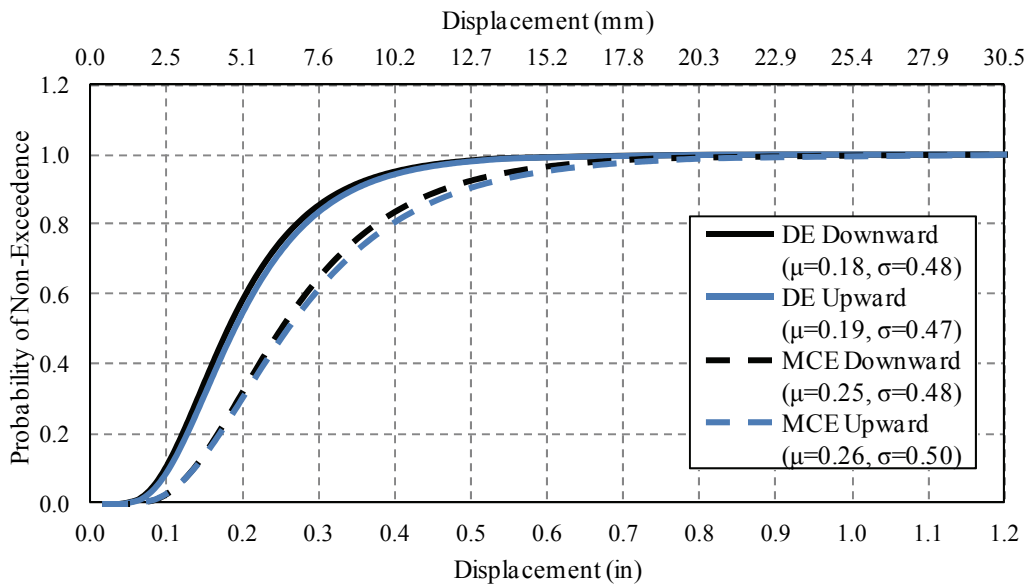


Figure 6-12: Cumulative probability distribution function of maximum downward vertical displacement of mid-span cross-section considering the DE and MCE intensity levels and different loading directions

The overall maximum response in terms of upward vertical displacement occurs for the case of the MCE and downward loading direction and equals 1.149 inches (29.18 mm). It should be noted that the maximum downward vertical displacement of the mid-span section of the eight-segment numerical model for the case of displacement-controlled loading is approximately equal to 10.0 inches (254 mm), as shown in Figure 5-30.

Through comparison of Table 6-4 and Table 6-5, it becomes apparent that the maximum downward vertical displacement of the superstructure model is considerably greater than the upward one. This can be attributed to the pre-stressing tendons which increase the strength of the bottom fiber of the superstructure's mid-span cross-section.

As for the case of maximum upward vertical displacement, the response for the case of downward and upward loading is not significantly different but slightly lower for the case of upward loading.

Another indicative response quantity of the model's non-linear behavior when subjected to vertical seismic loading is the maximum gap opening of the mid-span cross-section. The maximum gap opening is evaluated in terms of maximum elongation of the top (spring 1) and bottom (spring 11) compression springs of the mid-span contact zone. Both cases of upward and downward maximum displacement are considered.

In Table 6-6, an indication of the most severe response in terms of maximum top gap opening of the mid-span cross-section is given for both considered intensity levels and loading directions.

Additionally, the cumulative probability distribution function of the same response quantity is presented for both considered intensities, DE and MCE. In Figure 6-13, the cumulative probability distribution function of the maximum top gap opening is illustrated independently of the loading direction whereas; in Figure 6-14 the upward and downward loading curves are presented separately.

Table 6-6: Maximum top gap opening of mid-span cross-section

Max Top Gap Opening		
Intensity	Downward Loading	Upward Loading
DE	0.013 in (0.331 mm)	0.025 in (0.633 mm)
MCE	0.047 in (1.190 mm)	0.030 in (0.757 mm)

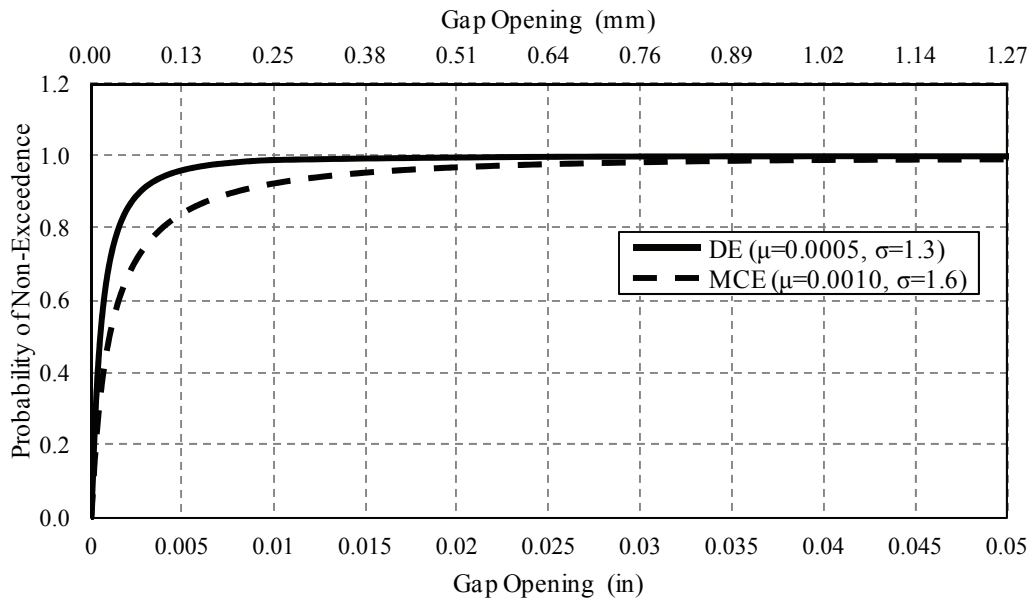


Figure 6-13: Cumulative probability distribution function of maximum top gap opening of mid-span cross-section considering the DE and MCE intensity levels

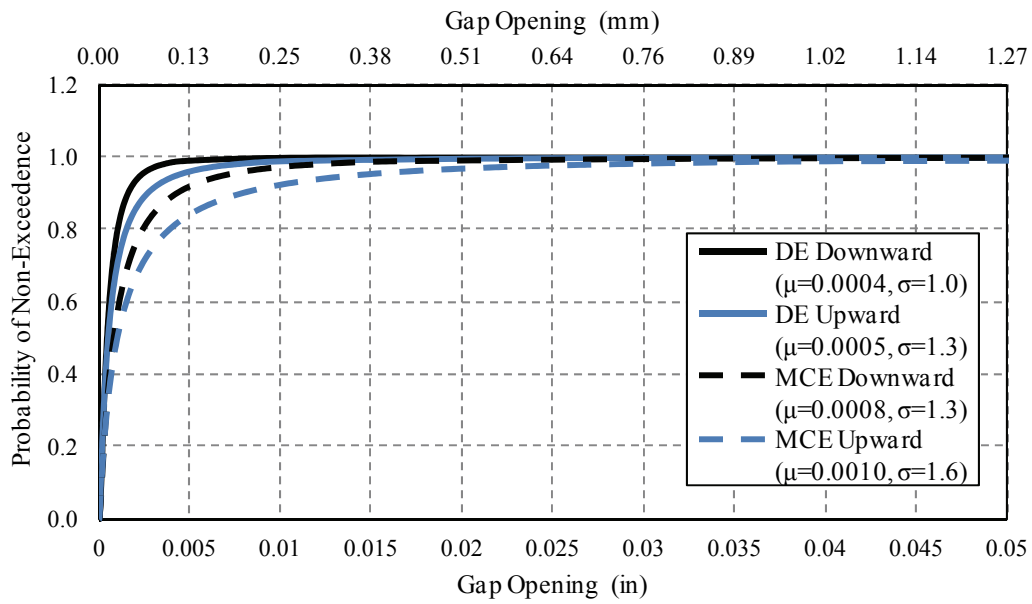


Figure 6-14: Cumulative probability distribution function of maximum top gap opening of mid-span cross-section considering the DE and MCE intensity levels and different loading directions

The shape of the probability of non-exceedance curves related to the maximum top gap opening indicates a great variability of the obtained response values. For the majority of records, the top gap opening is smaller than 0.01 inches (0.254 mm) for both intensity levels and loading directions whereas a significantly higher response is observed in some cases. Given that the behavior of the compression contact spring, which lay between two adjacent segments, is highly nonlinear their response is significantly dependant of the intensity and characteristics of the considered ground motion. As for the case of maximum vertical upward or downward displacement, the maximum top gap opening of the superstructure's mid-span cross-section is greater for the case of upward loading as illustrated in Figure 6-14.

In Table 6-7, an indication of the most severe response in terms of maximum bottom gap opening of the mid-span cross-section is given for both considered intensity levels and loading directions.

Table 6-7: Maximum bottom gap opening of mid-span cross-section

Max Bottom Gap Opening		
Intensity	Downward Loading	Upward Loading
DE	0.094 in (2.397 mm)	0.068 in (1.725 mm)
MCE	0.123 in (3.133 mm)	0.103 in (2.625 mm)

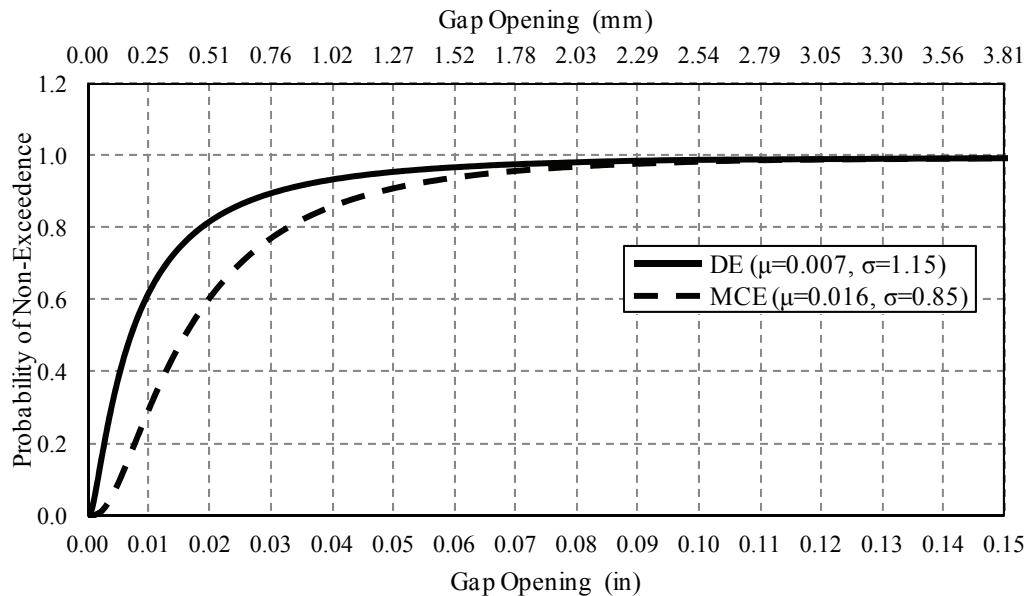


Figure 6-15: Cumulative probability distribution function of maximum bottom gap opening of mid-span cross-section considering the DE and MCE intensity levels

Additionally, the probability of non-exceedance of the same response quantity is presented for both considered intensities, DE and MCE. In Figure 6-15, the probability of non-exceedance for the maximum bottom gap opening is illustrated independently of the loading direction given that the response appears to be independent of the loading direction.

Through comparison of Figure 6-13 and Figure 6-15, it becomes apparent that the maximum gap opening of the bottom compression spring is significantly greater than the top one for all considered cases. Moreover, the shape of the probability of non-exceedance of the bottom gap opening of the mid-span cross-section indicates a normalized distribution of the response quantity. It should be noted that the gap opening of the bottom fiber of the mid-span cross-section is dominated by the response of the pre-stressed tendons.

The original vertical ATC-63 ground motions were modified in order to match the seismic intensity levels specified by FEMA ATC-63 [2008]. Based on the results presented above in terms of maximum vertical displacement and gap opening of the mid-span cross-section, the Maximum Considered Earthquake (MCE) level does not cause exceedance of the structural strength or collapse. However, the response of the superstructure model is highly nonlinear and it is therefore significantly affected by many parameters such as the direction, the magnitude and the frequency content of the loading as well as, the assigned percentage of critical damping. For this reason, it would be reasonable to conduct a series of incremental dynamic analyses considering higher seismic intensities [Vamvatsikos, 2002]. The variability of the model's behavior is recorded through these analyses, and the proposed structural system can be forced to instability.

SECTION 7

CONCLUSIONS

The use of precast segmental bridge construction has witnessed increased worldwide interest during the last decades due to its inarguable advantages comparing to traditional cast-in-place techniques. However, the adoption of precast segmental bridge systems in areas of moderate to high seismicity involves uncertainties in terms of their overall behavior, that need to be addressed.

This study focuses on designing a precast segmental bridge model, according to the Accelerated Bridge Construction (ABC) techniques, and investigating its response under earthquake induced loads. A key concept is introduced in the design: post-tensioned internal unbonded tendons are used as the only continuous reinforcement between adjacent segments of the bridge's superstructure and substructure. The use of internal unbonded tendons in order to post-tension precast segmental bridge superstructures has never been reported in the literature.

The bridge model described in this study was developed as part of an ongoing research project on precast segmental bridges undertaken by the Department of Civil, Structural and Environmental Engineering (CSEE) at the University at Buffalo and the Multidisciplinary Center for Earthquake Engineering Research (MCEER). The Structural Engineering and Earthquake Simulation Laboratory (SEESL), at the University at Buffalo, supports research projects pertinent to the seismic behavior of structures, equipment and non-structural components. Along with numerous testing capabilities, the SEESL facility is equipped with two high-performance six degrees-of-freedom relocatable shake tables. According to the testing capabilities of the two shake tables at SEESL, a large-scale precast segmental bridge model is designed to investigate the overall behavior of precast segmental bridge systems under earthquake induced loads.

A prototype bridge system [Megally et al., 2002] has been selected and modified to comply with the ABC techniques, as applied for precast segmental systems. The scaling of the prototype segmental bridge system resulted in a 1/2.39-scale test specimen based on the performance specifications of the dual shake tables at SEESL. The 1/2.39-scale model is then designed according to the AASHTO LRFD Bridge Design Specifications [2007] and the PCI Bridge Design Manual [2003]. For the design of the model's superstructure, the case of vertical earthquake loads is taken into account even though AASHTO specifications consider only horizontal design seismic loads. The vertical earthquake loads are assumed to be equal to 2/3 of the corresponding horizontal ones. Moreover, in order to account for the higher ductility and energy dissipation capabilities of the proposed segmental bridge system with internal unbonded tendons over the conventional monolithic systems, an overall response modification factor, R equal to 2.50 is selected. According to AASHTO [2007], the response modification factors for the bridge's superstructure and substructure ('critical' bridges) would equal 1.00 and 1.50,

respectively. In this report, the model's superstructure is designed for an R-factor that equals 2.50 (2.50×1.00) and, the columns are designed for an R-factor equal to 3.75 (2.50×1.50).

In addition to the design of the segmental bridge model according to current bridge design specifications, a two-dimensional numerical model of the superstructure model is developed in this study. An approach on the numerical modeling of the piers is presented by Sideris et al. [2010] whereas; a numerical model of the complete bridge specimen will be presented in future studies.

The two-dimensional numerical model of the bridge superstructure is developed accounting for material and geometric nonlinearities. The seismic response of the superstructure model is investigated considering vertical displacement-controlled loadings and, its analysis show that the segmental superstructure with unbonded tendons behaves as a self-centering system. The model's response is highly nonlinear and depends on the direction, magnitude and frequency content of the loading. Moreover, the geometry of the unbonded pre-stressed tendons along the superstructure's length affects the stiffness of the system and therefore, the response of the superstructure is dependant of the loading direction. Under a vertical sinusoidal displacement-controlled load pattern with a maximum displacement of 10.0 inches (254 mm) at the mid-span joint, the model exhibits gap opening of the segment-to-segment joints and yielding of the unbonded tendons.

The seismic response of the superstructure model is also investigated considering the vertical component of the ATC-63 far-field earthquake ground motion ensemble [FEMA ATC-63, 2008]. The historical records are scaled to satisfy the adopted similitude requirements and to account for different seismic intensity levels. The case of a prototype bridge structure located at Western United States ($S_{DS}=0.625$ g - design case) as well as, a higher seismic intensity case of a prototype bridge located at the City of Los Angeles ($S_{DS}=1.415$ g) are considered. Only the results of the second case are presented in the report, focusing on four characteristic response parameters: the maximum upward (top) and downward (bottom) vertical displacement of the mid-span cross-section; the maximum top and bottom gap opening of the mid-span contact zone (maximum elongation of top and bottom compression springs at mid-span section).

For the Maximum Considered Earthquake (MCE) level [ASCE/SEI 7-05, 2005] the vertical displacement of the mid-span cross-section reaches up to 1.2 inches (30.5 mm) whereas; the gap opening at the same location reaches up to 0.12 inches (3.1 mm). Comparing to the results obtained by applying a maximum vertical displacement of 10.0 inches (254 mm) at the mid-span joint, it becomes evident that the segmental superstructure model can sustain significantly greater vertical seismic induced loads.

An Incremental Dynamic Analysis (IDA) of the proposed two-dimensional numerical model would provide results on the probability of exceeding a specified limit state for given hazard intensity levels, such as the Design Earthquake (DE) or the Maximum Considered Earthquake (MCE) and, damage limit states could be defined. By scaling the ensemble of historical

earthquake records, presented in Section 6.2, to higher intensity levels the stability of the superstructure model could be monitored.

During this study, the adjacent segments of the precast bridge model are considered to be joined together through internal unbonded post-tensioned tendons. However, a common practice for this type of structural systems incorporates the use of internal or combination of internal and external tendons. After post-tensioning, the tendons are grouted in order to protect the strands from corrosion and other environmental effects. The proposed large-scale bridge specimen could be easily altered in order to accommodate a combination of bonded and unbonded strands or solely bonded strands by simply grouting a number or all unbonded tendons. In that case, the experimental response of different segmental bridge systems could be investigated and, the differences of their response under seismic induced loads could be evaluated.

The segmental precast bridge model, described in this report, was constructed and tested on the dual shake tables of SEESL during the months of April and May 2010 [Sideris et al., 2010]. Currently, processing of data obtained from the experimental investigation is undertaken at the University at Buffalo which will lead to robust conclusions on the behavior of precast segmental bridges under earthquake excitation. The results on the experimental investigation of the precast segmental bridge specimen, as conducted at SEESL, will be presented in a future study and will be used to calibrate the system's numerical model. The numerical model of the large-scale bridge specimen will be presented in a future study together with results on its response under uniaxial and multiaxial seismic excitations of various intensities. The experimental data processing and numerical investigation of the segmental bridge system will result in providing accurate design specifications and analysis procedures for such systems.

SECTION 8

REFERENCES

- AASHTO [2007] *AASHTO LRFD Bridge Design Specifications*, American Association of State Highway and Transportation Officials, Washington, D.C., United States.
- AASHTO – PCI – ASBI [2000] *Segmental Box Girder Standards for Span-by-Span and Balanced Cantilever Construction*, American Association of State Highway and Transportation Officials – Precast/Prestressed Concrete Institute – American Segmental Bridge Institute, United States.
- ASCE/SEI [2005] *Minimum Design Loads for Buildings and Other Structures, ASCE/SEI 7-05*, American Society of Civil Engineers, United States.
- Burnell, K.P., Megally, S.H., Restrepo, J.I., Seible, F. [2005] “Seismic Testing of Precast Segmental Systems Bridges: Phase III, Bridge System Tests,” *Structural Systems Research Project SSRP 2005/01*, University of California at San Diego, La Jolla, California, United States.
- Carr, A. [2007] *Ruaumoko 2D – Inelastic Dynamic Analysis*, Department of Civil Engineering, University of Canterbury, Christchurch, New Zealand.
- Chopra, A.K. [2007] *Dynamics of Structures*, Pearson Prentice Hall, New Jersey, United States.
- Christopoulos, C., Filiatrault, A. [2006] *Principles of Passive Supplemental Damping and Seismic Isolation*, IUSS Press, Pavia, Italy.
- DYWIDAG, DSI [2009] *DYWIDAG Unbonded Mono-strand Post-Tensioning Systems*, DYWIDAG – Systems International, Illinois, United States.
- FEMA [2008] *Quantification of Building Seismic Performance Factors, ATC-63 Project Report*, Federal Emergency Management Agency, Washington, D.C., United States.
- FHWA [2004] “Post-Tensioning Tendon Installation and Grouting Manual,” *U.S. Department of Transportation, Federal Highway Administration*, Washington, D.C., United States.
- Harris, H.G., Sabnis, G.M. [1999] *Structural Modeling and Experimental Techniques*, CRC Press.
- Hewes, J. T., Priestley, M. J. N. [2002] “Seismic design and performance of precast concrete segmental bridge columns,” *Structural Systems Research Project SSRP 2001/25*, University of California at San Diego, La Jolla, California, United States.
- Hewes, J. T. [2007] “Seismic tests on precast segmental concrete columns with unbonded tendons,” *Bridge Structures: Assessment, Design and Construction*, Vol. 3, No. 3, pp. 215-227.
- Kircher, C. [1996] *A Method for Scaling Horizontal Earthquake Time Histories*, Kircher and Associates, California, United States.

- Megally, S.H., Garg, M., Seible, F., Dowell, R.K. [2002] “Seismic Performance of precast Segmental bridge superstructures,” *Structural Systems Research Project SSRP 2001/24*, University of California at San Diego, La Jolla, California, United States.
- Nilson, A.H. [1978] *Design of Prestressed Concrete*, John Wiley & Sons.
- Ou, Y. C., Tsai, M. S., Chang, K. C., Lee, G. C. [2010] “Cyclic behavior of precast segmental concrete bridge columns with high performance or conventional steel reinforcing bars as energy dissipation bars,” *Earthquake Engineering and Structural Dynamics*, Vol. 39, No. 11, pp. 1181-1198.
- PCI [2003] *Precast/Prestressed Concrete Bridge Design Manual*, Precast/Prestressed Concrete Institute, Chicago, Illinois, United States.
- Rombach, G. [2002] “*Precast segmental box girder bridges with external prestressing, design and construction*,” Technical University of Hamburg, Hamburg, Germany.
- Sideris, P., Anagnostopoulou, M., Aref, A., Filiatrault, A. [2010] “Seismic Performance of Precast Segmental Bridges,” *9th U.S. National and 10th Canadian Conference on Earthquake Engineering: Reaching Beyond Borders*, Toronto, Canada.
- Spieth, H.A., Arnold, D., Davies, M., Mander, J.B., Carr, A.J. [2004] “Modelling of post-tensioned precast reinforced concrete frames with rocking beam-column connections,” *2004 NZSEE Conference*, Rotorua, New Zealand.
- Wang, J. C., Ou, Y. C., Chang, K. C., Lee, G. C. [2008] “Large-scale seismic tests of tall concrete bridge columns with precast segmental construction,” *Earthquake Engineering and Structural Dynamics*, Vol. 37, No. 12, pp. 1449-1465.
- Yamashita, R., Sanders, D. H. [2009] “Seismic Performance of Precast Unbonded Prestressed Concrete Columns,” *American Concrete Institute (ACI)*, Vol. 106, No. 6, pp. 821-830.
- Vamvatsikos, D., Cornell, C.A. [2002] “Incremental Dynamic Analysis,” *Earthquake Engineering and Structural Dynamics*, Vol. 31, No. 3, pp. 491-514.
- Veletzos, M.J., Restrepo, J.I., Seible, F. [2006] “Seismic Response of Precast Segmental Bridge Superstructures,” *Structural Systems Research Project SSRP 2006/18*, University of California at San Diego, La Jolla, California, United States.

APPENDIX A


Following the calculations presented in Chapter 3 and 4, detailed shop drawings of the superstructure's and substructure's geometry and reinforcement details are presented hereafter. The dimensions illustrated in the drawings are in inches.

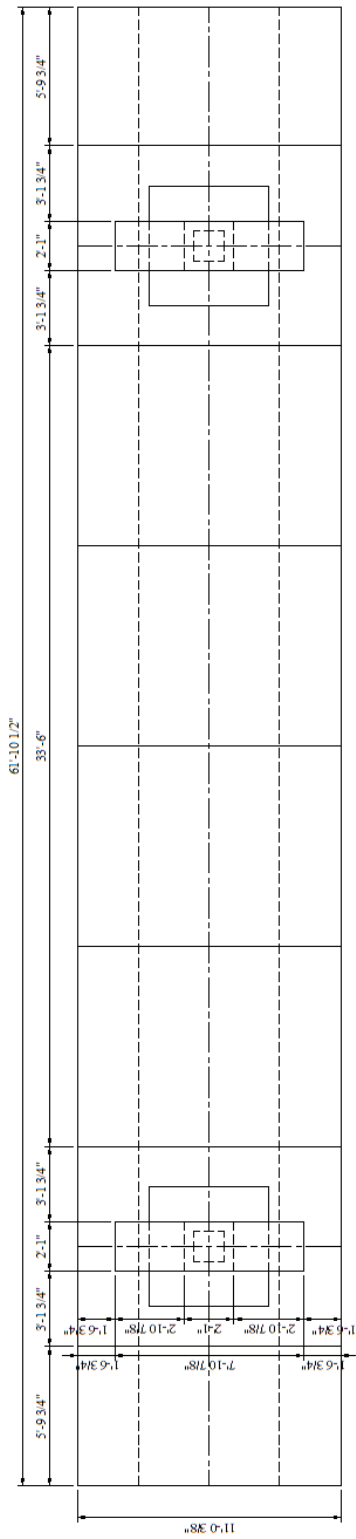
Drawings

D1/12 Bridge Specimen Geometry
D2/12 Bridge Side View & Typical Cross-Sections
D3/12 Superstructure Tendon Geometry
D4/12 S.1 and S.8 Superstructure Segment Geometry
D5/12 S.2 Superstructure Segment Geometry
D6/12 S.3 Superstructure Segment Geometry
D7/12 S.4 Superstructure Segment Geometry
D8/12 S.5 Superstructure Segment Geometry
D9/12 S.6 Superstructure Segment Geometry
D10/12 S.7 Superstructure Segment Geometry
D11/12 Superstructure Reinforcement Details
D12/12 Pier Reinforcement Details

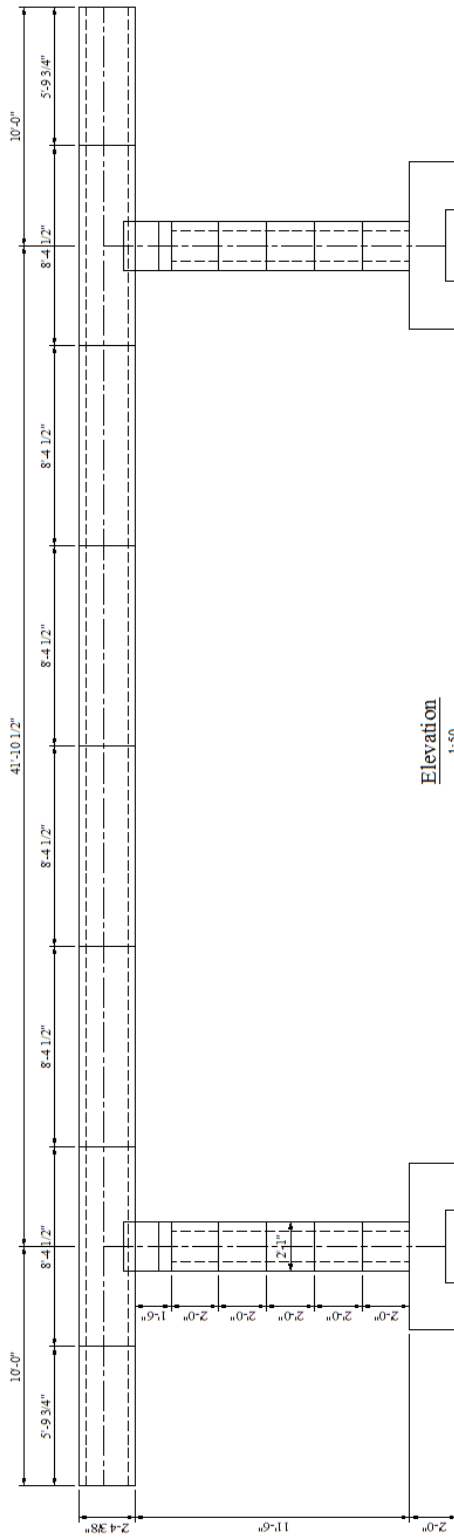
General Notes

1. Cover : 1/2"
2. Rebar : # 3, 3/8" diameter
3. Post-Tensioning : 0.5" diameter strand for superstructure
0.6" diameter strand for piers
4. Material properties:
Concrete : 28-day comp. strength = 5000 psi
Reinforcing bars : Grade 60
Pre-stressing strands : Seven-wire low-relaxation
strand Grade 270
5. All dimensions are in inches unless otherwise shown

 SEESL University of Memphis Center for Earthquake Engineering and Seismicity Research	Accelerated Bridge Construction System Testing		List of Drawings
	Drawn by: M. Anagnostopoulou	Date : 09-02-2009	Sheet: -

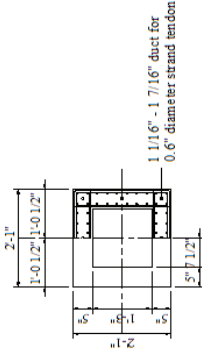
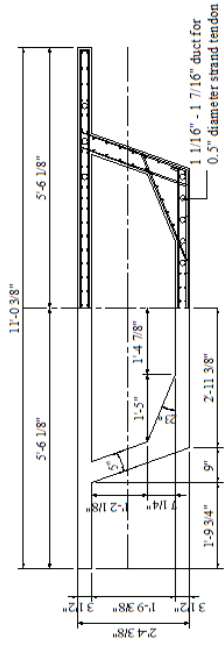
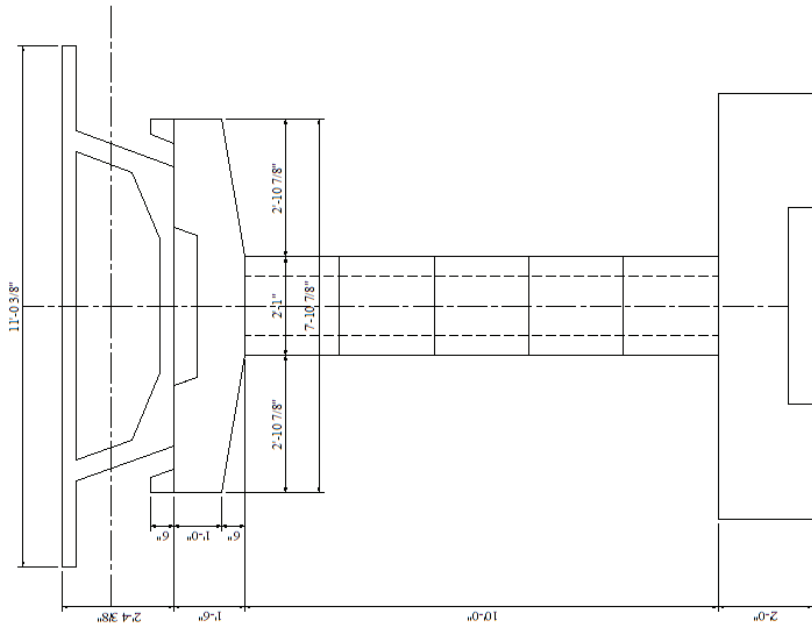


Plan View
1:50



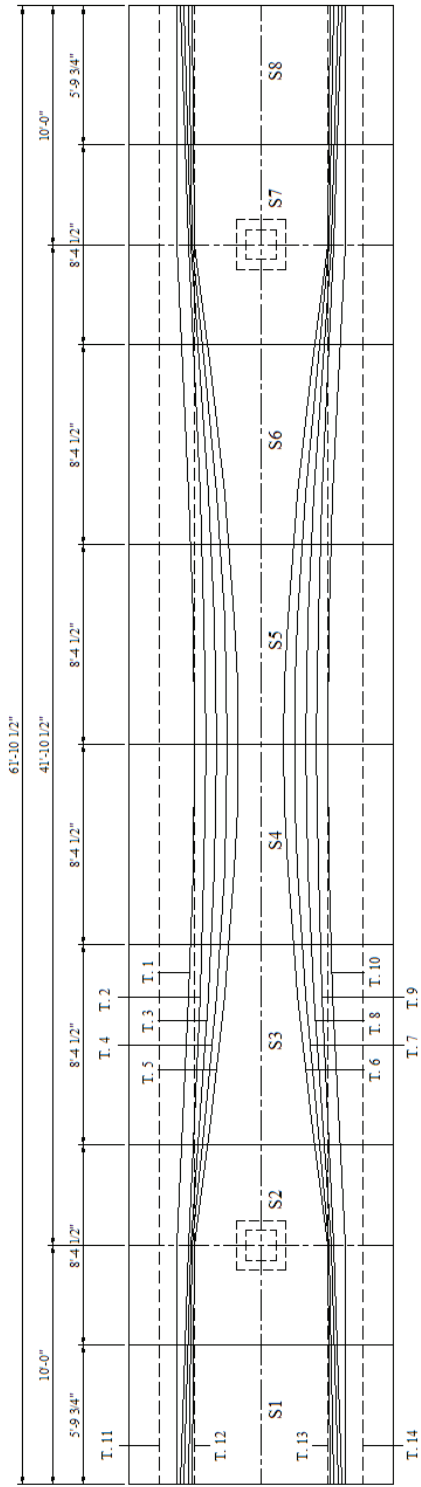
Elevation
1:50

 SEESL <small>University at Buffalo</small> <small>The State University of New York</small>	Accelerated Bridge Construction System Testing		Bridge Specimen Geometry	
	Drawn by: M. Anagnostopoulou	Date: 09-02-2009	Sheet: 1/12	

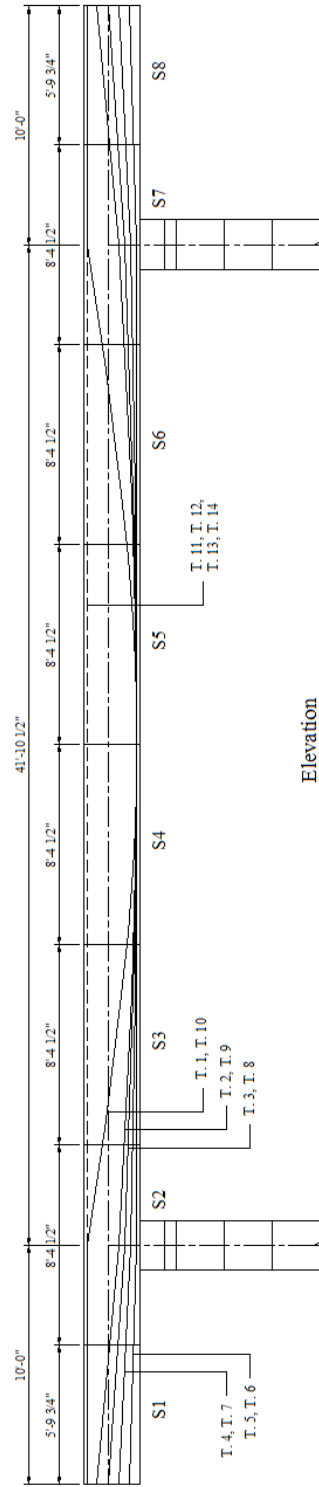


Accelerated Bridge Construction System Testing		Bridge Side View & Typical Cross-Sections	
Drawn by:	M. Anagnostopoulou	Date:	09-02-2009
			Sheet:
			2/12



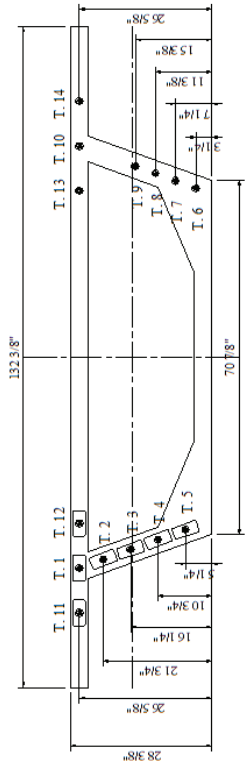


Plan View
1:50

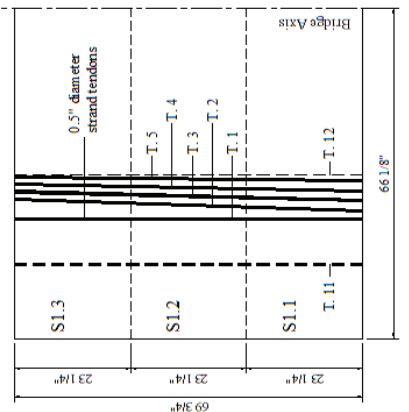
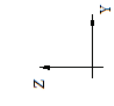


Elevation
1:50

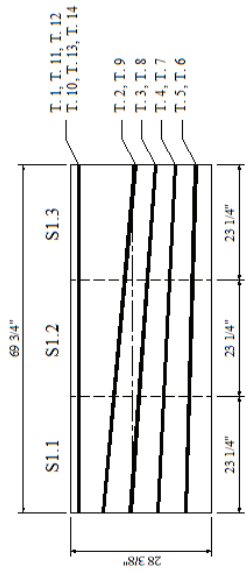
	Accelerated Bridge Construction System Testing		Superstructure Tendon Geometry	
	Drawn by:	M. Anagnostopolou	Date:	09-02-2009
			Sheet:	3/12



S.1 Typical Section
1:20



S.1 Plan View
1:20



S.1 Elevation
1:20

S	S1.1 Left				S1.1 Right - S1.2 Left				S1.2 Right - S1.3 Left				S1.3 Right					
	X	Y	Z	T	X	Y	Z	T	X	Y	Z	T	X	Y	Z	T		
T.1	0	-42.278	25.578	23.278	-42.278	35.578	46.478	-42.278	25.578	46.478	-42.278	25.578	69.678	-42.278	25.578	69.678	42.278	34.578
T.2	0	-42.278	21.678	23.278	38.678	15.578	46.478	38	57.478	46.478	38	57.478	69.678	38.678	35.578	69.678	38.678	35.578
T.3	0	-38.478	15.278	23.278	38	15.578	46.478	37.378	53	46.478	37.378	53	69.678	38.678	35.578	69.678	38.678	35.578
T.4	0	-36.578	10.678	23.278	36.178	9.578	46.478	36.678	8.478	46.478	36.678	8.478	69.678	35.578	35.578	69.678	35.578	35.578
T.5	0	-34.578	5.278	23.278	34.378	4.578	46.478	34.178	3.778	46.478	34.178	3.778	69.678	34.178	34.178	69.678	34.178	34.178
T.6	0	-34.578	5.278	23.278	-34.378	4.578	46.478	-34.178	3.778	46.478	-34.178	3.778	69.678	-34.178	-34.178	69.678	-34.178	-34.178
T.7	0	-36.578	10.678	23.278	-36.178	9.578	46.478	-36.678	8.478	46.478	-36.678	8.478	69.678	-35.578	35.578	69.678	-35.578	35.578
T.8	0	-38.478	15.278	23.278	-38	15.578	46.478	-37.378	53	46.478	-37.378	53	69.678	-38.678	35.578	69.678	-38.678	35.578
T.9	0	-42.278	21.678	23.278	-42.278	15.578	46.478	-42.278	25.578	46.478	-42.278	25.578	69.678	-42.278	25.578	69.678	-42.278	25.578
T.10	0	-42.278	25.578	23.278	-42.278	25.578	46.478	-42.278	25.578	46.478	-42.278	25.578	69.678	-42.278	25.578	69.678	-42.278	25.578

Accelerated Bridge Construction System Testing

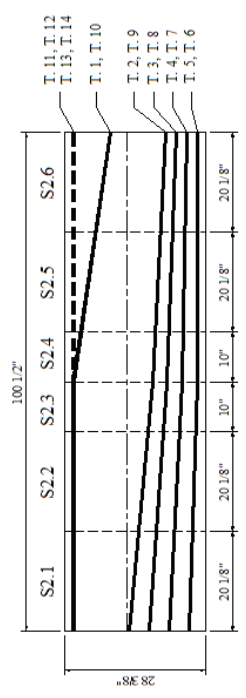
S.1 and S.8 Superstructure Segment Geometry

Drawn by: M. Anagnostopoulou

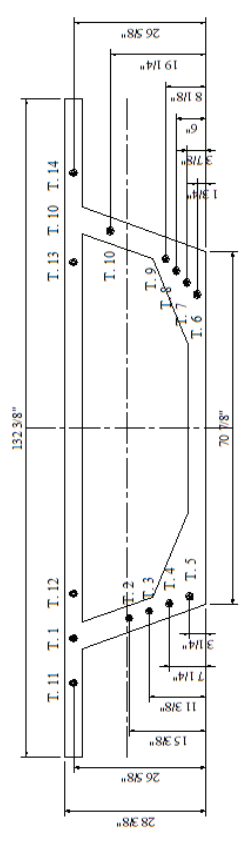
Date: 09-02-2009

Sheet: 4/12

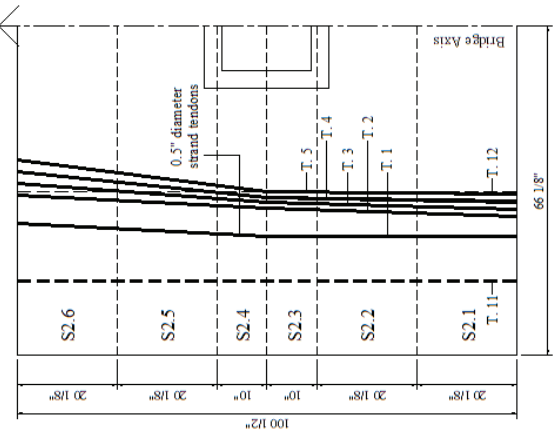




S.2 Elevation
1:20



S.2 Typical Section
1:20



Plan View
1:20

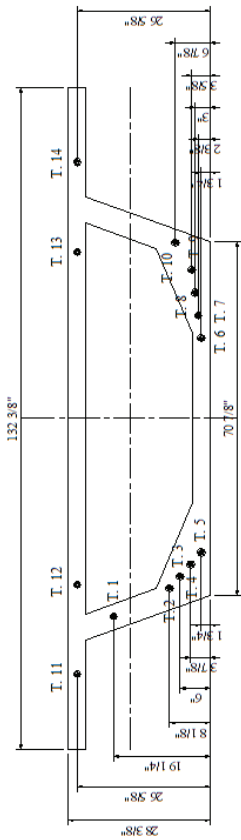
5	S2.1 Left			S2.1 Right- S2.7 Left			S2.2 Right- S2.3 Left			S2.3 Right- S2.4 Left		
	X	Y	Z	X	Y	Z	X	Y	Z	X	Y	Z
T.1	0	51.0	25.0	50.0	41.0	25.0	40.0	31.0	25.0	30.0	21.0	25.0
T.2	0	36.0	11.0	35.0	26.0	11.0	25.0	16.0	11.0	11.0	6.0	11.0
T.3	0	21.0	3.0	20.0	11.0	3.0	10.0	1.0	3.0	1.0	1.0	3.0
T.4	0	6.0	0.0	5.0	0.0	0.0	0.0	0.0	0.0	0.0	0.0	0.0
T.5	0	39.0	3.0	38.0	28.0	3.0	27.0	18.0	3.0	13.0	3.0	3.0
T.6	0	33.0	3.0	32.0	22.0	3.0	21.0	11.0	3.0	6.0	3.0	3.0
T.7	0	18.0	7.0	17.0	7.0	7.0	6.0	1.0	7.0	1.0	7.0	7.0
T.8	0	3.0	11.0	2.0	11.0	11.0	10.0	11.0	11.0	11.0	11.0	11.0
T.9	0	3.0	15.0	2.0	15.0	15.0	14.0	15.0	15.0	15.0	15.0	15.0
T.10	0	42.0	25.0	41.0	32.0	25.0	31.0	22.0	25.0	13.0	25.0	25.0

5	S2.4 Right- S2.5 Left			S2.5 Right- S2.6 Left			S2.6 Right		
	X	Y	Z	X	Y	Z	X	Y	Z
T.1	60.0	46.0	25.0	50.0	37.0	25.0	40.0	24.0	25.0
T.2	45.0	16.0	11.0	35.0	6.0	11.0	25.0	1.0	11.0
T.3	30.0	3.0	3.0	20.0	1.0	3.0	10.0	1.0	3.0
T.4	60.0	33.0	3.0	50.0	23.0	3.0	40.0	13.0	3.0
T.5	60.0	39.0	3.0	50.0	29.0	3.0	40.0	19.0	3.0
T.6	60.0	33.0	3.0	50.0	23.0	3.0	40.0	13.0	3.0
T.7	60.0	18.0	7.0	50.0	8.0	7.0	40.0	1.0	7.0
T.8	60.0	3.0	11.0	50.0	1.0	11.0	40.0	1.0	11.0
T.9	60.0	3.0	15.0	50.0	1.0	15.0	40.0	1.0	15.0
T.10	60.0	42.0	25.0	50.0	31.0	25.0	40.0	20.0	25.0

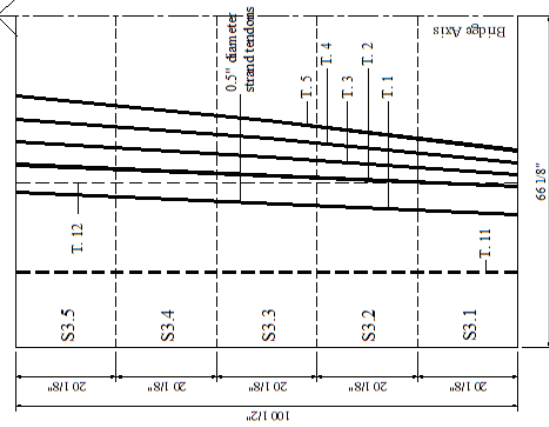
Accelerated Bridge Construction System Testing

SEESI
The Smart Construction System

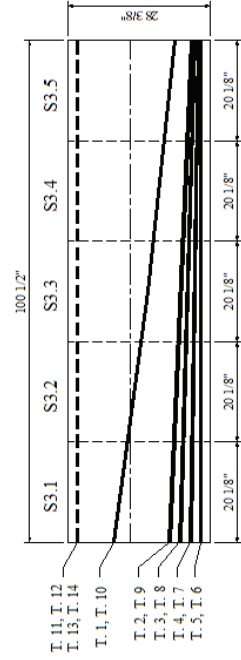
S.2 Superstructure Segment Geometry
 Drawn by: M. Anagnostopoulou Date: 09-02-2009 Sheet: 5/12



S.3 Typical Section
1:20



Plan View
1:20



S.3 Elevation
1:20

S	S3.1 Left			S3.1 Right- S2.1 Left			S2.1 Right- S3.1 Left		
	Y	V	Z	Y	V	Z	Y	V	Z
T.1	0	35.5	52.2	20.18	35.5	52.2	40.38	35.5	52.2
T.2	0	34	44.8	20.18	34	44.8	40.38	34	44.8
T.3	0	31.5	6	20.18	31.5	6	40.38	31.5	6
T.4	0	29.2	3.7	20.18	29.2	3.7	40.38	29.2	3.7
T.5	0	26.7	1.6	20.18	26.7	1.6	40.38	26.7	1.6
T.6	0	-25.7	1.6	20.18	-24.3	1.6	40.38	-22	1.6
T.7	0	-29.2	3.7	20.18	-27.2	3.4	40.38	-25.2	3.2
T.8	0	-31.5	6	20.18	-30.2	5.2	40.38	-28.2	4.2
T.9	0	-33.7	11.8	20.18	-32.2	10.2	40.38	-30.2	9.2
T.10	0	-35.5	21.2	20.18	-33.5	16.2	40.38	-32.2	15.2

S	S3.2 Right- S2.1 Left			S2.1 Right- S3.1 Left		
	Y	V	Z	Y	V	Z
T.1	0	35.5	52.2	20.18	35.5	52.2
T.2	0	34	44.8	20.18	34	44.8
T.3	0	31.5	6	20.18	31.5	6
T.4	0	29.2	3.7	20.18	29.2	3.7
T.5	0	26.7	1.6	20.18	26.7	1.6
T.6	0	-25.7	1.6	20.18	-24.3	1.6
T.7	0	-29.2	3.7	20.18	-27.2	3.4
T.8	0	-31.5	6	20.18	-30.2	5.2
T.9	0	-33.7	11.8	20.18	-32.2	10.2
T.10	0	-35.5	21.2	20.18	-33.5	16.2

S	S3.3 Right- S2.1 Left			S2.1 Right- S3.1 Left		
	Y	V	Z	Y	V	Z
T.1	0	35.5	52.2	20.18	35.5	52.2
T.2	0	34	44.8	20.18	34	44.8
T.3	0	31.5	6	20.18	31.5	6
T.4	0	29.2	3.7	20.18	29.2	3.7
T.5	0	26.7	1.6	20.18	26.7	1.6
T.6	0	-25.7	1.6	20.18	-24.3	1.6
T.7	0	-29.2	3.7	20.18	-27.2	3.4
T.8	0	-31.5	6	20.18	-30.2	5.2
T.9	0	-33.7	11.8	20.18	-32.2	10.2
T.10	0	-35.5	21.2	20.18	-33.5	16.2

Accelerated Bridge Construction System Testing

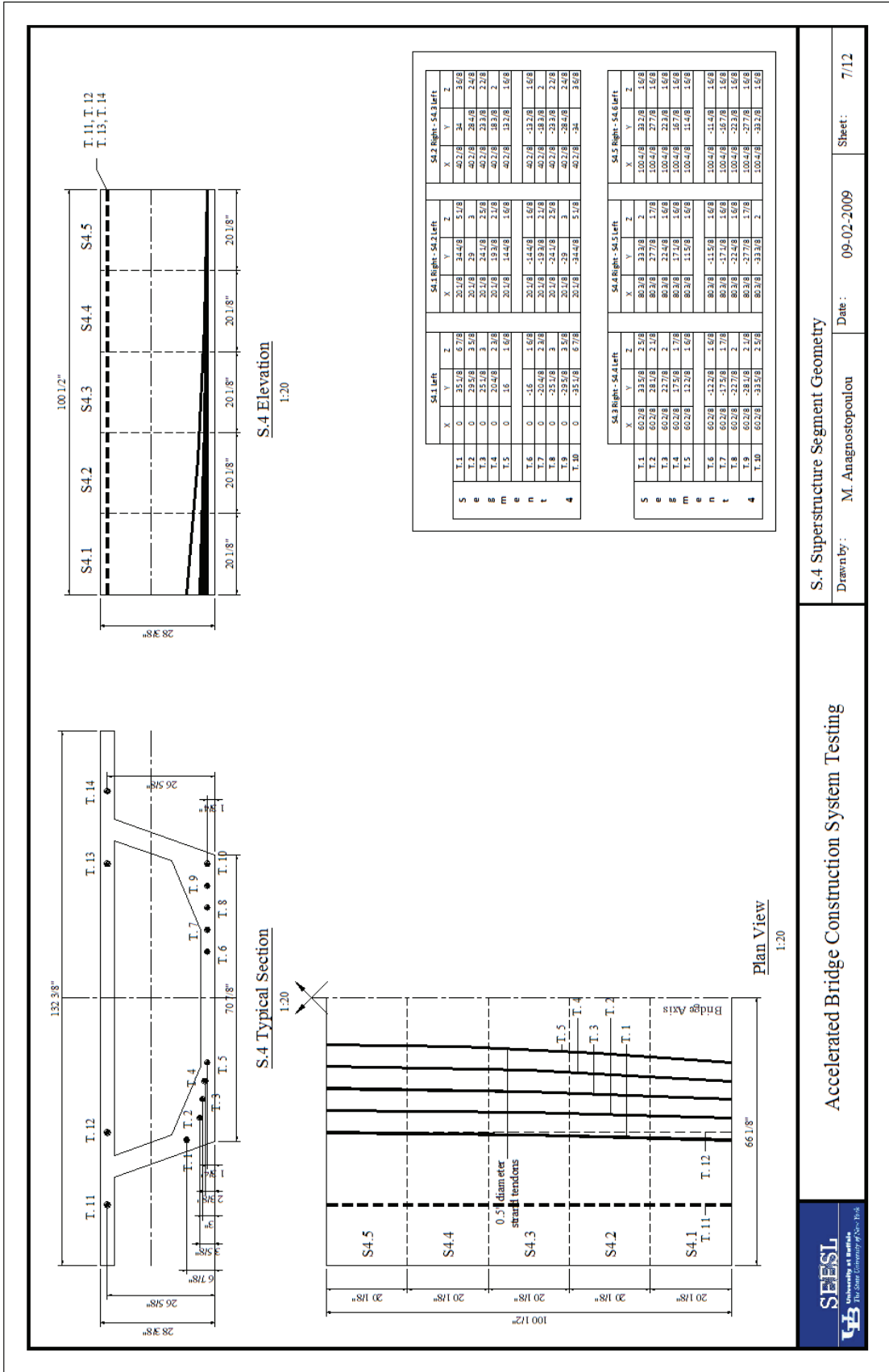
S.3 Superstructure Segment Geometry

Drawn by: M. Anagnostopoulou

Date: 09-02-2009

Sheet: 6/12





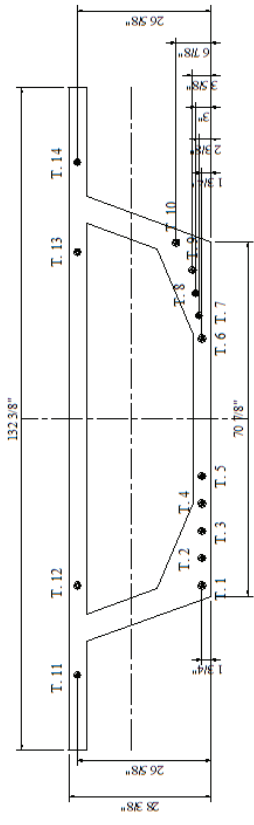
Accelerated Bridge Construction System Testing

S.4 Superstructure Segment Geometry

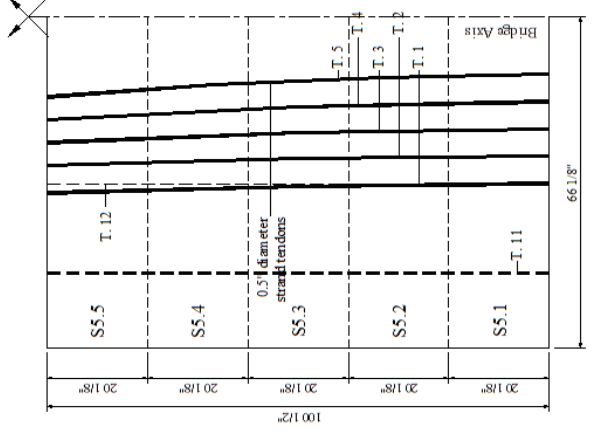
Drawn by: M. Anagnostopoulos

Date: 09-02-2009

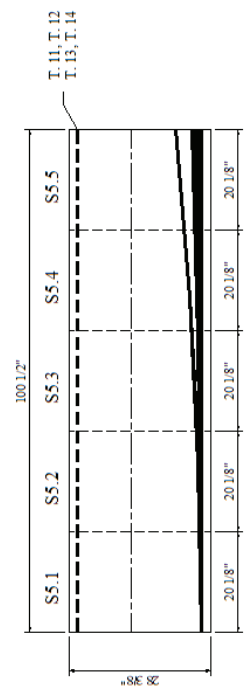
Sheet: 7/12



S.5 Typical Section
1:20



Plan View
1:20



S.5 Elevation
1:20

S	S5.1 Left			S5.1 Right, S5.2 Left			S5.2 Right, S5.3 Left		
	X	Y	Z	X	Y	Z	X	Y	Z
T.1	0	-35.718	1.678	20.178	-17.718	1.678	40.228	-33.218	1.678
T.2	0	-29.718	1.678	20.178	-17.718	1.678	40.228	-27.218	1.678
T.3	0	-23.718	1.678	20.178	-17.718	1.678	40.228	-21.218	1.678
T.4	0	-17.718	1.678	20.178	-17.718	1.678	40.228	-15.218	1.678
T.5	0	-11.478	1.678	20.178	-11.518	1.678	40.228	-9.218	1.678
T.6	0	-5.478	1.678	20.178	-5.518	1.678	40.228	-3.218	1.678
T.7	0	0.478	1.678	20.178	0.478	1.678	40.228	2.718	1.678
T.8	0	6.478	1.678	20.178	6.478	1.678	40.228	8.718	1.678
T.9	0	12.478	1.678	20.178	12.478	1.678	40.228	14.718	1.678
T.10	0	18.478	1.678	20.178	18.478	1.678	40.228	20.718	1.678

S	S5.2 Right, S5.4 Left			S5.4 Right, S5.5 Left		
	X	Y	Z	X	Y	Z
T.1	60.228	-34.478	1.678	80.328	-24.478	1.678
T.2	60.228	-28.478	1.678	80.328	-18.478	1.678
T.3	60.228	-22.478	1.678	80.328	-12.478	1.678
T.4	60.228	-16.478	1.678	80.328	-6.478	1.678
T.5	60.228	-10.478	1.678	80.328	-0.478	1.678
T.6	60.228	-4.478	1.678	80.328	5.478	1.678
T.7	60.228	1.478	1.678	80.328	11.478	1.678
T.8	60.228	7.478	1.678	80.328	17.478	1.678
T.9	60.228	13.478	1.678	80.328	23.478	1.678
T.10	60.228	19.478	1.678	80.328	29.478	1.678

Accelerated Bridge Construction System Testing

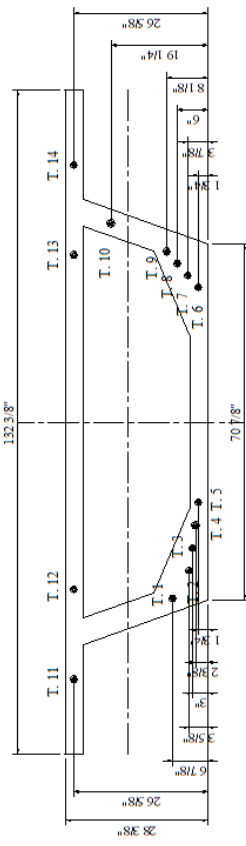
S.5 Superstructure Segment Geometry

Drawn by: M. Anagnostopoulou

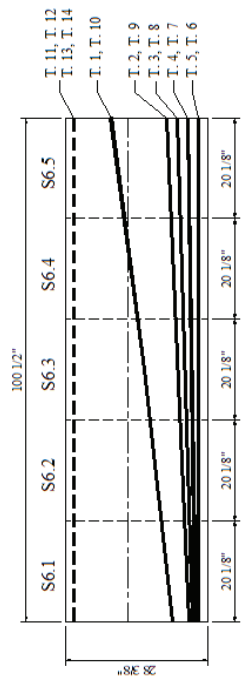
Date: 09-02-2009

Sheet: 8/12

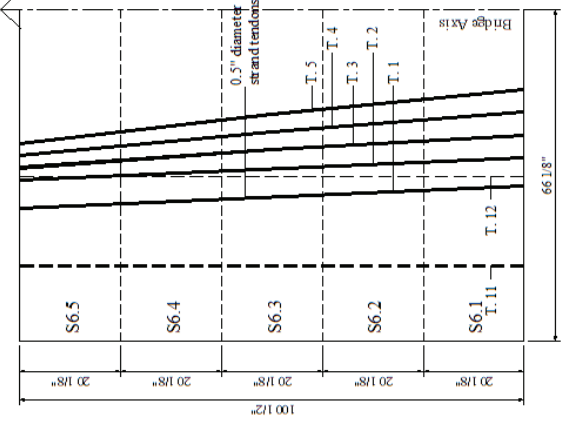




S.6 Typical Section
1:20



S.6 Elevation
1:20



Plan View
1:20

	S6.1 Left			S6.2 Right-S6.2 Left			S6.3 Right-S6.3 Left			
	X	Y	Z	X	Y	Z	X	Y	Z	
S	T.1	0	-25.1/8	6.7/8	20.1/8	-25.7/8	9	40.2/8	-26.6/8	11.2/8
e	T.2	0	-25.5/8	3.5/8	20.1/8	-20.2/8	4.2/8	40.2/8	-31.1/8	5.2/8
e	T.3	0	-25.1/8	3	20.1/8	-25.1/8	3.4/8	40.2/8	-27.8/8	4
e	T.4	0	-20.4/8	-2.3/8	20.1/8	22	2.5/8	40.2/8	-23.5/8	2.7/8
m	T.5	0	15	-1.6/8	20.1/8	-7.6/8	-1.6/8	40.2/8	-19.7/8	1.6/8
e	T.6	0	-15	-1.6/8	20.1/8	-17.6/8	-1.6/8	40.2/8	-19.7/8	-1.6/8
n	T.7	0	-25.4/8	3.2/8	20.1/8	-25.4/8	3.4/8	40.2/8	-31.1/8	4
t	T.8	0	-25.1/8	3	20.1/8	-25.1/8	3.4/8	40.2/8	-27.8/8	4
e	T.9	0	-25.5/8	3.5/8	20.1/8	-20.2/8	4.2/8	40.2/8	-31.1/8	5.2/8
6	T.10	0	-25.1/8	6.7/8	20.1/8	-25.7/8	9	40.2/8	-26.6/8	11.2/8

	S6.3 Right-S6.4 Left			S6.4 Right-S6.5 Left			S6.5 Right-S6.6 Left			
	X	Y	Z	X	Y	Z	X	Y	Z	
S	T.1	60.2/8	-37.5/8	13.6/8	80.2/8	-38.5/8	56.2/8	100.4/8	-39.5/8	19.2/8
e	T.2	60.2/8	35	6.1/8	80.2/8	33	7.1/8	100.4/8	34	8.1/8
e	T.3	60.2/8	-28.6/8	4.5/8	80.2/8	-30.1/8	5.2/8	100.4/8	-31.5/8	6
e	T.4	60.2/8	-25.3/8	3.2/8	80.2/8	-27.2/8	3.4/8	100.4/8	-29.2/8	3.7/8
m	T.5	60.2/8	22	1.6/8	80.2/8	-24.2/8	1.6/8	100.4/8	-25.7/8	1.6/8
e	T.6	60.2/8	-22	1.6/8	80.2/8	-24.2/8	1.6/8	100.4/8	-25.7/8	1.6/8
t	T.7	60.2/8	-25.3/8	3.2/8	80.2/8	-27.2/8	3.4/8	100.4/8	-29.2/8	3.7/8
e	T.8	60.2/8	-28.6/8	4.5/8	80.2/8	-30.1/8	5.2/8	100.4/8	-31.5/8	6
n	T.9	60.2/8	35	6.1/8	80.2/8	33	7.1/8	100.4/8	34	8.1/8
6	T.10	60.2/8	-37.5/8	13.6/8	80.2/8	-38.5/8	56.2/8	100.4/8	-39.5/8	19.2/8

Accelerated Bridge Construction System Testing

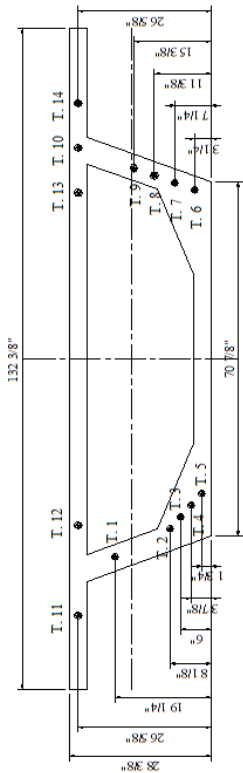
S.6 Superstructure Segment Geometry

Drawn by: M. Anagnostopoulou

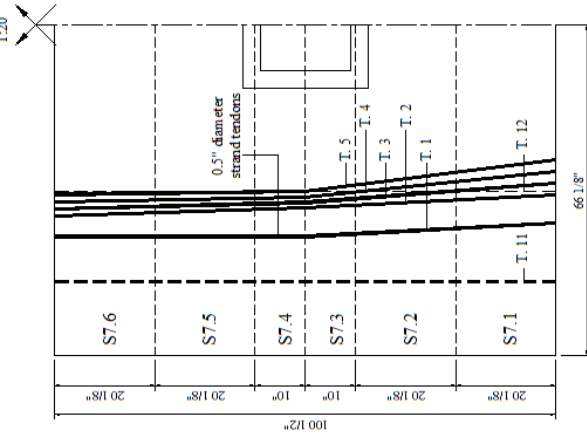
Date: 09-02-2009

Sheet: 9/12

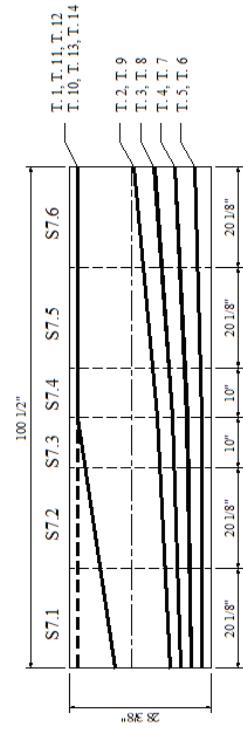




S.7 Typical Section
1:20



Plan View
1:20



S.7 Elevation
1:20

5	S7.1 Left		S7.1 Right-S7.3 Left		S7.3 Right-S7.4 Left		S7.4 Right-S7.6 Left	
	X	Z	X	Z	X	Z	X	Z
T.1	0	-35.98	20.18	-45.18	40.36	-41.68	60.54	-43.20
T.2	0	-34.81	20.18	-35	40.36	-36	60.54	-34.48
T.3	0	-31.58	20.18	-31.18	40.36	-31.68	60.54	-31.68
T.4	0	-29.28	20.18	-29.28	40.36	-29.28	60.54	-29.28
T.5	0	-26.78	20.18	-26.78	40.36	-26.78	60.54	-26.78
T.6	0	-25.78	20.18	-25.78	40.36	-25.78	60.54	-25.78
T.7	0	-25.28	20.18	-25.28	40.36	-25.28	60.54	-25.28
T.8	0	-31.58	20.18	-31.18	40.36	-31.68	60.54	-31.68
T.9	0	-34.81	20.18	-35	40.36	-36	60.54	-34.48
T.10	0	-35.98	20.18	-45.18	40.36	-41.68	60.54	-43.20

5	S7.4 Right-S7.6 Left		S7.6 Left	
	X	Z	X	Z
T.1	60.54	-43.20	100.48	-43.20
T.2	60.54	-34.48	100.48	-34.48
T.3	60.54	-31.68	100.48	-31.68
T.4	60.54	-29.28	100.48	-29.28
T.5	60.54	-26.78	100.48	-26.78
T.6	60.54	-25.78	100.48	-25.78
T.7	60.54	-25.28	100.48	-25.28
T.8	60.54	-31.68	100.48	-31.68
T.9	60.54	-34.48	100.48	-34.48
T.10	60.54	-43.20	100.48	-43.20

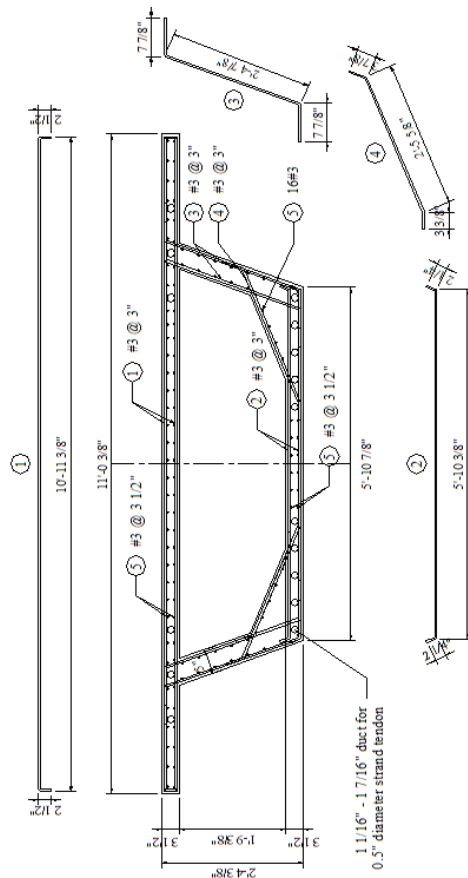
Accelerated Bridge Construction System Testing

S.7 Superstructure Segment Geometry

Drawn by: M. Anagnostopoulou Date: 09-02-2009

Sheet: 10/12

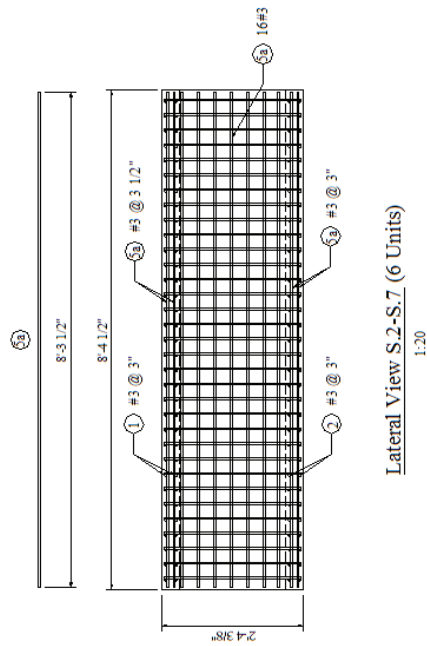




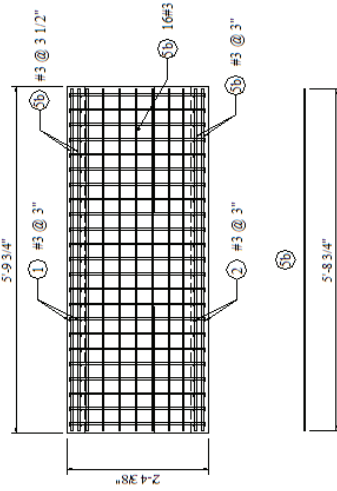
Typical Section
1:20

Notes

1. Cover = 1/2"
2. Rebar : # 3, 3/8" diameter
3. Post-Tensioning : 0.5" diameter strand
4. Material properties:
Concrete : 28-day comp. strength = 5000 psi
Reinforcing bars : Grade 60
Pre-stressing strands : Seven-wire low-relaxation strand Grade 270
5. All dimensions are in inches unless otherwise shown

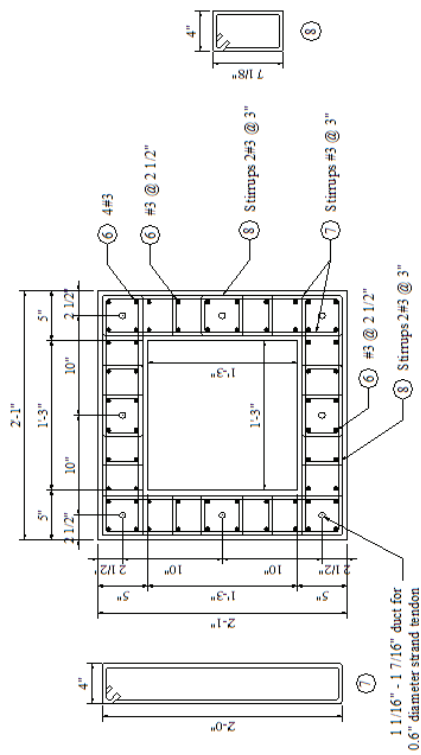


Lateral View S.2-S.7 (6 Units)
1:20

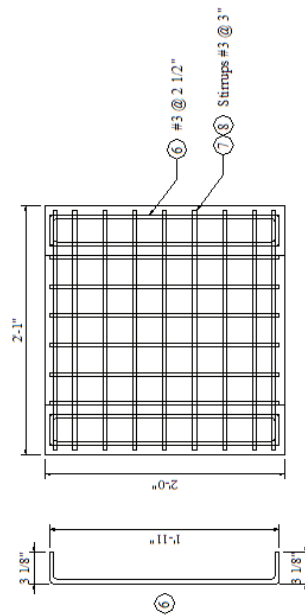


Lateral View S.1, S.8 (2 Units)
1:20

 SEESL University of Buffalo The State University of New York	Accelerated Bridge Construction System Testing		Superstructure Reinforcement Details
	Drawn by: M. Anagnostopoulou	Date : 09-02-2009	Sheet : 11/12



Typical Section (10 Units)
1:10



Lateral View
1:10

Pier Reinforcement Details	
Drawn by: M. Anagnostopoulou	Date: 09-02-2009
Sheet: 12/12	

Accelerated Bridge Construction System Testing



MCEER Technical Reports

MCEER publishes technical reports on a variety of subjects written by authors funded through MCEER. These reports are available from both MCEER Publications and the National Technical Information Service (NTIS). Requests for reports should be directed to MCEER Publications, MCEER, University at Buffalo, State University of New York, 133A Ketter Hall, Buffalo, New York 14260. Reports can also be requested through NTIS, P.O. Box 1425, Springfield, Virginia 22151. NTIS accession numbers are shown in parenthesis, if available.

- NCEER-87-0001 "First-Year Program in Research, Education and Technology Transfer," 3/5/87, (PB88-134275, A04, MF-A01).
- NCEER-87-0002 "Experimental Evaluation of Instantaneous Optimal Algorithms for Structural Control," by R.C. Lin, T.T. Soong and A.M. Reinhorn, 4/20/87, (PB88-134341, A04, MF-A01).
- NCEER-87-0003 "Experimentation Using the Earthquake Simulation Facilities at University at Buffalo," by A.M. Reinhorn and R.L. Ketter, to be published.
- NCEER-87-0004 "The System Characteristics and Performance of a Shaking Table," by J.S. Hwang, K.C. Chang and G.C. Lee, 6/1/87, (PB88-134259, A03, MF-A01). This report is available only through NTIS (see address given above).
- NCEER-87-0005 "A Finite Element Formulation for Nonlinear Viscoplastic Material Using a Q Model," by O. Gyebe and G. Dasgupta, 11/2/87, (PB88-213764, A08, MF-A01).
- NCEER-87-0006 "Symbolic Manipulation Program (SMP) - Algebraic Codes for Two and Three Dimensional Finite Element Formulations," by X. Lee and G. Dasgupta, 11/9/87, (PB88-218522, A05, MF-A01).
- NCEER-87-0007 "Instantaneous Optimal Control Laws for Tall Buildings Under Seismic Excitations," by J.N. Yang, A. Akbarpour and P. Ghaemmaghami, 6/10/87, (PB88-134333, A06, MF-A01). This report is only available through NTIS (see address given above).
- NCEER-87-0008 "IDARC: Inelastic Damage Analysis of Reinforced Concrete Frame - Shear-Wall Structures," by Y.J. Park, A.M. Reinhorn and S.K. Kunnath, 7/20/87, (PB88-134325, A09, MF-A01). This report is only available through NTIS (see address given above).
- NCEER-87-0009 "Liquefaction Potential for New York State: A Preliminary Report on Sites in Manhattan and Buffalo," by M. Budhu, V. Vijayakumar, R.F. Giese and L. Baumgras, 8/31/87, (PB88-163704, A03, MF-A01). This report is available only through NTIS (see address given above).
- NCEER-87-0010 "Vertical and Torsional Vibration of Foundations in Inhomogeneous Media," by A.S. Veletsos and K.W. Dotson, 6/1/87, (PB88-134291, A03, MF-A01). This report is only available through NTIS (see address given above).
- NCEER-87-0011 "Seismic Probabilistic Risk Assessment and Seismic Margins Studies for Nuclear Power Plants," by Howard H.M. Hwang, 6/15/87, (PB88-134267, A03, MF-A01). This report is only available through NTIS (see address given above).
- NCEER-87-0012 "Parametric Studies of Frequency Response of Secondary Systems Under Ground-Acceleration Excitations," by Y. Yong and Y.K. Lin, 6/10/87, (PB88-134309, A03, MF-A01). This report is only available through NTIS (see address given above).
- NCEER-87-0013 "Frequency Response of Secondary Systems Under Seismic Excitation," by J.A. HoLung, J. Cai and Y.K. Lin, 7/31/87, (PB88-134317, A05, MF-A01). This report is only available through NTIS (see address given above).
- NCEER-87-0014 "Modelling Earthquake Ground Motions in Seismically Active Regions Using Parametric Time Series Methods," by G.W. Ellis and A.S. Cakmak, 8/25/87, (PB88-134283, A08, MF-A01). This report is only available through NTIS (see address given above).
- NCEER-87-0015 "Detection and Assessment of Seismic Structural Damage," by E. DiPasquale and A.S. Cakmak, 8/25/87, (PB88-163712, A05, MF-A01). This report is only available through NTIS (see address given above).

- NCEER-87-0016 "Pipeline Experiment at Parkfield, California," by J. Isenberg and E. Richardson, 9/15/87, (PB88-163720, A03, MF-A01). This report is available only through NTIS (see address given above).
- NCEER-87-0017 "Digital Simulation of Seismic Ground Motion," by M. Shinozuka, G. Deodatis and T. Harada, 8/31/87, (PB88-155197, A04, MF-A01). This report is available only through NTIS (see address given above).
- NCEER-87-0018 "Practical Considerations for Structural Control: System Uncertainty, System Time Delay and Truncation of Small Control Forces," J.N. Yang and A. Akbarpour, 8/10/87, (PB88-163738, A08, MF-A01). This report is only available through NTIS (see address given above).
- NCEER-87-0019 "Modal Analysis of Nonclassically Damped Structural Systems Using Canonical Transformation," by J.N. Yang, S. Sarkani and F.X. Long, 9/27/87, (PB88-187851, A04, MF-A01).
- NCEER-87-0020 "A Nonstationary Solution in Random Vibration Theory," by J.R. Red-Horse and P.D. Spanos, 11/3/87, (PB88-163746, A03, MF-A01).
- NCEER-87-0021 "Horizontal Impedances for Radially Inhomogeneous Viscoelastic Soil Layers," by A.S. Veletsos and K.W. Dotson, 10/15/87, (PB88-150859, A04, MF-A01).
- NCEER-87-0022 "Seismic Damage Assessment of Reinforced Concrete Members," by Y.S. Chung, C. Meyer and M. Shinozuka, 10/9/87, (PB88-150867, A05, MF-A01). This report is available only through NTIS (see address given above).
- NCEER-87-0023 "Active Structural Control in Civil Engineering," by T.T. Soong, 11/11/87, (PB88-187778, A03, MF-A01).
- NCEER-87-0024 "Vertical and Torsional Impedances for Radially Inhomogeneous Viscoelastic Soil Layers," by K.W. Dotson and A.S. Veletsos, 12/87, (PB88-187786, A03, MF-A01).
- NCEER-87-0025 "Proceedings from the Symposium on Seismic Hazards, Ground Motions, Soil-Liquefaction and Engineering Practice in Eastern North America," October 20-22, 1987, edited by K.H. Jacob, 12/87, (PB88-188115, A23, MF-A01). This report is available only through NTIS (see address given above).
- NCEER-87-0026 "Report on the Whittier-Narrows, California, Earthquake of October 1, 1987," by J. Pantelic and A. Reinhorn, 11/87, (PB88-187752, A03, MF-A01). This report is available only through NTIS (see address given above).
- NCEER-87-0027 "Design of a Modular Program for Transient Nonlinear Analysis of Large 3-D Building Structures," by S. Srivastav and J.F. Abel, 12/30/87, (PB88-187950, A05, MF-A01). This report is only available through NTIS (see address given above).
- NCEER-87-0028 "Second-Year Program in Research, Education and Technology Transfer," 3/8/88, (PB88-219480, A04, MF-A01).
- NCEER-88-0001 "Workshop on Seismic Computer Analysis and Design of Buildings With Interactive Graphics," by W. McGuire, J.F. Abel and C.H. Conley, 1/18/88, (PB88-187760, A03, MF-A01). This report is only available through NTIS (see address given above).
- NCEER-88-0002 "Optimal Control of Nonlinear Flexible Structures," by J.N. Yang, F.X. Long and D. Wong, 1/22/88, (PB88-213772, A06, MF-A01).
- NCEER-88-0003 "Substructuring Techniques in the Time Domain for Primary-Secondary Structural Systems," by G.D. Manolis and G. Juhn, 2/10/88, (PB88-213780, A04, MF-A01).
- NCEER-88-0004 "Iterative Seismic Analysis of Primary-Secondary Systems," by A. Singhal, L.D. Lutes and P.D. Spanos, 2/23/88, (PB88-213798, A04, MF-A01).
- NCEER-88-0005 "Stochastic Finite Element Expansion for Random Media," by P.D. Spanos and R. Ghanem, 3/14/88, (PB88-213806, A03, MF-A01).

- NCEER-88-0006 "Combining Structural Optimization and Structural Control," by F.Y. Cheng and C.P. Pantelides, 1/10/88, (PB88-213814, A05, MF-A01).
- NCEER-88-0007 "Seismic Performance Assessment of Code-Designed Structures," by H.H-M. Hwang, J-W. Jaw and H-J. Shau, 3/20/88, (PB88-219423, A04, MF-A01). This report is only available through NTIS (see address given above).
- NCEER-88-0008 "Reliability Analysis of Code-Designed Structures Under Natural Hazards," by H.H-M. Hwang, H. Ushiba and M. Shinozuka, 2/29/88, (PB88-229471, A07, MF-A01). This report is only available through NTIS (see address given above).
- NCEER-88-0009 "Seismic Fragility Analysis of Shear Wall Structures," by J-W Jaw and H.H-M. Hwang, 4/30/88, (PB89-102867, A04, MF-A01).
- NCEER-88-0010 "Base Isolation of a Multi-Story Building Under a Harmonic Ground Motion - A Comparison of Performances of Various Systems," by F-G Fan, G. Ahmadi and I.G. Tadjbakhsh, 5/18/88, (PB89-122238, A06, MF-A01). This report is only available through NTIS (see address given above).
- NCEER-88-0011 "Seismic Floor Response Spectra for a Combined System by Green's Functions," by F.M. Lavelle, L.A. Bergman and P.D. Spanos, 5/1/88, (PB89-102875, A03, MF-A01).
- NCEER-88-0012 "A New Solution Technique for Randomly Excited Hysteretic Structures," by G.Q. Cai and Y.K. Lin, 5/16/88, (PB89-102883, A03, MF-A01).
- NCEER-88-0013 "A Study of Radiation Damping and Soil-Structure Interaction Effects in the Centrifuge," by K. Weissman, supervised by J.H. Prevost, 5/24/88, (PB89-144703, A06, MF-A01).
- NCEER-88-0014 "Parameter Identification and Implementation of a Kinematic Plasticity Model for Frictional Soils," by J.H. Prevost and D.V. Griffiths, to be published.
- NCEER-88-0015 "Two- and Three- Dimensional Dynamic Finite Element Analyses of the Long Valley Dam," by D.V. Griffiths and J.H. Prevost, 6/17/88, (PB89-144711, A04, MF-A01).
- NCEER-88-0016 "Damage Assessment of Reinforced Concrete Structures in Eastern United States," by A.M. Reinhorn, M.J. Seidel, S.K. Kunnath and Y.J. Park, 6/15/88, (PB89-122220, A04, MF-A01). This report is only available through NTIS (see address given above).
- NCEER-88-0017 "Dynamic Compliance of Vertically Loaded Strip Foundations in Multilayered Viscoelastic Soils," by S. Ahmad and A.S.M. Israil, 6/17/88, (PB89-102891, A04, MF-A01).
- NCEER-88-0018 "An Experimental Study of Seismic Structural Response With Added Viscoelastic Dampers," by R.C. Lin, Z. Liang, T.T. Soong and R.H. Zhang, 6/30/88, (PB89-122212, A05, MF-A01). This report is available only through NTIS (see address given above).
- NCEER-88-0019 "Experimental Investigation of Primary - Secondary System Interaction," by G.D. Manolis, G. Juhn and A.M. Reinhorn, 5/27/88, (PB89-122204, A04, MF-A01).
- NCEER-88-0020 "A Response Spectrum Approach For Analysis of Nonclassically Damped Structures," by J.N. Yang, S. Sarkani and F.X. Long, 4/22/88, (PB89-102909, A04, MF-A01).
- NCEER-88-0021 "Seismic Interaction of Structures and Soils: Stochastic Approach," by A.S. Veletsos and A.M. Prasad, 7/21/88, (PB89-122196, A04, MF-A01). This report is only available through NTIS (see address given above).
- NCEER-88-0022 "Identification of the Serviceability Limit State and Detection of Seismic Structural Damage," by E. DiPasquale and A.S. Cakmak, 6/15/88, (PB89-122188, A05, MF-A01). This report is available only through NTIS (see address given above).
- NCEER-88-0023 "Multi-Hazard Risk Analysis: Case of a Simple Offshore Structure," by B.K. Bhartia and E.H. Vanmarcke, 7/21/88, (PB89-145213, A05, MF-A01).

- NCEER-88-0024 "Automated Seismic Design of Reinforced Concrete Buildings," by Y.S. Chung, C. Meyer and M. Shinozuka, 7/5/88, (PB89-122170, A06, MF-A01). This report is available only through NTIS (see address given above).
- NCEER-88-0025 "Experimental Study of Active Control of MDOF Structures Under Seismic Excitations," by L.L. Chung, R.C. Lin, T.T. Soong and A.M. Reinhorn, 7/10/88, (PB89-122600, A04, MF-A01).
- NCEER-88-0026 "Earthquake Simulation Tests of a Low-Rise Metal Structure," by J.S. Hwang, K.C. Chang, G.C. Lee and R.L. Ketter, 8/1/88, (PB89-102917, A04, MF-A01).
- NCEER-88-0027 "Systems Study of Urban Response and Reconstruction Due to Catastrophic Earthquakes," by F. Kozin and H.K. Zhou, 9/22/88, (PB90-162348, A04, MF-A01).
- NCEER-88-0028 "Seismic Fragility Analysis of Plane Frame Structures," by H.H-M. Hwang and Y.K. Low, 7/31/88, (PB89-131445, A06, MF-A01).
- NCEER-88-0029 "Response Analysis of Stochastic Structures," by A. Kardara, C. Bucher and M. Shinozuka, 9/22/88, (PB89-174429, A04, MF-A01).
- NCEER-88-0030 "Nonnormal Accelerations Due to Yielding in a Primary Structure," by D.C.K. Chen and L.D. Lutes, 9/19/88, (PB89-131437, A04, MF-A01).
- NCEER-88-0031 "Design Approaches for Soil-Structure Interaction," by A.S. Veletsos, A.M. Prasad and Y. Tang, 12/30/88, (PB89-174437, A03, MF-A01). This report is available only through NTIS (see address given above).
- NCEER-88-0032 "A Re-evaluation of Design Spectra for Seismic Damage Control," by C.J. Turkstra and A.G. Tallin, 11/7/88, (PB89-145221, A05, MF-A01).
- NCEER-88-0033 "The Behavior and Design of Noncontact Lap Splices Subjected to Repeated Inelastic Tensile Loading," by V.E. Sagan, P. Gergely and R.N. White, 12/8/88, (PB89-163737, A08, MF-A01).
- NCEER-88-0034 "Seismic Response of Pile Foundations," by S.M. Mamoon, P.K. Banerjee and S. Ahmad, 11/1/88, (PB89-145239, A04, MF-A01).
- NCEER-88-0035 "Modeling of R/C Building Structures With Flexible Floor Diaphragms (IDARC2)," by A.M. Reinhorn, S.K. Kunnath and N. Panahshahi, 9/7/88, (PB89-207153, A07, MF-A01).
- NCEER-88-0036 "Solution of the Dam-Reservoir Interaction Problem Using a Combination of FEM, BEM with Particular Integrals, Modal Analysis, and Substructuring," by C-S. Tsai, G.C. Lee and R.L. Ketter, 12/31/88, (PB89-207146, A04, MF-A01).
- NCEER-88-0037 "Optimal Placement of Actuators for Structural Control," by F.Y. Cheng and C.P. Pantelides, 8/15/88, (PB89-162846, A05, MF-A01).
- NCEER-88-0038 "Teflon Bearings in Aseismic Base Isolation: Experimental Studies and Mathematical Modeling," by A. Mokha, M.C. Constantinou and A.M. Reinhorn, 12/5/88, (PB89-218457, A10, MF-A01). This report is available only through NTIS (see address given above).
- NCEER-88-0039 "Seismic Behavior of Flat Slab High-Rise Buildings in the New York City Area," by P. Weidlinger and M. Ettouney, 10/15/88, (PB90-145681, A04, MF-A01).
- NCEER-88-0040 "Evaluation of the Earthquake Resistance of Existing Buildings in New York City," by P. Weidlinger and M. Ettouney, 10/15/88, to be published.
- NCEER-88-0041 "Small-Scale Modeling Techniques for Reinforced Concrete Structures Subjected to Seismic Loads," by W. Kim, A. El-Attar and R.N. White, 11/22/88, (PB89-189625, A05, MF-A01).
- NCEER-88-0042 "Modeling Strong Ground Motion from Multiple Event Earthquakes," by G.W. Ellis and A.S. Cakmak, 10/15/88, (PB89-174445, A03, MF-A01).

- NCEER-88-0043 "Nonstationary Models of Seismic Ground Acceleration," by M. Grigoriu, S.E. Ruiz and E. Rosenblueth, 7/15/88, (PB89-189617, A04, MF-A01).
- NCEER-88-0044 "SARCF User's Guide: Seismic Analysis of Reinforced Concrete Frames," by Y.S. Chung, C. Meyer and M. Shinozuka, 11/9/88, (PB89-174452, A08, MF-A01).
- NCEER-88-0045 "First Expert Panel Meeting on Disaster Research and Planning," edited by J. Pantelic and J. Stoyke, 9/15/88, (PB89-174460, A05, MF-A01).
- NCEER-88-0046 "Preliminary Studies of the Effect of Degrading Infill Walls on the Nonlinear Seismic Response of Steel Frames," by C.Z. Chrysostomou, P. Gergely and J.F. Abel, 12/19/88, (PB89-208383, A05, MF-A01).
- NCEER-88-0047 "Reinforced Concrete Frame Component Testing Facility - Design, Construction, Instrumentation and Operation," by S.P. Pessiki, C. Conley, T. Bond, P. Gergely and R.N. White, 12/16/88, (PB89-174478, A04, MF-A01).
- NCEER-89-0001 "Effects of Protective Cushion and Soil Compliancy on the Response of Equipment Within a Seismically Excited Building," by J.A. HoLung, 2/16/89, (PB89-207179, A04, MF-A01).
- NCEER-89-0002 "Statistical Evaluation of Response Modification Factors for Reinforced Concrete Structures," by H.H-M. Hwang and J-W. Jaw, 2/17/89, (PB89-207187, A05, MF-A01).
- NCEER-89-0003 "Hysteretic Columns Under Random Excitation," by G-Q. Cai and Y.K. Lin, 1/9/89, (PB89-196513, A03, MF-A01).
- NCEER-89-0004 "Experimental Study of 'Elephant Foot Bulge' Instability of Thin-Walled Metal Tanks," by Z-H. Jia and R.L. Ketter, 2/22/89, (PB89-207195, A03, MF-A01).
- NCEER-89-0005 "Experiment on Performance of Buried Pipelines Across San Andreas Fault," by J. Isenberg, E. Richardson and T.D. O'Rourke, 3/10/89, (PB89-218440, A04, MF-A01). This report is available only through NTIS (see address given above).
- NCEER-89-0006 "A Knowledge-Based Approach to Structural Design of Earthquake-Resistant Buildings," by M. Subramani, P. Gergely, C.H. Conley, J.F. Abel and A.H. Zaghaw, 1/15/89, (PB89-218465, A06, MF-A01).
- NCEER-89-0007 "Liquefaction Hazards and Their Effects on Buried Pipelines," by T.D. O'Rourke and P.A. Lane, 2/1/89, (PB89-218481, A09, MF-A01).
- NCEER-89-0008 "Fundamentals of System Identification in Structural Dynamics," by H. Imai, C-B. Yun, O. Maruyama and M. Shinozuka, 1/26/89, (PB89-207211, A04, MF-A01).
- NCEER-89-0009 "Effects of the 1985 Michoacan Earthquake on Water Systems and Other Buried Lifelines in Mexico," by A.G. Ayala and M.J. O'Rourke, 3/8/89, (PB89-207229, A06, MF-A01).
- NCEER-89-R010 "NCEER Bibliography of Earthquake Education Materials," by K.E.K. Ross, Second Revision, 9/1/89, (PB90-125352, A05, MF-A01). This report is replaced by NCEER-92-0018.
- NCEER-89-0011 "Inelastic Three-Dimensional Response Analysis of Reinforced Concrete Building Structures (IDARC-3D), Part I - Modeling," by S.K. Kunnath and A.M. Reinhorn, 4/17/89, (PB90-114612, A07, MF-A01). This report is available only through NTIS (see address given above).
- NCEER-89-0012 "Recommended Modifications to ATC-14," by C.D. Poland and J.O. Malley, 4/12/89, (PB90-108648, A15, MF-A01).
- NCEER-89-0013 "Repair and Strengthening of Beam-to-Column Connections Subjected to Earthquake Loading," by M. Corazao and A.J. Durrani, 2/28/89, (PB90-109885, A06, MF-A01).
- NCEER-89-0014 "Program EXKAL2 for Identification of Structural Dynamic Systems," by O. Maruyama, C-B. Yun, M. Hoshiya and M. Shinozuka, 5/19/89, (PB90-109877, A09, MF-A01).

- NCEER-89-0015 "Response of Frames With Bolted Semi-Rigid Connections, Part I - Experimental Study and Analytical Predictions," by P.J. DiCorso, A.M. Reinhorn, J.R. Dickerson, J.B. Radzinski and W.L. Harper, 6/1/89, to be published.
- NCEER-89-0016 "ARMA Monte Carlo Simulation in Probabilistic Structural Analysis," by P.D. Spanos and M.P. Mignolet, 7/10/89, (PB90-109893, A03, MF-A01).
- NCEER-89-P017 "Preliminary Proceedings from the Conference on Disaster Preparedness - The Place of Earthquake Education in Our Schools," Edited by K.E.K. Ross, 6/23/89, (PB90-108606, A03, MF-A01).
- NCEER-89-0017 "Proceedings from the Conference on Disaster Preparedness - The Place of Earthquake Education in Our Schools," Edited by K.E.K. Ross, 12/31/89, (PB90-207895, A012, MF-A02). This report is available only through NTIS (see address given above).
- NCEER-89-0018 "Multidimensional Models of Hysteretic Material Behavior for Vibration Analysis of Shape Memory Energy Absorbing Devices, by E.J. Graesser and F.A. Cozzarelli, 6/7/89, (PB90-164146, A04, MF-A01).
- NCEER-89-0019 "Nonlinear Dynamic Analysis of Three-Dimensional Base Isolated Structures (3D-BASIS)," by S. Nagarajaiah, A.M. Reinhorn and M.C. Constantinou, 8/3/89, (PB90-161936, A06, MF-A01). This report has been replaced by NCEER-93-0011.
- NCEER-89-0020 "Structural Control Considering Time-Rate of Control Forces and Control Rate Constraints," by F.Y. Cheng and C.P. Pantelides, 8/3/89, (PB90-120445, A04, MF-A01).
- NCEER-89-0021 "Subsurface Conditions of Memphis and Shelby County," by K.W. Ng, T-S. Chang and H-H.M. Hwang, 7/26/89, (PB90-120437, A03, MF-A01).
- NCEER-89-0022 "Seismic Wave Propagation Effects on Straight Jointed Buried Pipelines," by K. Elhmadi and M.J. O'Rourke, 8/24/89, (PB90-162322, A10, MF-A02).
- NCEER-89-0023 "Workshop on Serviceability Analysis of Water Delivery Systems," edited by M. Grigoriu, 3/6/89, (PB90-127424, A03, MF-A01).
- NCEER-89-0024 "Shaking Table Study of a 1/5 Scale Steel Frame Composed of Tapered Members," by K.C. Chang, J.S. Hwang and G.C. Lee, 9/18/89, (PB90-160169, A04, MF-A01).
- NCEER-89-0025 "DYNA1D: A Computer Program for Nonlinear Seismic Site Response Analysis - Technical Documentation," by Jean H. Prevost, 9/14/89, (PB90-161944, A07, MF-A01). This report is available only through NTIS (see address given above).
- NCEER-89-0026 "1:4 Scale Model Studies of Active Tendon Systems and Active Mass Dampers for Aseismic Protection," by A.M. Reinhorn, T.T. Soong, R.C. Lin, Y.P. Yang, Y. Fukao, H. Abe and M. Nakai, 9/15/89, (PB90-173246, A10, MF-A02). This report is available only through NTIS (see address given above).
- NCEER-89-0027 "Scattering of Waves by Inclusions in a Nonhomogeneous Elastic Half Space Solved by Boundary Element Methods," by P.K. Hadley, A. Askar and A.S. Cakmak, 6/15/89, (PB90-145699, A07, MF-A01).
- NCEER-89-0028 "Statistical Evaluation of Deflection Amplification Factors for Reinforced Concrete Structures," by H.H.M. Hwang, J-W. Jaw and A.L. Ch'ng, 8/31/89, (PB90-164633, A05, MF-A01).
- NCEER-89-0029 "Bedrock Accelerations in Memphis Area Due to Large New Madrid Earthquakes," by H.H.M. Hwang, C.H.S. Chen and G. Yu, 11/7/89, (PB90-162330, A04, MF-A01).
- NCEER-89-0030 "Seismic Behavior and Response Sensitivity of Secondary Structural Systems," by Y.Q. Chen and T.T. Soong, 10/23/89, (PB90-164658, A08, MF-A01).
- NCEER-89-0031 "Random Vibration and Reliability Analysis of Primary-Secondary Structural Systems," by Y. Ibrahim, M. Grigoriu and T.T. Soong, 11/10/89, (PB90-161951, A04, MF-A01).

- NCEER-89-0032 "Proceedings from the Second U.S. - Japan Workshop on Liquefaction, Large Ground Deformation and Their Effects on Lifelines, September 26-29, 1989," Edited by T.D. O'Rourke and M. Hamada, 12/1/89, (PB90-209388, A22, MF-A03).
- NCEER-89-0033 "Deterministic Model for Seismic Damage Evaluation of Reinforced Concrete Structures," by J.M. Bracci, A.M. Reinhorn, J.B. Mander and S.K. Kunnath, 9/27/89, (PB91-108803, A06, MF-A01).
- NCEER-89-0034 "On the Relation Between Local and Global Damage Indices," by E. DiPasquale and A.S. Cakmak, 8/15/89, (PB90-173865, A05, MF-A01).
- NCEER-89-0035 "Cyclic Undrained Behavior of Nonplastic and Low Plasticity Silts," by A.J. Walker and H.E. Stewart, 7/26/89, (PB90-183518, A10, MF-A01).
- NCEER-89-0036 "Liquefaction Potential of Surficial Deposits in the City of Buffalo, New York," by M. Budhu, R. Giese and L. Baumgrass, 1/17/89, (PB90-208455, A04, MF-A01).
- NCEER-89-0037 "A Deterministic Assessment of Effects of Ground Motion Incoherence," by A.S. Veletsos and Y. Tang, 7/15/89, (PB90-164294, A03, MF-A01).
- NCEER-89-0038 "Workshop on Ground Motion Parameters for Seismic Hazard Mapping," July 17-18, 1989, edited by R.V. Whitman, 12/1/89, (PB90-173923, A04, MF-A01).
- NCEER-89-0039 "Seismic Effects on Elevated Transit Lines of the New York City Transit Authority," by C.J. Costantino, C.A. Miller and E. Heymsfield, 12/26/89, (PB90-207887, A06, MF-A01).
- NCEER-89-0040 "Centrifugal Modeling of Dynamic Soil-Structure Interaction," by K. Weissman, Supervised by J.H. Prevost, 5/10/89, (PB90-207879, A07, MF-A01).
- NCEER-89-0041 "Linearized Identification of Buildings With Cores for Seismic Vulnerability Assessment," by I-K. Ho and A.E. Aktan, 11/1/89, (PB90-251943, A07, MF-A01).
- NCEER-90-0001 "Geotechnical and Lifeline Aspects of the October 17, 1989 Loma Prieta Earthquake in San Francisco," by T.D. O'Rourke, H.E. Stewart, F.T. Blackburn and T.S. Dickerman, 1/90, (PB90-208596, A05, MF-A01).
- NCEER-90-0002 "Nonnormal Secondary Response Due to Yielding in a Primary Structure," by D.C.K. Chen and L.D. Lutes, 2/28/90, (PB90-251976, A07, MF-A01).
- NCEER-90-0003 "Earthquake Education Materials for Grades K-12," by K.E.K. Ross, 4/16/90, (PB91-251984, A05, MF-A05). This report has been replaced by NCEER-92-0018.
- NCEER-90-0004 "Catalog of Strong Motion Stations in Eastern North America," by R.W. Busby, 4/3/90, (PB90-251984, A05, MF-A01).
- NCEER-90-0005 "NCEER Strong-Motion Data Base: A User Manual for the GeoBase Release (Version 1.0 for the Sun3)," by P. Friberg and K. Jacob, 3/31/90 (PB90-258062, A04, MF-A01).
- NCEER-90-0006 "Seismic Hazard Along a Crude Oil Pipeline in the Event of an 1811-1812 Type New Madrid Earthquake," by H.H.M. Hwang and C-H.S. Chen, 4/16/90, (PB90-258054, A04, MF-A01).
- NCEER-90-0007 "Site-Specific Response Spectra for Memphis Sheahan Pumping Station," by H.H.M. Hwang and C.S. Lee, 5/15/90, (PB91-108811, A05, MF-A01).
- NCEER-90-0008 "Pilot Study on Seismic Vulnerability of Crude Oil Transmission Systems," by T. Ariman, R. Dobry, M. Grigoriu, F. Kozin, M. O'Rourke, T. O'Rourke and M. Shinozuka, 5/25/90, (PB91-108837, A06, MF-A01).
- NCEER-90-0009 "A Program to Generate Site Dependent Time Histories: EQGEN," by G.W. Ellis, M. Srinivasan and A.S. Cakmak, 1/30/90, (PB91-108829, A04, MF-A01).
- NCEER-90-0010 "Active Isolation for Seismic Protection of Operating Rooms," by M.E. Talbott, Supervised by M. Shinozuka, 6/8/9, (PB91-110205, A05, MF-A01).

- NCEER-90-0011 "Program LINEARID for Identification of Linear Structural Dynamic Systems," by C-B. Yun and M. Shinozuka, 6/25/90, (PB91-110312, A08, MF-A01).
- NCEER-90-0012 "Two-Dimensional Two-Phase Elasto-Plastic Seismic Response of Earth Dams," by A.N. Yiagos, Supervised by J.H. Prevost, 6/20/90, (PB91-110197, A13, MF-A02).
- NCEER-90-0013 "Secondary Systems in Base-Isolated Structures: Experimental Investigation, Stochastic Response and Stochastic Sensitivity," by G.D. Manolis, G. Juhn, M.C. Constantinou and A.M. Reinhorn, 7/1/90, (PB91-110320, A08, MF-A01).
- NCEER-90-0014 "Seismic Behavior of Lightly-Reinforced Concrete Column and Beam-Column Joint Details," by S.P. Pessiki, C.H. Conley, P. Gergely and R.N. White, 8/22/90, (PB91-108795, A11, MF-A02).
- NCEER-90-0015 "Two Hybrid Control Systems for Building Structures Under Strong Earthquakes," by J.N. Yang and A. Daniellians, 6/29/90, (PB91-125393, A04, MF-A01).
- NCEER-90-0016 "Instantaneous Optimal Control with Acceleration and Velocity Feedback," by J.N. Yang and Z. Li, 6/29/90, (PB91-125401, A03, MF-A01).
- NCEER-90-0017 "Reconnaissance Report on the Northern Iran Earthquake of June 21, 1990," by M. Mehrain, 10/4/90, (PB91-125377, A03, MF-A01).
- NCEER-90-0018 "Evaluation of Liquefaction Potential in Memphis and Shelby County," by T.S. Chang, P.S. Tang, C.S. Lee and H. Hwang, 8/10/90, (PB91-125427, A09, MF-A01).
- NCEER-90-0019 "Experimental and Analytical Study of a Combined Sliding Disc Bearing and Helical Steel Spring Isolation System," by M.C. Constantinou, A.S. Mokha and A.M. Reinhorn, 10/4/90, (PB91-125385, A06, MF-A01). This report is available only through NTIS (see address given above).
- NCEER-90-0020 "Experimental Study and Analytical Prediction of Earthquake Response of a Sliding Isolation System with a Spherical Surface," by A.S. Mokha, M.C. Constantinou and A.M. Reinhorn, 10/11/90, (PB91-125419, A05, MF-A01).
- NCEER-90-0021 "Dynamic Interaction Factors for Floating Pile Groups," by G. Gazetas, K. Fan, A. Kaynia and E. Kausel, 9/10/90, (PB91-170381, A05, MF-A01).
- NCEER-90-0022 "Evaluation of Seismic Damage Indices for Reinforced Concrete Structures," by S. Rodriguez-Gomez and A.S. Cakmak, 9/30/90, PB91-171322, A06, MF-A01).
- NCEER-90-0023 "Study of Site Response at a Selected Memphis Site," by H. Desai, S. Ahmad, E.S. Gazetas and M.R. Oh, 10/11/90, (PB91-196857, A03, MF-A01).
- NCEER-90-0024 "A User's Guide to Strongmo: Version 1.0 of NCEER's Strong-Motion Data Access Tool for PCs and Terminals," by P.A. Friberg and C.A.T. Susch, 11/15/90, (PB91-171272, A03, MF-A01).
- NCEER-90-0025 "A Three-Dimensional Analytical Study of Spatial Variability of Seismic Ground Motions," by L-L. Hong and A.H.-S. Ang, 10/30/90, (PB91-170399, A09, MF-A01).
- NCEER-90-0026 "MUMOID User's Guide - A Program for the Identification of Modal Parameters," by S. Rodriguez-Gomez and E. DiPasquale, 9/30/90, (PB91-171298, A04, MF-A01).
- NCEER-90-0027 "SARCF-II User's Guide - Seismic Analysis of Reinforced Concrete Frames," by S. Rodriguez-Gomez, Y.S. Chung and C. Meyer, 9/30/90, (PB91-171280, A05, MF-A01).
- NCEER-90-0028 "Viscous Dampers: Testing, Modeling and Application in Vibration and Seismic Isolation," by N. Makris and M.C. Constantinou, 12/20/90 (PB91-190561, A06, MF-A01).
- NCEER-90-0029 "Soil Effects on Earthquake Ground Motions in the Memphis Area," by H. Hwang, C.S. Lee, K.W. Ng and T.S. Chang, 8/2/90, (PB91-190751, A05, MF-A01).

- NCEER-91-0001 "Proceedings from the Third Japan-U.S. Workshop on Earthquake Resistant Design of Lifeline Facilities and Countermeasures for Soil Liquefaction, December 17-19, 1990," edited by T.D. O'Rourke and M. Hamada, 2/1/91, (PB91-179259, A99, MF-A04).
- NCEER-91-0002 "Physical Space Solutions of Non-Proportionally Damped Systems," by M. Tong, Z. Liang and G.C. Lee, 1/15/91, (PB91-179242, A04, MF-A01).
- NCEER-91-0003 "Seismic Response of Single Piles and Pile Groups," by K. Fan and G. Gazetas, 1/10/91, (PB92-174994, A04, MF-A01).
- NCEER-91-0004 "Damping of Structures: Part 1 - Theory of Complex Damping," by Z. Liang and G. Lee, 10/10/91, (PB92-197235, A12, MF-A03).
- NCEER-91-0005 "3D-BASIS - Nonlinear Dynamic Analysis of Three Dimensional Base Isolated Structures: Part II," by S. Nagarajaiah, A.M. Reinhorn and M.C. Constantinou, 2/28/91, (PB91-190553, A07, MF-A01). This report has been replaced by NCEER-93-0011.
- NCEER-91-0006 "A Multidimensional Hysteretic Model for Plasticity Deforming Metals in Energy Absorbing Devices," by E.J. Graesser and F.A. Cozzarelli, 4/9/91, (PB92-108364, A04, MF-A01).
- NCEER-91-0007 "A Framework for Customizable Knowledge-Based Expert Systems with an Application to a KBES for Evaluating the Seismic Resistance of Existing Buildings," by E.G. Ibarra-Anaya and S.J. Fennes, 4/9/91, (PB91-210930, A08, MF-A01).
- NCEER-91-0008 "Nonlinear Analysis of Steel Frames with Semi-Rigid Connections Using the Capacity Spectrum Method," by G.G. Deierlein, S-H. Hsieh, Y-J. Shen and J.F. Abel, 7/2/91, (PB92-113828, A05, MF-A01).
- NCEER-91-0009 "Earthquake Education Materials for Grades K-12," by K.E.K. Ross, 4/30/91, (PB91-212142, A06, MF-A01). This report has been replaced by NCEER-92-0018.
- NCEER-91-0010 "Phase Wave Velocities and Displacement Phase Differences in a Harmonically Oscillating Pile," by N. Makris and G. Gazetas, 7/8/91, (PB92-108356, A04, MF-A01).
- NCEER-91-0011 "Dynamic Characteristics of a Full-Size Five-Story Steel Structure and a 2/5 Scale Model," by K.C. Chang, G.C. Yao, G.C. Lee, D.S. Hao and Y.C. Yeh," 7/2/91, (PB93-116648, A06, MF-A02).
- NCEER-91-0012 "Seismic Response of a 2/5 Scale Steel Structure with Added Viscoelastic Dampers," by K.C. Chang, T.T. Soong, S-T. Oh and M.L. Lai, 5/17/91, (PB92-110816, A05, MF-A01).
- NCEER-91-0013 "Earthquake Response of Retaining Walls; Full-Scale Testing and Computational Modeling," by S. Alampalli and A-W.M. Elgamal, 6/20/91, to be published.
- NCEER-91-0014 "3D-BASIS-M: Nonlinear Dynamic Analysis of Multiple Building Base Isolated Structures," by P.C. Tsopelas, S. Nagarajaiah, M.C. Constantinou and A.M. Reinhorn, 5/28/91, (PB92-113885, A09, MF-A02).
- NCEER-91-0015 "Evaluation of SEAOC Design Requirements for Sliding Isolated Structures," by D. Theodossiou and M.C. Constantinou, 6/10/91, (PB92-114602, A11, MF-A03).
- NCEER-91-0016 "Closed-Loop Modal Testing of a 27-Story Reinforced Concrete Flat Plate-Core Building," by H.R. Somaprasad, T. Toksoy, H. Yoshiyuki and A.E. Aktan, 7/15/91, (PB92-129980, A07, MF-A02).
- NCEER-91-0017 "Shake Table Test of a 1/6 Scale Two-Story Lightly Reinforced Concrete Building," by A.G. El-Attar, R.N. White and P. Gergely, 2/28/91, (PB92-222447, A06, MF-A02).
- NCEER-91-0018 "Shake Table Test of a 1/8 Scale Three-Story Lightly Reinforced Concrete Building," by A.G. El-Attar, R.N. White and P. Gergely, 2/28/91, (PB93-116630, A08, MF-A02).
- NCEER-91-0019 "Transfer Functions for Rigid Rectangular Foundations," by A.S. Veletsos, A.M. Prasad and W.H. Wu, 7/31/91, to be published.

- NCEER-91-0020 "Hybrid Control of Seismic-Excited Nonlinear and Inelastic Structural Systems," by J.N. Yang, Z. Li and A. Daniellians, 8/1/91, (PB92-143171, A06, MF-A02).
- NCEER-91-0021 "The NCEER-91 Earthquake Catalog: Improved Intensity-Based Magnitudes and Recurrence Relations for U.S. Earthquakes East of New Madrid," by L. Seeber and J.G. Armbruster, 8/28/91, (PB92-176742, A06, MF-A02).
- NCEER-91-0022 "Proceedings from the Implementation of Earthquake Planning and Education in Schools: The Need for Change - The Roles of the Changemakers," by K.E.K. Ross and F. Winslow, 7/23/91, (PB92-129998, A12, MF-A03).
- NCEER-91-0023 "A Study of Reliability-Based Criteria for Seismic Design of Reinforced Concrete Frame Buildings," by H.H.M. Hwang and H-M. Hsu, 8/10/91, (PB92-140235, A09, MF-A02).
- NCEER-91-0024 "Experimental Verification of a Number of Structural System Identification Algorithms," by R.G. Ghanem, H. Gavin and M. Shinozuka, 9/18/91, (PB92-176577, A18, MF-A04).
- NCEER-91-0025 "Probabilistic Evaluation of Liquefaction Potential," by H.H.M. Hwang and C.S. Lee," 11/25/91, (PB92-143429, A05, MF-A01).
- NCEER-91-0026 "Instantaneous Optimal Control for Linear, Nonlinear and Hysteretic Structures - Stable Controllers," by J.N. Yang and Z. Li, 11/15/91, (PB92-163807, A04, MF-A01).
- NCEER-91-0027 "Experimental and Theoretical Study of a Sliding Isolation System for Bridges," by M.C. Constantinou, A. Kartoum, A.M. Reinhorn and P. Bradford, 11/15/91, (PB92-176973, A10, MF-A03).
- NCEER-92-0001 "Case Studies of Liquefaction and Lifeline Performance During Past Earthquakes, Volume 1: Japanese Case Studies," Edited by M. Hamada and T. O'Rourke, 2/17/92, (PB92-197243, A18, MF-A04).
- NCEER-92-0002 "Case Studies of Liquefaction and Lifeline Performance During Past Earthquakes, Volume 2: United States Case Studies," Edited by T. O'Rourke and M. Hamada, 2/17/92, (PB92-197250, A20, MF-A04).
- NCEER-92-0003 "Issues in Earthquake Education," Edited by K. Ross, 2/3/92, (PB92-222389, A07, MF-A02).
- NCEER-92-0004 "Proceedings from the First U.S. - Japan Workshop on Earthquake Protective Systems for Bridges," Edited by I.G. Buckle, 2/4/92, (PB94-142239, A99, MF-A06).
- NCEER-92-0005 "Seismic Ground Motion from a Haskell-Type Source in a Multiple-Layered Half-Space," A.P. Theoharis, G. Deodatis and M. Shinozuka, 1/2/92, to be published.
- NCEER-92-0006 "Proceedings from the Site Effects Workshop," Edited by R. Whitman, 2/29/92, (PB92-197201, A04, MF-A01).
- NCEER-92-0007 "Engineering Evaluation of Permanent Ground Deformations Due to Seismically-Induced Liquefaction," by M.H. Baziar, R. Dobry and A-W.M. Elgamal, 3/24/92, (PB92-222421, A13, MF-A03).
- NCEER-92-0008 "A Procedure for the Seismic Evaluation of Buildings in the Central and Eastern United States," by C.D. Poland and J.O. Malley, 4/2/92, (PB92-222439, A20, MF-A04).
- NCEER-92-0009 "Experimental and Analytical Study of a Hybrid Isolation System Using Friction Controllable Sliding Bearings," by M.Q. Feng, S. Fujii and M. Shinozuka, 5/15/92, (PB93-150282, A06, MF-A02).
- NCEER-92-0010 "Seismic Resistance of Slab-Column Connections in Existing Non-Ductile Flat-Plate Buildings," by A.J. Durrani and Y. Du, 5/18/92, (PB93-116812, A06, MF-A02).
- NCEER-92-0011 "The Hysteretic and Dynamic Behavior of Brick Masonry Walls Upgraded by Ferrocement Coatings Under Cyclic Loading and Strong Simulated Ground Motion," by H. Lee and S.P. Prawel, 5/11/92, to be published.
- NCEER-92-0012 "Study of Wire Rope Systems for Seismic Protection of Equipment in Buildings," by G.F. Demetriades, M.C. Constantinou and A.M. Reinhorn, 5/20/92, (PB93-116655, A08, MF-A02).

- NCEER-92-0013 "Shape Memory Structural Dampers: Material Properties, Design and Seismic Testing," by P.R. Witting and F.A. Cozzarelli, 5/26/92, (PB93-116663, A05, MF-A01).
- NCEER-92-0014 "Longitudinal Permanent Ground Deformation Effects on Buried Continuous Pipelines," by M.J. O'Rourke, and C. Nordberg, 6/15/92, (PB93-116671, A08, MF-A02).
- NCEER-92-0015 "A Simulation Method for Stationary Gaussian Random Functions Based on the Sampling Theorem," by M. Grigoriu and S. Balopoulou, 6/11/92, (PB93-127496, A05, MF-A01).
- NCEER-92-0016 "Gravity-Load-Designed Reinforced Concrete Buildings: Seismic Evaluation of Existing Construction and Detailing Strategies for Improved Seismic Resistance," by G.W. Hoffmann, S.K. Kunnath, A.M. Reinhorn and J.B. Mander, 7/15/92, (PB94-142007, A08, MF-A02).
- NCEER-92-0017 "Observations on Water System and Pipeline Performance in the Limón Area of Costa Rica Due to the April 22, 1991 Earthquake," by M. O'Rourke and D. Ballantyne, 6/30/92, (PB93-126811, A06, MF-A02).
- NCEER-92-0018 "Fourth Edition of Earthquake Education Materials for Grades K-12," Edited by K.E.K. Ross, 8/10/92, (PB93-114023, A07, MF-A02).
- NCEER-92-0019 "Proceedings from the Fourth Japan-U.S. Workshop on Earthquake Resistant Design of Lifeline Facilities and Countermeasures for Soil Liquefaction," Edited by M. Hamada and T.D. O'Rourke, 8/12/92, (PB93-163939, A99, MF-E11).
- NCEER-92-0020 "Active Bracing System: A Full Scale Implementation of Active Control," by A.M. Reinhorn, T.T. Soong, R.C. Lin, M.A. Riley, Y.P. Wang, S. Aizawa and M. Higashino, 8/14/92, (PB93-127512, A06, MF-A02).
- NCEER-92-0021 "Empirical Analysis of Horizontal Ground Displacement Generated by Liquefaction-Induced Lateral Spreads," by S.F. Bartlett and T.L. Youd, 8/17/92, (PB93-188241, A06, MF-A02).
- NCEER-92-0022 "IDARC Version 3.0: Inelastic Damage Analysis of Reinforced Concrete Structures," by S.K. Kunnath, A.M. Reinhorn and R.F. Lobo, 8/31/92, (PB93-227502, A07, MF-A02).
- NCEER-92-0023 "A Semi-Empirical Analysis of Strong-Motion Peaks in Terms of Seismic Source, Propagation Path and Local Site Conditions, by M. Kamiyama, M.J. O'Rourke and R. Flores-Berrones, 9/9/92, (PB93-150266, A08, MF-A02).
- NCEER-92-0024 "Seismic Behavior of Reinforced Concrete Frame Structures with Nonductile Details, Part I: Summary of Experimental Findings of Full Scale Beam-Column Joint Tests," by A. Beres, R.N. White and P. Gergely, 9/30/92, (PB93-227783, A05, MF-A01).
- NCEER-92-0025 "Experimental Results of Repaired and Retrofitted Beam-Column Joint Tests in Lightly Reinforced Concrete Frame Buildings," by A. Beres, S. El-Borgi, R.N. White and P. Gergely, 10/29/92, (PB93-227791, A05, MF-A01).
- NCEER-92-0026 "A Generalization of Optimal Control Theory: Linear and Nonlinear Structures," by J.N. Yang, Z. Li and S. Vongchavalitkul, 11/2/92, (PB93-188621, A05, MF-A01).
- NCEER-92-0027 "Seismic Resistance of Reinforced Concrete Frame Structures Designed Only for Gravity Loads: Part I - Design and Properties of a One-Third Scale Model Structure," by J.M. Bracci, A.M. Reinhorn and J.B. Mander, 12/1/92, (PB94-104502, A08, MF-A02).
- NCEER-92-0028 "Seismic Resistance of Reinforced Concrete Frame Structures Designed Only for Gravity Loads: Part II - Experimental Performance of Subassemblages," by L.E. Aycaardi, J.B. Mander and A.M. Reinhorn, 12/1/92, (PB94-104510, A08, MF-A02).
- NCEER-92-0029 "Seismic Resistance of Reinforced Concrete Frame Structures Designed Only for Gravity Loads: Part III - Experimental Performance and Analytical Study of a Structural Model," by J.M. Bracci, A.M. Reinhorn and J.B. Mander, 12/1/92, (PB93-227528, A09, MF-A01).

- NCEER-92-0030 "Evaluation of Seismic Retrofit of Reinforced Concrete Frame Structures: Part I - Experimental Performance of Retrofitted Subassemblages," by D. Choudhuri, J.B. Mander and A.M. Reinhorn, 12/8/92, (PB93-198307, A07, MF-A02).
- NCEER-92-0031 "Evaluation of Seismic Retrofit of Reinforced Concrete Frame Structures: Part II - Experimental Performance and Analytical Study of a Retrofitted Structural Model," by J.M. Bracci, A.M. Reinhorn and J.B. Mander, 12/8/92, (PB93-198315, A09, MF-A03).
- NCEER-92-0032 "Experimental and Analytical Investigation of Seismic Response of Structures with Supplemental Fluid Viscous Dampers," by M.C. Constantinou and M.D. Symans, 12/21/92, (PB93-191435, A10, MF-A03). This report is available only through NTIS (see address given above).
- NCEER-92-0033 "Reconnaissance Report on the Cairo, Egypt Earthquake of October 12, 1992," by M. Khater, 12/23/92, (PB93-188621, A03, MF-A01).
- NCEER-92-0034 "Low-Level Dynamic Characteristics of Four Tall Flat-Plate Buildings in New York City," by H. Gavin, S. Yuan, J. Grossman, E. Pekelis and K. Jacob, 12/28/92, (PB93-188217, A07, MF-A02).
- NCEER-93-0001 "An Experimental Study on the Seismic Performance of Brick-Infilled Steel Frames With and Without Retrofit," by J.B. Mander, B. Nair, K. Wojtkowski and J. Ma, 1/29/93, (PB93-227510, A07, MF-A02).
- NCEER-93-0002 "Social Accounting for Disaster Preparedness and Recovery Planning," by S. Cole, E. Pantoja and V. Razak, 2/22/93, (PB94-142114, A12, MF-A03).
- NCEER-93-0003 "Assessment of 1991 NEHRP Provisions for Nonstructural Components and Recommended Revisions," by T.T. Soong, G. Chen, Z. Wu, R-H. Zhang and M. Grigoriu, 3/1/93, (PB93-188639, A06, MF-A02).
- NCEER-93-0004 "Evaluation of Static and Response Spectrum Analysis Procedures of SEAOC/UBC for Seismic Isolated Structures," by C.W. Winters and M.C. Constantinou, 3/23/93, (PB93-198299, A10, MF-A03).
- NCEER-93-0005 "Earthquakes in the Northeast - Are We Ignoring the Hazard? A Workshop on Earthquake Science and Safety for Educators," edited by K.E.K. Ross, 4/2/93, (PB94-103066, A09, MF-A02).
- NCEER-93-0006 "Inelastic Response of Reinforced Concrete Structures with Viscoelastic Braces," by R.F. Lobo, J.M. Bracci, K.L. Shen, A.M. Reinhorn and T.T. Soong, 4/5/93, (PB93-227486, A05, MF-A02).
- NCEER-93-0007 "Seismic Testing of Installation Methods for Computers and Data Processing Equipment," by K. Kosar, T.T. Soong, K.L. Shen, J.A. HoLung and Y.K. Lin, 4/12/93, (PB93-198299, A07, MF-A02).
- NCEER-93-0008 "Retrofit of Reinforced Concrete Frames Using Added Dampers," by A. Reinhorn, M. Constantinou and C. Li, to be published.
- NCEER-93-0009 "Seismic Behavior and Design Guidelines for Steel Frame Structures with Added Viscoelastic Dampers," by K.C. Chang, M.L. Lai, T.T. Soong, D.S. Hao and Y.C. Yeh, 5/1/93, (PB94-141959, A07, MF-A02).
- NCEER-93-0010 "Seismic Performance of Shear-Critical Reinforced Concrete Bridge Piers," by J.B. Mander, S.M. Waheed, M.T.A. Chaudhary and S.S. Chen, 5/12/93, (PB93-227494, A08, MF-A02).
- NCEER-93-0011 "3D-BASIS-TABS: Computer Program for Nonlinear Dynamic Analysis of Three Dimensional Base Isolated Structures," by S. Nagarajaiah, C. Li, A.M. Reinhorn and M.C. Constantinou, 8/2/93, (PB94-141819, A09, MF-A02).
- NCEER-93-0012 "Effects of Hydrocarbon Spills from an Oil Pipeline Break on Ground Water," by O.J. Helweg and H.H.M. Hwang, 8/3/93, (PB94-141942, A06, MF-A02).
- NCEER-93-0013 "Simplified Procedures for Seismic Design of Nonstructural Components and Assessment of Current Code Provisions," by M.P. Singh, L.E. Suarez, E.E. Matheu and G.O. Maldonado, 8/4/93, (PB94-141827, A09, MF-A02).
- NCEER-93-0014 "An Energy Approach to Seismic Analysis and Design of Secondary Systems," by G. Chen and T.T. Soong, 8/6/93, (PB94-142767, A11, MF-A03).

- NCEER-93-0015 "Proceedings from School Sites: Becoming Prepared for Earthquakes - Commemorating the Third Anniversary of the Loma Prieta Earthquake," Edited by F.E. Winslow and K.E.K. Ross, 8/16/93, (PB94-154275, A16, MF-A02).
- NCEER-93-0016 "Reconnaissance Report of Damage to Historic Monuments in Cairo, Egypt Following the October 12, 1992 Dahshur Earthquake," by D. Sykora, D. Look, G. Croci, E. Karaesmen and E. Karaesmen, 8/19/93, (PB94-142221, A08, MF-A02).
- NCEER-93-0017 "The Island of Guam Earthquake of August 8, 1993," by S.W. Swan and S.K. Harris, 9/30/93, (PB94-141843, A04, MF-A01).
- NCEER-93-0018 "Engineering Aspects of the October 12, 1992 Egyptian Earthquake," by A.W. Elgamal, M. Amer, K. Adalier and A. Abul-Fadl, 10/7/93, (PB94-141983, A05, MF-A01).
- NCEER-93-0019 "Development of an Earthquake Motion Simulator and its Application in Dynamic Centrifuge Testing," by I. Krstelj, Supervised by J.H. Prevost, 10/23/93, (PB94-181773, A-10, MF-A03).
- NCEER-93-0020 "NCEER-Taisei Corporation Research Program on Sliding Seismic Isolation Systems for Bridges: Experimental and Analytical Study of a Friction Pendulum System (FPS)," by M.C. Constantinou, P. Tsopelas, Y-S. Kim and S. Okamoto, 11/1/93, (PB94-142775, A08, MF-A02).
- NCEER-93-0021 "Finite Element Modeling of Elastomeric Seismic Isolation Bearings," by L.J. Billings, Supervised by R. Shepherd, 11/8/93, to be published.
- NCEER-93-0022 "Seismic Vulnerability of Equipment in Critical Facilities: Life-Safety and Operational Consequences," by K. Porter, G.S. Johnson, M.M. Zadeh, C. Scawthorn and S. Eder, 11/24/93, (PB94-181765, A16, MF-A03).
- NCEER-93-0023 "Hokkaido Nansei-oki, Japan Earthquake of July 12, 1993, by P.I. Yanev and C.R. Scawthorn, 12/23/93, (PB94-181500, A07, MF-A01).
- NCEER-94-0001 "An Evaluation of Seismic Serviceability of Water Supply Networks with Application to the San Francisco Auxiliary Water Supply System," by I. Markov, Supervised by M. Grigoriu and T. O'Rourke, 1/21/94, (PB94-204013, A07, MF-A02).
- NCEER-94-0002 "NCEER-Taisei Corporation Research Program on Sliding Seismic Isolation Systems for Bridges: Experimental and Analytical Study of Systems Consisting of Sliding Bearings, Rubber Restoring Force Devices and Fluid Dampers," Volumes I and II, by P. Tsopelas, S. Okamoto, M.C. Constantinou, D. Ozaki and S. Fujii, 2/4/94, (PB94-181740, A09, MF-A02 and PB94-181757, A12, MF-A03).
- NCEER-94-0003 "A Markov Model for Local and Global Damage Indices in Seismic Analysis," by S. Rahman and M. Grigoriu, 2/18/94, (PB94-206000, A12, MF-A03).
- NCEER-94-0004 "Proceedings from the NCEER Workshop on Seismic Response of Masonry Infills," edited by D.P. Abrams, 3/1/94, (PB94-180783, A07, MF-A02).
- NCEER-94-0005 "The Northridge, California Earthquake of January 17, 1994: General Reconnaissance Report," edited by J.D. Goltz, 3/11/94, (PB94-193943, A10, MF-A03).
- NCEER-94-0006 "Seismic Energy Based Fatigue Damage Analysis of Bridge Columns: Part I - Evaluation of Seismic Capacity," by G.A. Chang and J.B. Mander, 3/14/94, (PB94-219185, A11, MF-A03).
- NCEER-94-0007 "Seismic Isolation of Multi-Story Frame Structures Using Spherical Sliding Isolation Systems," by T.M. Al-Hussaini, V.A. Zayas and M.C. Constantinou, 3/17/94, (PB94-193745, A09, MF-A02).
- NCEER-94-0008 "The Northridge, California Earthquake of January 17, 1994: Performance of Highway Bridges," edited by I.G. Buckle, 3/24/94, (PB94-193851, A06, MF-A02).
- NCEER-94-0009 "Proceedings of the Third U.S.-Japan Workshop on Earthquake Protective Systems for Bridges," edited by I.G. Buckle and I. Friedland, 3/31/94, (PB94-195815, A99, MF-A06).

- NCEER-94-0010 "3D-BASIS-ME: Computer Program for Nonlinear Dynamic Analysis of Seismically Isolated Single and Multiple Structures and Liquid Storage Tanks," by P.C. Tsopelas, M.C. Constantinou and A.M. Reinhorn, 4/12/94, (PB94-204922, A09, MF-A02).
- NCEER-94-0011 "The Northridge, California Earthquake of January 17, 1994: Performance of Gas Transmission Pipelines," by T.D. O'Rourke and M.C. Palmer, 5/16/94, (PB94-204989, A05, MF-A01).
- NCEER-94-0012 "Feasibility Study of Replacement Procedures and Earthquake Performance Related to Gas Transmission Pipelines," by T.D. O'Rourke and M.C. Palmer, 5/25/94, (PB94-206638, A09, MF-A02).
- NCEER-94-0013 "Seismic Energy Based Fatigue Damage Analysis of Bridge Columns: Part II - Evaluation of Seismic Demand," by G.A. Chang and J.B. Mander, 6/1/94, (PB95-18106, A08, MF-A02).
- NCEER-94-0014 "NCEER-Taisei Corporation Research Program on Sliding Seismic Isolation Systems for Bridges: Experimental and Analytical Study of a System Consisting of Sliding Bearings and Fluid Restoring Force/Damping Devices," by P. Tsopelas and M.C. Constantinou, 6/13/94, (PB94-219144, A10, MF-A03).
- NCEER-94-0015 "Generation of Hazard-Consistent Fragility Curves for Seismic Loss Estimation Studies," by H. Hwang and J-R. Huo, 6/14/94, (PB95-181996, A09, MF-A02).
- NCEER-94-0016 "Seismic Study of Building Frames with Added Energy-Absorbing Devices," by W.S. Pong, C.S. Tsai and G.C. Lee, 6/20/94, (PB94-219136, A10, A03).
- NCEER-94-0017 "Sliding Mode Control for Seismic-Excited Linear and Nonlinear Civil Engineering Structures," by J. Yang, J. Wu, A. Agrawal and Z. Li, 6/21/94, (PB95-138483, A06, MF-A02).
- NCEER-94-0018 "3D-BASIS-TABS Version 2.0: Computer Program for Nonlinear Dynamic Analysis of Three Dimensional Base Isolated Structures," by A.M. Reinhorn, S. Nagarajaiah, M.C. Constantinou, P. Tsopelas and R. Li, 6/22/94, (PB95-182176, A08, MF-A02).
- NCEER-94-0019 "Proceedings of the International Workshop on Civil Infrastructure Systems: Application of Intelligent Systems and Advanced Materials on Bridge Systems," Edited by G.C. Lee and K.C. Chang, 7/18/94, (PB95-252474, A20, MF-A04).
- NCEER-94-0020 "Study of Seismic Isolation Systems for Computer Floors," by V. Lambrou and M.C. Constantinou, 7/19/94, (PB95-138533, A10, MF-A03).
- NCEER-94-0021 "Proceedings of the U.S.-Italian Workshop on Guidelines for Seismic Evaluation and Rehabilitation of Unreinforced Masonry Buildings," Edited by D.P. Abrams and G.M. Calvi, 7/20/94, (PB95-138749, A13, MF-A03).
- NCEER-94-0022 "NCEER-Taisei Corporation Research Program on Sliding Seismic Isolation Systems for Bridges: Experimental and Analytical Study of a System Consisting of Lubricated PTFE Sliding Bearings and Mild Steel Dampers," by P. Tsopelas and M.C. Constantinou, 7/22/94, (PB95-182184, A08, MF-A02).
- NCEER-94-0023 "Development of Reliability-Based Design Criteria for Buildings Under Seismic Load," by Y.K. Wen, H. Hwang and M. Shinozuka, 8/1/94, (PB95-211934, A08, MF-A02).
- NCEER-94-0024 "Experimental Verification of Acceleration Feedback Control Strategies for an Active Tendon System," by S.J. Dyke, B.F. Spencer, Jr., P. Quast, M.K. Sain, D.C. Kaspari, Jr. and T.T. Soong, 8/29/94, (PB95-212320, A05, MF-A01).
- NCEER-94-0025 "Seismic Retrofitting Manual for Highway Bridges," Edited by I.G. Buckle and I.F. Friedland, published by the Federal Highway Administration (PB95-212676, A15, MF-A03).
- NCEER-94-0026 "Proceedings from the Fifth U.S.-Japan Workshop on Earthquake Resistant Design of Lifeline Facilities and Countermeasures Against Soil Liquefaction," Edited by T.D. O'Rourke and M. Hamada, 11/7/94, (PB95-220802, A99, MF-E08).

- NCEER-95-0001 “Experimental and Analytical Investigation of Seismic Retrofit of Structures with Supplemental Damping: Part 1 - Fluid Viscous Damping Devices,” by A.M. Reinhorn, C. Li and M.C. Constantinou, 1/3/95, (PB95-266599, A09, MF-A02).
- NCEER-95-0002 “Experimental and Analytical Study of Low-Cycle Fatigue Behavior of Semi-Rigid Top-And-Seat Angle Connections,” by G. Pekcan, J.B. Mander and S.S. Chen, 1/5/95, (PB95-220042, A07, MF-A02).
- NCEER-95-0003 “NCEER-ATC Joint Study on Fragility of Buildings,” by T. Anagnos, C. Rojahn and A.S. Kiremidjian, 1/20/95, (PB95-220026, A06, MF-A02).
- NCEER-95-0004 “Nonlinear Control Algorithms for Peak Response Reduction,” by Z. Wu, T.T. Soong, V. Gattulli and R.C. Lin, 2/16/95, (PB95-220349, A05, MF-A01).
- NCEER-95-0005 “Pipeline Replacement Feasibility Study: A Methodology for Minimizing Seismic and Corrosion Risks to Underground Natural Gas Pipelines,” by R.T. Eguchi, H.A. Seligson and D.G. Honegger, 3/2/95, (PB95-252326, A06, MF-A02).
- NCEER-95-0006 “Evaluation of Seismic Performance of an 11-Story Frame Building During the 1994 Northridge Earthquake,” by F. Naeim, R. DiSulio, K. Benuska, A. Reinhorn and C. Li, to be published.
- NCEER-95-0007 “Prioritization of Bridges for Seismic Retrofitting,” by N. Basöz and A.S. Kiremidjian, 4/24/95, (PB95-252300, A08, MF-A02).
- NCEER-95-0008 “Method for Developing Motion Damage Relationships for Reinforced Concrete Frames,” by A. Singhal and A.S. Kiremidjian, 5/11/95, (PB95-266607, A06, MF-A02).
- NCEER-95-0009 “Experimental and Analytical Investigation of Seismic Retrofit of Structures with Supplemental Damping: Part II - Friction Devices,” by C. Li and A.M. Reinhorn, 7/6/95, (PB96-128087, A11, MF-A03).
- NCEER-95-0010 “Experimental Performance and Analytical Study of a Non-Ductile Reinforced Concrete Frame Structure Retrofitted with Elastomeric Spring Dampers,” by G. Pekcan, J.B. Mander and S.S. Chen, 7/14/95, (PB96-137161, A08, MF-A02).
- NCEER-95-0011 “Development and Experimental Study of Semi-Active Fluid Damping Devices for Seismic Protection of Structures,” by M.D. Symans and M.C. Constantinou, 8/3/95, (PB96-136940, A23, MF-A04).
- NCEER-95-0012 “Real-Time Structural Parameter Modification (RSPM): Development of Innervated Structures,” by Z. Liang, M. Tong and G.C. Lee, 4/11/95, (PB96-137153, A06, MF-A01).
- NCEER-95-0013 “Experimental and Analytical Investigation of Seismic Retrofit of Structures with Supplemental Damping: Part III - Viscous Damping Walls,” by A.M. Reinhorn and C. Li, 10/1/95, (PB96-176409, A11, MF-A03).
- NCEER-95-0014 “Seismic Fragility Analysis of Equipment and Structures in a Memphis Electric Substation,” by J-R. Huo and H.H.M. Hwang, 8/10/95, (PB96-128087, A09, MF-A02).
- NCEER-95-0015 “The Hanshin-Awaji Earthquake of January 17, 1995: Performance of Lifelines,” Edited by M. Shinozuka, 11/3/95, (PB96-176383, A15, MF-A03).
- NCEER-95-0016 “Highway Culvert Performance During Earthquakes,” by T.L. Youd and C.J. Beckman, available as NCEER-96-0015.
- NCEER-95-0017 “The Hanshin-Awaji Earthquake of January 17, 1995: Performance of Highway Bridges,” Edited by I.G. Buckle, 12/1/95, to be published.
- NCEER-95-0018 “Modeling of Masonry Infill Panels for Structural Analysis,” by A.M. Reinhorn, A. Madan, R.E. Valles, Y. Reichmann and J.B. Mander, 12/8/95, (PB97-110886, MF-A01, A06).
- NCEER-95-0019 “Optimal Polynomial Control for Linear and Nonlinear Structures,” by A.K. Agrawal and J.N. Yang, 12/11/95, (PB96-168737, A07, MF-A02).

- NCEER-95-0020 "Retrofit of Non-Ductile Reinforced Concrete Frames Using Friction Dampers," by R.S. Rao, P. Gergely and R.N. White, 12/22/95, (PB97-133508, A10, MF-A02).
- NCEER-95-0021 "Parametric Results for Seismic Response of Pile-Supported Bridge Bents," by G. Mylonakis, A. Nikolaou and G. Gazetas, 12/22/95, (PB97-100242, A12, MF-A03).
- NCEER-95-0022 "Kinematic Bending Moments in Seismically Stressed Piles," by A. Nikolaou, G. Mylonakis and G. Gazetas, 12/23/95, (PB97-113914, MF-A03, A13).
- NCEER-96-0001 "Dynamic Response of Unreinforced Masonry Buildings with Flexible Diaphragms," by A.C. Costley and D.P. Abrams, 10/10/96, (PB97-133573, MF-A03, A15).
- NCEER-96-0002 "State of the Art Review: Foundations and Retaining Structures," by I. Po Lam, to be published.
- NCEER-96-0003 "Ductility of Rectangular Reinforced Concrete Bridge Columns with Moderate Confinement," by N. Wehbe, M. Saiidi, D. Sanders and B. Douglas, 11/7/96, (PB97-133557, A06, MF-A02).
- NCEER-96-0004 "Proceedings of the Long-Span Bridge Seismic Research Workshop," edited by I.G. Buckle and I.M. Friedland, to be published.
- NCEER-96-0005 "Establish Representative Pier Types for Comprehensive Study: Eastern United States," by J. Kulicki and Z. Prucz, 5/28/96, (PB98-119217, A07, MF-A02).
- NCEER-96-0006 "Establish Representative Pier Types for Comprehensive Study: Western United States," by R. Imbsen, R.A. Schamber and T.A. Osterkamp, 5/28/96, (PB98-118607, A07, MF-A02).
- NCEER-96-0007 "Nonlinear Control Techniques for Dynamical Systems with Uncertain Parameters," by R.G. Ghanem and M.I. Bujakov, 5/27/96, (PB97-100259, A17, MF-A03).
- NCEER-96-0008 "Seismic Evaluation of a 30-Year Old Non-Ductile Highway Bridge Pier and Its Retrofit," by J.B. Mander, B. Mahmoodzadegan, S. Bhadra and S.S. Chen, 5/31/96, (PB97-110902, MF-A03, A10).
- NCEER-96-0009 "Seismic Performance of a Model Reinforced Concrete Bridge Pier Before and After Retrofit," by J.B. Mander, J.H. Kim and C.A. Ligozio, 5/31/96, (PB97-110910, MF-A02, A10).
- NCEER-96-0010 "IDARC2D Version 4.0: A Computer Program for the Inelastic Damage Analysis of Buildings," by R.E. Valles, A.M. Reinhorn, S.K. Kunnath, C. Li and A. Madan, 6/3/96, (PB97-100234, A17, MF-A03).
- NCEER-96-0011 "Estimation of the Economic Impact of Multiple Lifeline Disruption: Memphis Light, Gas and Water Division Case Study," by S.E. Chang, H.A. Seligson and R.T. Eguchi, 8/16/96, (PB97-133490, A11, MF-A03).
- NCEER-96-0012 "Proceedings from the Sixth Japan-U.S. Workshop on Earthquake Resistant Design of Lifeline Facilities and Countermeasures Against Soil Liquefaction, Edited by M. Hamada and T. O'Rourke, 9/11/96, (PB97-133581, A99, MF-A06).
- NCEER-96-0013 "Chemical Hazards, Mitigation and Preparedness in Areas of High Seismic Risk: A Methodology for Estimating the Risk of Post-Earthquake Hazardous Materials Release," by H.A. Seligson, R.T. Eguchi, K.J. Tierney and K. Richmond, 11/7/96, (PB97-133565, MF-A02, A08).
- NCEER-96-0014 "Response of Steel Bridge Bearings to Reversed Cyclic Loading," by J.B. Mander, D-K. Kim, S.S. Chen and G.J. Premus, 11/13/96, (PB97-140735, A12, MF-A03).
- NCEER-96-0015 "Highway Culvert Performance During Past Earthquakes," by T.L. Youd and C.J. Beckman, 11/25/96, (PB97-133532, A06, MF-A01).
- NCEER-97-0001 "Evaluation, Prevention and Mitigation of Pounding Effects in Building Structures," by R.E. Valles and A.M. Reinhorn, 2/20/97, (PB97-159552, A14, MF-A03).
- NCEER-97-0002 "Seismic Design Criteria for Bridges and Other Highway Structures," by C. Rojahn, R. Mayes, D.G. Anderson, J. Clark, J.H. Hom, R.V. Nutt and M.J. O'Rourke, 4/30/97, (PB97-194658, A06, MF-A03).

- NCEER-97-0003 "Proceedings of the U.S.-Italian Workshop on Seismic Evaluation and Retrofit," Edited by D.P. Abrams and G.M. Calvi, 3/19/97, (PB97-194666, A13, MF-A03).
- NCEER-97-0004 "Investigation of Seismic Response of Buildings with Linear and Nonlinear Fluid Viscous Dampers," by A.A. Seleemah and M.C. Constantinou, 5/21/97, (PB98-109002, A15, MF-A03).
- NCEER-97-0005 "Proceedings of the Workshop on Earthquake Engineering Frontiers in Transportation Facilities," edited by G.C. Lee and I.M. Friedland, 8/29/97, (PB98-128911, A25, MR-A04).
- NCEER-97-0006 "Cumulative Seismic Damage of Reinforced Concrete Bridge Piers," by S.K. Kunnath, A. El-Bahy, A. Taylor and W. Stone, 9/2/97, (PB98-108814, A11, MF-A03).
- NCEER-97-0007 "Structural Details to Accommodate Seismic Movements of Highway Bridges and Retaining Walls," by R.A. Imbsen, R.A. Schamber, E. Thorkildsen, A. Kartoum, B.T. Martin, T.N. Rosser and J.M. Kulicki, 9/3/97, (PB98-108996, A09, MF-A02).
- NCEER-97-0008 "A Method for Earthquake Motion-Damage Relationships with Application to Reinforced Concrete Frames," by A. Singhal and A.S. Kiremidjian, 9/10/97, (PB98-108988, A13, MF-A03).
- NCEER-97-0009 "Seismic Analysis and Design of Bridge Abutments Considering Sliding and Rotation," by K. Fishman and R. Richards, Jr., 9/15/97, (PB98-108897, A06, MF-A02).
- NCEER-97-0010 "Proceedings of the FHWA/NCEER Workshop on the National Representation of Seismic Ground Motion for New and Existing Highway Facilities," edited by I.M. Friedland, M.S. Power and R.L. Mayes, 9/22/97, (PB98-128903, A21, MF-A04).
- NCEER-97-0011 "Seismic Analysis for Design or Retrofit of Gravity Bridge Abutments," by K.L. Fishman, R. Richards, Jr. and R.C. Divito, 10/2/97, (PB98-128937, A08, MF-A02).
- NCEER-97-0012 "Evaluation of Simplified Methods of Analysis for Yielding Structures," by P. Tsopelas, M.C. Constantinou, C.A. Kircher and A.S. Whittaker, 10/31/97, (PB98-128929, A10, MF-A03).
- NCEER-97-0013 "Seismic Design of Bridge Columns Based on Control and Repairability of Damage," by C-T. Cheng and J.B. Mander, 12/8/97, (PB98-144249, A11, MF-A03).
- NCEER-97-0014 "Seismic Resistance of Bridge Piers Based on Damage Avoidance Design," by J.B. Mander and C-T. Cheng, 12/10/97, (PB98-144223, A09, MF-A02).
- NCEER-97-0015 "Seismic Response of Nominally Symmetric Systems with Strength Uncertainty," by S. Balopoulou and M. Grigoriu, 12/23/97, (PB98-153422, A11, MF-A03).
- NCEER-97-0016 "Evaluation of Seismic Retrofit Methods for Reinforced Concrete Bridge Columns," by T.J. Wipf, F.W. Klaiber and F.M. Russo, 12/28/97, (PB98-144215, A12, MF-A03).
- NCEER-97-0017 "Seismic Fragility of Existing Conventional Reinforced Concrete Highway Bridges," by C.L. Mullen and A.S. Cakmak, 12/30/97, (PB98-153406, A08, MF-A02).
- NCEER-97-0018 "Loss Assessment of Memphis Buildings," edited by D.P. Abrams and M. Shinozuka, 12/31/97, (PB98-144231, A13, MF-A03).
- NCEER-97-0019 "Seismic Evaluation of Frames with Infill Walls Using Quasi-static Experiments," by K.M. Mosalam, R.N. White and P. Gergely, 12/31/97, (PB98-153455, A07, MF-A02).
- NCEER-97-0020 "Seismic Evaluation of Frames with Infill Walls Using Pseudo-dynamic Experiments," by K.M. Mosalam, R.N. White and P. Gergely, 12/31/97, (PB98-153430, A07, MF-A02).
- NCEER-97-0021 "Computational Strategies for Frames with Infill Walls: Discrete and Smeared Crack Analyses and Seismic Fragility," by K.M. Mosalam, R.N. White and P. Gergely, 12/31/97, (PB98-153414, A10, MF-A02).

- NCEER-97-0022 "Proceedings of the NCEER Workshop on Evaluation of Liquefaction Resistance of Soils," edited by T.L. Youd and I.M. Idriss, 12/31/97, (PB98-155617, A15, MF-A03).
- MCEER-98-0001 "Extraction of Nonlinear Hysteretic Properties of Seismically Isolated Bridges from Quick-Release Field Tests," by Q. Chen, B.M. Douglas, E.M. Maragakis and I.G. Buckle, 5/26/98, (PB99-118838, A06, MF-A01).
- MCEER-98-0002 "Methodologies for Evaluating the Importance of Highway Bridges," by A. Thomas, S. Eshenaur and J. Kulicki, 5/29/98, (PB99-118846, A10, MF-A02).
- MCEER-98-0003 "Capacity Design of Bridge Piers and the Analysis of Overstrength," by J.B. Mander, A. Dutta and P. Goel, 6/1/98, (PB99-118853, A09, MF-A02).
- MCEER-98-0004 "Evaluation of Bridge Damage Data from the Loma Prieta and Northridge, California Earthquakes," by N. Basoz and A. Kiremidjian, 6/2/98, (PB99-118861, A15, MF-A03).
- MCEER-98-0005 "Screening Guide for Rapid Assessment of Liquefaction Hazard at Highway Bridge Sites," by T. L. Youd, 6/16/98, (PB99-118879, A06, not available on microfiche).
- MCEER-98-0006 "Structural Steel and Steel/Concrete Interface Details for Bridges," by P. Ritchie, N. Kaulh and J. Kulicki, 7/13/98, (PB99-118945, A06, MF-A01).
- MCEER-98-0007 "Capacity Design and Fatigue Analysis of Confined Concrete Columns," by A. Dutta and J.B. Mander, 7/14/98, (PB99-118960, A14, MF-A03).
- MCEER-98-0008 "Proceedings of the Workshop on Performance Criteria for Telecommunication Services Under Earthquake Conditions," edited by A.J. Schiff, 7/15/98, (PB99-118952, A08, MF-A02).
- MCEER-98-0009 "Fatigue Analysis of Unconfined Concrete Columns," by J.B. Mander, A. Dutta and J.H. Kim, 9/12/98, (PB99-123655, A10, MF-A02).
- MCEER-98-0010 "Centrifuge Modeling of Cyclic Lateral Response of Pile-Cap Systems and Seat-Type Abutments in Dry Sands," by A.D. Gadre and R. Dobry, 10/2/98, (PB99-123606, A13, MF-A03).
- MCEER-98-0011 "IDARC-BRIDGE: A Computational Platform for Seismic Damage Assessment of Bridge Structures," by A.M. Reinhorn, V. Simeonov, G. Mylonakis and Y. Reichman, 10/2/98, (PB99-162919, A15, MF-A03).
- MCEER-98-0012 "Experimental Investigation of the Dynamic Response of Two Bridges Before and After Retrofitting with Elastomeric Bearings," by D.A. Wendichansky, S.S. Chen and J.B. Mander, 10/2/98, (PB99-162927, A15, MF-A03).
- MCEER-98-0013 "Design Procedures for Hinge Restrainers and Hinge Sear Width for Multiple-Frame Bridges," by R. Des Roches and G.L. Fenves, 11/3/98, (PB99-140477, A13, MF-A03).
- MCEER-98-0014 "Response Modification Factors for Seismically Isolated Bridges," by M.C. Constantinou and J.K. Quarshie, 11/3/98, (PB99-140485, A14, MF-A03).
- MCEER-98-0015 "Proceedings of the U.S.-Italy Workshop on Seismic Protective Systems for Bridges," edited by I.M. Friedland and M.C. Constantinou, 11/3/98, (PB2000-101711, A22, MF-A04).
- MCEER-98-0016 "Appropriate Seismic Reliability for Critical Equipment Systems: Recommendations Based on Regional Analysis of Financial and Life Loss," by K. Porter, C. Scawthorn, C. Taylor and N. Blais, 11/10/98, (PB99-157265, A08, MF-A02).
- MCEER-98-0017 "Proceedings of the U.S. Japan Joint Seminar on Civil Infrastructure Systems Research," edited by M. Shinozuka and A. Rose, 11/12/98, (PB99-156713, A16, MF-A03).
- MCEER-98-0018 "Modeling of Pile Footings and Drilled Shafts for Seismic Design," by I. PoLam, M. Kapuskar and D. Chaudhuri, 12/21/98, (PB99-157257, A09, MF-A02).

- MCEER-99-0001 "Seismic Evaluation of a Masonry Infilled Reinforced Concrete Frame by Pseudodynamic Testing," by S.G. Buonopane and R.N. White, 2/16/99, (PB99-162851, A09, MF-A02).
- MCEER-99-0002 "Response History Analysis of Structures with Seismic Isolation and Energy Dissipation Systems: Verification Examples for Program SAP2000," by J. Scheller and M.C. Constantinou, 2/22/99, (PB99-162869, A08, MF-A02).
- MCEER-99-0003 "Experimental Study on the Seismic Design and Retrofit of Bridge Columns Including Axial Load Effects," by A. Dutta, T. Kokorina and J.B. Mander, 2/22/99, (PB99-162877, A09, MF-A02).
- MCEER-99-0004 "Experimental Study of Bridge Elastomeric and Other Isolation and Energy Dissipation Systems with Emphasis on Uplift Prevention and High Velocity Near-source Seismic Excitation," by A. Kasalanati and M. C. Constantinou, 2/26/99, (PB99-162885, A12, MF-A03).
- MCEER-99-0005 "Truss Modeling of Reinforced Concrete Shear-flexure Behavior," by J.H. Kim and J.B. Mander, 3/8/99, (PB99-163693, A12, MF-A03).
- MCEER-99-0006 "Experimental Investigation and Computational Modeling of Seismic Response of a 1:4 Scale Model Steel Structure with a Load Balancing Supplemental Damping System," by G. Pekcan, J.B. Mander and S.S. Chen, 4/2/99, (PB99-162893, A11, MF-A03).
- MCEER-99-0007 "Effect of Vertical Ground Motions on the Structural Response of Highway Bridges," by M.R. Button, C.J. Cronin and R.L. Mayes, 4/10/99, (PB2000-101411, A10, MF-A03).
- MCEER-99-0008 "Seismic Reliability Assessment of Critical Facilities: A Handbook, Supporting Documentation, and Model Code Provisions," by G.S. Johnson, R.E. Sheppard, M.D. Quilici, S.J. Eder and C.R. Scawthorn, 4/12/99, (PB2000-101701, A18, MF-A04).
- MCEER-99-0009 "Impact Assessment of Selected MCEER Highway Project Research on the Seismic Design of Highway Structures," by C. Rojahn, R. Mayes, D.G. Anderson, J.H. Clark, D'Appolonia Engineering, S. Gloyd and R.V. Nutt, 4/14/99, (PB99-162901, A10, MF-A02).
- MCEER-99-0010 "Site Factors and Site Categories in Seismic Codes," by R. Dobry, R. Ramos and M.S. Power, 7/19/99, (PB2000-101705, A08, MF-A02).
- MCEER-99-0011 "Restrainer Design Procedures for Multi-Span Simply-Supported Bridges," by M.J. Randall, M. Saiidi, E. Maragakis and T. Isakovic, 7/20/99, (PB2000-101702, A10, MF-A02).
- MCEER-99-0012 "Property Modification Factors for Seismic Isolation Bearings," by M.C. Constantinou, P. Tsopelas, A. Kasalanati and E. Wolff, 7/20/99, (PB2000-103387, A11, MF-A03).
- MCEER-99-0013 "Critical Seismic Issues for Existing Steel Bridges," by P. Ritchie, N. Kauh and J. Kulicki, 7/20/99, (PB2000-101697, A09, MF-A02).
- MCEER-99-0014 "Nonstructural Damage Database," by A. Kao, T.T. Soong and A. Vender, 7/24/99, (PB2000-101407, A06, MF-A01).
- MCEER-99-0015 "Guide to Remedial Measures for Liquefaction Mitigation at Existing Highway Bridge Sites," by H.G. Cooke and J. K. Mitchell, 7/26/99, (PB2000-101703, A11, MF-A03).
- MCEER-99-0016 "Proceedings of the MCEER Workshop on Ground Motion Methodologies for the Eastern United States," edited by N. Abrahamson and A. Becker, 8/11/99, (PB2000-103385, A07, MF-A02).
- MCEER-99-0017 "Quindío, Colombia Earthquake of January 25, 1999: Reconnaissance Report," by A.P. Asfura and P.J. Flores, 10/4/99, (PB2000-106893, A06, MF-A01).
- MCEER-99-0018 "Hysteretic Models for Cyclic Behavior of Deteriorating Inelastic Structures," by M.V. Sivaselvan and A.M. Reinhorn, 11/5/99, (PB2000-103386, A08, MF-A02).

- MCEER-99-0019 "Proceedings of the 7th U.S.- Japan Workshop on Earthquake Resistant Design of Lifeline Facilities and Countermeasures Against Soil Liquefaction," edited by T.D. O'Rourke, J.P. Bardet and M. Hamada, 11/19/99, (PB2000-103354, A99, MF-A06).
- MCEER-99-0020 "Development of Measurement Capability for Micro-Vibration Evaluations with Application to Chip Fabrication Facilities," by G.C. Lee, Z. Liang, J.W. Song, J.D. Shen and W.C. Liu, 12/1/99, (PB2000-105993, A08, MF-A02).
- MCEER-99-0021 "Design and Retrofit Methodology for Building Structures with Supplemental Energy Dissipating Systems," by G. Pekcan, J.B. Mander and S.S. Chen, 12/31/99, (PB2000-105994, A11, MF-A03).
- MCEER-00-0001 "The Marmara, Turkey Earthquake of August 17, 1999: Reconnaissance Report," edited by C. Scawthorn; with major contributions by M. Bruneau, R. Eguchi, T. Holzer, G. Johnson, J. Mander, J. Mitchell, W. Mitchell, A. Papageorgiou, C. Scaethorn, and G. Webb, 3/23/00, (PB2000-106200, A11, MF-A03).
- MCEER-00-0002 "Proceedings of the MCEER Workshop for Seismic Hazard Mitigation of Health Care Facilities," edited by G.C. Lee, M. Ettouney, M. Grigoriu, J. Hauer and J. Nigg, 3/29/00, (PB2000-106892, A08, MF-A02).
- MCEER-00-0003 "The Chi-Chi, Taiwan Earthquake of September 21, 1999: Reconnaissance Report," edited by G.C. Lee and C.H. Loh, with major contributions by G.C. Lee, M. Bruneau, I.G. Buckle, S.E. Chang, P.J. Flores, T.D. O'Rourke, M. Shinozuka, T.T. Soong, C-H. Loh, K-C. Chang, Z-J. Chen, J-S. Hwang, M-L. Lin, G-Y. Liu, K-C. Tsai, G.C. Yao and C-L. Yen, 4/30/00, (PB2001-100980, A10, MF-A02).
- MCEER-00-0004 "Seismic Retrofit of End-Sway Frames of Steel Deck-Truss Bridges with a Supplemental Tendon System: Experimental and Analytical Investigation," by G. Pekcan, J.B. Mander and S.S. Chen, 7/1/00, (PB2001-100982, A10, MF-A02).
- MCEER-00-0005 "Sliding Fragility of Unrestrained Equipment in Critical Facilities," by W.H. Chong and T.T. Soong, 7/5/00, (PB2001-100983, A08, MF-A02).
- MCEER-00-0006 "Seismic Response of Reinforced Concrete Bridge Pier Walls in the Weak Direction," by N. Abo-Shadi, M. Saiidi and D. Sanders, 7/17/00, (PB2001-100981, A17, MF-A03).
- MCEER-00-0007 "Low-Cycle Fatigue Behavior of Longitudinal Reinforcement in Reinforced Concrete Bridge Columns," by J. Brown and S.K. Kunnath, 7/23/00, (PB2001-104392, A08, MF-A02).
- MCEER-00-0008 "Soil Structure Interaction of Bridges for Seismic Analysis," I. PoLam and H. Law, 9/25/00, (PB2001-105397, A08, MF-A02).
- MCEER-00-0009 "Proceedings of the First MCEER Workshop on Mitigation of Earthquake Disaster by Advanced Technologies (MEDAT-1), edited by M. Shinozuka, D.J. Inman and T.D. O'Rourke, 11/10/00, (PB2001-105399, A14, MF-A03).
- MCEER-00-0010 "Development and Evaluation of Simplified Procedures for Analysis and Design of Buildings with Passive Energy Dissipation Systems, Revision 01," by O.M. Ramirez, M.C. Constantinou, C.A. Kircher, A.S. Whittaker, M.W. Johnson, J.D. Gomez and C. Chrysostomou, 11/16/01, (PB2001-105523, A23, MF-A04).
- MCEER-00-0011 "Dynamic Soil-Foundation-Structure Interaction Analyses of Large Caissons," by C-Y. Chang, C-M. Mok, Z-L. Wang, R. Settgast, F. Waggoner, M.A. Ketchum, H.M. Gonnermann and C-C. Chin, 12/30/00, (PB2001-104373, A07, MF-A02).
- MCEER-00-0012 "Experimental Evaluation of Seismic Performance of Bridge Restrainers," by A.G. Vlassis, E.M. Maragakis and M. Saiid Saiidi, 12/30/00, (PB2001-104354, A09, MF-A02).
- MCEER-00-0013 "Effect of Spatial Variation of Ground Motion on Highway Structures," by M. Shinozuka, V. Saxena and G. Deodatis, 12/31/00, (PB2001-108755, A13, MF-A03).
- MCEER-00-0014 "A Risk-Based Methodology for Assessing the Seismic Performance of Highway Systems," by S.D. Werner, C.E. Taylor, J.E. Moore, II, J.S. Walton and S. Cho, 12/31/00, (PB2001-108756, A14, MF-A03).

- MCEER-01-0001 “Experimental Investigation of P-Delta Effects to Collapse During Earthquakes,” by D. Vian and M. Bruneau, 6/25/01, (PB2002-100534, A17, MF-A03).
- MCEER-01-0002 “Proceedings of the Second MCEER Workshop on Mitigation of Earthquake Disaster by Advanced Technologies (MEDAT-2),” edited by M. Bruneau and D.J. Inman, 7/23/01, (PB2002-100434, A16, MF-A03).
- MCEER-01-0003 “Sensitivity Analysis of Dynamic Systems Subjected to Seismic Loads,” by C. Roth and M. Grigoriu, 9/18/01, (PB2003-100884, A12, MF-A03).
- MCEER-01-0004 “Overcoming Obstacles to Implementing Earthquake Hazard Mitigation Policies: Stage 1 Report,” by D.J. Alesch and W.J. Petak, 12/17/01, (PB2002-107949, A07, MF-A02).
- MCEER-01-0005 “Updating Real-Time Earthquake Loss Estimates: Methods, Problems and Insights,” by C.E. Taylor, S.E. Chang and R.T. Eguchi, 12/17/01, (PB2002-107948, A05, MF-A01).
- MCEER-01-0006 “Experimental Investigation and Retrofit of Steel Pile Foundations and Pile Bents Under Cyclic Lateral Loadings,” by A. Shama, J. Mander, B. Blabac and S. Chen, 12/31/01, (PB2002-107950, A13, MF-A03).
- MCEER-02-0001 “Assessment of Performance of Bolu Viaduct in the 1999 Duzce Earthquake in Turkey” by P.C. Roussis, M.C. Constantinou, M. Erdik, E. Durukal and M. Dicleli, 5/8/02, (PB2003-100883, A08, MF-A02).
- MCEER-02-0002 “Seismic Behavior of Rail Counterweight Systems of Elevators in Buildings,” by M.P. Singh, Rildova and L.E. Suarez, 5/27/02. (PB2003-100882, A11, MF-A03).
- MCEER-02-0003 “Development of Analysis and Design Procedures for Spread Footings,” by G. Mylonakis, G. Gazetas, S. Nikolaou and A. Chauncey, 10/02/02, (PB2004-101636, A13, MF-A03, CD-A13).
- MCEER-02-0004 “Bare-Earth Algorithms for Use with SAR and LIDAR Digital Elevation Models,” by C.K. Huyck, R.T. Eguchi and B. Houshmand, 10/16/02, (PB2004-101637, A07, CD-A07).
- MCEER-02-0005 “Review of Energy Dissipation of Compression Members in Concentrically Braced Frames,” by K.Lee and M. Bruneau, 10/18/02, (PB2004-101638, A10, CD-A10).
- MCEER-03-0001 “Experimental Investigation of Light-Gauge Steel Plate Shear Walls for the Seismic Retrofit of Buildings” by J. Berman and M. Bruneau, 5/2/03, (PB2004-101622, A10, MF-A03, CD-A10).
- MCEER-03-0002 “Statistical Analysis of Fragility Curves,” by M. Shinozuka, M.Q. Feng, H. Kim, T. Uzawa and T. Ueda, 6/16/03, (PB2004-101849, A09, CD-A09).
- MCEER-03-0003 “Proceedings of the Eighth U.S.-Japan Workshop on Earthquake Resistant Design of Lifeline Facilities and Countermeasures Against Liquefaction,” edited by M. Hamada, J.P. Bardet and T.D. O’Rourke, 6/30/03, (PB2004-104386, A99, CD-A99).
- MCEER-03-0004 “Proceedings of the PRC-US Workshop on Seismic Analysis and Design of Special Bridges,” edited by L.C. Fan and G.C. Lee, 7/15/03, (PB2004-104387, A14, CD-A14).
- MCEER-03-0005 “Urban Disaster Recovery: A Framework and Simulation Model,” by S.B. Miles and S.E. Chang, 7/25/03, (PB2004-104388, A07, CD-A07).
- MCEER-03-0006 “Behavior of Underground Piping Joints Due to Static and Dynamic Loading,” by R.D. Meis, M. Maragakis and R. Siddharthan, 11/17/03, (PB2005-102194, A13, MF-A03, CD-A00).
- MCEER-04-0001 “Experimental Study of Seismic Isolation Systems with Emphasis on Secondary System Response and Verification of Accuracy of Dynamic Response History Analysis Methods,” by E. Wolff and M. Constantinou, 1/16/04 (PB2005-102195, A99, MF-E08, CD-A00).
- MCEER-04-0002 “Tension, Compression and Cyclic Testing of Engineered Cementitious Composite Materials,” by K. Kesner and S.L. Billington, 3/1/04, (PB2005-102196, A08, CD-A08).

- MCEER-04-0003 "Cyclic Testing of Braces Laterally Restrained by Steel Studs to Enhance Performance During Earthquakes," by O.C. Celik, J.W. Berman and M. Bruneau, 3/16/04, (PB2005-102197, A13, MF-A03, CD-A00).
- MCEER-04-0004 "Methodologies for Post Earthquake Building Damage Detection Using SAR and Optical Remote Sensing: Application to the August 17, 1999 Marmara, Turkey Earthquake," by C.K. Huyck, B.J. Adams, S. Cho, R.T. Eguchi, B. Mansouri and B. Houshmand, 6/15/04, (PB2005-104888, A10, CD-A00).
- MCEER-04-0005 "Nonlinear Structural Analysis Towards Collapse Simulation: A Dynamical Systems Approach," by M.V. Sivaselvan and A.M. Reinhorn, 6/16/04, (PB2005-104889, A11, MF-A03, CD-A00).
- MCEER-04-0006 "Proceedings of the Second PRC-US Workshop on Seismic Analysis and Design of Special Bridges," edited by G.C. Lee and L.C. Fan, 6/25/04, (PB2005-104890, A16, CD-A00).
- MCEER-04-0007 "Seismic Vulnerability Evaluation of Axially Loaded Steel Built-up Laced Members," by K. Lee and M. Bruneau, 6/30/04, (PB2005-104891, A16, CD-A00).
- MCEER-04-0008 "Evaluation of Accuracy of Simplified Methods of Analysis and Design of Buildings with Damping Systems for Near-Fault and for Soft-Soil Seismic Motions," by E.A. Pavlou and M.C. Constantinou, 8/16/04, (PB2005-104892, A08, MF-A02, CD-A00).
- MCEER-04-0009 "Assessment of Geotechnical Issues in Acute Care Facilities in California," by M. Lew, T.D. O'Rourke, R. Dobry and M. Koch, 9/15/04, (PB2005-104893, A08, CD-A00).
- MCEER-04-0010 "Scissor-Jack-Damper Energy Dissipation System," by A.N. Sigaher-Boyle and M.C. Constantinou, 12/1/04 (PB2005-108221).
- MCEER-04-0011 "Seismic Retrofit of Bridge Steel Truss Piers Using a Controlled Rocking Approach," by M. Pollino and M. Bruneau, 12/20/04 (PB2006-105795).
- MCEER-05-0001 "Experimental and Analytical Studies of Structures Seismically Isolated with an Uplift-Restraint Isolation System," by P.C. Roussis and M.C. Constantinou, 1/10/05 (PB2005-108222).
- MCEER-05-0002 "A Versatile Experimentation Model for Study of Structures Near Collapse Applied to Seismic Evaluation of Irregular Structures," by D. Kusumastuti, A.M. Reinhorn and A. Rutenberg, 3/31/05 (PB2006-101523).
- MCEER-05-0003 "Proceedings of the Third PRC-US Workshop on Seismic Analysis and Design of Special Bridges," edited by L.C. Fan and G.C. Lee, 4/20/05, (PB2006-105796).
- MCEER-05-0004 "Approaches for the Seismic Retrofit of Braced Steel Bridge Piers and Proof-of-Concept Testing of an Eccentrically Braced Frame with Tubular Link," by J.W. Berman and M. Bruneau, 4/21/05 (PB2006-101524).
- MCEER-05-0005 "Simulation of Strong Ground Motions for Seismic Fragility Evaluation of Nonstructural Components in Hospitals," by A. Wanitkorkul and A. Filiatrault, 5/26/05 (PB2006-500027).
- MCEER-05-0006 "Seismic Safety in California Hospitals: Assessing an Attempt to Accelerate the Replacement or Seismic Retrofit of Older Hospital Facilities," by D.J. Alesch, L.A. Arendt and W.J. Petak, 6/6/05 (PB2006-105794).
- MCEER-05-0007 "Development of Seismic Strengthening and Retrofit Strategies for Critical Facilities Using Engineered Cementitious Composite Materials," by K. Kesner and S.L. Billington, 8/29/05 (PB2006-111701).
- MCEER-05-0008 "Experimental and Analytical Studies of Base Isolation Systems for Seismic Protection of Power Transformers," by N. Murota, M.Q. Feng and G-Y. Liu, 9/30/05 (PB2006-111702).
- MCEER-05-0009 "3D-BASIS-ME-MB: Computer Program for Nonlinear Dynamic Analysis of Seismically Isolated Structures," by P.C. Tsopelas, P.C. Roussis, M.C. Constantinou, R. Buchanan and A.M. Reinhorn, 10/3/05 (PB2006-111703).
- MCEER-05-0010 "Steel Plate Shear Walls for Seismic Design and Retrofit of Building Structures," by D. Vian and M. Bruneau, 12/15/05 (PB2006-111704).


- MCEER-05-0011 "The Performance-Based Design Paradigm," by M.J. Astrella and A. Whittaker, 12/15/05 (PB2006-111705).
- MCEER-06-0001 "Seismic Fragility of Suspended Ceiling Systems," H. Badillo-Almaraz, A.S. Whittaker, A.M. Reinhorn and G.P. Cimellaro, 2/4/06 (PB2006-111706).
- MCEER-06-0002 "Multi-Dimensional Fragility of Structures," by G.P. Cimellaro, A.M. Reinhorn and M. Bruneau, 3/1/06 (PB2007-106974, A09, MF-A02, CD A00).
- MCEER-06-0003 "Built-Up Shear Links as Energy Dissipators for Seismic Protection of Bridges," by P. Dusicka, A.M. Itani and I.G. Buckle, 3/15/06 (PB2006-111708).
- MCEER-06-0004 "Analytical Investigation of the Structural Fuse Concept," by R.E. Vargas and M. Bruneau, 3/16/06 (PB2006-111709).
- MCEER-06-0005 "Experimental Investigation of the Structural Fuse Concept," by R.E. Vargas and M. Bruneau, 3/17/06 (PB2006-111710).
- MCEER-06-0006 "Further Development of Tubular Eccentrically Braced Frame Links for the Seismic Retrofit of Braced Steel Truss Bridge Piers," by J.W. Berman and M. Bruneau, 3/27/06 (PB2007-105147).
- MCEER-06-0007 "REDARS Validation Report," by S. Cho, C.K. Huyck, S. Ghosh and R.T. Eguchi, 8/8/06 (PB2007-106983).
- MCEER-06-0008 "Review of Current NDE Technologies for Post-Earthquake Assessment of Retrofitted Bridge Columns," by J.W. Song, Z. Liang and G.C. Lee, 8/21/06 (PB2007-106984).
- MCEER-06-0009 "Liquefaction Remediation in Silty Soils Using Dynamic Compaction and Stone Columns," by S. Thevanayagam, G.R. Martin, R. Nashed, T. Shenthan, T. Kanagalingam and N. Ecemis, 8/28/06 (PB2007-106985).
- MCEER-06-0010 "Conceptual Design and Experimental Investigation of Polymer Matrix Composite Infill Panels for Seismic Retrofitting," by W. Jung, M. Chiewanichakorn and A.J. Aref, 9/21/06 (PB2007-106986).
- MCEER-06-0011 "A Study of the Coupled Horizontal-Vertical Behavior of Elastomeric and Lead-Rubber Seismic Isolation Bearings," by G.P. Warn and A.S. Whittaker, 9/22/06 (PB2007-108679).
- MCEER-06-0012 "Proceedings of the Fourth PRC-US Workshop on Seismic Analysis and Design of Special Bridges: Advancing Bridge Technologies in Research, Design, Construction and Preservation," Edited by L.C. Fan, G.C. Lee and L. Ziang, 10/12/06 (PB2007-109042).
- MCEER-06-0013 "Cyclic Response and Low Cycle Fatigue Characteristics of Plate Steels," by P. Dusicka, A.M. Itani and I.G. Buckle, 11/1/06 (PB2007-106987).
- MCEER-06-0014 "Proceedings of the Second US-Taiwan Bridge Engineering Workshop," edited by W.P. Yen, J. Shen, J-Y. Chen and M. Wang, 11/15/06 (PB2008-500041).
- MCEER-06-0015 "User Manual and Technical Documentation for the REDARSTM Import Wizard," by S. Cho, S. Ghosh, C.K. Huyck and S.D. Werner, 11/30/06 (PB2007-114766).
- MCEER-06-0016 "Hazard Mitigation Strategy and Monitoring Technologies for Urban and Infrastructure Public Buildings: Proceedings of the China-US Workshops," edited by X.Y. Zhou, A.L. Zhang, G.C. Lee and M. Tong, 12/12/06 (PB2008-500018).
- MCEER-07-0001 "Static and Kinetic Coefficients of Friction for Rigid Blocks," by C. Kafali, S. Fathali, M. Grigoriu and A.S. Whittaker, 3/20/07 (PB2007-114767).
- MCEER-07-0002 "Hazard Mitigation Investment Decision Making: Organizational Response to Legislative Mandate," by L.A. Arendt, D.J. Alesch and W.J. Petak, 4/9/07 (PB2007-114768).
- MCEER-07-0003 "Seismic Behavior of Bidirectional-Resistant Ductile End Diaphragms with Unbonded Braces in Straight or Skewed Steel Bridges," by O. Celik and M. Bruneau, 4/11/07 (PB2008-105141).

- MCEER-07-0004 “Modeling Pile Behavior in Large Pile Groups Under Lateral Loading,” by A.M. Dodds and G.R. Martin, 4/16/07(PB2008-105142).
- MCEER-07-0005 “Experimental Investigation of Blast Performance of Seismically Resistant Concrete-Filled Steel Tube Bridge Piers,” by S. Fujikura, M. Bruneau and D. Lopez-Garcia, 4/20/07 (PB2008-105143).
- MCEER-07-0006 “Seismic Analysis of Conventional and Isolated Liquefied Natural Gas Tanks Using Mechanical Analogs,” by I.P. Christovasilis and A.S. Whittaker, 5/1/07.
- MCEER-07-0007 “Experimental Seismic Performance Evaluation of Isolation/Restraint Systems for Mechanical Equipment – Part 1: Heavy Equipment Study,” by S. Fathali and A. Filiatrault, 6/6/07 (PB2008-105144).
- MCEER-07-0008 “Seismic Vulnerability of Timber Bridges and Timber Substructures,” by A.A. Sharma, J.B. Mander, I.M. Friedland and D.R. Allicock, 6/7/07 (PB2008-105145).
- MCEER-07-0009 “Experimental and Analytical Study of the XY-Friction Pendulum (XY-FP) Bearing for Bridge Applications,” by C.C. Marin-Artieda, A.S. Whittaker and M.C. Constantinou, 6/7/07 (PB2008-105191).
- MCEER-07-0010 “Proceedings of the PRC-US Earthquake Engineering Forum for Young Researchers,” Edited by G.C. Lee and X.Z. Qi, 6/8/07 (PB2008-500058).
- MCEER-07-0011 “Design Recommendations for Perforated Steel Plate Shear Walls,” by R. Purba and M. Bruneau, 6/18/07, (PB2008-105192).
- MCEER-07-0012 “Performance of Seismic Isolation Hardware Under Service and Seismic Loading,” by M.C. Constantinou, A.S. Whittaker, Y. Kalpakidis, D.M. Fenz and G.P. Warn, 8/27/07, (PB2008-105193).
- MCEER-07-0013 “Experimental Evaluation of the Seismic Performance of Hospital Piping Subassemblies,” by E.R. Goodwin, E. Maragakis and A.M. Itani, 9/4/07, (PB2008-105194).
- MCEER-07-0014 “A Simulation Model of Urban Disaster Recovery and Resilience: Implementation for the 1994 Northridge Earthquake,” by S. Miles and S.E. Chang, 9/7/07, (PB2008-106426).
- MCEER-07-0015 “Statistical and Mechanistic Fragility Analysis of Concrete Bridges,” by M. Shinozuka, S. Banerjee and S-H. Kim, 9/10/07, (PB2008-106427).
- MCEER-07-0016 “Three-Dimensional Modeling of Inelastic Buckling in Frame Structures,” by M. Schachter and AM. Reinhorn, 9/13/07, (PB2008-108125).
- MCEER-07-0017 “Modeling of Seismic Wave Scattering on Pile Groups and Caissons,” by I. Po Lam, H. Law and C.T. Yang, 9/17/07 (PB2008-108150).
- MCEER-07-0018 “Bridge Foundations: Modeling Large Pile Groups and Caissons for Seismic Design,” by I. Po Lam, H. Law and G.R. Martin (Coordinating Author), 12/1/07 (PB2008-111190).
- MCEER-07-0019 “Principles and Performance of Roller Seismic Isolation Bearings for Highway Bridges,” by G.C. Lee, Y.C. Ou, Z. Liang, T.C. Niu and J. Song, 12/10/07 (PB2009-110466).
- MCEER-07-0020 “Centrifuge Modeling of Permeability and Pinning Reinforcement Effects on Pile Response to Lateral Spreading,” by L.L Gonzalez-Lagos, T. Abdoun and R. Dobry, 12/10/07 (PB2008-111191).
- MCEER-07-0021 “Damage to the Highway System from the Pisco, Perú Earthquake of August 15, 2007,” by J.S. O’Connor, L. Mesa and M. Nykamp, 12/10/07, (PB2008-108126).
- MCEER-07-0022 “Experimental Seismic Performance Evaluation of Isolation/Restraint Systems for Mechanical Equipment – Part 2: Light Equipment Study,” by S. Fathali and A. Filiatrault, 12/13/07 (PB2008-111192).
- MCEER-07-0023 “Fragility Considerations in Highway Bridge Design,” by M. Shinozuka, S. Banerjee and S.H. Kim, 12/14/07 (PB2008-111193).

- MCEER-07-0024 "Performance Estimates for Seismically Isolated Bridges," by G.P. Warn and A.S. Whittaker, 12/30/07 (PB2008-112230).
- MCEER-08-0001 "Seismic Performance of Steel Girder Bridge Superstructures with Conventional Cross Frames," by L.P. Carden, A.M. Itani and I.G. Buckle, 1/7/08, (PB2008-112231).
- MCEER-08-0002 "Seismic Performance of Steel Girder Bridge Superstructures with Ductile End Cross Frames with Seismic Isolators," by L.P. Carden, A.M. Itani and I.G. Buckle, 1/7/08 (PB2008-112232).
- MCEER-08-0003 "Analytical and Experimental Investigation of a Controlled Rocking Approach for Seismic Protection of Bridge Steel Truss Piers," by M. Pollino and M. Bruneau, 1/21/08 (PB2008-112233).
- MCEER-08-0004 "Linking Lifeline Infrastructure Performance and Community Disaster Resilience: Models and Multi-Stakeholder Processes," by S.E. Chang, C. Pasion, K. Tatebe and R. Ahmad, 3/3/08 (PB2008-112234).
- MCEER-08-0005 "Modal Analysis of Generally Damped Linear Structures Subjected to Seismic Excitations," by J. Song, Y-L. Chu, Z. Liang and G.C. Lee, 3/4/08 (PB2009-102311).
- MCEER-08-0006 "System Performance Under Multi-Hazard Environments," by C. Kafali and M. Grigoriu, 3/4/08 (PB2008-112235).
- MCEER-08-0007 "Mechanical Behavior of Multi-Spherical Sliding Bearings," by D.M. Fenz and M.C. Constantinou, 3/6/08 (PB2008-112236).
- MCEER-08-0008 "Post-Earthquake Restoration of the Los Angeles Water Supply System," by T.H.P. Tabucchi and R.A. Davidson, 3/7/08 (PB2008-112237).
- MCEER-08-0009 "Fragility Analysis of Water Supply Systems," by A. Jacobson and M. Grigoriu, 3/10/08 (PB2009-105545).
- MCEER-08-0010 "Experimental Investigation of Full-Scale Two-Story Steel Plate Shear Walls with Reduced Beam Section Connections," by B. Qu, M. Bruneau, C-H. Lin and K-C. Tsai, 3/17/08 (PB2009-106368).
- MCEER-08-0011 "Seismic Evaluation and Rehabilitation of Critical Components of Electrical Power Systems," S. Ersoy, B. Feizi, A. Ashrafi and M. Ala Saadeghvaziri, 3/17/08 (PB2009-105546).
- MCEER-08-0012 "Seismic Behavior and Design of Boundary Frame Members of Steel Plate Shear Walls," by B. Qu and M. Bruneau, 4/26/08 . (PB2009-106744).
- MCEER-08-0013 "Development and Appraisal of a Numerical Cyclic Loading Protocol for Quantifying Building System Performance," by A. Filiatrault, A. Wanitkorkul and M. Constantinou, 4/27/08 (PB2009-107906).
- MCEER-08-0014 "Structural and Nonstructural Earthquake Design: The Challenge of Integrating Specialty Areas in Designing Complex, Critical Facilities," by W.J. Petak and D.J. Alesch, 4/30/08 (PB2009-107907).
- MCEER-08-0015 "Seismic Performance Evaluation of Water Systems," by Y. Wang and T.D. O'Rourke, 5/5/08 (PB2009-107908).
- MCEER-08-0016 "Seismic Response Modeling of Water Supply Systems," by P. Shi and T.D. O'Rourke, 5/5/08 (PB2009-107910).
- MCEER-08-0017 "Numerical and Experimental Studies of Self-Centering Post-Tensioned Steel Frames," by D. Wang and A. Filiatrault, 5/12/08 (PB2009-110479).
- MCEER-08-0018 "Development, Implementation and Verification of Dynamic Analysis Models for Multi-Spherical Sliding Bearings," by D.M. Fenz and M.C. Constantinou, 8/15/08 (PB2009-107911).
- MCEER-08-0019 "Performance Assessment of Conventional and Base Isolated Nuclear Power Plants for Earthquake Blast Loadings," by Y.N. Huang, A.S. Whittaker and N. Luco, 10/28/08 (PB2009-107912).


- MCEER-08-0020 “Remote Sensing for Resilient Multi-Hazard Disaster Response – Volume I: Introduction to Damage Assessment Methodologies,” by B.J. Adams and R.T. Eguchi, 11/17/08 (PB2010-102695).
- MCEER-08-0021 “Remote Sensing for Resilient Multi-Hazard Disaster Response – Volume II: Counting the Number of Collapsed Buildings Using an Object-Oriented Analysis: Case Study of the 2003 Bam Earthquake,” by L. Gusella, C.K. Huyck and B.J. Adams, 11/17/08 (PB2010-100925).
- MCEER-08-0022 “Remote Sensing for Resilient Multi-Hazard Disaster Response – Volume III: Multi-Sensor Image Fusion Techniques for Robust Neighborhood-Scale Urban Damage Assessment,” by B.J. Adams and A. McMillan, 11/17/08 (PB2010-100926).
- MCEER-08-0023 “Remote Sensing for Resilient Multi-Hazard Disaster Response – Volume IV: A Study of Multi-Temporal and Multi-Resolution SAR Imagery for Post-Katrina Flood Monitoring in New Orleans,” by A. McMillan, J.G. Morley, B.J. Adams and S. Chesworth, 11/17/08 (PB2010-100927).
- MCEER-08-0024 “Remote Sensing for Resilient Multi-Hazard Disaster Response – Volume V: Integration of Remote Sensing Imagery and VIEWS™ Field Data for Post-Hurricane Charley Building Damage Assessment,” by J.A. Womble, K. Mehta and B.J. Adams, 11/17/08 (PB2009-115532).
- MCEER-08-0025 “Building Inventory Compilation for Disaster Management: Application of Remote Sensing and Statistical Modeling,” by P. Sarabandi, A.S. Kiremidjian, R.T. Eguchi and B. J. Adams, 11/20/08 (PB2009-110484).
- MCEER-08-0026 “New Experimental Capabilities and Loading Protocols for Seismic Qualification and Fragility Assessment of Nonstructural Systems,” by R. Retamales, G. Mosqueda, A. Filiatrault and A. Reinhorn, 11/24/08 (PB2009-110485).
- MCEER-08-0027 “Effects of Heating and Load History on the Behavior of Lead-Rubber Bearings,” by I.V. Kalpakidis and M.C. Constantinou, 12/1/08 (PB2009-115533).
- MCEER-08-0028 “Experimental and Analytical Investigation of Blast Performance of Seismically Resistant Bridge Piers,” by S.Fujikura and M. Bruneau, 12/8/08 (PB2009-115534).
- MCEER-08-0029 “Evolutionary Methodology for Aseismic Decision Support,” by Y. Hu and G. Dargush, 12/15/08.
- MCEER-08-0030 “Development of a Steel Plate Shear Wall Bridge Pier System Conceived from a Multi-Hazard Perspective,” by D. Keller and M. Bruneau, 12/19/08 (PB2010-102696).
- MCEER-09-0001 “Modal Analysis of Arbitrarily Damped Three-Dimensional Linear Structures Subjected to Seismic Excitations,” by Y.L. Chu, J. Song and G.C. Lee, 1/31/09 (PB2010-100922).
- MCEER-09-0002 “Air-Blast Effects on Structural Shapes,” by G. Ballantyne, A.S. Whittaker, A.J. Aref and G.F. Dargush, 2/2/09 (PB2010-102697).
- MCEER-09-0003 “Water Supply Performance During Earthquakes and Extreme Events,” by A.L. Bonneau and T.D. O’Rourke, 2/16/09 (PB2010-100923).
- MCEER-09-0004 “Generalized Linear (Mixed) Models of Post-Earthquake Ignitions,” by R.A. Davidson, 7/20/09 (PB2010-102698).
- MCEER-09-0005 “Seismic Testing of a Full-Scale Two-Story Light-Frame Wood Building: NEESWood Benchmark Test,” by I.P. Christovasilis, A. Filiatrault and A. Wanitkorkul, 7/22/09 (PB2012-102401).
- MCEER-09-0006 “IDARC2D Version 7.0: A Program for the Inelastic Damage Analysis of Structures,” by A.M. Reinhorn, H. Roh, M. Sivaselvan, S.K. Kunnath, R.E. Valles, A. Madan, C. Li, R. Lobo and Y.J. Park, 7/28/09 (PB2010-103199).
- MCEER-09-0007 “Enhancements to Hospital Resiliency: Improving Emergency Planning for and Response to Hurricanes,” by D.B. Hess and L.A. Arendt, 7/30/09 (PB2010-100924).

- MCEER-09-0008 “Assessment of Base-Isolated Nuclear Structures for Design and Beyond-Design Basis Earthquake Shaking,” by Y.N. Huang, A.S. Whittaker, R.P. Kennedy and R.L. Mayes, 8/20/09 (PB2010-102699).
- MCEER-09-0009 “Quantification of Disaster Resilience of Health Care Facilities,” by G.P. Cimellaro, C. Fumo, A.M. Reinhorn and M. Bruneau, 9/14/09 (PB2010-105384).
- MCEER-09-0010 “Performance-Based Assessment and Design of Squat Reinforced Concrete Shear Walls,” by C.K. Gulec and A.S. Whittaker, 9/15/09 (PB2010-102700).
- MCEER-09-0011 “Proceedings of the Fourth US-Taiwan Bridge Engineering Workshop,” edited by W.P. Yen, J.J. Shen, T.M. Lee and R.B. Zheng, 10/27/09 (PB2010-500009).
- MCEER-09-0012 “Proceedings of the Special International Workshop on Seismic Connection Details for Segmental Bridge Construction,” edited by W. Phillip Yen and George C. Lee, 12/21/09 (PB2012-102402).
- MCEER-10-0001 “Direct Displacement Procedure for Performance-Based Seismic Design of Multistory Woodframe Structures,” by W. Pang and D. Rosowsky, 4/26/10 (PB2012-102403).
- MCEER-10-0002 “Simplified Direct Displacement Design of Six-Story NEESWood Capstone Building and Pre-Test Seismic Performance Assessment,” by W. Pang, D. Rosowsky, J. van de Lindt and S. Pei, 5/28/10 (PB2012-102404).
- MCEER-10-0003 “Integration of Seismic Protection Systems in Performance-Based Seismic Design of Woodframed Structures,” by J.K. Shinde and M.D. Symans, 6/18/10 (PB2012-102405).
- MCEER-10-0004 “Modeling and Seismic Evaluation of Nonstructural Components: Testing Frame for Experimental Evaluation of Suspended Ceiling Systems,” by A.M. Reinhorn, K.P. Ryu and G. Maddaloni, 6/30/10 (PB2012-102406).
- MCEER-10-0005 “Analytical Development and Experimental Validation of a Structural-Fuse Bridge Pier Concept,” by S. El-Bahey and M. Bruneau, 10/1/10 (PB2012-102407).
- MCEER-10-0006 “A Framework for Defining and Measuring Resilience at the Community Scale: The PEOPLES Resilience Framework,” by C.S. Renschler, A.E. Frazier, L.A. Arendt, G.P. Cimellaro, A.M. Reinhorn and M. Bruneau, 10/8/10 (PB2012-102408).
- MCEER-10-0007 “Impact of Horizontal Boundary Elements Design on Seismic Behavior of Steel Plate Shear Walls,” by R. Purba and M. Bruneau, 11/14/10 (PB2012-102409).
- MCEER-10-0008 “Seismic Testing of a Full-Scale Mid-Rise Building: The NEESWood Capstone Test,” by S. Pei, J.W. van de Lindt, S.E. Pryor, H. Shimizu, H. Isoda and D.R. Rammer, 12/1/10 (PB2012-102410).
- MCEER-10-0009 “Modeling the Effects of Detonations of High Explosives to Inform Blast-Resistant Design,” by P. Sherkar, A.S. Whittaker and A.J. Aref, 12/1/10 (PB2012-102411).
- MCEER-10-0010 “L’Aquila Earthquake of April 6, 2009 in Italy: Rebuilding a Resilient City to Withstand Multiple Hazards,” by G.P. Cimellaro, I.P. Christovasilis, A.M. Reinhorn, A. De Stefano and T. Kirova, 12/29/10.
- MCEER-11-0001 “Numerical and Experimental Investigation of the Seismic Response of Light-Frame Wood Structures,” by I.P. Christovasilis and A. Filiatrault, 8/8/11 (PB2012-102412).
- MCEER-11-0002 “Seismic Design and Analysis of a Precast Segmental Concrete Bridge Model,” by M. Anagnostopoulou, A. Filiatrault and A. Aref, 9/15/11.



EARTHQUAKE ENGINEERING TO EXTREME EVENTS

University at Buffalo, The State University of New York
Red Jacket Quadrangle ■ Buffalo, New York 14261
Phone: (716) 645-3391 ■ Fax: (716) 645-3399
E-mail: mceer@buffalo.edu ■ WWW Site <http://mceer.buffalo.edu>



University at Buffalo *The State University of New York*

ISSN 1520-295X